THIRD ANNUAL HEDS-UP FORUM

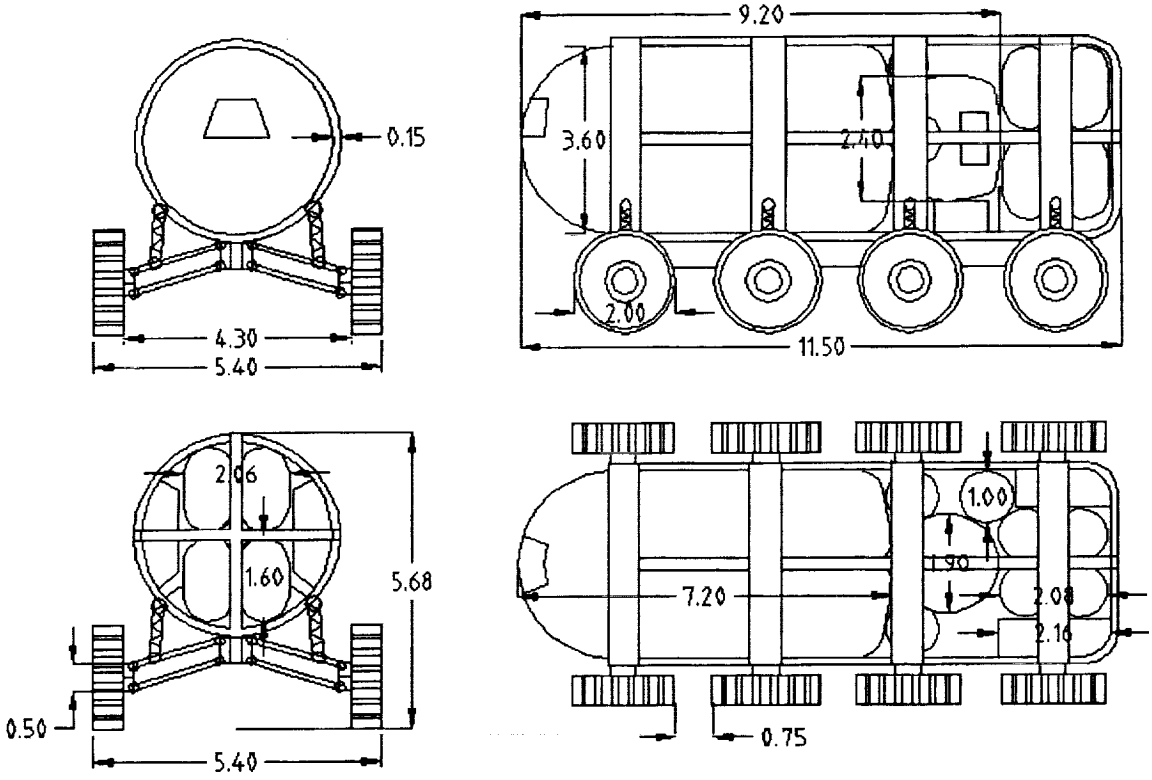

May 4–5, 2000
Lunar and Planetary Institute, Houston, Texas

LPI Contribution No. 1063

THIRD ANNUAL HEDS-UP FORUM

May 4–5, 2000
Lunar and Planetary Institute, Houston, Texas

Edited by
Michael B. Duke

Sponsored by
Lunar and Planetary Institute
National Aeronautics and Space Administration
Office of Space Flight, Advanced Projects Office

Lunar and Planetary Institute 3600 Bay Area Boulevard Houston TX 77058-1113

LPI Contribution No. 1063

Compiled in 2000 by
LUNAR AND PLANETARY INSTITUTE

The Institute is operated by the Universities Space Research Association under Contract No. NASW-4574 with the National Aeronautics and Space Administration.

This volume may be cited as

Duke M. B., ed. (2000) *Third Annual HEDS-UP Forum.* LPI Contribution No. 1063, Lunar and Planetary Institute, Houston. 237 pp.

This volume is distributed by

ORDER DEPARTMENT
Lunar and Planetary Institute
3600 Bay Area Boulevard
Houston TX 77058-1113
Phone: 281-486-2172
Fax: 281-486-2186
E-mail: order@lpi.usra.edu

Mail order requestors will be invoiced for the cost of shipping and handling.

Cover: Lunar rover designed by the team from the University of Maryland.

PREFACE

The HEDS-UP (Human Exploration and Development of Space–University Partners) program has been instituted to build new relationships between university faculty and students and NASA in support of the Human Exploration and Development of Space. The program provides a mechanism whereby university students can explore problems of interest to NASA through student design projects, led by a university professor or mentor, and aided by the HEDS-UP staff. HEDS-UP advises on the type of project that is of interest and provides contacts to NASA and industry professionals who may serve as mentors to the student project. Students become acquainted with objectives, strategies, development issues, and technologic characteristics of space exploration programs. In doing so, they are preparing themselves for future engineering challenges and may well find that the program is on their critical path to professional advancement. Many of the ideas are novel and are of interest to NASA. Industry finds in HEDS-UP a mechanism to meet many bright and enthusiastic students who are about to enter the work force. The universities become more involved with space exploration and the students are encouraged to include an outreach element in their work, to bring their efforts and their excitement to others in their universities or in their communities.

The climax of the HEDS-UP program each year is the HEDS-UP Forum, held at the Lunar and Planetary Institute. Here, the university teams bring their projects — written reports, oral reports, models, prototypes, and experiment demonstrations — to show to one another and to NASA and industry participants. NASA, industry, and academic professionals present discussions of problems of current interest to space exploration. All meet informally around the posters that each of the teams brings to the Forum.

This year the HEDS-UP Forum was held May 4–5 at the Lunar and Planetary Institute in Houston. Thirteen university teams from twelve universities participated. Eleven teams were undergraduate teams; two were composed of graduate students. Each team contributed a 20-page written report, and these reports are reproduced in this volume. The agenda for the Forum shows the order of presentation of the talks by the universities and by NASA and Lunar and Planetary Institute presenters. The specially invited NASA presenters included Mr. John Connolly, Dr. David McKay and Dr. Donald Henninger of the NASA Johnson Space Center, Dr. Paul Spudis and Dr. Steve Clifford of the Lunar and Planetary Institute, and Dr. Pascal Lee of the NASA Ames Research Center.

The Forum could not have been carried out without the efforts of Sharon Steahle and Kay Labuda of the Lunar and Planetary Institute, and many other Institute staff members contributed to the effort. Mike Duke and Kay Labuda took the photographs that are included in this report. Renee Dotson was responsible for the final editing.

This report, including its downloadable photos, is accessible through the HEDS-UP Web site (http://www.lpi.usra.edu/lpi/HEDS-UP/). The Web site also includes additional information for prospective participants.

The LPI staff is looking forward to the next year of HEDS-UP, in which we hope to make further improvements and involve additional university teams.

Funding for HEDS-UP is provided by the Advanced Projects Office of the Office of Space Flight, NASA Headquarters.

Michael B. Duke
Lunar and Planetary Institute
May 2000

CONTENTS

AGENDA

May 4, 2000

7:30 a.m.	Continental Breakfast
8:30	Welcome to LPI — David Black, Director
8:45	John Connolly, NASA Johnson Space Center — "Strategic Directions for HEDS"
9:30	Break
9:45	University of California, Berkeley — "The Hunt for Liquid Water, Life and Landing Sites on the Surface of Mars Today"
10:30	University of Washington — "Studies on Closed Ecosystems: Biosphere in a Bottle"
11:15	University of Texas, Austin — "Automated Construction of a Martian Base"
12:00	Lunch
1:30 p.m.	University of Colorado — "MARV: Mars Aerial Research Vehicle"
2:15	University of Maryland — "Project Magellan: Racing the Sun around the Moon"
3:00	California Institute of Technology — "Mars SCHEME: The Mars Society-Caltech Human Exploration of Mars Endeavor"
3:45	Break
4:00	Embry Riddle Aeronautical University — "LIRA: Lunar Interferometric Radio Array"
4:45	Wichita State University — "Mars Airborne Exploration Vehicle"
5:30	Posters and Reception

May 5, 2000

7:30 a.m.	Continental Breakfast
8:30	Colorado School of Mines — "Excavating Martian Regolith to Extract Water"
9:15	Rowan University — "A Comparison of Preliminary Design Configurations for Liquid, Solid and Hybrid Mars Ascent Vehicles using In Situ Propellants"
10:00	Break
10:15	Pennsylvania State University — "Scaling the Martian Walls of Time"
11:00	Georgia Institute of Technology — "A Moon-based Advanced Reusable Transportation Architecture: The MARTA Project"
11:45	Embry-Riddle Aeronautical University — "Red Mars – Green Mars? Martian Regolith as a Plant Growth Medium"
12:30 p.m.	Lunch
2:00	"Exploration of the Moon," P. Spudis, LPI
2:30	"Searching for Life on Mars," D. McKay, JSC
3:00	"Drilling for Water on Mars," S. Clifford, LPI
3:30	"The Haughton Crater Mars Analog," P. Lee, Ames Research Center
4:00	"Advanced Life Support for Long-Duration Missions," D. Henninger, JSC
4:30	Presentation of Awards
5:00	Adjourn

The Forum

The Forum is a two-way communication event, with university teams presenting the results of their studies and NASA, industry, and others presenting recent advances in space exploration. The interchange is productive and stimulating, with ideas for next year's HEDS-UP program emerging.

Dr. Pascal Lee, an astrobiologist at the NASA Ames Research Labororatory, discusses plans for a Mars analog test facility at the Haughton meteorite crater in the Canadian Arctic.

Dr. David S. McKay, a geologist at NASA's Johnson Space Center, discussed the problems of finding evidence for ancient life on Mars. Mars may once have been water-rich, though now only traces of water can be found in its atmosphere.

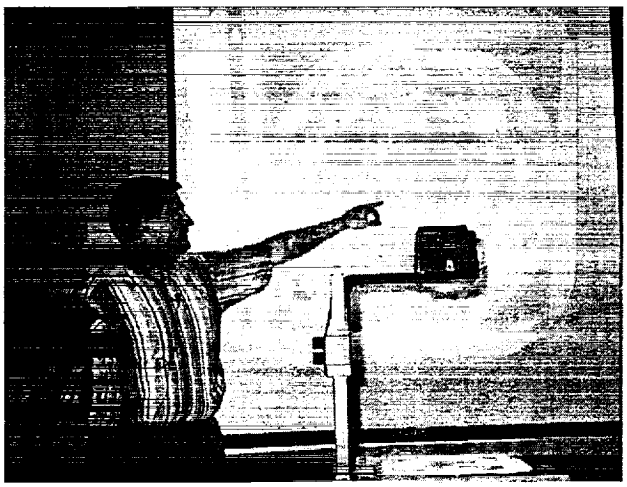

Dr. Paul Spudis, Assistant Director of the Lunar and Planetary Institute, discussed the future exploration of the Moon. Here he explains how water ice might be trapped in permanently shadowed areas near the lunar poles.

The Teams

A team of graduate students from the Georgia Institute of Technology worked with Dr. John Olds (arrow) on an analytical study of the cost of transporting materials from the Moon to space.

A team of students, under the direction of Dr. Anthony Marchese (left) of Rowan University in New Jersey, studied the variety of propulsion systems that might be used to take people off the surface of Mars on their trip back to Earth.

Dr. Frieda Taub, of the University of Washington, advised a student team that studied "Biospheres in a Bottle," an approach intended to learn about characteristics of small closed systems such as would exist in a spacecraft on its way to Mars.

The Pennsylvania State University team was advised by Professor Wojiech Klimkiewicz (arrow). They studied a novel concept that allows instruments to descend a steep-sided canyon wall on Mars to study the layering. They tied for third place among the undergraduate teams at the HEDS-UP Forum.

The Caltech student chapter of The Mars Society, with the advice of Jim Burke (not shown) of the Jet Propulsion Laboratory and Caltech, presented their integrated study of a complete round trip for humans to go to Mars (tied for third place).

Wichita State University contributed a study of an research vehicle (a glider of sorts) for studying the atmosphere on Mars. Their advisor, Dr. Gawad Nagati, is not shown.

The University of California at Berkeley contributed two studies. This one, presented only as a poster, studied the relationship of metabolic activity to the design of spacesuits for astronauts.

The other UCB team, shown here with their advisor Dr. Larry Kuznetz (arrow) and mentor David Gan (right), studied the question of whether liquid water might be able to form under some circumstances on the surface of Mars.

A team from the University of Maryland, with their advisor Dr. David Akin (arrow), presented Project Magellan, the first human circumnavigation of the Moon's equator, using a pressurized roving vehicle. They were awarded second place among the undergraduate teams.

Students at the University of Texas, Austin, are shown here with their faculty advisor, Dr. Wallace Fowler. The students were one of four UT teams, who worked on different problems. This team studied the possibility of robotic construction of a human outpost on the Moon.

A team of graduate students from Embry-Riddle Aeronautical University worked on the question of whether plants would grow well in the surface regolith on Mars. They were organized and led by Tony De Tora (right), a graduate student who also contributed to the study.

The University of Colorado, Boulder, considered the design of a Mars Airplane, as initially specified by NASA for the 2003 mission to Mars. Here the team is shown with their faculty advisor, Jason Hinkle (in front).

An undergraduate team from Embry-Riddle University, shown here with advisor Mehmet Reyhanoglu (left), described the design and construction of an interferometric array of radiotelescopes that could be erected on the Moon.

The Colorado School of Mines Engineering Practices Initial Course Sequence (EPICS) program involved over 400 students in a contest to design an robotic excavator for Mars. C.R.A.T.E.R., the winning team from their competition, also won first place at the HEDS-UP Forum among undergraduate teams. Their advisor, Dr. Robert Knecht, is not shown.

The Poster Session

One of the highlights of the HEDS-UP Forum is the poster session and reception, during which the students, faculty, and NASA/industry guests can meet one another and show off their wares. Several of the teams brought models, prototypes, or experimental apparatus.

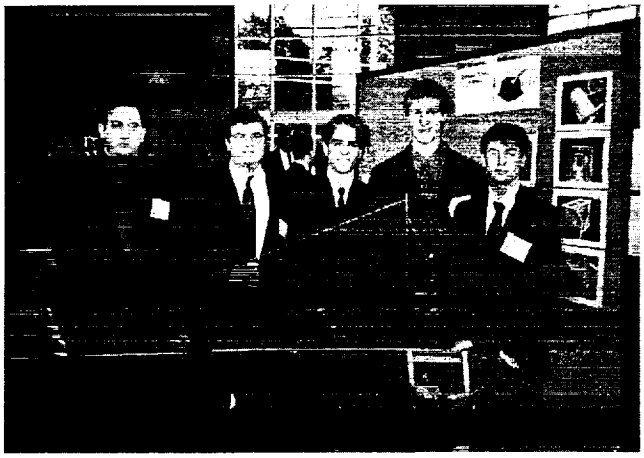

Members of the Colorado School of Mines team demonstrate their Mars drag-line concept.

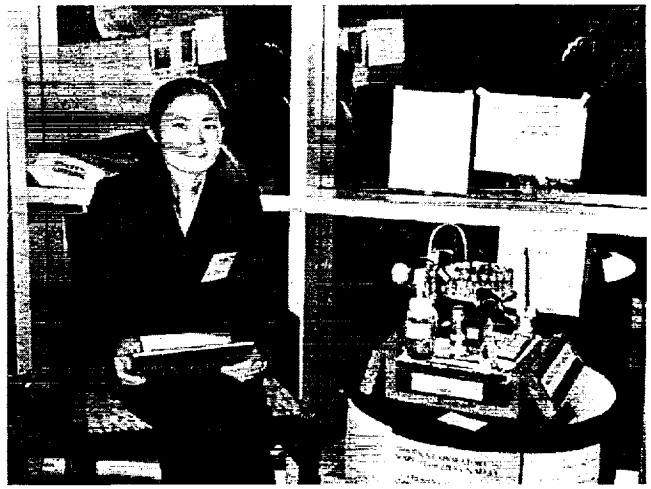

The University of California, Berkeley's experimental apparatus for producing liquid water under martian atmospheric conditions.

Wichita State University student Ravi Malla shows the model they had constructed to illustrate their concept for a martian aerial reconnaissance vehicle.

Professor Gawad Nagati of Wichita State University in discussion with a HEDS-UP student.

The Winners

A panel of judges based their awards on both a written report and the oral presentation made to the Forum. And the winners are . . .

Dr. Michael Duke of the Lunar and Planetary Institute (at right) presents the first-place award for undergraduates to team C.R.A.T.E.R. from the Colorado School of Mines.

The team from Georgia Institute of Technology was awarded first place among graduate teams for their study of the economics of lunar transportation systems.

Among the undergraduate teams, the University of Maryland placed second and a tie for third was awarded to the teams from Caltech and Penn States. Only a first-place award was made to the graduate teams. Each team received a HEDS-UP plaque for their efforts.

The Hunt for Liquid Water, Life and Landing Sites on the Surface of Mars Today

University of California, Berkeley
Contributors: Vincent Chang, David Chu, Christina Lee, Robert Lee, Dalziel Wilson, and Miki Yamada
Teaching Staff: Larry Kuznetz and David Gan

Abstract: As the debate rages on about past or present life on Mars, the prevailing assumption has been that the liquid water essential for its existence is absent because pressures and temperatures are too low. This study presents data, anecdotal and experimental evidence to challenge that assumption.

1.0 Introduction and Background

"Liquid water does not exist on the surface of Mars...Without liquid water, life as we know it cannot exist."
Principal Viking investigator Norman Horowitz made these statements over two decades ago, establishing the contemporary paradigm of a barren Mars today. Since that time, a wealth of new knowledge has been accumulated in the form of images and data on soil, air composition and climate from the robotic probes of the 90s, Pathfinder and Mars Global Surveyer (MGS). We now have extensive pressure and temperature data from all three probes (Figure 1a and Figure 1b) demonstrating pressures above the triple point and temperatures above freezing for long periods of time, meeting the criteria for liquid water. Pathfinder also found 20...C variations along its mast, suggesting ice can melt on the surface even with air temperatures above it below freezing. Spacial variations in temperature may also permit ice to melt against sunlit, smooth, dark rocks despite immediately adjacent temperatures being below zero. Other issues of concern include boiling, evaporation and stability. Under observed Martian pressures, there exists only a 7°C window exists between freezing and boiling. Though narrow, the Viking orbiter observed such a window. As for stability, even if liquid water could exist, skeptics argue, it would be rapidly driven off by high evaporation rates into the dry atmosphere. On the other hand, frost was observed to persist at Viking s Utopia Planitia landing site, implying condensation and stability.

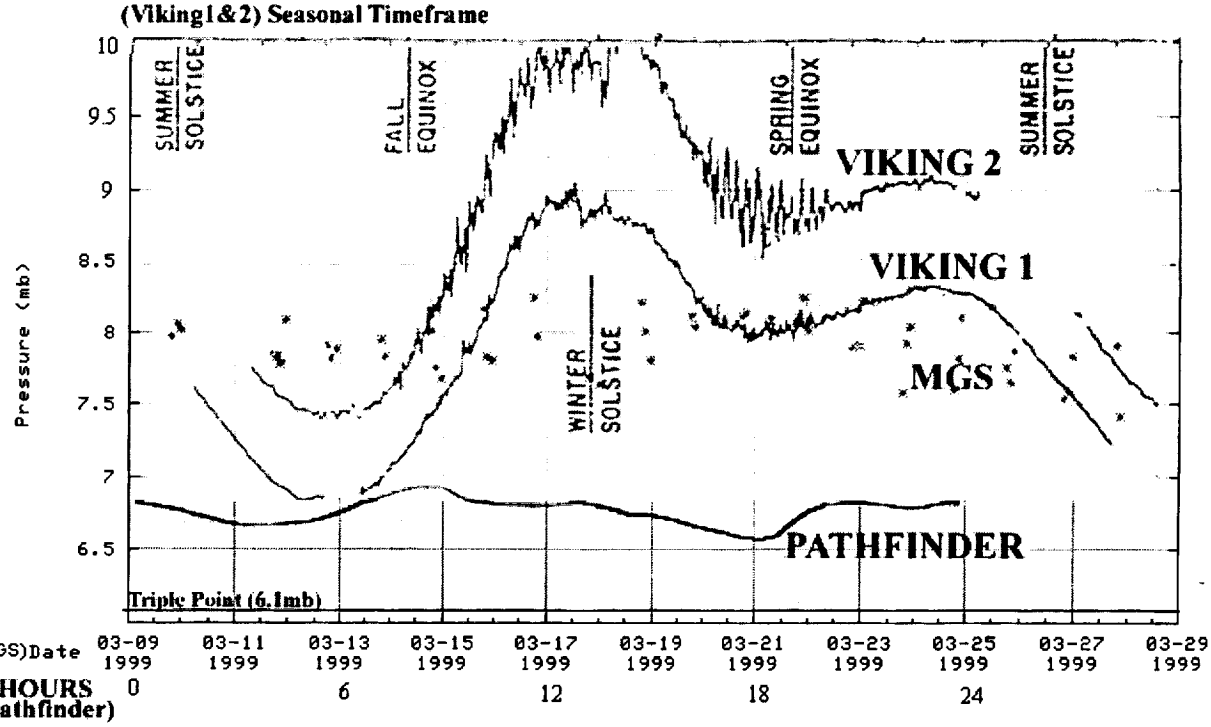

Figure 1a. Probe Pressure Data

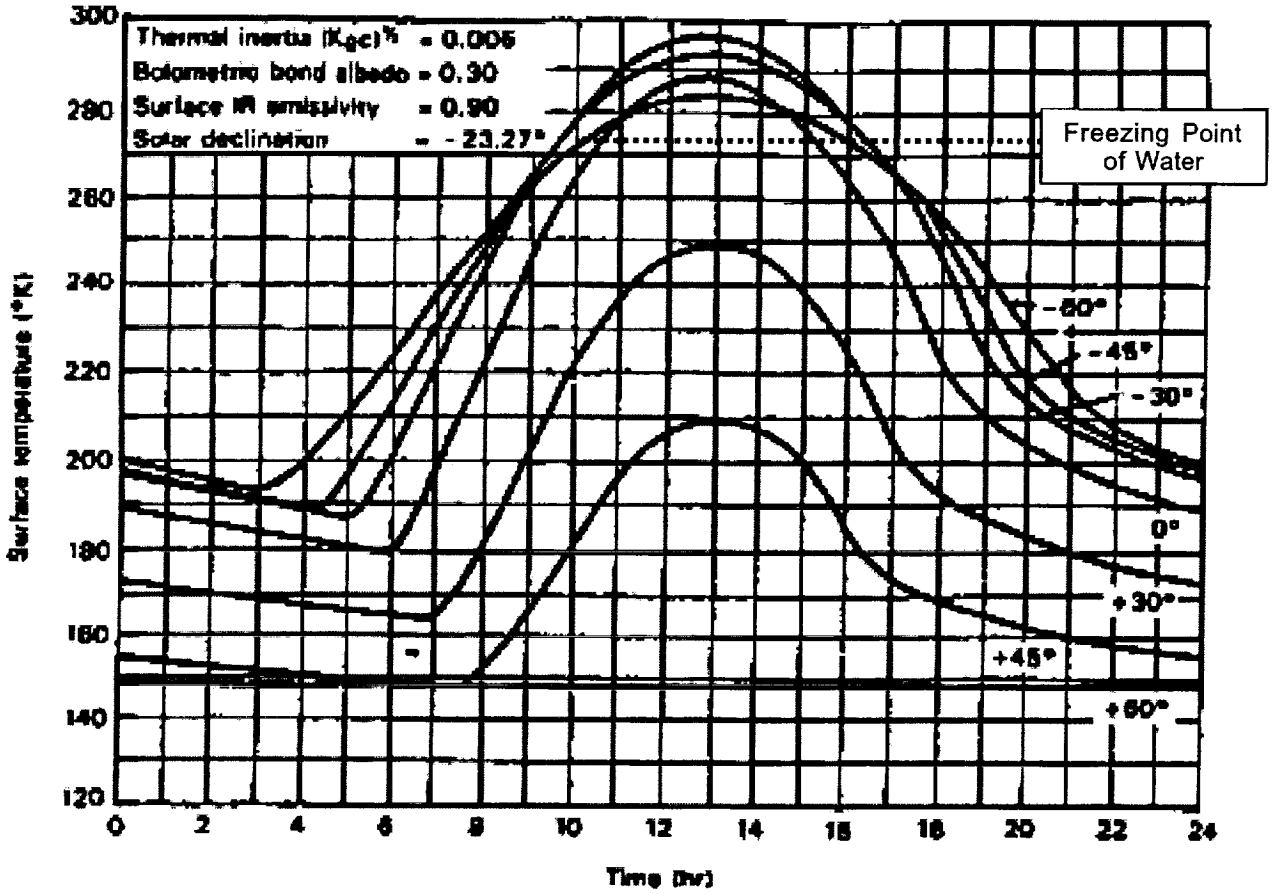

Figure 1b. Viking Temperature Data

If conditions are stable and above the triple point, thermodynamics dictate that liquid water must exist. But does it? The results of this study suggest it can, although precariously. Can life exist in water that remains liquid for just a few hours a day? The answer is less clear. To resolve the questions raised above, a multi-tiered study of theoretical models, empirical evidence and experiments has been performed.

2.0 Theoretical Considerations

Martian Atmospheric Conditions

The Martian atmosphere is composed almost entirely of $C0_2$, with minor fractions of O_2, water vapor and trace gases (Table 1). The NASA-Ames AEPS study[1] analyzed this atmosphere and concluded that it can be treated as an ideal gas.

MAJOR	Composition	Percentage
	Carbon Dioxide (CO_2)	95.32
°	Nitrogen (N_2)	2.7
°	Argon (Ar)	1.6
°	Oxygen (O_2)	0.13
°	Carbon Monoxide (CO)	0.08
MINOR	**Composition**	**ppm (parts per million)**
°	Water (Vapor) (H_2O)	210

TABLE 1: Compositions of Martian atmosphere

As such, the laws governing its behavior can be summarized as follows:

The Knudson number, is on the order of 10^{-5}, where:

$$K_n = \frac{\lambda}{L}$$

λ = mean free path
L = container dimension

Dalton law of additive pressure

$$P_{mix} = \sum_{i=1}^{k} P_i(T_{mix}, V_{mix})$$

Where P_{mix} = pressure of a gas mixture,
P_i = pressure of one composition of the mixture,
T_{mix}, V_{mix} = temperature and pressure of the mixture.

Amagat s law of additive volume

$$V_{mix} = \sum_{i=1}^{k} V_i(T_{mix}, P_{mix})$$

Fick s law

$$M = -D\frac{\partial C}{\partial x}(H_2O)$$

Where M is evaporation or sublimation rate, D is a property of the binary diffusion coefficient, and C denotes concentration.

Psychrometry

For a multiphase medium, evaporation is governed by partial pressure and temperature differences between each component on the surface and in the air stream, according to the following equation:

$$S_2 - S_1 = nN\left[\bar{C}_v N \ln\frac{T_2}{T_{IN}} + \bar{R}\ln\frac{V_2}{V_{IN}}\right] + nO\left[\bar{C}_v O \ln\frac{T_2}{T_{IN}} + \bar{R}\ln\frac{V_2}{V_{IN}}\right]$$

Heat/mass transfer analysis

Using the preceding equations together with ones that govern the flow of fluids, heat, and mass, a mathematical model of the Martian climate system accounting for conduction, convection, radiation, evaporation, sublimation, atmospheric properties and soil properties can be constructed (Figure 2)[2]. Such a model has been used by Haberle[3] et al to indicate that liquid water is not only feasible, but potentially stable for up to 150 days/year near the equator.

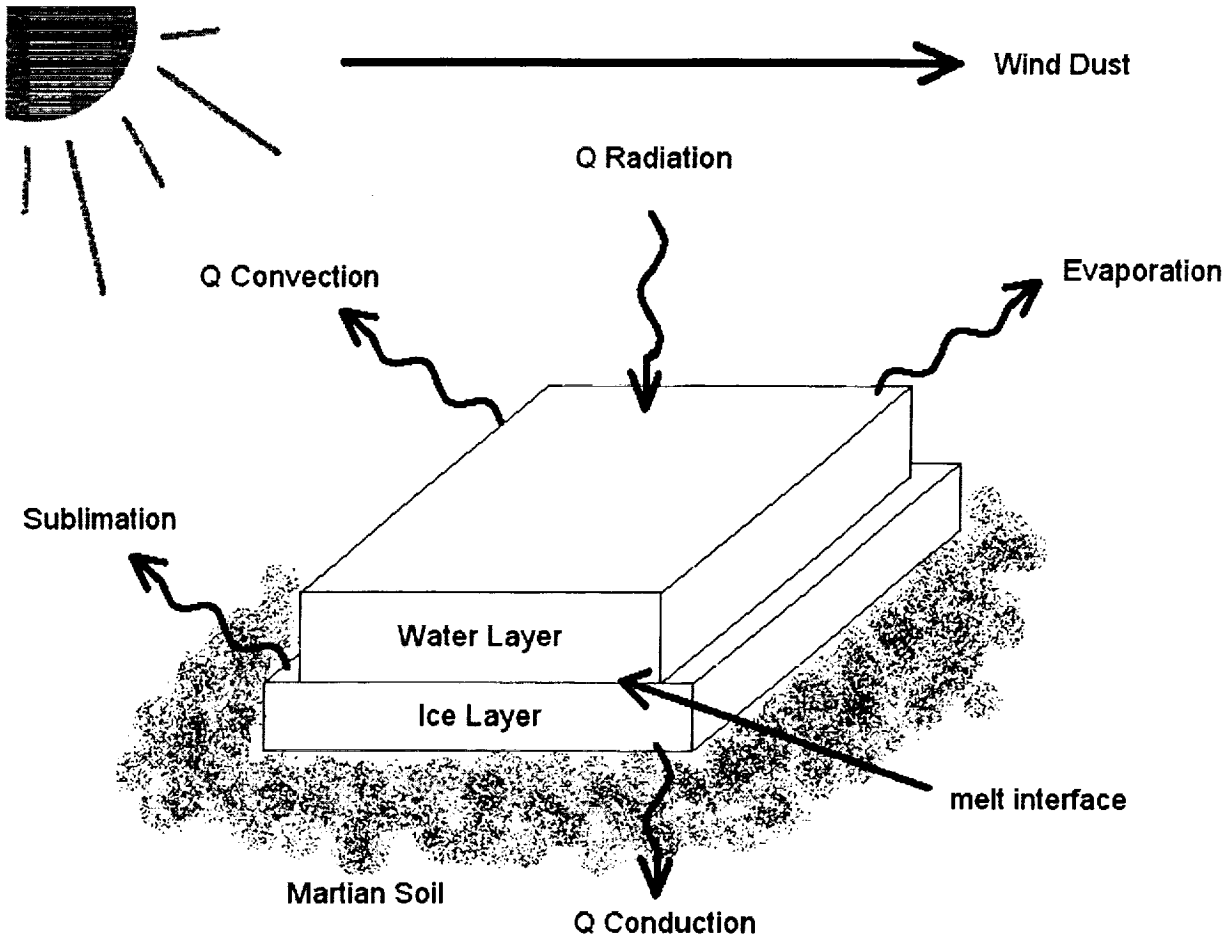

Figure 2: Water on Mars Thermal Model

Thermodynamics

The phase diagram for pure water (Figure 3) shows the pressures and temperatures at which water can exist in a solid, liquid, or vapor form. As seen from this diagram, liquid water cannot exist below 6.1mb. Since Martian pressures range between 3-10mb and temperatures frequently fall in the 0-7...Gwindow, between freezing and boiling, thermodynamics dictate that liquid water must exist at certain times. A question frequently asked is whether the abscissa in Figure 3 is total pressure or partial pressure of water vapor. If the former, the pressure on Mars is frequently above the triple point. If the latter, the pressure would always be below it since the partial pressure of water vapor in the atmosphere is only a fraction of a millibar. This question will be addressed in the experimental methods section of this paper. Another issue is water purity. The triple point diagram is for pure distilled water. Water with brine, sand, or impurities such as on Mars, would have a depressed freezing/melt point, shifting the boundaries of Figure 3 down and increasing the probability of liquid water.

Empirical Evidence

The porous plate sublimator used in all astronaut EMU's (Extravehicular Mobility Units) since the Apollo program makes use of the fact that water goes directly from ice to vapor at pressures below the triple point. The design of this sublimator incorporates a feedwater tank under pressure that supplies water to the plate, a ventilation gas loop, a liquid cooled garment loop that carries body and equipment heat from the EMU to the sublimator, and associated pumps, fans, batteries, diverter valves, tubing and ancillary equipment.

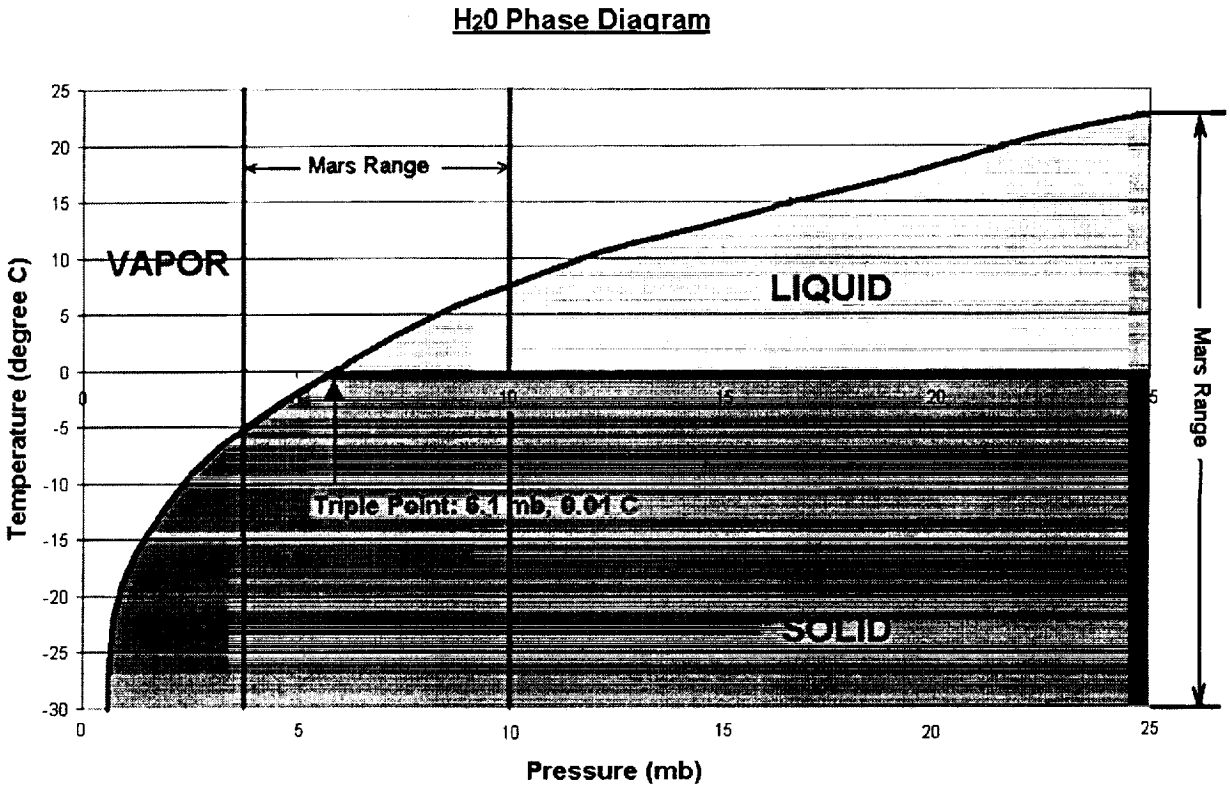

Figure 3. Triple Point Diagram. Source: handbook of Chemistry and Physics

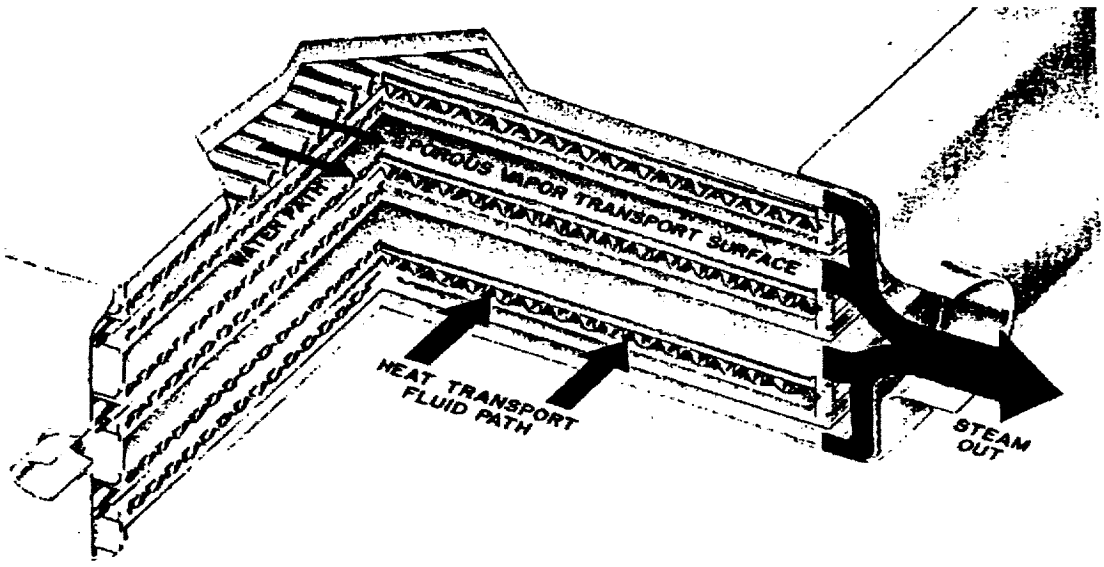

Figure 4. Porous Plate Sublimator Cross-Section Source: Hamilton Standard, Division of United Technologies

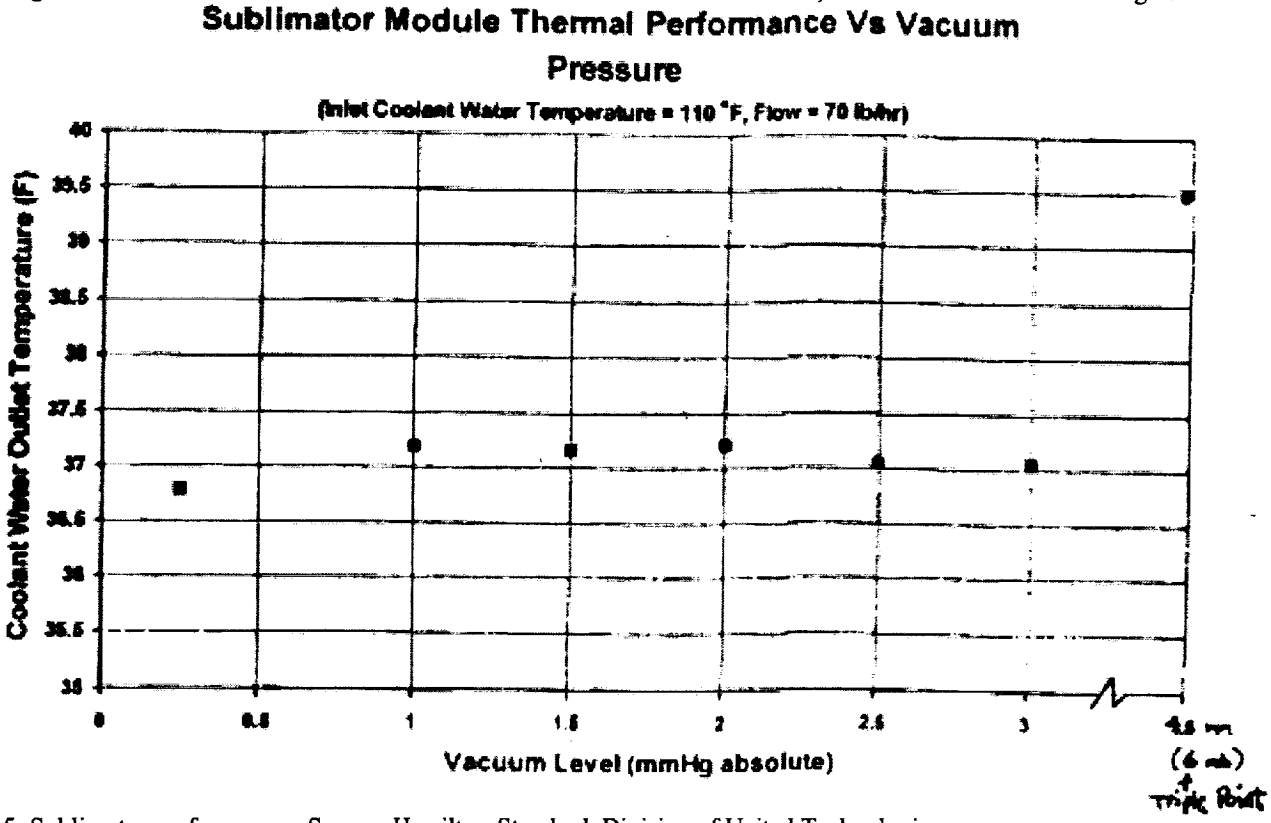

5. Sublimator performance. Source: Hamilton Standard, Division of United Technologies

The system functions as follows:

An ice layer forms within the porous plate when the feedwater tank directs water to it because it is exposed to ambient vacuum. As long as heat is not supplied to it, this ice layer stays intact. However, when the suit ventilation and liquid cooled garment loops enter the sublimator carrying body and equipment heat (Figure 4), the ice layer sublimates to steam in direct proportion to the amount of heat being carried in. The feedwater tank resupplies water to the sublimator plate in proportion to heat loss, until its eight-pound supply is exhausted. The passage of heat from the suit, air and water loops to the sublimator takes place by conduction through aluminum heat exchanger fins integral to the design. As a consequence of this design, ambient pressures rising above the triple point will cause the ice layer on the plate to melt when heated. If this happens, unlike traditional water boilers or evaporators that continue to operate at low pressures, the unit will experience "breakthrough" and stop functioning. Such functional degradation is rapid and marked and has been observed in suit testing within vacuum chambers. Test data has established that this process occurs at pressures above 3.5mb with Mars-like temperatures (Figure 5).

The implication is inescapable. If sublimation is indeed replaced by evaporation at Martian pressures in a vacuum chamber on Earth, evaporation from a liquid phase must occur on Mars as well. It must be added, however, that since the sublimator tests described here were for EMU performance, not Mars simulation, this evidence for liquid water is circumstantial.

3.0 Experimental Evidence

Protocol:

Simulating Martian conditions in a bell jar was the objective of the experimental phase of this study. An ice cube in a glass funnel placed inside a bell jar containing Drierite (a desiccant), calibrated thermometers, and dry ice (to create a CO_2 atmosphere) was kept under Martian pressures by a vacuum pump. A lamp placed over the bell jar simulated Martian sunlight (38% of Earth) and time, temperature and pressure readings were recorded (Figure 6). The end point for each run was defined as the first appearance of a water droplet or film.

Results:

Over 80 runs were made, 23 using tap water and the remainder using distilled water, diluted sea water, bacterial culture media and other mixtures. Typical results are shown for tap water in Figures 7-9 and are summarized as follows:

As seen in figure 7, with mean atmospheric temperature of 26...C liquid water was observed at pressures between 12 mb and 16 mb. These runs, taken at higher pressures than Martian conditions, demonstrated that the sublimation process is total-pressure-driven and not driven by the partial pressure of water vapor, since the latter was below the triple point.

At a mean ice temperature of 0...C as seen in figure 8, liquid water was observed at pressures between 3 mb and 10 mb, Mars like conditions. This data demonstrates that liquid water can exist under these simulated Martian conditions.

Figure 9 shows transient results for a typical run. At the beginning of the experiment, the ice cube is frosted over, yielding no liquid water even when touched by a warm body. Half way through the experiment, temperatures have grown significantly and the pressure has dropped. It is at this time that micro-ice crystals and vapor films are observed on the sides of the funnel. The ice cube has also changed appearance, changing its white exterior for a glossy one. Towards the end of the experiment, white and frozen films are seen, suggesting concurrent sublimation at low pressures.

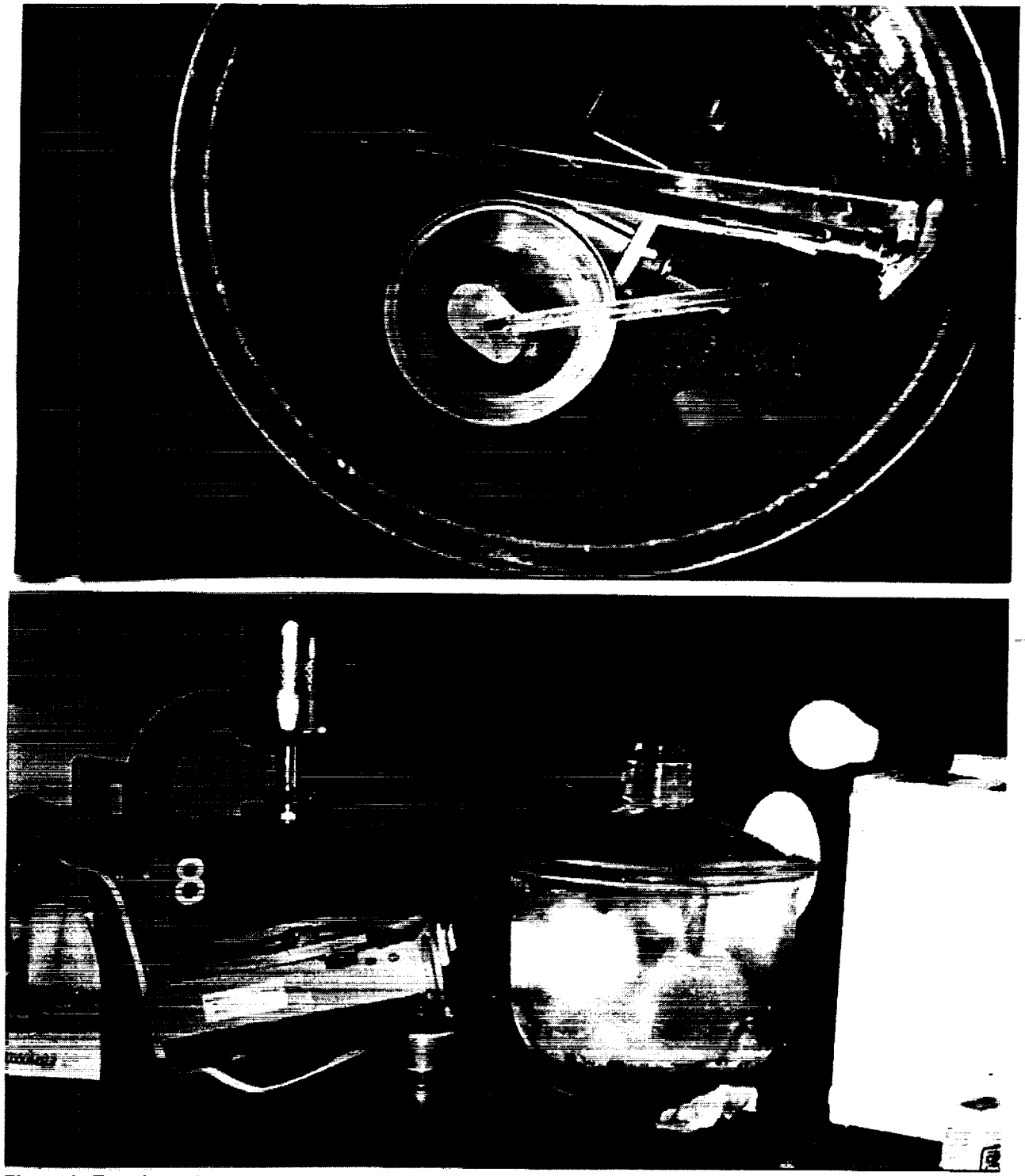

Figure 6. Experimental setup

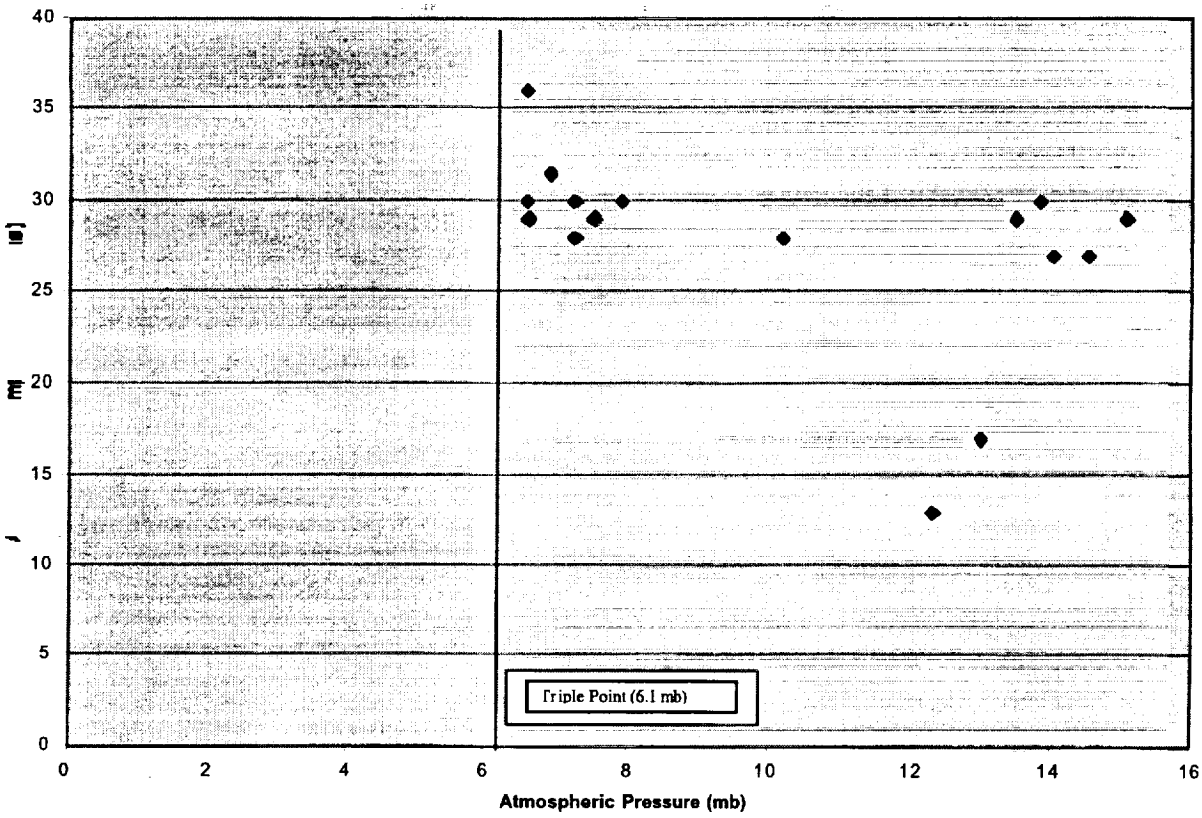

Figure 7. Atmospheric temperature vs. pressure endpoints

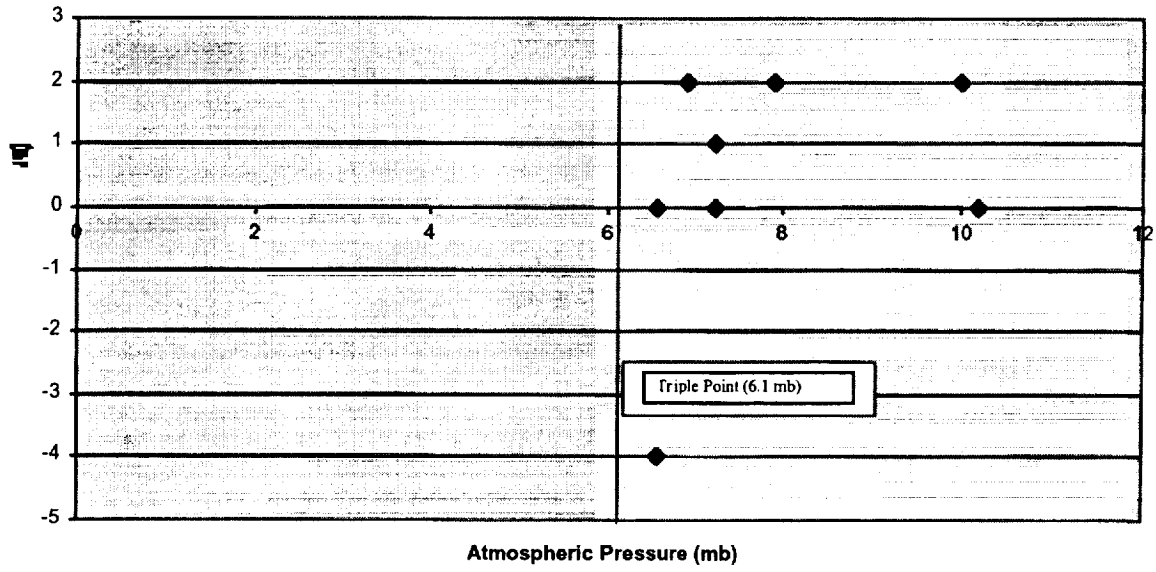

Figure 8. Ice cube temperature vs. pressure endpoints

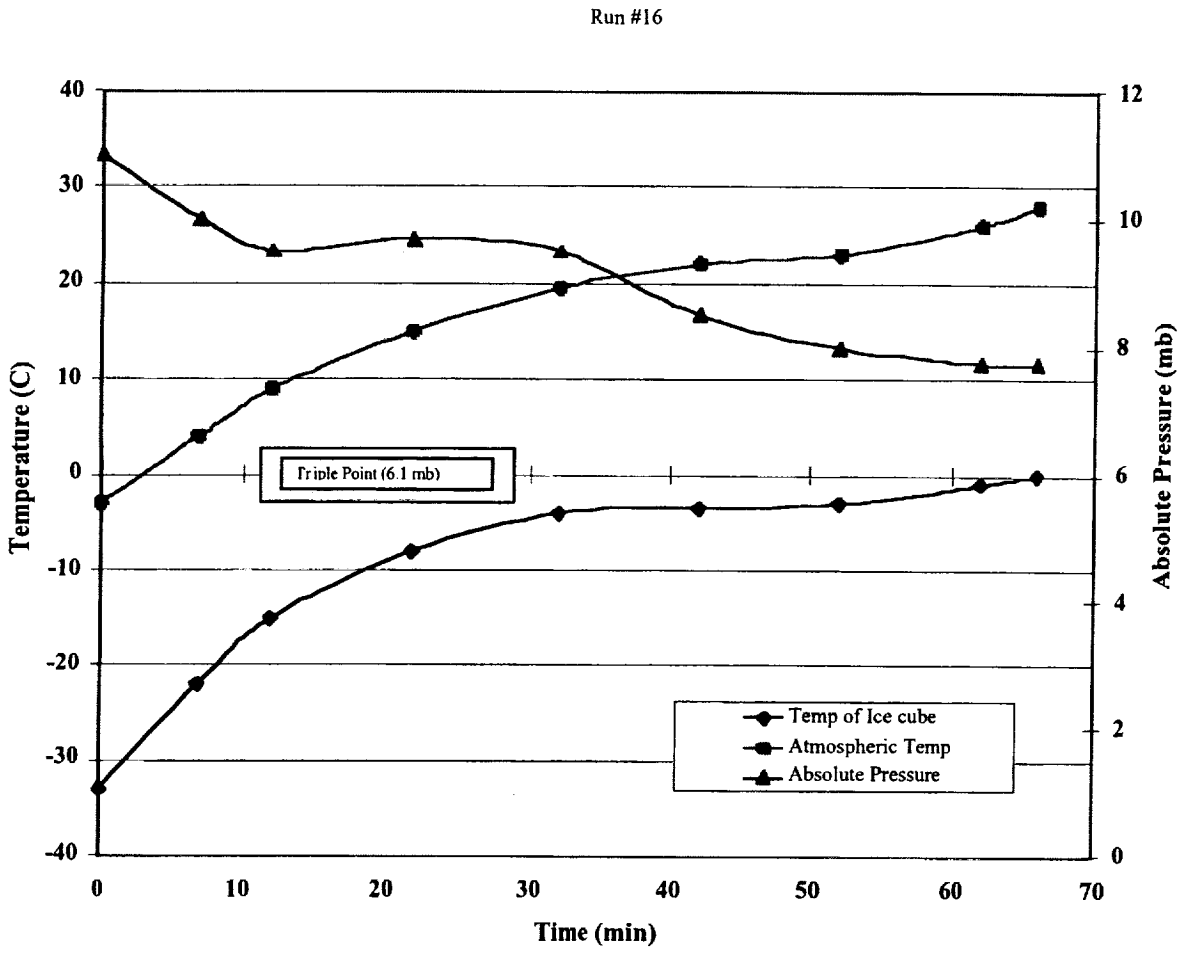

Figure 9. Transient temperature and pressure graph

Discussion and Errors:

The protocol had certain inherent errors. First, observations were subjectively based on the eyes of the observer. To counter this, a team of observers was utilized, as well as photographs and videotape recordings. Secondly, the atmosphere provided was pure CO_2, not the exact mix of the Martian atmosphere specified by Table 1. However, since 95% of the atmosphere is CO_2 and the remaining 5% is either inert or trace gases, this is a reasonable approximation. Thirdly, although Drierite, a desiccant, was used to keep the bell jar free of water vapor, humidity sensors were not available to test exactly how dry. The Drierite, on the other hand, contained an indicator that would change color when exposed to persistent water vapor. Since it never did, we can reasonably assume water vapor quantities were extremely low. Fourthly, the dual thermometers used to measure air and ice cube temperatures recorded different data depending on the placement within the ice cube and air stream. This was likely caused by radiant heating of the thermometer bulbs by the sun lamps. As such, actual atmospheric temperatures were likely lower than the sensed air temperatures, an error having little effect on the final results because temperatures were within the Martian range, as shown in figure 1b. Lastly, ice was seen to swivel on its own, suggesting the presence of a liquid film, when a visual confirmation of liquid could not be made.

Conclusions:

The purpose of the bell jar experiment was to determine the feasibility of liquid water under Martian conditions. This condition was met. Additionally, we can conclude that total pressure drives the phase change of water, not the partial pressure of water vapor in the atmosphere.

4.0 Implications

Implications for Geology:

McKay et al[4] have assumed the absence of liquid water as a significant geologic force for billions of years (Figure 10). If it can be shown that water persists in liquid form today, it would shift the timeline and paradigm of the forces that shaped the planet.

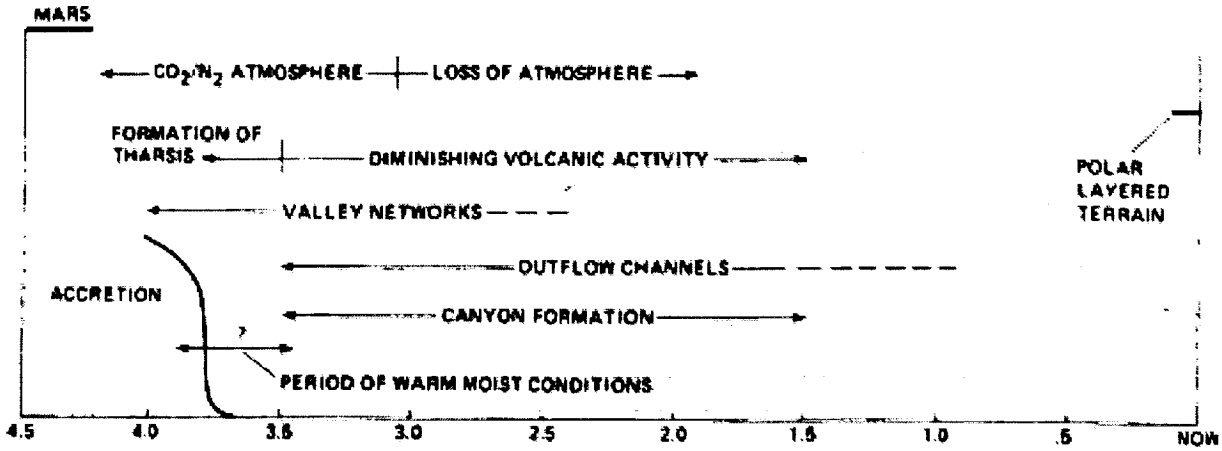

Figure 10. Geologic history of Mars. McKay and Stoker (ref. 4)

Implications of Life:

The viability of liquid water on the Martian surface may provide an environment for fringe organisms that live in conditions far more extreme than a temporary film of cold water. If extremophiles can be found living in ice 2.3 miles below the frozen surface of Lake Vostok in Antartica[5], why not Archea, Eubacteria, or Protista on Mars? Sites that demonstrate the possibility of liquid water may likely be temperate enough to sustain such life today.

Figure 11. Extremophiles found in Antartica. (ref. 5)

Implications for Landing Site Selection:

If liquid water were on the surface today, it would not only shift the paradigm of how geologic forces shaped the planet, but effect human mission planners who assume its absence. On-site water would provide resources for drinking, oxygen, and hygiene, saving the cost of shipping it from Earth or making it on the surface. Decreased mass, complexity and power requirements would decrease costs, possibly even making the difference between an affordable or extravagant mission. The question then becomes how best to locate water, and after having done so, how to let it influence landing site selection. One way of doing this is by using theoretical models such as Haberle s[6]. Another is by utilizing Mars Global Surveyor mapping data.

Global Surveyor Mapping Data.

The presence of liquid water on the Martian surface would greatly impact human landing site selection, and we have presented evidence for it under simulated Mars conditions. The next phase of this study will evaluate the feasibility of these conditions on the planet itself and map the locations where they might occur. Haberle s theoretical model provides one method of doing this and another is the utilization of mapping data from Mars Global Surveyor.

MGS, currently in orbit, records pressures and temperatures using radio occultation. Microwave radiation is transmitted by the spacecraft into the Martian atmosphere and received at tracking stations on Earth. Analyzing the phase shift of these waves provides data for specific longitudes, latitudes and time of day. Table 2 shows MGS pressure and temperature profiles for a site in Hellas Crater collected this way. Although the data suggests a liquid phase cannot exist, trend analysis may show otherwise. It s important to note that temperature and pressure increase as one nears the surface from higher elevations (Figure 9), and that the vertical resolution of the MGS oscillator can only approximate abrupt topographical surface changes.

Indeed, "sounding" the atmosphere within a canyon is possible in only rare cases[7] and radio occultation may prove over-generalized for deep and chaotic surfaces like Hebbes and Ophir Chasma. If so, another way of determining conditions in these sites would be to extrapolate surface data to lower depths using theoretical models, pressure decay curves, and other techniques. This approach, using figure 9 for pressure augmentation and the Monte Carlo radiant interchange analysis of spherical cavities for temperature is one we hope to utilize in the future. This analysis may reveal higher probabilities for liquid surface water than expected from current MGS data. For example, if the pressure was only a scant 15mb instead of 10mb at the bottom of Vallis Marinaris, the probability of liquid water would nearly triple and the span between freezing and boiling would nearly double (see cross-hatched region of Figure 12).

Martian Weather Observation

http://www-star.stanford.edu/projects/mgs/sun/

Martian Weather Observation

This martian weather observation is brought to you courtesy of the MGS Radio Science Team. The time of the atmospheric measurement and the local time of the measurement on Mars are specified on a 24 hour clock. The elevation is with respect to a standard martian reference surface (geoid). The typical atmospheric pressure on the surface of the Earth is approximately 1000 millibars (1 bar).

Date of Measurement	04-02-1998
Time of Measurement	09:51 GMT
Local Time on Mars	18:38
Latitude	33.5 degrees S
Longitude	63.2 degrees E
Elevation	-7137 meters
Surface Temperature	2.0 Fahrenheit
	-16.7 Celsius
Surface Pressure	9.94 millibars
Martian Season	Middle Summer

Table 2. MGS Observation Data Source: MGS Website

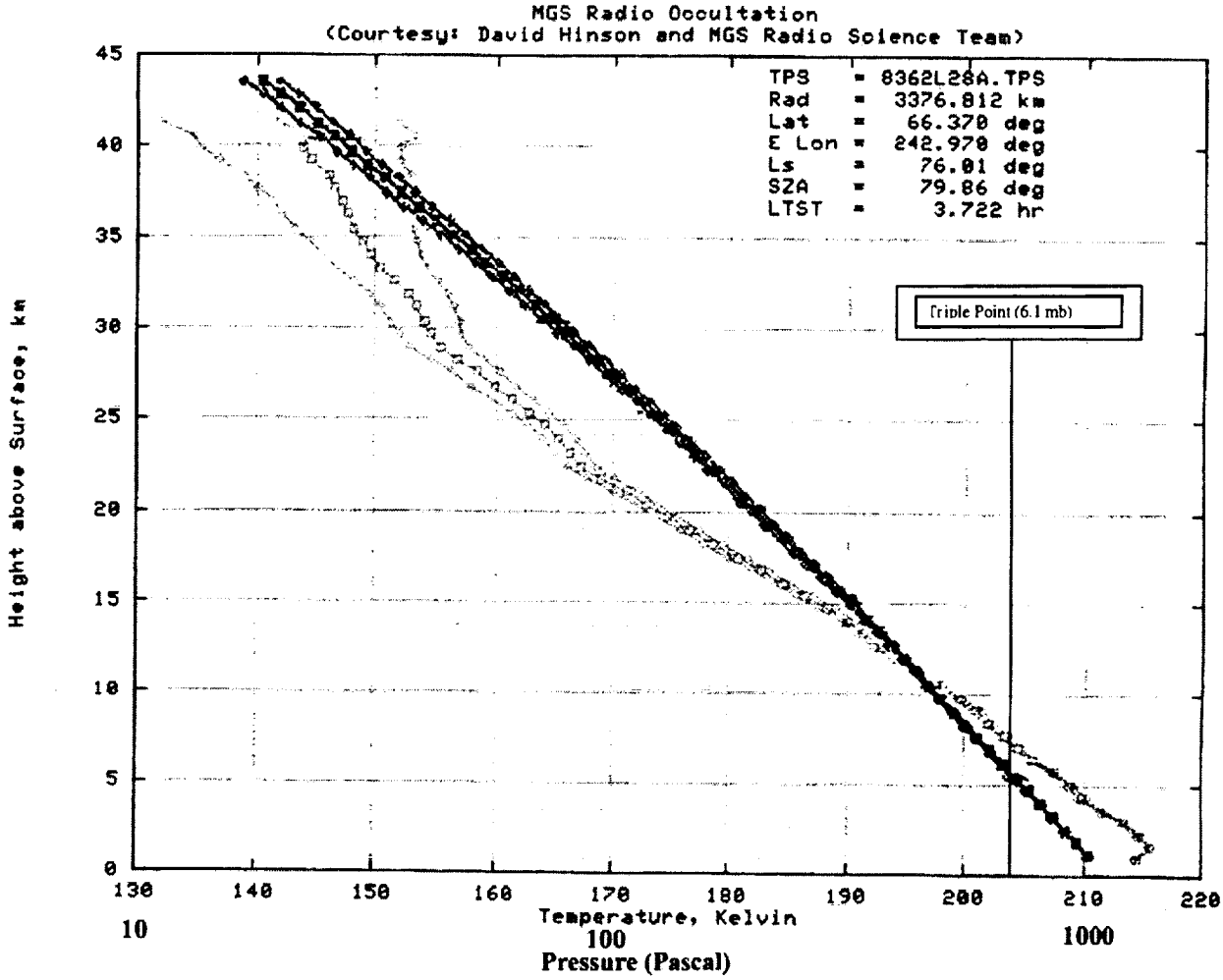

Figure 12. Altitude vs. Temperature/Pressure (MGS) Source: MGS Website

5.0 Summary and Future Work

By examining Viking, Pathfinder, and MGS data, theoretical considerations, and a simulation experiment, we have set down the conditions under which liquid water can exist on the surface of Mars today and found clear indications that it does. Since liquid water is a deciding factor on where to send human missions, it would also influence landing site selection. Two approaches to finding such sites have been discussed: the theoretical approach of Haberle at NASA Ames and the use of MGS data to extrapolate desirable sub-datum level landing sites.

The experimental protocol described was only used for pure liquid water. Future work involves testing water in soil under Martian conditions, a study currently underway by Quinn et al at NASA Ames, and a study incorporating microbial life in simulated Mars soil samples, which we hope to perform shortly. If these tests yield positive results, they could form the basis of a Pathfinder-like proposal to search for liquid water and surface microbes on Mars itself.

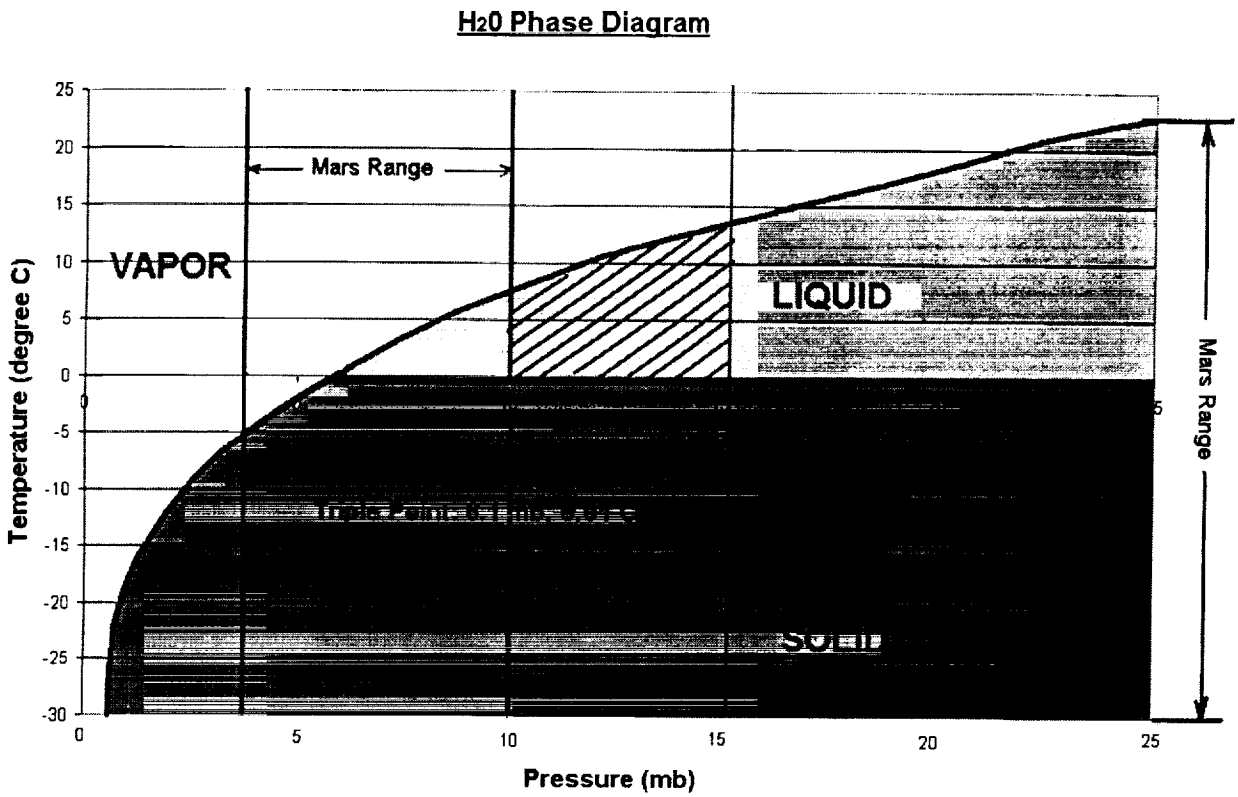

Figure 10. Triple Point diagram showing range for liquid water at 15mb

Acknowledgements

Our thanks to Professor Richard Muller and Professor Ron Shen of the UC Berkeley Physics Department for their advice, Dr. Daniel Mills, Microbial Diseases Section of the California State Department of Health Services, Berkeley for material support and calibration of our thermometer and Mr. Don Stiver for technical support.

References

Kuznetz, L and Gan, D (1999). Hunt for Liquid Water on Mars Today. Mars Society Proceedings, May 1999, Boulder, CO.

Rodriguez-Navarro, Carlos (1998), Evidence of Honeycomb Weathering on Mars .

[1] NASA Advanced Environmental Protective System Study (AEPS), NASA Ames Res. Center, Advanced EVA Branch, 1982

[2] Kaplan. "Environment of Mars". NASA-TM-100470 (1988)

[3] Haberle, et al. (2000). "Meteorological Control on the Formation of Martian Paleolakes". Abstract in the proceedings of the 33rd Lunar and Planetary Science Conference, Houston, TX.

[4] McKay, C. P and Stoker, C. R. "The Early Environment and Its Evolution on Mars: Implications for Life" in Reviews for Geophysics, 27, 2/May 1989, p. 189-214.

[5] Science, (Priscu and Karl, Dec. 10, 1999)

[6] Haberle et al. (2000). "On the Stability of liquid water on Present Day Mars". Abstract in proceedings of the First Astrobiology Conference, NASA Ames Research Center

[7] Conversation with David Hillman at Stanford University.

Studies in Closed Ecological Systems: Biosphere in a Bottle

Authors: Ben Armentrout[1] and Heidi Kappes[2]

Research Team: Ben Armentrout[1], Heidi Kappes[2], Kimberly Genther[3], Rosa Kim[4], Hilary Mathis[6], Matt Morasch[1], Brian Riley[5], Victoria Stone[3]

University of Washington, Seattle, WA: [1]Department of Biology, [2]Department of Botany, [3]School of Fisheries, [4]Department of Chemistry, [5]Department of Biochemistry, [6]Department of Astronomy

Faculty Advisor: Dr. Frieda Taub, University of Washington, School of Fisheries

Abstract

Small closed ecological chambers are an efficient model for developing principles of bioregenerative systems. Knowing these principles can enhance long distance space travel and remote human habitation. Closed systems were constructed in the laboratory using tissue culture flasks and one-liter glass bottles. All nutrients, micro algae and aquatic macro-invertebrates were added approximately one week before sealing. Viability of the closed system was judged by continued survival and activity of macro-invertebrates. Teams studied varying light intensity, nutrient concentration, temperature and varying air space. We found that *Tigriopus californicus* (a salt water copepod detritus feeder) populations maintained a steady abundance at high intensity light, increased quickly at moderate light and declined quickly at low light. *Daphnia magna* (a fresh water zooplankton) population increased more rapidly at high temperature. Within the levels of nutrient concentration we tested, *T. californicus* population growth increased with more algal nutrients. While trying to test the relationship between air space and viability, we observed that when refuges were present for algae and macro-invertebrates, populations outlived those without refuge space. Studies are continuing.

Introduction

Attempting to reconstruct nature in a bottle appears to be a formidable task. Nature is very complex with organisms at all levels, from macro to micro, interacting with each other and changing abiotic factors. However, developing closed environments will benefit our studies of life and the universe. Small materially closed microcosms have been studied since the late 1960's (Folsome, 1986). Since then several books, journal articles and PhD dissertations have been published about closed microcosms. We have taken a small piece of nature to produce a small, simple closed systems to test the systems responses and tolerance to varying initial conditions (nutrient, air:water volumes) and energy inputs. For the purpose of this study, we define

a successful ecosystem as one in which all the macro-zooplankton populations persist. The survival of the organisms serves as a biomarker that oxygen is available and chemical conditions do not exceed their tolerance.

The Earth's biosphere is made up of interacting ecosystems, each characterized by abiotic and biotic factors. Abiotic factors, such as temperature and light, influence the distribution of biotic factors and may in turn influence the abiotic factors of other ecosystems. For example, local wind and water currents can eventually influence global atmospheric and oceanic circulation patterns. It is difficult to predict what constraint may limit the growth of organisms, or cause a decline in population. It is even harder to determine which species will dominate due to the availability of certain resources.

The four most important chemical elements for living organisms are hydrogen, oxygen, carbon and nitrogen (Adey and Loveland 1998). Many other elements are necessary for sustained life, but in much smaller quantities. Life is constrained when any needed element is in short supply. Alternately, a needed element may be abundant, but in an unusable form. Free nitrogen (N_2) is plentiful in the atmosphere, but is often a limiting factor for plant growth in the absence of nitrogen fixing bacteria such as Cyanobacteria. Also, a needed element may be missing entirely in a particular ecosystem, but its absence overlooked for some time, because it is needed in such small quantities.

Some ecosystems on earth seem to have obvious abiotic constraints. In the Gobi Desert, we expect water to be the primary constraint on biomass growth. Other ecosystems have constraints that are not as obvious. This is the case in the equatorial Pacific, which is a barren ocean that blooms profusely when iron levels in an available form are boosted by only a few parts per billion (Martin et. al. 1994; Rue & Bruland, 1997). Subtle constraints may lead to problems that appear to be caused by more obvious constraints. For example a lack of magnesium would inhibit photosynthesis and may lead to a lack of O_2; the lack of O_2 may appear to be the primary constraint when in fact it is secondary.

Density dependent growth refers to the constraints that are put on a population as it expands relative to its ecosystem. If it grows too quickly, the population can

deplete the necessary nutrients it needs to grow and survive. The rapid increase may be followed by death of part or all of the population. In a closed system, the growth of the population must be controlled so that production of nutrients can keep up with the growing population's increasing demand. There are several ways to do this in a small system. Temperature is one way. Low temperature slows the metabolism of many animals. With a slowed metabolism, the animal will eat less, thus grow and reproduce less. Temperature is not as much of a restraining factor for plants. If plants are able to grow and reproduce at a normal level, both the food for the animals and the available O_2 will increase, hopefully at a rate equal to that of the consumption by the animal.

In an open ecosystem, organisms can migrate between ecosystems. Plant seeds / spores may be dispersed far from the parent plant by animals, ocean currents or wind. Both biotic and abiotic factors can buffer the ecosystem from some extremes by migrating to neighboring ecosystems in this way. On Earth, with its complex ecosystem and diverse terrain, it is often possible to compensate for material deficiency at one locale, simply by moving to a new one. For example, humans may have populated North America as hunters following one of their constraints, large herd animals, across the Bering land bridge. Also, O_2 and CO_2 can diffuse between the air and the aquatic community compensating for imbalances.

In a closed system, nutrients may be limited because they are not cycled through the system fast enough and/or it is not possible to compensate for deficiencies by migration. In closed ecosystems, outside influences are eliminated. Therefore closed ecosystems test the adequacy of the initial organism and nutrient supply. The challenge in finding appropriate initial conditions and radiant energy inputs for a closed system lies in the constraints of these factors. Once the system is sealed, we can observe the interplay of the organisms.

We have defined the success of our model ecosystems as the persistence of macro-invertebrate populations. There may be several periods of population fluctuation. In some systems, an initial species of the system may be reduced or go extinct as it is followed by a subsequent species. In this way an early dominant species may be replaced by another species, previously rare, that becomes dominant. This is an example of succession. In primary succession, the initial colonizing species often

prepares a new ecosystem condition with necessary nutrients for a secondary species that will replace the primary species. A terrestrial example of this is a nitrogen fixing plant that colonizes a barren area after a major disturbance. The nitrogen fixing plant will build up the nitrogen store in the soil, providing the secondary species the necessary nutrients to populate the area, after which the secondary species may crowd out the earlier dominant species.

Balanced ecosystems do not always start out as balanced systems. Given the correct initial conditions, however, they may evolve to a balanced state. In closed ecosystems, the primary species may be an alga that grows quickly, providing an initial food source for the invertebrate while a secondary, hardier algal species accumulates. In a second example, the primary species may be an invertebrate that grows and reproduces quickly, adding to the carbon storage by molt and/or skeletons while a second, hardier but slower growing species gets started. Since there is no immigration into the system, it is difficult to find the right balance of organisms to start a system. In a closed system with sustainable population fluctuations, populations rarely grow as large as they would in an open system. The population size is dependent on the available nutrients. Thus the population is density dependent. An example of this was found in an experiment on sewage oxidation in 1959. An in vitro system was made in an attempt to mimic an oxidation pond. In the synthetic system, a succession began with a bacterial bloom, followed by an algal bloom of Chlorella, and then followed by an increase in invertebrate population. The climax was observed to be similar to the population from the original pond. One of the links that allowed this succession to take place was the excretion by the bacteria of thiamine, a vitamin necessary for growth of the strain of Chlorella (Byers & Odum 1993).

We can monitor small, closed ecosystems more fully than large open systems, because the complexity is reduced, allowing for easier measurements and experimental controls. If we can learn which initial conditions and energy inputs allow the small system to sustain macro-invertebrate populations, we can scale up these small ecosystem models to predict the requirements for sustainability in larger ecosystems.

Experimental Background

Small, simple closed microcosms are a means of monitoring short-term pressures on an ecological system. Claire Folsome (1986) pioneered work on closed ecological systems in the late 1960's, and many journal articles, books (Giesey, 1978; Byers & Odum, 1993), and PhD dissertations have followed. Despite this, small closed ecological systems are rarely used as serious research tools, but marketed to the public as curiosities. One reason for not using them for research may be expense. Biosphere II and NASA's Closed Ecological (or Engineering) Life Support Systems (CELSS) are very expensive. Small microcosms developed in tissue culture flasks are inexpensive, enabling us to study simple questions, while providing the opportunity for several replicates and controls.

There are two major controversies about small, synthesized ecosystems or microcosms. The first is that ecosystems are too complex for human synthesis. It is believed that there are too many interactions between abiotic and biotic factors for a human to produce a working ecosystem. The other controversy is that in order to control an ecosystem it must be simple - i.e. a monoculture or single species gardening approach. These two controversies need to be considered and accommodated when building a closed system that will be used to study the interaction of species in an ecosystem and to test the effects of constraints (i.e. limited nutrients, light energy or toxicity) or to allow for human habitation in barren habitats.

"The process occurring in microcosms are the same as those found in ecosystems, but they are simplified since the system is closed and isolated" (Byers & Odum, 1993). Knowing the fundamentals of closed system constraints will be necessary for human habitation of such systems in the context of space travel and colonization.

One hypothesis is that an important constraint on a closed ecological system is oxygen, since it is almost entirely biologically produced. Plants and some bacteria produce oxygen by photosynthesis. Photosynthesis is the process by which organisms use light energy to break apart water and fix carbon as glucose. The equation for photosynthesis is:

$$nCO_2 + nH_2O \rightarrow (CH_2O)n + nO_2$$

Respiration is the same process in reverse, where glucose is broken apart and combined with O_2 to get energy, CO_2 and H_2O. Especially in small systems, periods of low levels of O_2 or no O_2 can kill some organisms very quickly. There are several ways to buffer against this catastrophe. Increasing the plant population will increase the ability of the system to maintain O_2 levels. Likewise decreasing the animal's metabolism, and thus respiration, will decrease the amount of O_2 used. Adding pH buffers to the system via air space or salts in the water will protect against extreme pH changes and add a place for O_2 to be stored. Another unexplored option is to use species that are anoxia tolerant. These species can produce spores or eggs that can tolerate anoxic conditions for long periods of time, allowing the system to recharge its oxygen stores. Some species may even be active in anoxic conditions. Nematodes are an example of this.

If a crew of astronauts runs out of oxidative potential while on the long trip to Mars, they cannot stick their heads out the window to catch their breath. Once on Mars, they will continue to need oxygen. In addition to the long-term balance that must be obtained, short-term constraints must also be monitored. It does us no good to get to Mars with a full load of oxygen, if all of the Astronauts are dead from asphyxiation because six weeks into the trip an unexpected bacterial bloom used up all of the oxygen for two hours. Plants will probably produce this oxygen, but if there is a shortage of nitrogen, an element that is in short supply on Mars compared to Earth, then the plants cannot grow and will not produce oxygen. Furthermore, the nitrogen must be in a usable form, and so nitrogen-fixing bacteria may be needed. But Cyanobacteria depend on complex water chemistry, which often involves hundreds or thousands of species. It will be much easier to get a general grasp of these systems, than to engineer a complex network of dependencies from individual biochemical reactions.

We ran a series of pilot studies to investigate the range of conditions for constraints for O_2 / CO_2 equilibrium in closed aquatic systems. The biomarker we used to determine anoxia in systems was obtained by quantifying populations of macro-invertebrates determined to be tolerant of anoxic conditions for times in excess of 24 hours (fig. 6). This allowed us to experimentally examine the effects of a number of

constraints on the O_2 / CO_2 equilibrium of the enclosed system. Our experiments attempted to develop isolated ecosystems that functioned normally for reasonably extended periods under a series of pressures. "The general tactic [has been] to enclose aliquants of ecosystems; to observe how and, if possible, deduce why the systems changed or failed; to modify conditions appropriately; and to experiment again" (Macguire 1980). Any system that contains living macro-invertebrates is assumed to have not had chronic anoxia.

Approach

All systems were constructed in glass or thick plastic containers and sealed with screw caps. All water, chemicals, and algae were added two to seven days before invertebrates to allow for any unexpected organic material oxidation. Systems were sealed on the same day the macro-invertebrates were added. Unless mentioned, all systems were kept in normal room temperature (~21° C) away from direct sun light, room temperature or light controls.

The three types of micro algae used for freshwater were *Selenastrum*, *Chlamydomonas*, and *Ankistrodesmus* - all micro algae that serves as a food source for the freshwater invertebrates. The freshwater invertebrates that were used were *Daphnia magna* and / or *Ceriodaphnia*. T82, a freshwater algal media served as the source of micronutrients for the algae (table 1). Kent water (table 3) was used as the source for freshwater.

For salt water systems, the three types of micro algae used were *Nannochloropussis*, *Isochrysis*, and a green mixture - which served as a food source for the invertebrate *Tigriopis californicus*. f/2, a marine algae media served as the source of micronutrients for the algae (table 2). Filtered, UV disinfected salt water was obtained through the Seattle Aquarium.

Light Intensity Experiment: Tissue culture flasks (65 ml) were filled with 60 ml seawater, 5% f/2 media, and 0.1 ml of each salt-water micro algae (*Nannochloropussis*, *Isochrysis*, and a green mixture). Seven days after filling the flasks, 6 *Tigriopis californicus* were added to each flask and each flask was sealed. Each flask was slipped into a pocket constructed out of 50% light-blocking greenhouse shade cloth. Replicates of 3-4 were set up at four light intensities, created by putting different layers of shade cloth around each flask.

Temperature Experiment: Glass bottles (1 L) were filled with 800 ml Kent water, 200 ml T82 media, and some of each freshwater micro algae (*Ankistrodesmus* and *Scenedesmus*). Seven days after filling the flasks, 5 *Daphnia magna* were added to each bottle and the bottles were sealed. Each bottle was then placed in a water bath at varying temperatures (25° C, 15° C, and 20° C) and control bottles were placed at room

temperature (approx. 21° C). The water baths were kept at a constant temp by using an aquarium heater for heat or running cold water to cool. Fluorescent lights were mounted above systems to provide light and were on a 12 hour on / 12 hour off timer.

Nutrient Experiment: Tissue culture flasks (65 ml) were filled to the rim with varying concentrations of seawater / f/2 media (2%, 10% and 20%), and 0.1 ml of each salt water micro algae (*Nannochloropussis*, *Isochrysis*, and a green mixture). Two days after filling the flasks, 6 *Tigriopis californicus* were added to each flask and each flask was sealed.

Air Space Experiment: 65 ml tissue culture flasks were filled with 30 ml Kent water, 10 ml T82 media, and 0.1 ml of each of the freshwater micro algae (*Selenastrum*, *Ankistrodesmus*, and *Chlamydomonas*). A 48-hour toxicity test was performed to determine possible toxic effects of the styrofoam on the *Daphnia.* There were no apparent adverse effects, so the experiment set-up proceeded. Seven days after filling the flasks, 6 *Daphnia magna* and 6 *Ceriodaphnia* were added to each flask. Styrofoam was then added to each flask at varying volumes (20 ml, 10 ml, and 5 ml; measured by water displacement) to displace air in the flask. 14 ml of T82 media was then added to each flask to raise the level of liquid in the flask with the highest volume of styrofoam to the rim (to displace any remaining air) and each flask was sealed.

Salinity Experiment: Tissue culture flasks (1000 ml) were filled with varying concentrations of salt water (6.25%, 12.5%, and 25%), Kent water, and 25% T82 to which 25 ml of *Selanstrum* was added. Five days after filling, five *Daphnia magna* were added to each flask and each flask was sealed.

Results:

Tigriopis californicus populations grew at a faster rate when systems were in environments with intermediate light intensities (13.7 to 23.4 μEinsteins). At the highest light intensities the population persisted but did not increase. At the lowest light level, 7.7 μEinsteins, the poulation was low, but started increasing at day 30 and by the end of the experiment equaled the highest density. No populations went extinct during the 40-day experiment (fig 1).

T. californicus populations were the highest at the end of the 42-day experiment in flasks with intermediate (10%) concentrations of T82 algae growth media. Populations in flasks with higher concentrations had the highest daily average population throughout the course of the experiment, and had the lowest final population. No populations went extinct during the course of the experiment (fig 2).

Daphnia magna grew at the fastest rate in bottles kept at the highest temperature (25° C) and also declined the fastest. Populations kept at room temperature kept a constant population size the longest. Populations in the highest temperature (25° C) were extinct within 49 days and the populations kept at the lowest temperature (15° C) were close to extinction (fig, 3).

D. magna in flasks with no free air space declined at a faster rate, but lasted longer than those in flasks with air space (except control). All flasks went extinct by day 17, except one control flask and one flask with no air space - both that went extinct by day 20. Populations grew in all flasks, except those without free air space (fig. 4).

Conclusion:

We produced simple model systems for ecological studies by enclosing micro algae and invertebrates in closed flasks. These model systems are similar to *Arabidopsis* for botany studies, *Drosphila* for zoology studies, Zebra fish for fisheries studies, and yeast for genetics studies. Oxygen levels were monitored by observation of invertebrate populations that are sensitive to anoxia. Various constraints (light, temperature, algal nutrient concentration, salinity and air space) were placed on the systems to quantify the range of the sensitivity to these pressures.

Results showed that a difference in our variables led to different population patterns. Medium light intensities (13.7-23.4 micro Einsteins), 10% algal growth media, intermediate temperature (20-21°C), and 6.25% salinity were found to support higher populations of invertebrates than variables at other levels. The addition of seawater was to supply trace levels of elements that might be lacking in the chemically defined algal medium (T82) or the Kent water. The salt water also served to test the osmotic tolerance of the organisms.

Further experiments need to be done to assess the effects of complexity of species assemblage, complexity of environment (refuges) and anaerobic microzones.

Our studies are beginning to give us an idea of the time scale of these types of systems as well as the kinds of factors that affect their population patterns. (Our salinity experiment showed a definite effect, whereas our variation in air space did not have a conclusive effect). Our next step will be to define base systems to work with. Using

variations of these systems, we will build a mathematical model. We will continue to work with variation in air space (gas buffer), nutrient concentration, light intensity, temperature and toxicity (salinity). In addition, we plan to look at genetic variation (of a single species), size variation of the system, a harvesting situation where the system is expected to produce a needed commodity (food, O_2) and complexity of space within the closed system (refuges).

We will also develop assays for better determining the health of our systems. We will refine our understanding of the needs of our chosen indicator species (*Daphnia magna*). We will start monitoring pH and O_2 concentrations extracted from our systems. We will also attempt to analyze the long-term viability of some of our systems using energy in equals energy out model.

Ecosystems have been modeled mathematically for some time. In the best case of a simple system, the mathematics are both intricate and, over long periods, inaccurate. One aspect which all of these have in common is the input of the light and the output of heat. Since these are the only input and output in our systems, they may give us an overall view of what the system will do down the road. If input and output are not equal, then something is building up or is being depleted within the system. This will most likely lead to succession of species as conditions change. Our system model will look something like figure 7 with $E_{in} = E_{out}$ being our goal. The diagram was drawn using the system developed by Byers and Odum (1993).

References

Addey and Loveland, 1998. Dyanamic Aquaria. Academic Press.

Byers, R. J. and H. T. Odum. 1993. Ecological Microcosms. Springer-Verlag.

Folsome, C. E. and J. A. Hanson, 1986. The emergence of materially closed system ecology. p. 269-288 in Polunin, N. (ed.) Ecosystem Theory and Application. John Wiley & Sons Ltd.

Giesy, J. P. Jr. (ed.), 1978. Microcosms in Ecological Research. Technical Information Center.

Kearnes, E. A. and C. E. Folsome, 1981. Measurement of biological activity in materially closed microbial ecosystems. Biosystems. 14: 205-209.

Maguire, Bassett Jr. 1978. Some Patterns in post-closure ecosystem dynamics (failure) p. 319-332 in Giesy, J. P. Jr. (ed.) Microcosms in Ecological Research. Technical Information Center.

Martin, J.H. and others, 1994. Testing the iron hypothesis in ecosystems of the equatorial Pacific Ocean. Nature. 371: 123-129.

McLachlan, J. 1973. p. 42-45 in Stein, J. R. (ed.) Handbook of Phycological Methods: Culture Methods and Growth Measurements. Cambridge University Press.

Rue, E. L. and K. W. Bruland, 1997. The role of organic complexation on ambient iron chemistry in the equatorial Pacific Ocean and the response of a mesocale iron addition experiement. Liminology and Oceanography. 42(5): 901-910.

Stum, W. and J.J. Morgan, 1996. Aquatic Chemistry. J. Wiley & Sons, Inc.

Taub, F. B. 1993. Standardizing an aquatic microcosm test. p. 159-188 in Soares, A. and P. Calow. (eds) Progress in Standardization of Aquatic Toxicity Tests. Pergamon Press.

Table 1

Freshwater Algal Media (T82)	**(Taub, 1993)**	
Compound	Element	
$NaNO_3$	N	7.0 mg/L
$MgSO_4 \bullet 7H_20$	Mg	2.43 mg/L
KH_2PO_4	P	1.23 mg/L
NaOH	Na	2.27 mg/L
$CaCl_2 \bullet 2H_20$	Ca	40.0 mg/L
NaCl	Na	34.5 mg/L
$Al_2(SO_4)_3 \bullet 18H_20$	Al	0.26 mg/L
$Na_2SiO_3 \bullet 9H_20$	Na	36.8 mg/L
	Si	22.4 mg/L
$FeSO_4 \bullet 7H_20$	Fe	0.0625 mg/L
EDTA	EDTA	0.4145 mg/L
H_3BO_3	B	0.008 mg/L
$ZnSO_4 \bullet 7H_20$	Zn	0.0015 mg/L
$MnCl_2 \bullet 4H_20$	Mn	0.0135 mg/L
$Na2MoO_4 \bullet 5H_20$	Mo	0.0024 mg/L
$CuSO_4 \bullet 5H_20$	Cu	0.00032 mg/L
$Co(NO_30_2 \bullet 6H_20$	Co	0.00015 mg/L

Table 2

Salt Water Algal Medium (f/2)	**(McLachlin, 1973)**
$NaNO_3$	0.075 g/L
$NaH_2PO_4 \bullet H_20$	0.005 g/L
$CuSO_4 \bullet 5H_20$	0.25 ml/L
$ZnSO_4 \bullet 7H_20$	0.25 ml/L
$CoCl_2 \bullet 6H_20$	0.25 ml/L
$MnCl_2 \bullet 4H_20$	0.25 ml/L
$Na_2MoO_4 \bullet 2H_20$	0.25 ml/L
O3 Stock A	0.76 ml/L
f/2 vitamins	0.5 ml/L
TRIS	5.0 ml/L

Table 3

Kent Water	**(Kent Marine, Marietta, GA)**
A combination of carbonates, sulfates and chlorides of sodium, magnesium, calcium and potassium with all necessary minor and trace metals necessary for cichlid fish. Contains no phosphates, nitrates or organics.	

Figure 1:

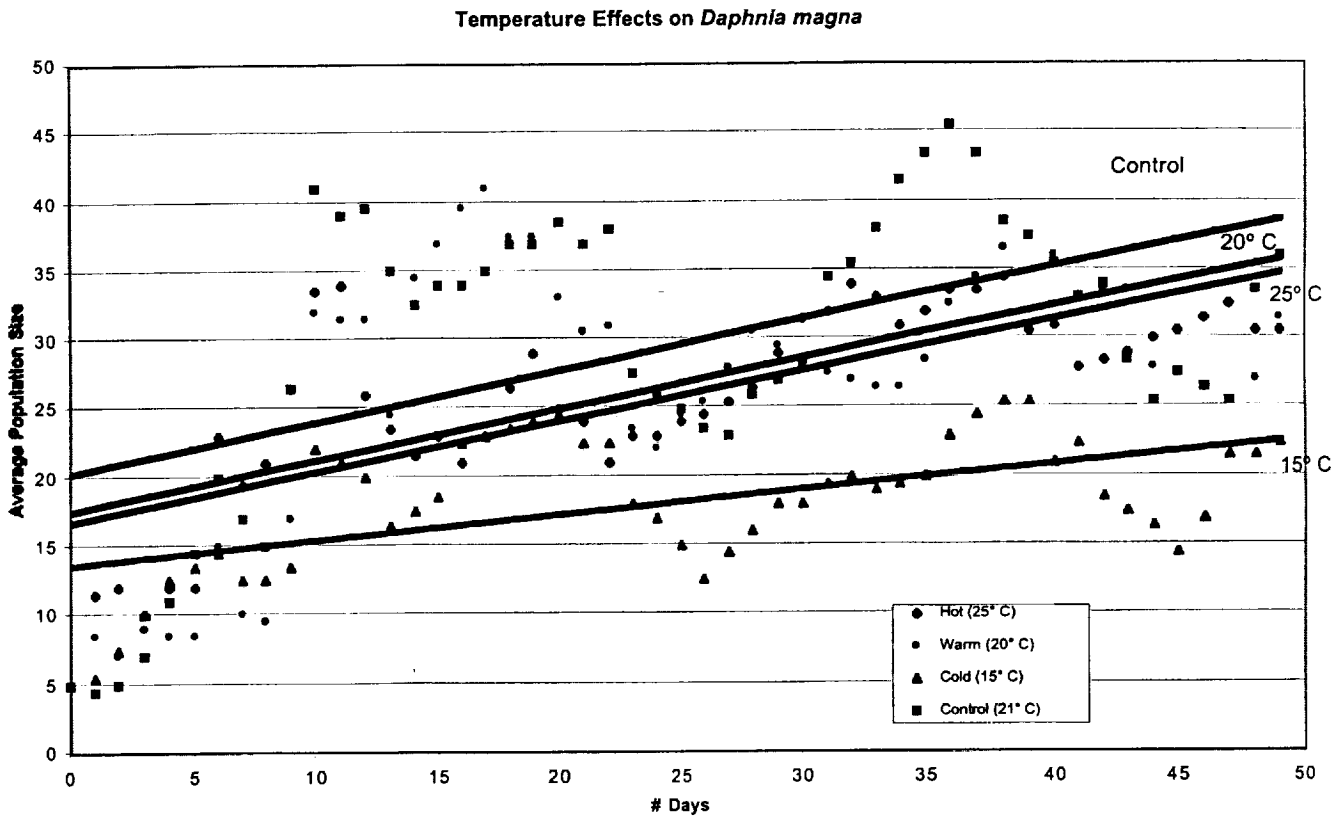
Temperature Effects on *Daphnia magna*
Average Population Size
Days
Control
20° C
25° C
15° C
Hot (25° C)
Warm (20° C)
Cold (15° C)
Control (21° C)
0
5
10
15
20
25
30
35
40
45
50

Figure 2:

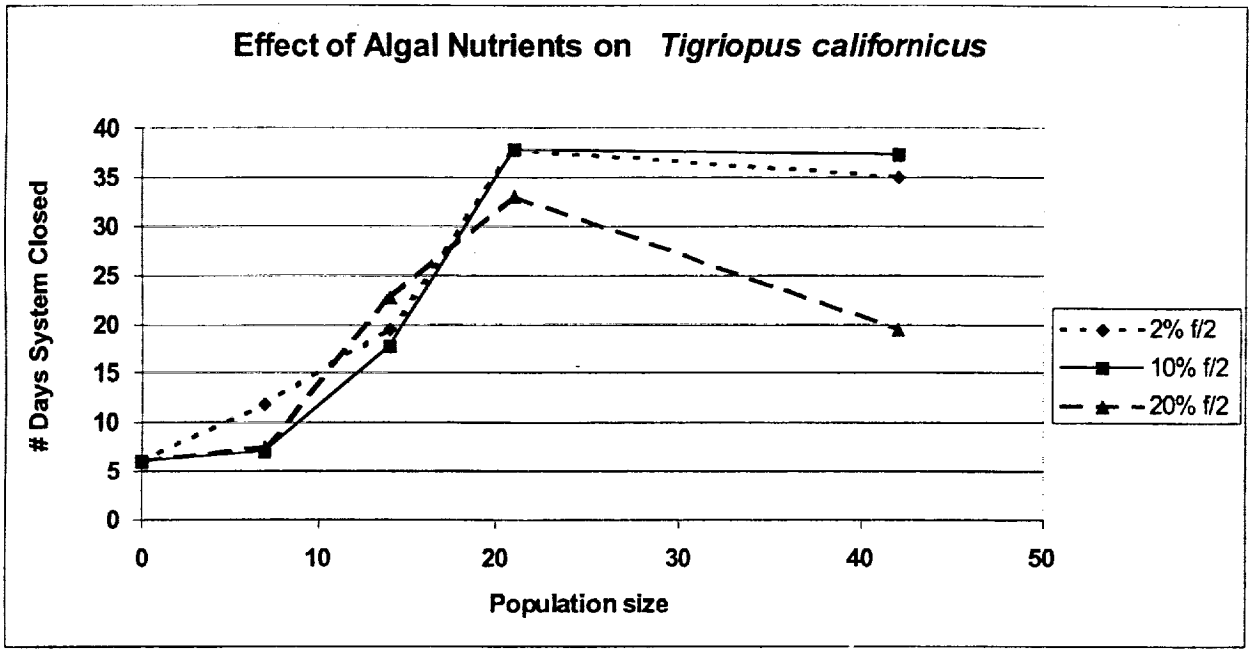
Effect of Algal Nutrients on *Tigriopus californicus*
Days System Closed
40
35
30
25
20
15
10
5
0
0
10
20
30
40
50
Population size
2% f/2
10% f/2
20% f/2

Figure 3:

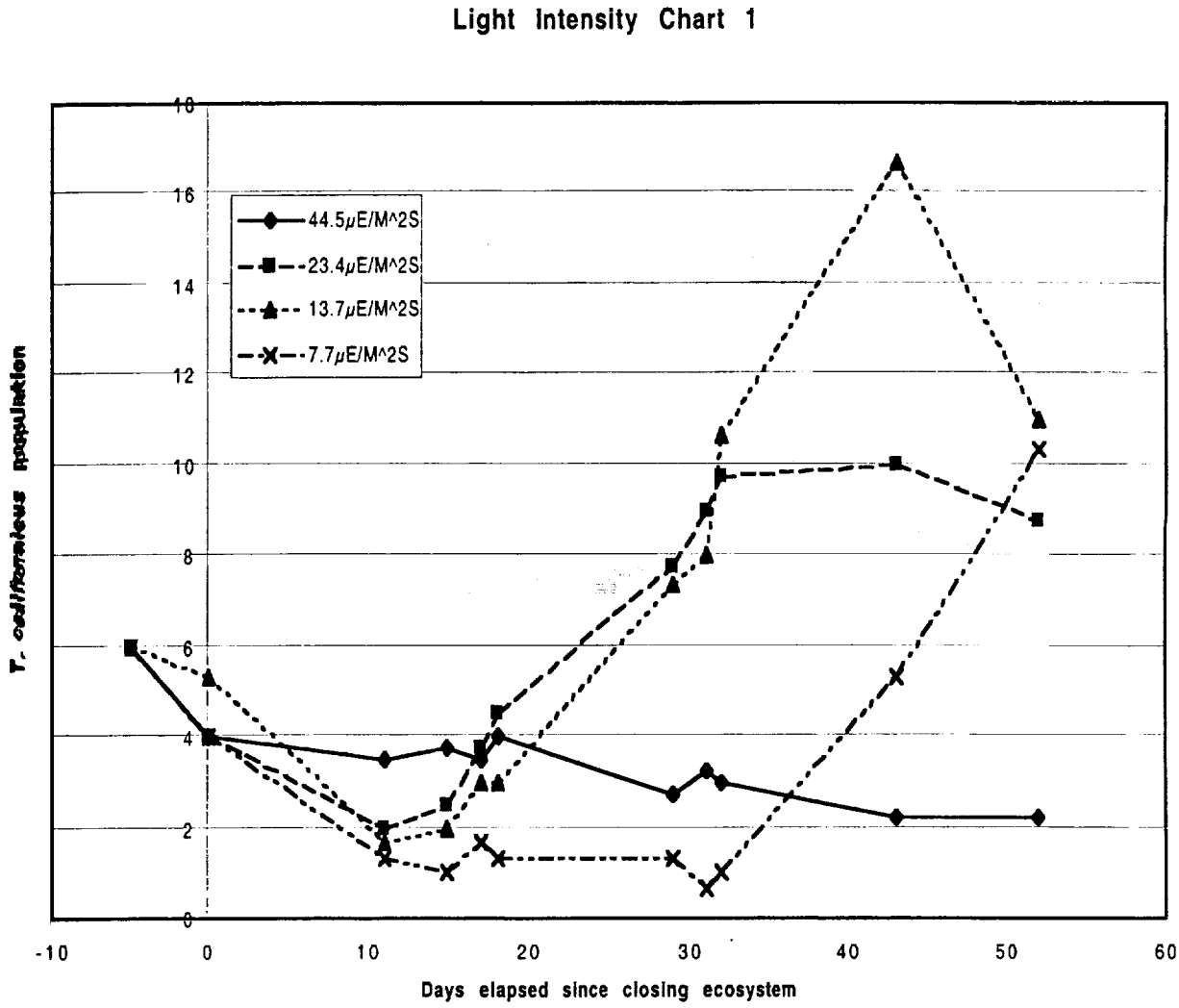
Light Intensity Chart 1
44.5μE/M^2S
23.4μE/M^2S
13.7μE/M^2S
7.7μE/M^2S
T. californicus population
Days elapsed since closing ecosystem
-10
0
10
20
30
40
50
60
0
2
4
6
8
10
12
14
16
18

Figure 4:

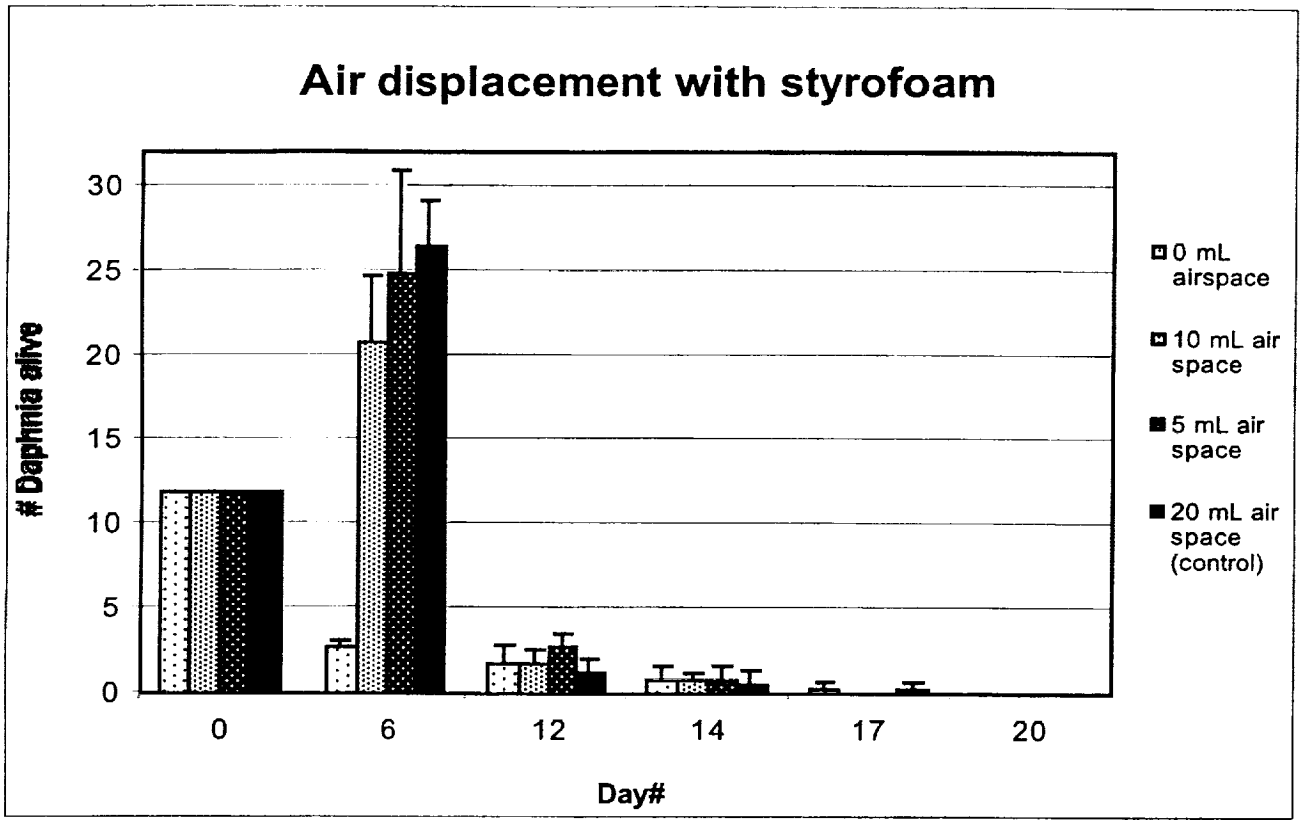
Air displacement with styrofoam
Daphnia alive
30
25
20
15
10
5
0
0
6
12
14
17
20
Day#
0 mL airspace
10 mL air space
5 mL air space
20 mL air space (control)

Figure 5:

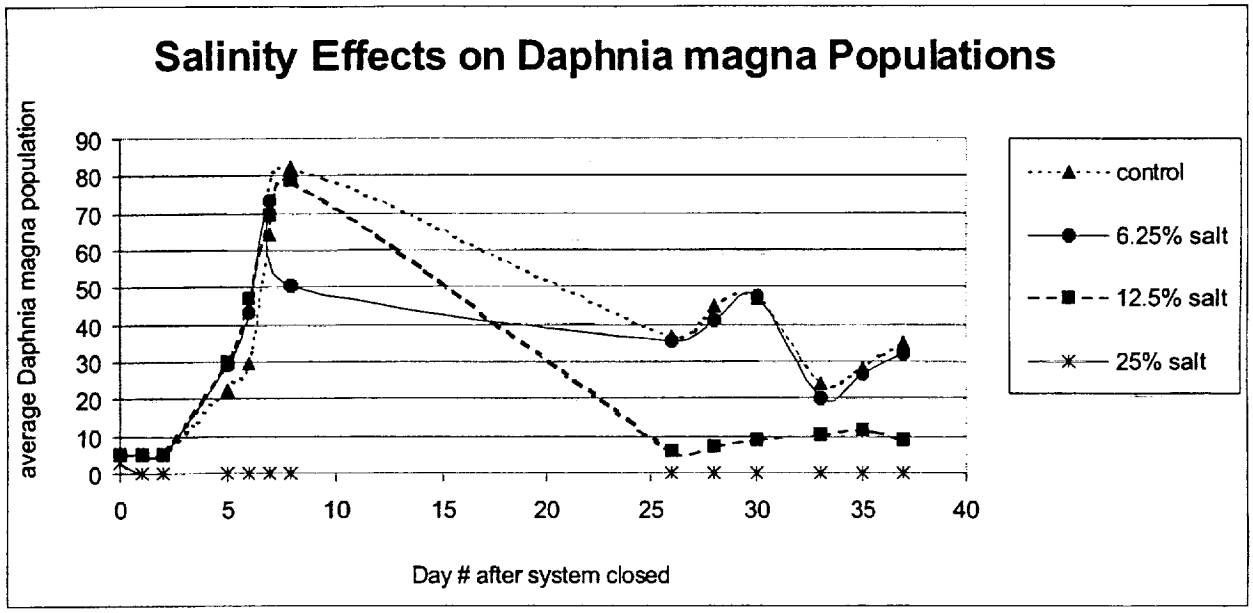
Salinity Effects on Daphnia magna Populations
average Daphnia magna population
90
80
70
60
50
40
30
20
10
0
0
5
10
15
20
25
30
35
40
Day # after system closed
control
6.25% salt
12.5% salt
25% salt

Figure 6:

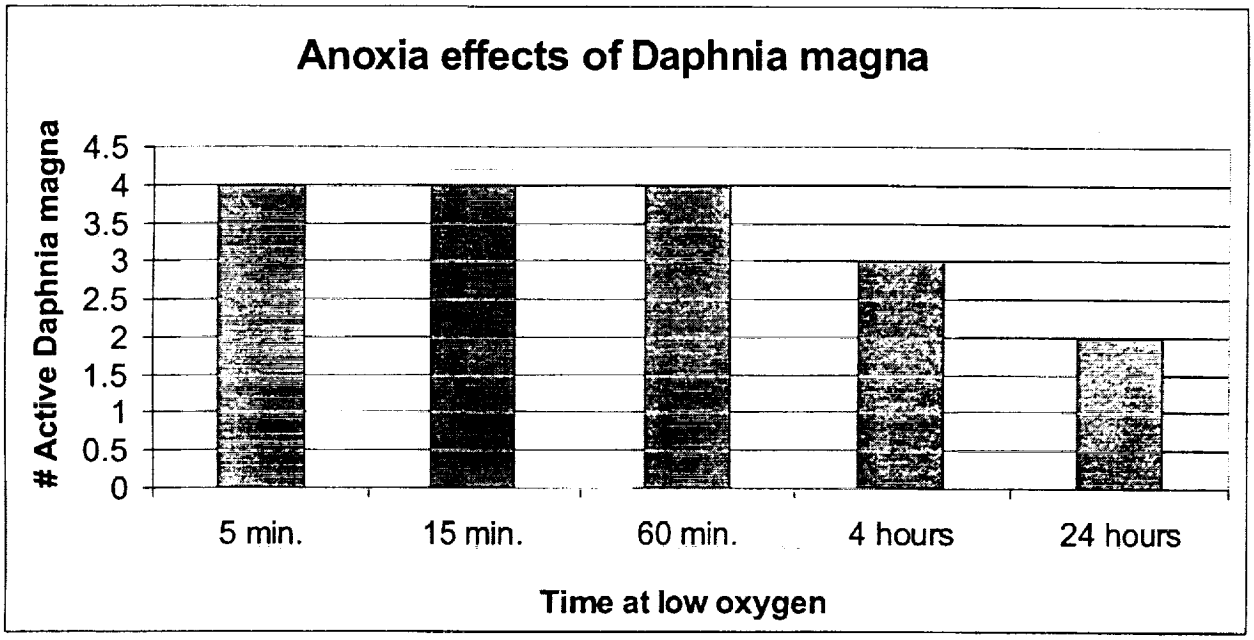
Anoxia effects of Daphnia magna
Active Daphnia magna
4.5
4
3.5
3
2.5
2
1.5
1
0.5
0
5 min.
15 min.
60 min.
4 hours
24 hours
Time at low oxygen

Figure 7: Energy Flow Diagram

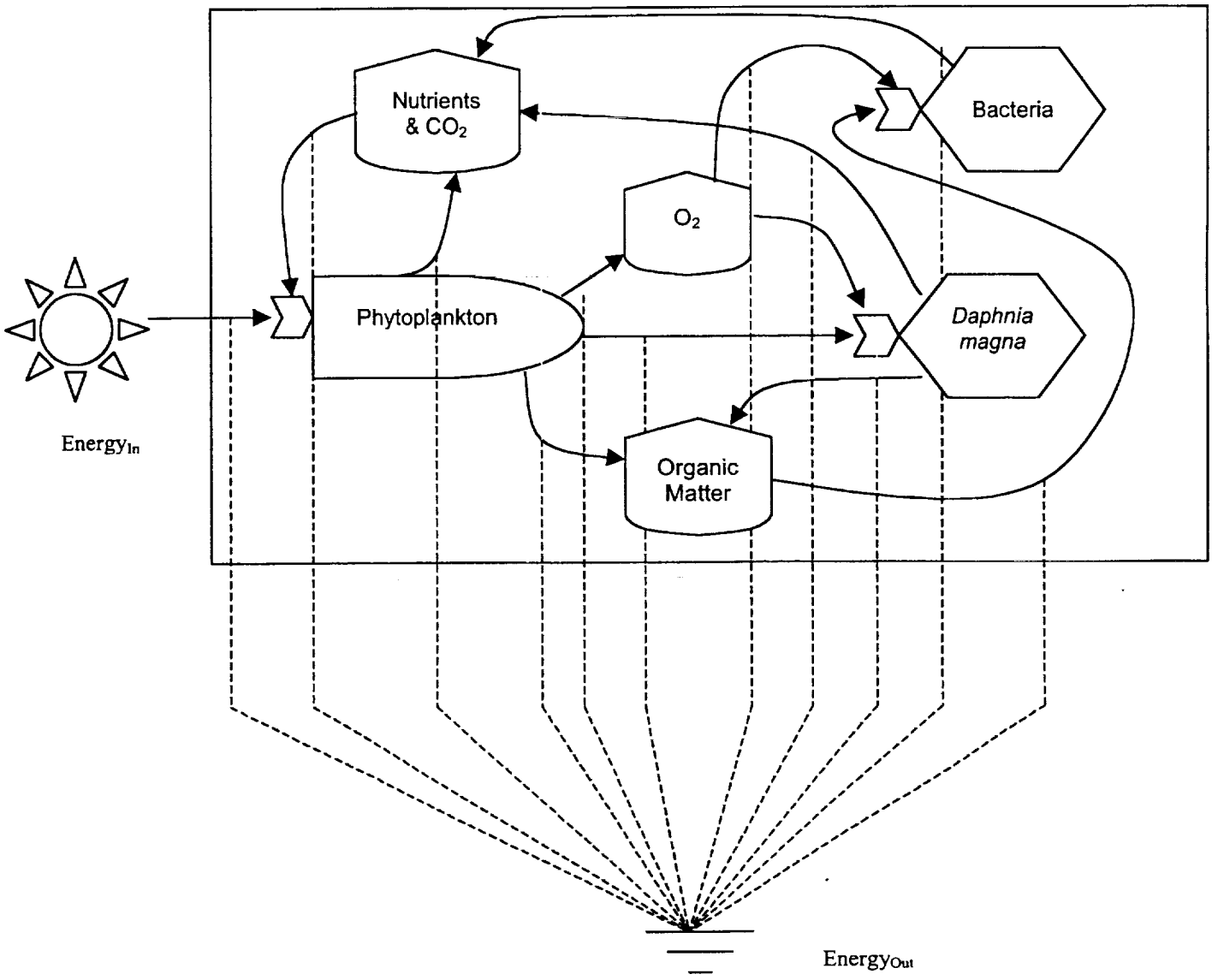

Automated Construction of a Martian Base

Angela Nicole Braun
Dan Bordeaux Burk Butler
Benjamin Shelton Kirk
Scott William White

The University of Texas at Austin
Austin, TX 78712

May 2, 2000

1 Introduction

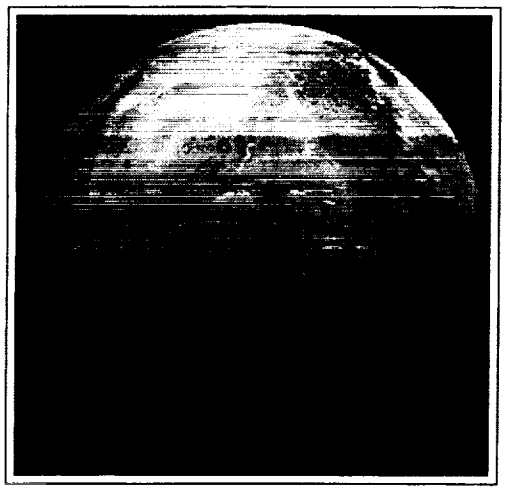

This document describes the construction of a Martian base that will support human exploration. The base will be constructed without a human presence in order to minimize the risk to the crew. The base will be verified remotely before the crew leaves Earth to ensure that all systems are performing as expected.

Life support is the most obvious function the base will have to perform. The crew will require consumables such as food and water. They must also be provided with a controlled atmosphere. The base will use in-situ resource generation (ISRG) as the primary means to provide these services. The ISRG system will extract chemicals from the Martian atmosphere and convert them to usable resources.

Power is a key resource for the base. The primary power needs will be met by an SP-100 nuclear reactor and three Stirling engines. This primary power source can provide 375 kW of power under nominal conditions, which is sufficient to support all base operations. Backup systems are present that can sustain critical functions such as life support and communications in the case of primary system failure.

The base will provide a substantial communications infrastructure. Both Earth to Mars and surface communications are supported. A satellite constellation will be used to provide this capability. Backup systems are also provided that can be used in the event of primary system failure.

Surface operations and science capability is an important aspect of the base design. The base includes two primary laboratories. One laboratory is contained in a lab module that is stationary, and the other is part of a pressurized rover. This mobile science unit (MSU) gives the exploration team the capability of collecting samples and exploring geologic features up to 500 km away. The MSU can operate autonomously from the base for periods up to two weeks with a crew, or it can function robotically for longer periods of time.

A transportation and delivery scheme has also been developed. This scheme requires 4 cargo and assembly missions. The cargo modules will transfer from Earth to Mars on a low energy, near-Hohmann trajectory and then aerocapture into Martian orbit. The cargo modules will then descend to the Martian surface and land within 1km of the chosen landing site. Each cargo module can land up to 15 metric tons on the surface.

Construction will begin as soon as the cargo modules land. The first launch opportunity will send the power and resource generation systems for the base as well as the surface communications infrastructure and two unpressurized rovers in a single launch package. Resource generation will begin as soon as possible. The second launch package will contain the water extraction system, an ascent vehicle, and scientific equipment and instruments.

The remainder of the base will be second launch opportunity. The first cargo mission in this opportunity will transport the science and utility modules and a pressurized science rover to the surface. The final launch will contain the habitation module, crew consumables, and a supplemental life support system.

Base assembly is accomplished through component movement and integration. This work is accomplished primarily with the two unpressurized rovers. The assembly procedure is controlled from the surface with the help of artificial intelligence. The final base is comprised of a central hub, three inflatable utility modules, the power system, and the ascent module.

The base is validated using telemetry from each subsystem. The validation must be successfully completed before sending a crew to Mars.

2 Systems

Here several options are investigated for the primary base systems. The advantages and disadvantages of each option are carefully analyzed, and initial system selection is made.

2.1 Power

Several methods for providing power to the habitat were considered. Photovoltaic arrays were considered first, but were ruled out for several reasons:

- Martian day/night cycle decreases power output
- Intermittent dust storms on the surface decrease sunlight and degrade cell efficiency
- Hydrogen/Oxygen regenerative fuel cell technology for night storage still in development [8]
- Extremely large surface area required to compensate for low sunlight intensity at Mars orbit
- Temperature fluctuations can change the quantum efficiency of the cells

Wind power was also considered. Windmill systems are not a feasible option for supplying power to the base because the Martian atmosphere is too thin. Batteries and fuel cells were investigated as well. A great deal of heritage surrounding the use of batteries in spacecraft exists, but the long duration of this mission's surface stay makes batteries an inadequate option for power.

The most viable method for delivering power to the base is via a nuclear plant. There has been a significant amount of research into surface nuclear power to support Lunar and Martian bases [8, 7, 5]. We recommend the deployment of a nuclear reactor system to provide the base with power.

2.2 Surface Operations

An anticipated surface stay of over 600 days causes surface operations to be particularly important. The crew must be provided adequate tools for scientific exploration and investigation. The crew will be conducting science in both the immediate base vicinity and in remote locations in order to maximize the scientific achievements of the mission.

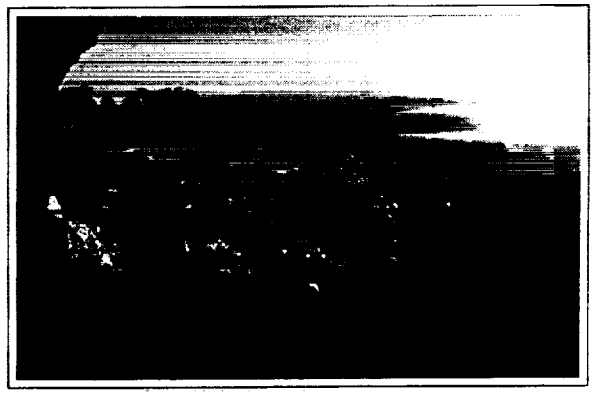

2.2.1 Science

The promise of increased scientific knowledge is a major motivating factor for the human exploration of Mars. Science is thus an important aspect of crew surface operations that must be adequately supported. Our design will include the power and laboratory infrastructure necessary to provide scientific capabilities equal to the International Space Station.

An important part of exploration is geology and sample collection. To facilitate this we will include a

mobile laboratory environment capable of conducting scientific studies at remote locations.

The International Space Station allocates approximately 45 kW of electric power to scientific experiments [2]. We will provide the same amount of power to the laboratory module of the base. Unlike the ISS, the base science requirements are geared more towards exploration and sample collection. A considerable amount of hardware to support exploration (microscopes, instruments, sample storage, etc ...) will also be made available. We will also provide a greenhouse environment for agricultural experiments.

2.2.2 Mobility

The extended surface stay for the crew makes surface mobility a necessity. Mars contains many geological features, and access to geological sites of interest is predicated upon the ability to traverse the terrain. Vehicle range is obviously a key consideration in selecting a device for surface operations. A number of vehicle types were considered.

Ballistic Vehicles
Robert Zubrin of Martin Marietta Astronautics has conducted an investigation of ballistic vehicles for surface mobility. These "ballistic hoppers" have the capability of bypassing particularly rough terrain to access geologic sites that are inaccessible to surface rovers. This advantage, however is offset by the fact that ballistic vehicles are generally less safe, require more fuel, and are heavier than surface rovers.

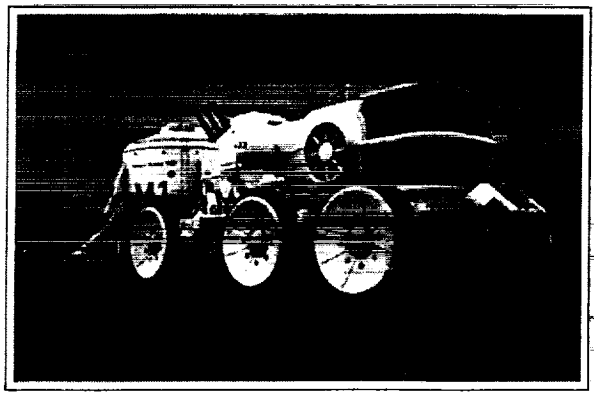

Surface Rovers
The most likely candidate for mobility on Mars is a surface rover. The Apollo Lunar rover was used in the 1970s and proved the usefulness of surface vehicles in the geologic exploration of planetary bodies. The Lunar rover had a one-way range of 20 kilometers [11]. It is obvious that a vehicle with substantially longer range will be required to conduct a thorough geologic survey of the area surrounding the landing site. We will employ surface rovers for mobility.

We have decided not to use the system described in the MSTS document [1] because of the difficulty associated with constructing the vehicle. Additionally, this vehicle is in an early design stage and at this point would remain an enabling technology for the mission. We therefore conclude that the assumptions governing the MSTS and the goals of our project are mutually exclusive.

2.2.3 Intra–Base Mobility

The main base is comprised of a number of pressurized modules. It is crucial to give the crew members the ability to move between modules to perform scientific or maintenance tasks, access sleeping quarters, transfer equipment between modules, utilize communications system, and retrieve dry goods from stowage.

A number of methods to facilitate mobility between modules were considered. These include suited EVA, pressurized "Tram" cablecar that moves between airlocks, and pressurized tunnels for IVA.

The concept of a "shirtsleeve" working environment dates back to the origins of the manned space program. The convenience and ease of working in a pressurized environment without the cumbersome bulk of a spacesuit increases productivity for crew members. The first method for moving between modules, suited EVAs, was ruled out for this reason. The considerable costs and time associated with suiting up to move between modules makes EVAs a poor option. EVAs are best left for sample collection and remote exploration.

The second consideration, a pressurized cablecar that could cycle between module airlocks was also ruled out, for a number of reasons ranging from weight to the precise module orientation required.

The third consideration, a pressurized tunnel system, was decided upon. The Pressurized Mobility Tunnels (PMT) will be constructed of the same material as the TransHab. These flexible tunnels allow the

modules to be misaligned and still connected. Crew members are free to move between modules without suiting up or going through lengthy pressurization and airlock interface procedures. The important tasks listed above that rely on ease of mobility are all easily accomplished via PMT. The PMTs will also house interfaces that permit power, communications, air, and water transfer between the modules.

2.3 In–Situ Resource Generation

The In–Situ Resource Generator (ISRG) is a device that will utilize elements of the Martian atmosphere to produce consumables for surface operations. The enormous cost per kilogram of payload to transport from Earth to Mars makes surface manufacturing an extremely attractive option.

2.3.1 System Types

Many experiments with In-Situ Resource Utilization (ISRU) have been conducted over the years, and the processes involved have become more efficient with each generation. Three ISRG systems were considered, each utilizing a different chemical process. All three processes extract carbon dioxide from the Martian atmosphere and process it to form other, usable chemicals.

Zirconia/Electrolysis
The zirconia electrolysis process [12] was conceived of by Dr. Robert Ash of JPL in the 1970s [12]. Carbon dioxide gas is heated to 1000°C, causing dissociation into CO and O_2. The gas is piped through porous zirconia tubes, and an electrochemical voltage potential facilitates the collection of O_2 molecules. Waste gas consists of CO_2 and CO molecules. It has been proposed that the CO be collected and used to manufacture CO/O_2 propellant, but the technical difficulties associated with development of engines compatible with a CO/O_2 bipropellant have relegated this idea to Mars ascent vehicles [12]. There are a number of disadvantages to a zirconia electrolysis system. A large quantity of zirconia tubes is required to produce enough O_2 to support a manned mission, and there is a significant power requirement to support these systems.

Sabatier-Electrolysis (SE)
The SE system is based largely on gaslight-era chemical engineering. Components for SE systems have been manufactured for the ISS [12]. SE systems are based on a carbon dioxide/hydrogen reaction which produces methane and water. The water can be electrolyzed to produce O_2 and recover half of the hydrogen molecules utilized in the initial reaction. Sabatier reactors developed by Lockheed-Martin have proven 96% reaction efficient, a marked improvement over zirconia electrolysis systems. The system is more robust and energy efficient than ZE systems, but it requires hydrogen to facilitate production. This hydrogen must either be imported from Earth or extracted from the Martian atmosphere.

Reverse Water Gas Shift (RWGS)
The RWGS reaction involves reacting hydrogen with carbon dioxide, resulting in carbon monoxide and water. Water electrolysis reaction allows recovery of all hydrogen, making a RWGS reactor an "infinite leverage oxygen machine [12]." The chief power requirement for an RWGS system is in the water electrolysis step (57 kcal/mole compared to 9 kcal/mole for the RWGS reaction).

2.3.2 Recommended ISRG System

We recommend the deployment of an SE-RWGS system. Dr. Robert Zubrin has experimented with a combination of an SE and RWGS system such that the heat generated by the SE reactor can be used to provide the heat required by the RWGS reactor [12]. A combined system can thus be modeled by the following reaction [12]:

$$3CO_2 + 6H_2 = CH_4 + 4H_2O + 2CO \qquad (1)$$

and water electrolysis is as follows [12]:

$$2H_2O = 2H_2 + O_2 \qquad (2)$$

The result is a system that creates 4 kg of methane and 16 kg of oxygen for each 1 kg of hydrogen provided to the system.

2.4 Life Support

One of the major obstacles to human exploration of the universe is our dependence on a rigid set of environmental conditions. Humans need food to eat, water to drink, oxygen to breathe, and an atmosphere within strict tolerances of temperature, pressure, and gas concentrations to live in. Our species is fragile, and in order to survive in space we must take our

atmosphere with us wherever we go. The function of an Environmental Control and Life Support System (ECLSS) is to provide these basic human needs in inhospitable environments, such as in space or on the surface of Mars.

2.4.1 Functions of the ECLSS

The ECLSS must perform several critical functions including:

- Atmosphere revitalization
- Atmosphere control and supply
- Temperature and humidity control
- Water recovery and management
- Food supply, storage, and preparation
- Waste management
- Radiation protection

These functions must be performed for a crew of five continuously and reliably for up to a 650-day mission on the Martian surface.

The ECLSS is critical to the success of the mission and the safety of the astronauts. With this in mind, the ECLSS for this base design will strive to have several levels of functional and design redundancy in order to ensure crew safety.

2.4.2 ECLSS Types

There are three general types of life support systems that can be used for a Martian base: open loop, physical/chemical, and bioregenerative. These general types of systems will now be defined, and the advantages and disadvantages of each will be discussed.

Open Loop Systems

Open loop life support systems operate by replacing consumables on a regular basis from the Earth. This type of system is the easiest to implement, as supplies are constantly replenished and used materials are simply discarded from the base. This is a feasible option for a single, short-duration mission; however, in order to sustain a prolonged presence on the Martian surface this option becomes far too costly to implement as the primary base life support system.

Physical/Chemical Systems

Physical/chemical systems operate using a combination of physical and chemical processes to recycle resources brought from the Earth. These types of systems are currently employed on the Space Shuttle and International Space Station. An example of this type of system is the Lithium Hydroxide canisters used to scrub the air of CO_2 during Shuttle missions.

The disadvantage in using a physical/chemical system, however, is that it cannot be one-hundred percent efficient. This lack of total efficiency results in consumable losses that have to be replaced in some manner; either from stored reserves or in-situ resource utilization. In addition, many physical/chemical systems are not recyclable. Once these systems reach their design limit they must be discarded and replaced with new systems that must be transported from Earth. The water vaporation and recovery process (WAVAR, shown schematically in Figure 1) is one such physical/chemical system that we will use to extract water from the Martian atmosphere.

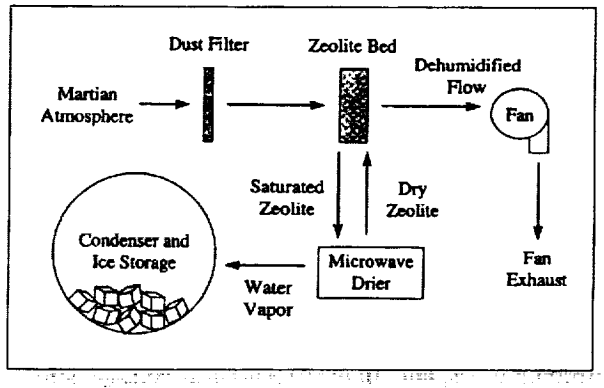

Figure 1: Schematic WAVAR Process [4]

Bioregenerative Systems

Bioregenerative systems are systems that use only biological elements (such as higher plant life) to regenerate organic products. This type of system "takes care of itself," and an example of one is the Earth itself. The development of this type of system is absolutely necessary for a continued human presence on Mars.

2.4.3 Recommended ECLSS

For the base, a combination of all three types of life support systems will be utilized. In this manner, mul-

tiple levels of redundancy can be built into the system to provide an adequate measure of safety for the crew.

2.5 Communications

Hardware on the surface of Mars is useless without reliable communications back to Earth. A Martian communication network must address Earth-Mars and Mars-Mars transmission. The exploration of Mars will greatly stretch the current space communication network. For example, the Mars Pathfinder mission returned 30 Megabits per day (Mb/sol). The time averaged bandwidth for the Mars-to-Earth link was 300 bits per second (bps) [3]. A communications link to support a permanent base on Mars must provide much more bandwidth. There are two basic networking methodologies that can used to create a Mars Network: peer-to-peer networking and a central-relay (or hub) network.

2.5.1 Peer-to-Peer Networking

A peer-to-peer network uses direct links between all the deployed assets and Earth. This method has been used for the majority of the NASA interplanetary mission. These missions included Mariner, Viking, and Pathfinder.

These types of systems have the benefit of being stand-alone and based on heritage technology. However, this means each asset must have the weight, complexity, and power penalties associated with a Mars-Earth link. A typical link will require:

- A directional antenna
- Steering mechanism
- Power amplifier
- Heat-removal device
- Large solar panels
- Battery capacity
- Power handling electronics

In the Mars Pathfinder and the Mars Surveyor '98, the mass of the link hardware outweighed the science payload [10].

2.5.2 Central Relay Networking

A more modern approach is the relay station/satellite. This method requires a single Mars-to-Earth direct link coupled with low power UHF (ultra-high frequency) communications for the Mars system. The relay station may be a single satellite, a satellite constellation, a high power ground based system, or some combination. The ground station is the most limited option (because it decreases the amount of time the base could be in contact with the Earth), and would likely only be used as a secondary system for a manned base on Mars. Whatever system is used must provide high-bandwidth, reliability, and expandibility.

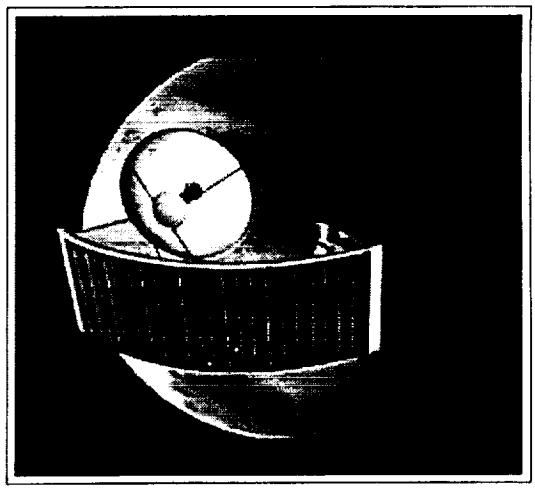

Figure 2: A MicroSat Design Configuration [9]

Relay satellites (a possible configuration shown in Figure 2) allow the science rovers to be lighter and use less power. The satellites will increase data return and allow improved surface navigation/landing. There are a multitude of design options for a communications satellite constellation. These constellations range from the low cost single craft [10] to larger constellations consisting of low orbit microsats coupled with larger aerostationary satellites [9]. Aerostationary satellites are in similar orbits to Earth geostationary communication satellites; that is, they stay above the same spot on the Mars surface. The Mars Network system currently under design by JPL is a central relay network that provides high bandwidth data return, reliable coverage with multiple satellites, and plans for expandibility [9].

3 Base Design

The initial Mars outpost will consist of six modules. The three living and working modules will be based on the current TransHab being developed at NASA Johnson Space Center [6]. The fourth module will be the ascent stage coupled with the resource generation systems. The final module will be the nuclear based power plant. The three living/working space modules will be design for critical failure redundancy. The hub of the base contains the primary base infrastructure components. These components include:

- ISRG
- Docking Adapters
- Communications Array
- Power Distribution System
- Airlock

A schematic design for the base is shown in Figure 3.

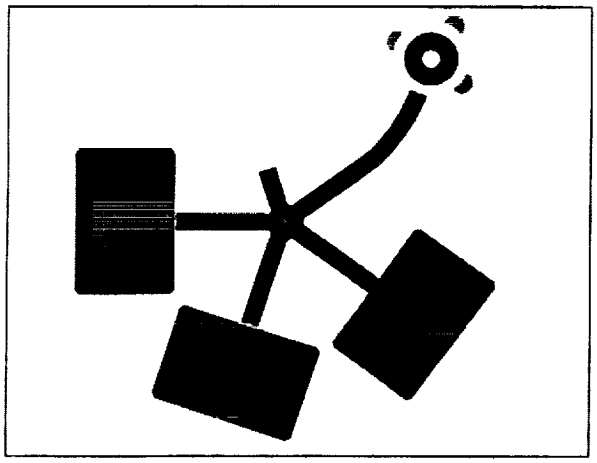

Figure 3: Schematic Base Design

3.1 Passageways

The astronauts will move between modules through inflatable tunnels made of the same material as the TransHab. The heating and air circulation for each hall will be provided from the modules connected to the hall. The tunnels will be flexible and extendable. This will allow small shifts in the location of each module without stressing the interconnecting passages. The flexibility will facilitate the construction of the base.

Without flexible interconnections all of the modules would have to aligned accurately in all six degrees of freedom and moved into place. Current estimate for the TransHab indicate a mass of 13 metric tons [6]. The alignment of two or more ten-ton objects would require an unnecessarily heavy infrastructure for the construction. The weight of the construction equipment can be better used for scientific or life support equipment.

3.2 Docking Interface

Each habitat module on Mars will be equipped will standard connector interfaces. The interfaces will permit the redundant transfer of power, communications network, air, and water throughout the base. The connections will also provide hallways between modules for the crew members. The connectors will be available on each end of all the modules. The connectors will come in male and female flavors.

The docking interface will act as a multi-use extension cord to connect the living/working modules. The use of these connectors will allow the flexibility in the assembly of the base. The docking interface will provide 15 meters of linkage between two modules.

3.2.1 Power Connection Requirements

The power conduit will have two separate connections. Each connection will be able to handle two-thirds of the base power requirements. All fully operational interfaces will pass 133% of the base power to the downstream modules. All power connections will be equipped with resetable circuit breakers. This will protect one module from being influenced by a power overload or short circuit in other portions of the base.

3.2.2 Communications Network Requirements

The base will be equipped with a network for computer communications through out the base. This methodology should leverage the large commercial sector involved involved in computer networking. The interface will have two fully redundant connections. The physical wiring should allow for computer connections as well as for stand-alone sensors based in and around the base. The network systems should be sized for the future growth of the station.

3.2.3 Water Transfer

The plumbing of the station will be very important. Water will be needed throughout the station. Clean potable water will be needed in the galley and living quarters. Water is also used in lab environments and other work areas. Each interface should provide the capacity to deliver 100% of the base daily requirements.

The disposal of water may pose a greater problem. The water must be filtered and recycled. Various levels of contamination will require different filtering methods. Three levels of disposal water will be provided. Each system will be separate and routed to the corresponding to filter/cleaning system. The disposal system must be sized to match the supply system with a safety and growth factor.

3.2.4 Air Transfer

The base will require central air recycling and heating for the base. If air circulation and heating ducts are used, they must be routed through the connectors. The air ducts will require a significant amount of volume and must be sized for the heating of the base. For the detailed design of the base heating and cooling systems it be easier and more efficient to circulate the air through the human passages themselves rather than through separate ducts.

3.2.5 Physical Connection

The connection system between the modules must provide an airtight seal and a strong connection. The connection of two modules must be accomplished without astronaut EVA intervention. The system must be made of materials that are inert in the Martian environment. The thermal expansion of all the materials must be closely matched because of the large temperature gradients the structure will face on the Mars surface.

The docking interface will have an independent backup system. Airlocks will be provided at each end of each module to allow suited crew member ingress and egress. These airlocks can be sealed to isolate any leaks that may develop in the seal or the hallway material. Multiple airlocks also increase base modularity.

The initial physical contact will be achieved via the use of cables that move from the male connector to the female connector. These guide cables provide alignment, strength for the passageway, and are used as a method for moving the docking systems together.

Once the two faces are touching electromagnetic latches will be closed to hold the joint together.

3.3 Construction Rover

The construction rover is based on the technology pioneered by JPL missions to explore Mars and the rover technology used to explore the oceans of the world. Current technology allows unmanned rovers to lay telecommunications cable, retrieve artifacts, inspect oil rigs, and more. This work is all done in the harsh environment of the ocean floor. The Martian environment poses similar obstacles to robotics.

The construction rover will have wheels for mobility. The system will be powered by batteries and will have the ability to recharge from the base power grid. The major component of the rover is the robotic arm. The arm can be a miniature version of the shuttle or space station arm. A manipulator hand is very important to pickup parts, place things, and flip switches.

One of the major limiting factors in current robotics is the controlling artificial intelligence. The majority of the working robots are tele-operated. This method of control is not feasible for Mars because of the time lag in communications. The Martian rover must be able to complete tasks without human intervention. However, the rover needs to be relatively lightweight and robust enough inspect a nuclear system. Therefore, the rover will contain sensors including stereo vision and lights, but the intelligence of the system will be contained in the base computers. In this way, the rover will be tele-operated by a computer program running on the base system. This setup will provide more processing power and storage than otherwise available on a rover. The system should have the ability to act in wireless mode (through an UHF radio link) or with an umbilical cord to provide power and control inputs.

4 Base Construction

The robotic assembly of the outpost on Mars requires a complicated set of steps to provide the functionality for human habitation.

The general construction sequence includes:

1. Land initial units on Mars
2. Move to assembly area

3. Align first two units within 15 meters
4. Begin docking procedure
5. Once docking procedure has be completed the modules are connected
6. Base validation begins

This procedure will be repeated for each new elements added to the outpost. Certain cargo missions use a different assembly procedure, however, that will be described later.

4.1 Launch Manifest

The orbits of Earth and Mars result in a 15 year trajectory cycle which is divided into 7 launch windows. This configuration results in a launch opportunity about every 26 months. The Reference Mission begins with the first launch of a Mars cargo transport in the year 2007, and this mission will begin with the same initial launch opportunity. For each of the launch windows, it is assumed that 2 successful launches will be made (for a total of 4 launch packages delivered to the Martian surface). This split launch approach will allow base components to be validated before additional pieces are sent. The following launch manifest assumes the capability to lift 15 metric tons to the surface of Mars. This more feasible than the reference mission assumption of 50 metric tons deliverable to the surface [7].

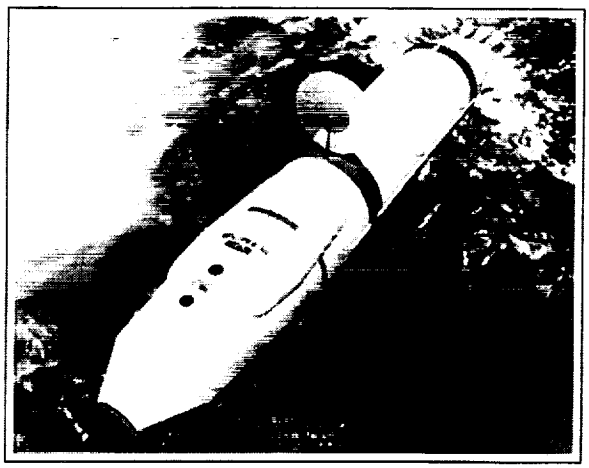

4.2 Base Deployment

The base will be composed of the modules mentioned previously and a number of subsystems. All systems must be deployed and integrated before the base will be fully functional.

Table 1: First Launch, September 2007

System	Mass (tons)
Power System (NPU, PDS)	8.7
Resource Generator (ISRG)	1.0
S-Band Communication System	1.0
Construction Rover	0.5
Utility Rover (UPR)	2.0
Seed Hydrogen	1.5
Total Launch Weight	14.7

Table 2: Second Launch, September 2007

System	Mass (tons)
Water Extraction (WAVAR)	5.0
Ascent Module (MAM)	5.4
Scientific Equipment (terrain mapping, soil sample collection and analysis, etc.)	up to 4.6
Total Launch Weight	10.4-15

4.2.1 NPU Deployment

The NPU is the primary power source for the base. Radiation considerations dictate that the reactor be placed 2.5 km from the main base. The reactor will be separated from the NPU deployment cart. The NPU deployment cart contains wheels, a spool with 2.5 km of power cable, and the Power Distribution System (PDS). The PDS is the "wall outlet" that the main base draws power from. The deployment cart also houses the ISRG and an s-band communications antenna and will be the eventual "hub" of the main

Table 3: Third Launch, October 2009

System	Mass (tons)
Science Module (SM)	7.5
Utility Module (UM)	6.5
Science Rover (MSU)	0.885
Total Launch Weight	14.885

Table 4: Fourth Launch, October 2009

System	Mass (tons)
Habitation Module (HM)	5.5
Food Cache	2.2
Experimental ECLSS (life support)	up to 7.3
Total Launch Weight	7.3-15

base. The UPR will tow the NPU's deployment cart 2.5 km and set down the PDS and ISRG on the site selected for the main base.

4.2.2 ISRG Deployment

The ISRG, which arrives in the first launch package with the NPU, is situated below the PDS. It will already be connected to the PDS and will begin receiving power when the NPU powers up. The ISRG requires no external assistance to begin manufacturing oxygen and bipropellant. One metric ton of seed hydrogen will be included in the first launch package for use the surface. The ISRG will immediately begin to process the seed hydrogen and will exhaust its stores, creating 12 metric tons of bipropellant and 8 metric tons of excess oxygen. The bipropellant will be used to fuel the UPR which will in turn be used to tow the ISRG/PDS "hub" to the site selected for the main base.

4.2.3 Rover Deployment

Three rovers are included in the mission scenario. They arrive on the surface unpowered and unfueled. The UPR and construction rover are included in the first launch package. When the NPU powers up, the ISRG utilizes seed hydrogen and creates bipropellant for the UPR. The UPR then moves the ISRG/PDS hub away from the reactor towards the main base site. The construction rover is a battery-operated rover that remains close to the central hub and is capable of using the PDS to recharge its power supply. The MSU arrives in the third launch package. The UPR will retrieve it and tow it to the ISRG for fueling and power.

4.2.4 WAVAR Deployment

WAVAR arrives in the second launch package. It requires power from the PDS to operate. The UPR will go to the second launch landing site, retrieve the WAVAR, and transport it to the central hub. Once receiving power from the PDS, WAVAR will provide water for the crew and seed hydrogen for the ISRG.

4.2.5 Mars Ascent Module Deployment

The Mars ascent module (MAM) arrives in the same launch package as the WAVAR. The 5.5 metric ton [7] vehicle will be moved by the UPR to the main base site. A PMT will link the MAM to the central hub. This will allow the crew to access the MAM without EVA. This is an obvious advantage over mission scenarios that require crew members to suit up in order to access an ascent vehicle. The time required to prepare all crew members for EVA can be crucial to survivability in an emergency, and the ability to quickly ingress the MAM in a crisis could save lives.

4.2.6 TransHab Deployment

The majority of habitable crew space is comprised of three TransHab modules (the SM, HM, and UM). These are scaled-down versions of the element envisioned for deployment on ISS. Each module serves a different purpose, but all three are deployed in an identical manner.

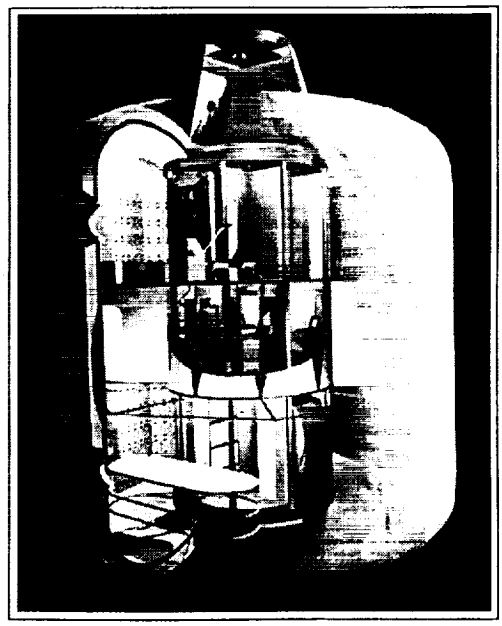

Preliminary Movement/Orientation
Regardless of the launch package or module purpose, each module will be moved from its landing site to an area near the main base by the UPR. Each module contains a 15 meter section of PMT on one end. It will also be necessary for the UPR to orient the module such that the end containing the section of PMT is oriented toward its designated docking ring on the hub. The UPR must therefore move the module to within 15 meters of the base and orient the PMT ring to mate with the hub. The PMTs are flexible enough to mate module to hub even though the two are misaligned or off axis. It should be obvious that a module positioned closer to the hub will have more PMT available to take up any misalignment.

Guide Cable Connection
After the UPR aligns the module with its mating adapter on the hub, the construction rover will connect three guide cables from the module to the hub. The cables will be contained in the PMT of the module. The cable holder and the corresponding catch will be painted to allow easy identification by the rover vision system. After all three cables are secure, the PMT will be ready to dock the hub.

PMT Extension and Docking
Once the module is physically connected to the hub by guide cables, the docking plate from the module is pulled into place by wheel bogeys housed in the PMT. The rover can provide video of the connection or in case of motor failure, it could extend the tunnel by pushing the docking plates together. The hub contains a winch that can be used to pull the PMT to the docking adaptor in the event of wheel bogey failure. Once the plates are flush, electromagnetic latches will seal the PMT to the hub and allow the module to be pressurized. The configuration of the docking plates is polarized and machined so that the pieces slide together creating the electrical, network, water, and air connections. After the physical connection, the circuit breakers can be thrown to power up the module. After all modules are fully powered, base validation can begin.

5 Base Validation

Base validation is a key aspect of the mission that must be satisfactorily completed before any human crew is sent to Mars. Validation will require testing all of the critical functions of the base and ensuring that they work to within given specifications. the validation phase of base construction is greatly facilitated by the extensive telemetry data that will be collected in the base during nominal operations. The key components that must be validated include:

- Power Systems
- Communications
- Life Support Systems
- Science Systems
- Transportation Systems
- Ascent Module

5.1 Power Systems

The power system is a key system that all base functions depend upon. The power system is so critical that if it is not functioning properly the validation phase cannot even be initiated.

A key element of the power system validation is that the nuclear reactor is functioning intact and within specifications. It is critically important that the NPU not leak excessive amounts of radiation, as this would endanger the crew. Geiger counters will be used at the base site to measure radiation levels and verify that they are within expected limits. These measurements will also be useful in determining the ambient radiation level due to solar activity. The base will already have been designed to withstand known levels of Martian radiation, but these tests will serve to validate those design limits.

The reactor core temperature must also be monitored to predict meltdown. Fluctuations in reactor core temperature can indicate a heat exchanger malfunction. The offending heat exchanger can be isolated via onboard thermocouples.

Additionally, each of the four Stirling engines will need to be validated. This can be done on an individual basis before the base is operating at its nominal power level. Each engine will be run up to its maximum rated power while its health is monitored. We will look for particular operational anomalies such as severe outlet temperature fluctuations, excessive vibration, inconsistent rotational speed, and inconsistent power output.

A mathematical model of the power system will be created. This model will be run on Earth during

the construction and validation phases. Results from the model will be compared to system sensor output as a means to detect differences and failures. The mathematical model can also detect failures in the sensors themselves by detecting results that are not physically possible. Once the base is operational, the model will be run in real time on the base control computer systems.

5.2 Communications

The communications system is another system that must be functioning properly when the validation phase of the base construction is begun. This system will be required to send massive amounts of data between Earth and Mars while validating all other systems.

Both the satellite transmitter relay and the base backup system will be verified for data integrity and reliability. This is particularly important for detecting any unanticipated interference that might be present in the base vicinity. Additionally, the communications subsystems on the MSU and UPR must be verified. These systems should be able to talk to each other, the base, the central relay satellite, and (to a very limited extent) to Earth.

5.3 Life Support Systems

Validating the life support system will concern the module artificial atmospheres and produced resources. The atmosphere in each module (and the MSU) must be verified as conforming to predetermined specifications. These specifications will prescribe the temperature and partial pressures of gases. The carbon dioxide filtration systems must be verified by introducing CO_2 into the closed system and monitoring the atmosphere throughout the filtration process. All of these atmospheric monitoring processes will continue for the lifetime of the base. The validation functions will therefore be an intrinsic part of the base design. Validation simply requires transferring this data to Earth for analysis.

The water and oxygen production functions of the ISRG and WAVAR systems must also be verified. Chemical tests will be performed to guarantee that the purity of these resources are within tolerable limits.

5.4 Science Systems

The individual science packages will be validated by their respective Earth-based support teams. The main base computer will run a battery of tests and transmit the results to Earth via the communications infrastructure for debugging purposes.

5.5 Transportation Systems

The MSU and UPR will be validated during the construction phase of the base. The UPR will already be validated through the construction procedure since it will be used to position components on the surface. These two devices must be capable of powering up and operating autonomously. The internal combustion engines will be verified by checking for excessive vibration and inconsistent torque output. These devices will be preprogrammed with a set of validation tasks that can be conducted on the surface under the guidance of the base control computers.

The surface rovers depend heavily on the ISRG's ability to produce and transfer fuel. The ISRG must therefore be fully functioning and have stored a sufficient amount of fuel. Again, the base construction is dependent on this functionality, so a successful construction phase will validate the ISRG fuel production capabilities.

5.6 Ascent Module

The Ascent Module will be powered up and pressurized before the crew arrives. This will check for leaks and allow engineers on Earth to verify that all its computer systems are functioning properly. It will also be partially fueled to check for leaks in the propulsion system tanks, hoses, valves, etc...

References

[1] Collins, C., Gomez, A., Muñiz, R., Musson, D., *The Conceptual Design of a Mars Surface Transportation System (MSTS)*, The University of Texas at Austin, Spring 1999.

[2] DeFelice, D., "NASA Factsheet," *http://www.lerc.nasa.gov/WWW/PAO/PAIS/fs06grc.htm*, 1999.

[3] Edwards, C., "Mars Network: First Stop On The Interplanetary Internet," TMOD Lecture Series presentation, Oct. 5, 1999.

[4] "Extraction of Atmospheric Water on Mars," *HEDS-UP Mars Exploration Forum*, May 4-5, 1998.

[5] Hoffman, S., Kaplan, D., "Human Exploration of Mars: The Reference Mission of the NASA Mars Exploration Study Team," *http://spaceflight.nasa.gov/mars/reference/hem/hem1.html*, July 1997.

[6] HSF–International Space Station, *http://spaceflight.nasa.gov/station/assembly/elements/transhab/index.html*, Accessed January, 2000..

[7] Human Mission Table, *http://cmex-www.arc.nasa.gov/MarsNews/Missions/human_missions/Human_Mission_Table.html*, Internet.

[8] Landis, G., Photovoltaic Power Options for Mars, *http://powerweb.grc.nasa.gov/pvsee/publications/mars/marspower.html*, October 1996.

[9] Mars Network- Gateway to the Mars Frontier, *http://marsnet.jpl.nasa.gov/index.html*, accessed February 2000.

[10] Svitek, T. et. al., *Mars Relay Spacecraft: A Low-Cost Approach*, 9th Annual AIAA Conference on Small Satellites, September 1995.

[11] Zubrin, R., *Methods for Achieving Long Range Mobility on Mars*, Martin Marietta Astronautics, Denver, CO, 1992.

[12] Zubrin, R., Frankie, B., and Kito, T., *Mars In-Situ Resource Utilization Based on the Reverse Water Gas Shift: Experiments and Mission Applications*, AIAA 97-2767 Pioneer Astronautics, 1997.

Mars Aerial Research Vehicle
M.A.R.V.

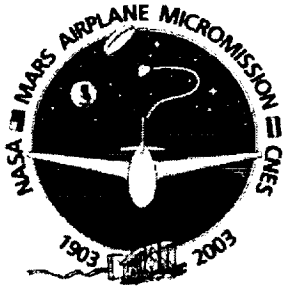

University of Colorado at Boulder

Undergraduate Aerospace Engineering
Ben Mottinger *Jason Muckenthaler*
Dan Wicklund *Corissa Young*

Undergraduate Computer Science
Colin Graham *Eric Schell*

Undergraduate Electrical Engineering
Ted Kutrumbos

Faculty Advisors
Dr. Brian Argrow
Dr. Jason Hinkle
Dr. John Sunkel

ABSTRACT

Mars Aerial Research Vehicle (MARV) is based on the NASA Langley mission Mars Airplane Package (MAP). The deployment sequence of the MAP was designed, as well as the method of separation from the aeroshell. To determine the stability behavior during separation from the aeroshell, a wind tunnel model of the airplane was constructed and tested for pitching moment. Also, a VxWorks based software system was implemented to provide video imaging and to control the airplane deployment and camera position. The ground software was written in Java to provide a portable data evaluation system.

TABLE OF CONTENTS

MISSION OVERVIEW

NASA has a vision statement that reads, "NASA is an investment in America's future. As explorers, pioneers, and innovators, we boldly expand frontiers in air and space to inspire and serve America and to benefit the quality of life on Earth." This is a very bold statement that encompasses many areas of Space exploration. One specific area it speaks to is the Human Exploration and Development of Space (HEDS), which is one of the foci of the Mars Aerial Research Vehicle (MARV) project. The HEDS division of NASA has generated it's own mission statement that reads, "To open the Space frontier by exploring, using and enabling the development of Space and to expand the human experience into the far reaches of Space."

Human exploration of Space has truly been and continues to be a driving force for the entire Space industry. Not only has it been responsible for much of the advancement and development of Space exploration materials and techniques, but it has also been a significant contributor to the excitement and interest of the general public in that vast expansion referred to as "Space: the final frontier". Sending people into Space has been the source of much pride for the United States since the early 1960's. In order for the United States to remain a leader in the Space industry, we must continue the advancement of human exploration of Space.

Langley Research Center (LaRC) has proposed the development and launch of a mission that will include the powered flight of an aircraft in the atmosphere of Mars. The mission will demonstrate the technology needed to fly an aircraft on another planet for the purpose of collecting science data, as well as taking high-resolution pictures of the Martian surface. The mission, known as the Mars Airplane Package (MAP), will also celebrate the first powered flight of the Wright Brothers in 1903. The Mars Airplane will be taken to Mars on the 2003 Mars spacecraft mission. The transfer spacecraft will drop the airplane package into the atmosphere, where the airplane will separate from the aeroshell (heat shield) and deploy autonomously wings and a tail. The airplane will then attain and begin powered, level flight, which will last a minimum of 120 seconds. The airplane will continue flying until the end of the usable communications window, which is estimated to be 20 minutes. During the entire flight, science and engineering data from the airplane will be relayed to Earth via the orbiting satellite.

The MARV team selected the deployment of the wings of the MAP as the design project focus. This problem encompasses many different engineering disciplines including aerospace, computer science, and electrical. For this reason, the MARV team is comprised of 4 aerospace engineering students, 2 computer science engineering students, 1 electrical engineering student, a computer science advisor, an electrical advisor, a structural advisor, and an aerodynamic advisor. This interdisciplinary team has been able to complete a more comprehensive and complete design for the wing deployment of the MAP.

The MARV project was divided into four phases:

- *Phase I*: the preliminary design portion of the project. During this time the group researched the design (aerodynamic and software) of the MAP on a very high level.
- *Phase II*: focused on one aspect of the MAP design, specifically the deployment system.
- *Phase III*: hardware acquisition, machining, and construction
- *Phase IV*: integration and testing phase.

The end goal for the project was to design the wing packaging and wing deployment for the MAP, with the end result being a fully deployable wing with the accompanying actuator, microprocessor, and supporting software. The secondary goal for the deployable wing was to conduct wind tunnel testing of its pitch stability. A complete software architecture design was also developed for the MAP along with all of the accompanying electrical components that were necessary for integrating the aerospace portion of the project with the software (computer science) portion of the project.

Phase I involved extensive research of the MAP design proposed by NASA Langley including aerodynamic plane designs along with software architecture concepts. This research served as the basis for the remainder of the MARV project. Previously developed concepts (from LaRC) and ideas were expanded upon to include the design of the deployment mechanism and sequence for the wings of the MAP.

Phases II and *III* will see the MARV group divided three ways:

- The first group was comprised of three of the four aerospace engineering students and will focus on the structural design and building of the MAP wing model, followed by the design of the wing packaging and deployment system. The portion of the deployment system situated on the wings consisted of shape memory actuators.
- The second group had the remaining aerospace student and the electrical engineering student. Group number two designed the electrical deployment mechanism that was initiated by the software developed by group three. The complete deployment mechanism is comprised of two shape memory actuators (on the wings) and the supporting power electronics. This group was also responsible for creating the necessary circuitry for a digital camera, which was implemented because of the requirement of MAP to take high-resolution pictures of the surface of Mars.
- The third group comprised of the two remaining students – both Computer Science majors – designed and implemented the control software for the supporting electronics for the deployment mechanism and the control software for the digital video camera.

Phase IV involved testing of the individual components including software code, electrical circuits, and wing stability. Then, final integration produced the demonstration of a fully deployable wing system for the MAP project.

AERIAL VEHICLES AS PLANETARY EXPLORERS

The Mars Airplane Project (MAP) concept was designed as a low-cost atmospheric research vehicle. Although the mission requires interplanetary space travel, the MAP was conceived along with its transfer vehicle to be launched as a secondary payload aboard an Ariane 5 launch vehicle. The implications of launching an interplanetary mission as a secondary payload are profound for NASA's exploration program. Secondary payloads require a fraction of the cost-to-orbit that primary payloads do.

The drawback to secondary payloads has always been two-fold. Secondary payloads are essentially hitchhikers and thus do not have the command of the launch vehicle that the primary does. Interplanetary missions often have narrow launch windows, making it difficult to rely on the primary payload's schedule. In addition to the scheduling constraints, secondary payloads suffer from extreme volume and mass constraints.

The MAP was conceived as a small vehicle with a short mission lifetime, translating into very limited, but valuable science returns. The planetary transfer vehicle – the Mars Micromission Spacecraft (MMSC) – was designed to carry several modules and deposit them into the Martian Atmosphere using an aeroshell-parachute system similar to that used on the Viking Missions. The MMSC would then act as the main communications relay for the objects deposited onto the planet. Multiple missions would build on the communications coverage by supplanting the previous MMSCs already in Martian Orbit.

Because of the inexpensive, disposable, and simplistic nature of airplanes similar to MAP, multiple missions could be sent at low cost. These missions have potential for other planetary exploration missions as well. Due to the proximity of Mars and the relative similarity in atmosphere and gravity, the MAP was well suited to atmospheric exploration and imaging. However, the potential for this type of exploration is not limited to aircraft. Dirigibles also present definite possibilities for atmospheric exploration due to their significantly increased mission lifetime and payload capability.

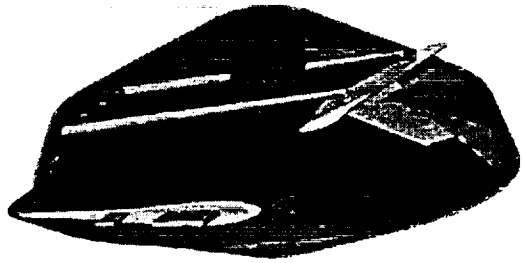

Figure 1: MAP in stowed configuration inside aeroshell (top). MAP separating from aeroshell (right)

MAP DEPLOYMENT DESIGN

The preliminary design for the Mars Air Plane (MAP) called for a disk shaped fuselage with deployable wings and deployable tail structure. The MAP shape was developed out of the general desire to maximize the scientific payload housed with in the fuselage. In order to maximize this payload and thus the scientific return from the mission, the wing area needed to be as large as possible. After looking at several possible deployment configurations for the MAP, it was decided that the wings needed to fold on top of each other:

This packaging method requires a more complicated wing deployment mechanism that will allow the wings to fold flat on top of each other. The most significant impact of this design decision is on the aerodynamics of the airplane during the deployment phase.

Deployment Design Assumptions

Because of the uncertainties associated with a free fall trajectory on Mars – wind, exact densities, exact orientation – assumptions were made to facilitate the design of the deployment sequence while not sacrificing requirements.

- Because of the unknown trajectory once the MAP is inside the atmosphere, it was assumed that the aeroshell's transverse velocity would remain much smaller than the vertical velocity during the free fall phase of the deployment.
- The orientation of the aeroshell is assumed to be roughly horizontal.
- The attitude of the aeroshell relative to the martian surface does not need to be known for a successful deployment and flight.

Pre-Deployment Conditions

Altitude	6.5 Km
MACH Number	0.9
Vertical Velocity	~207 m/s
Transverse Velocity	~0 or Vh << Vz
Orientation	~ Horizontal

Post Deployment Conditions

Minimum Altitude	5.0 Km
MACH Number	0.8
Vertical Velocity	~207 m/s
Transverse Velocity	~0 or Vh << Vz
Orientation	~ Horizontal

Aeroshell Deployment

The mission profile calls for the airplane to be deployed from the aeroshell at close to a 90° angle of attack relative to the oncoming airflow and then assume steady level flight. The deployment phase thus has to be designed such that the airplane can separate from the aeroshell, deploy its tail and wings, and recover from the ensuing dive while still maintaining as much altitude as possible, while accounting for the fact that the desired orientation for deployment may be achieved with a only a certain uncertainty.

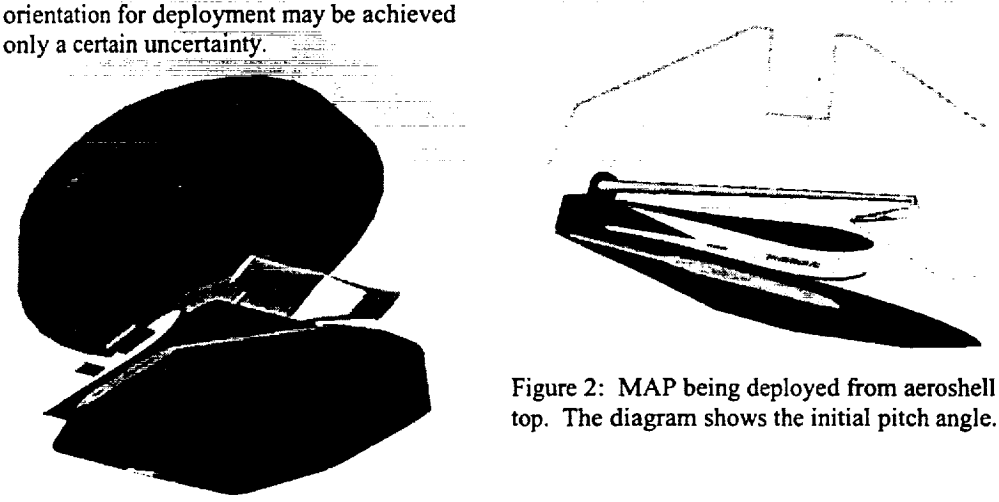

Figure 2: MAP being deployed from aeroshell top. The diagram shows the initial pitch angle.

The aeroshell deployment sequence was then designed so as to ensure that the MAP would attain a pitch forward dive in all but the most extreme circumstances upon separation from the top part of the aeroshell. Because the

airplane is essentially a flat disc upon ejection from the aeroshell, the aeroshell must have a mechanism to impart a nose-down pitch on the airplane.

The nose-down pitch would be accomplished by a set of separation springs. The springs would be set to kick the airplane out of the aeroshell with enough of a moment to prevent the MAP from falling back on itself. The springs would also serve to prevent the aeroshell from interfering with the deployment of the mechanisms.

Airplane Deployment Sequence

Time	Event	Description
Stage 1:		
T_{-1}	Aeroshell Bottom Separation	Aeroshell Mechanism
Stage 2:		
T_0	Aeroshell Top Separation	Release from MAP
Stage 3:		
T_1	Tail Deployment	
T_2	Wing 1 Deployment	
T_3	Wing 2 Deployment	
Stage 4:		
T_4	Horizontal Stabilizer Deflection	
T_5	Ignite Engine	
T_6	Begin Level Flight	

Immediately after the MAP is kicked out of the aeroshell, the tail assembly will deploy further pitching the nose of the aircraft down and causing the airplane to go into a nosedive. The reason for the desire to have the plane in a known orientation – specifically a nose dive – is to allow for the least amount of control needed while simultaneously allowing the vehicle to develop a velocity vector parallel to its nose as opposed to its belly, allowing the wings to produce lift and minimizing the amount of thrust necessary from the engine to produce this forward velocity.

At this stage of deployment, the MAP has a deployed tail and stowed wings and is free falling with a pitch down pitching moment. The wings are then deployed at a certain delta t from the tail to ensure that the tail has been locked into place and the wing deployment will not cause the plane to pitch unrecoverably.

The wing deployment presents one of the more interesting challenges for the deployment phase in terms of stability. The wings are deploying asynchronously in free fall. Therefore, the possibility exists for not only changes in the pitching moment that might be outside the correctibility range of the control surfaces, but also a rolling moment and associated coupled yawing moment.

THE MARV PROJECT

MARV is a quarter scale model of the MAP built to test the aerodynamics associated with the asynchronous and asymmetric nature of the aircraft during deployment. Specifically, MARV looks at the pitching moment during the wing deployment. MARV was built with the tail section fixed, but with deployable wings.

Test Article Design

The wind tunnel model design requirements were driven by the pitch moment measurement. Several test constraints including the test section size of the wind tunnel descoped the original model design. The wind tunnel test section limited the model to quarter scale, which imposed constraints on the size of deployment actuators and the release mechanism. Therefore, the wing deployment actuators (torsion springs), were mounted on the top of the fuselage. A small penalty in drag resulted from the external mounts, but the assembly and manufacturing complexity was reduced.

The original aeroshell volume constraint was also considered when designing the wing stowage. The wings fold flat on the fuselage, parallel to each other. This configuration requires a double hinge mechanism for the wing that folds on top of the other one (Fig. 3).

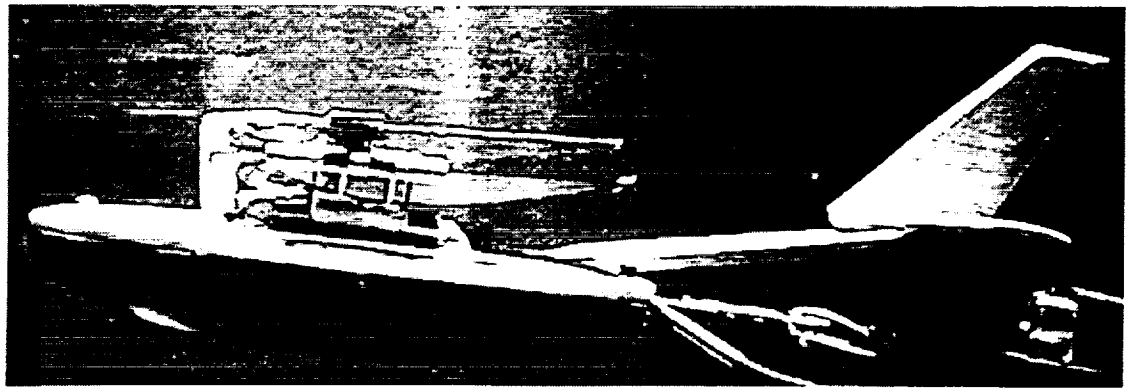

Figure 3: Stowed configuration showing double hinge mechanism

The release mechanism was also designed from a function/simplicity standpoint. The wings were held in the stowed position by lever arms that were actuated by NiTi shape memory alloy (SMA) electric pistons (see Fig. 4 & 5). The SMA pistons are activated by current, and the temperature change in the NiTi that results causes the alloy to contract in length, providing the linear force to pull the levers. When the alloy cools, it can be moved back to its original shape. The particular pistons used for the wind tunnel model provide about 1 lbf of force.

The fuselage was designed in two halves so that the SMA actuators could be mounted in the bottom half and accessed by removing the top.

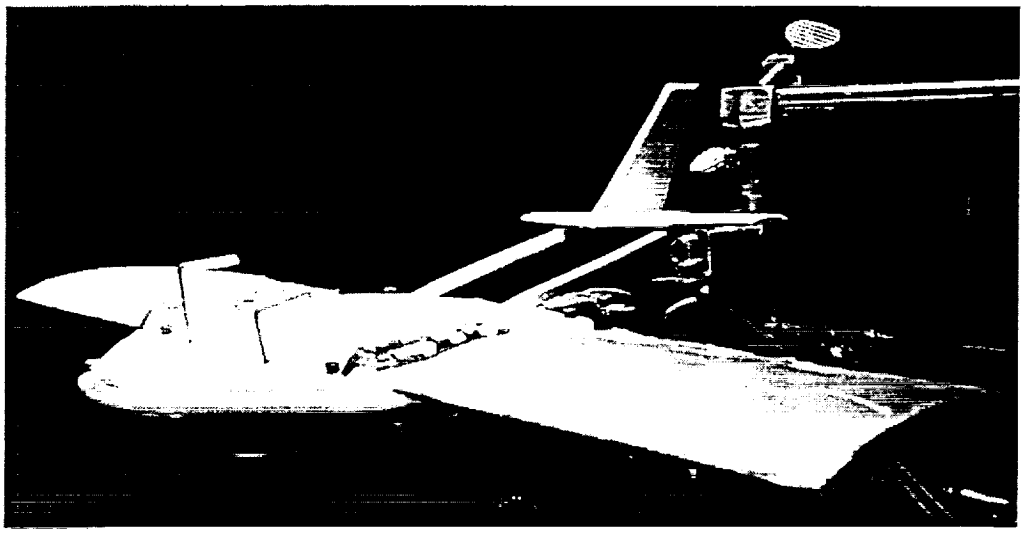

Figure 4: **MARV deployed in the wind tunnel**

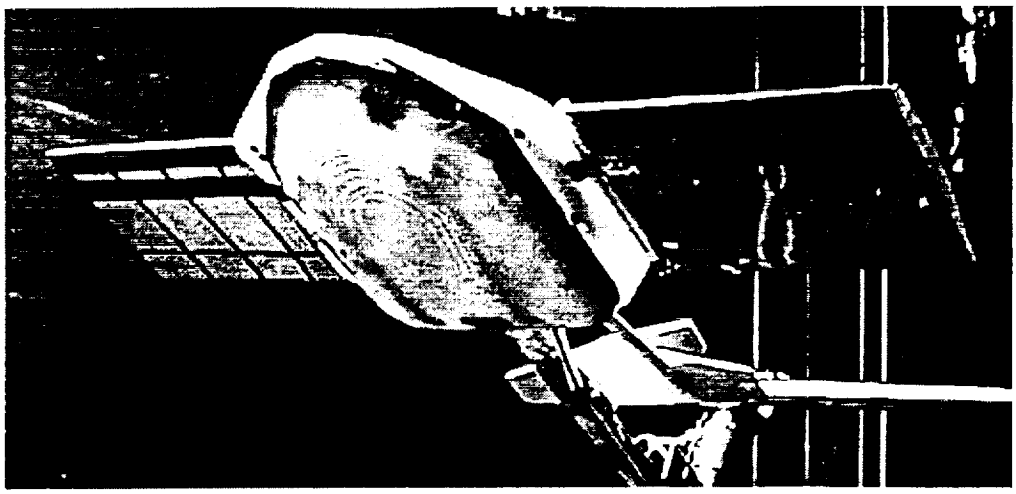

Figure 5: **Wind tunnel model at 45° angle of attack**

Test Article Manufacturing

The entire wind tunnel model and attachment hardware was manufactured by the MARV team at the University of Colorado. The fuselage was processed by a Rapid Prototype Device (RPD) using stereo lithography SolidWorks part files. Each half was processed in about 8 hours running continuously. The tail assembly was made from balsa wood by hand. The wing ribs were cut from maple wood on a Laser CNC to exactly match the Eppler 387 airfoil section (Fig. 5 shows wing ribs and spars). Covering for the wings was MonoKote™ model airplane iron-on material.

Experiment Overview

A pitch test was designed to determine the static pitching moment at angles of attack ranging from zero to 90 degrees (orthogonal to flow). By determining the static pitching moment of MARV at all angles of attack, a prediction of its behavior after aeroshell separation could be made. Additionally, a static pitch test was designed to measure the pitching moment during the wing deployment, to assist in determining pitching trends during wing deployment. A computer model was programmed to model the theoretical pitching moment of the static, deployed MARV at angles of attack up to 90 degrees, for comparison purposes with the measured wind tunnel data.

Experimental Setup

The testing was completed in a low-speed wind tunnel, with a 2x2 ft test section. The model was attached to the tunnel via a 15-cm rectangular cross-section, brass sting attached to a cross-flow bar. The sting was instrumented with four strain gauges, which measured strain along the axial direction of the sting. The moment measured at each strain gauge was determined via a calibration curve, created from tests during no-flow conditions. The full-velocity tests were run at 15m/s in both the (wings) stowed and (wings & tail) deployed configurations, with angles of attack varying from zero to 75 degrees.

The pitching moment was backed out of the measurements by taking strain measurements at two different points on the sting. The difference between the strains allowed the pitching moment to be differentiated from the moment in the sting due to the effective tip load (summed lift and weight of the model).

Experimental Results and Analysis

Flutter was encountered at angles of attack approximately 5 degrees on either side of stall, preventing the data precision obtained in other measurements. In the deployed configuration, MARV was found to stall at an angle of attack of approximately 12 degrees above the zero-lift AoA. In the stowed configuration, the stall point moved up to approximately 22 degrees above zero-lift.

The computer model was based on predictions of drag and lift, and is only accurate to use as a reference for pitching *trends*, as the ultra-high angle of attack regions of the model are relatively unexplored in terms of lift

and drag. Functions were developed based on approximate trends to model the lift coefficient and drag coefficients at angles of attack above stall. The computer model was based upon MARV dimensions, and flow characteristics present during the wind tunnel testing, for the sake of comparison with the measured data.

The model shows stable pitching trends from zero degrees up to stall, neutral pitch tendencies up to nearly 30 degrees AoA, and unstable pitch tendencies at higher angles of attack. These trends can be seen in Figure 6. The wind tunnel data obtained shows different pitching trends from the theory. The data shows unstable pitch tendencies throughout the range of angle of attack. The comparison between the wind tunnel data and the computer prediction is shown in figure 6.

Due to the aforementioned flutter at angles of attack around stall, the data in this range have a large uncertainty associated with them, which accounts for some of the discrepancy between the theoretical and predicted models. Additional error was encountered at large angles of attack because the flow over the tail was disturbed by the sting attachment prior to reaching the tail. This disturbed flow drastically reduced any lift acting from the tail, which would have helped to stabilize the aircraft. The model itself was comprised of many approximations, and, as previously stated, the figure below provides trends of the data and prediction.

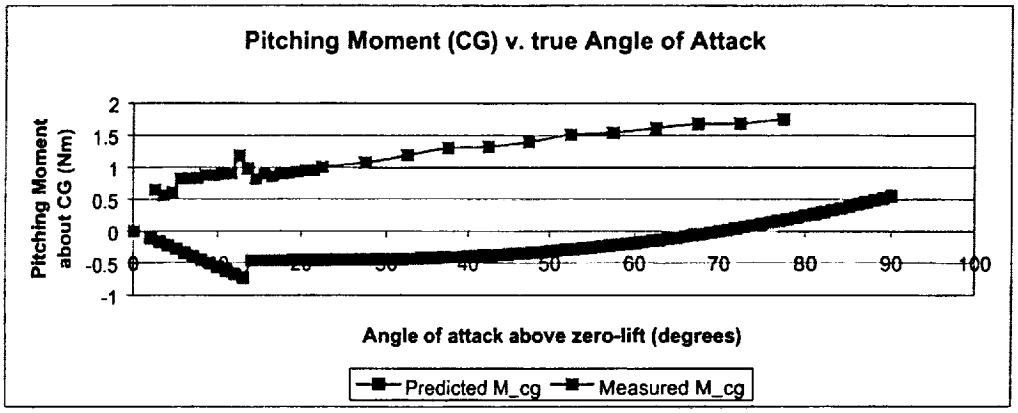

Figure 6: Measured and predicted pitching moments about MARV cg

The instability in the wind tunnel testing is likely due to two factors: the first is that the contribution of the body to lift was neglected, when it was found to represent a significant portion of the total lift. The second factor is that the tail was not sized for stability purposes in the MARV design. Contributing further to this factor is the disturbed flow from the sting, which was seen by the tail at high angles of attack.

The instability encountered in the wind tunnel testing would result in a massive pitch up moment during the wing deployment of the MAP, possibly sending the aircraft into an unrecoverable spin. Redesign of the MAP would be necessary to provide a large pitch down moment, even at ultra-high angles of attack. This negative pitching moment would serve to place the MAP into a dive, which would provide stability during the pull-out maneuver and engine firing. This pitch down moment would partly come from the separation springs in the aeroshell, and could be increased by increasing the tail size. Also, moving the cg forward would ensure dramatic stability increases.

ELECTRONICS SYSTEM:

The electronics system also known as the Control and Sensing System (CSS) is the integration point between the MARV flight software and the MARV plane (Figure 7). The main goal of the CSS is to control the deployment of the wings of the MARV plane when signaled from the flight software. The CSS also controls the position of the video acquisition unit. The CSS is best explained if broken into four subsystems; the micro-controller, the serial interface, camera controller, and the power amplifier.

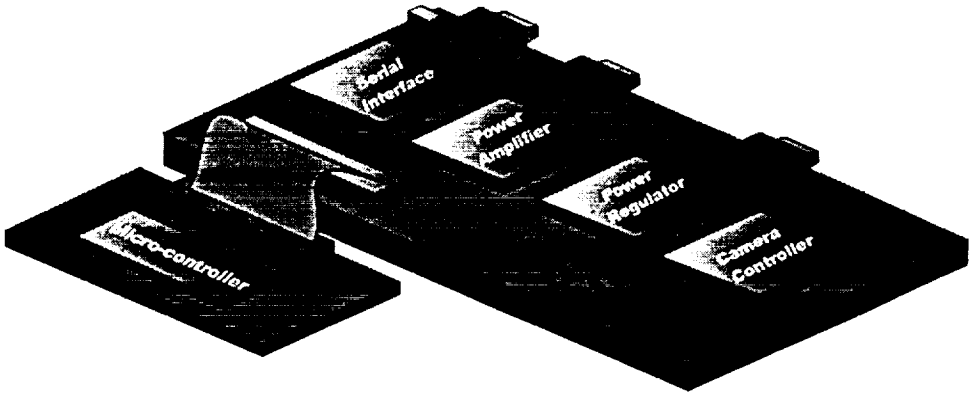

Figure 7: Control and sensing System (CSS)

Micro-controller

The micro-controller is the brain of the electronics system. The micro-controller must be capable of converting an acsii signal from the flight software into a TTL voltage level that will control the other subsystems. It was found that the best suited micro-controller for this project is the OOPic from savage Innovations (Figure 8). The OOPic is the first micro-controller that uses an object oriented programming language. The ease of programming in an object oriented language drastically reduced the programming time and allowed more time to be devoted to the actual electronics. The OOPic communicates with the flight software, which is located on a x86 target running VxWorks through a RS232 serial connection. The control and sensing system (CSS) recognizes acsii character sets sent by the VxWorks target. The communication between the target and the CSS is separated into three parts:

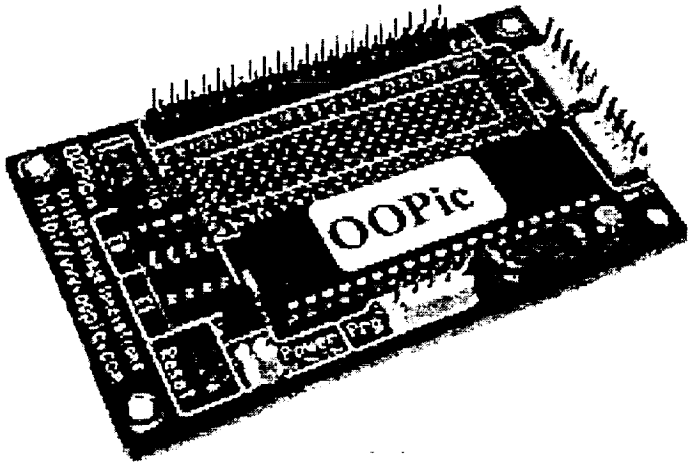

Figure 8: OOPic Micro-Controller

Initiation sequence:
On power up the CSS sends the target:

Ok
&

Upon the reception of "&" the CSS is ready to be controlled.

Camera control:
Camera control is the following:

>xxzz

Where acsii character ">" activates the control routine. Pan is controlled by "xx", which represents a two digit decimal number. Tilt is controlled by "zz", which also represents a two digit decimal number.

Pan values range from 10 (right limit) to 52 (left limit), with the value 31 being the center of rotation. Tilt values range from 10 (top limit) to 52 (bottom limit), with the value 25 being parallel to the base. Each character is echoed back to the target after being processed by the CSS.

Deployment Control:

Deployment control is the following:

>d (to start deployment)

s (to stop deployment)

Where acsii character ">" activates the control routine, and the acsii character "d" commands the deployment of the wings.

Each character is echoed back to the target after being processed by the CSS. The character "s" will be echoed when the CSS stops supplying power to the Signiture Memory Aloys (SMA) which deploy the wings of the MARV plane.

Serial interface:

The serial input and output signals from the OOPic are TTL level signals providing 0 and 5 volts. The TTL signals from the OOPic must be converted to +/-12 volts to register as serial communication on the VxWorks target. Conversion to RS232 signals was done with the MAX203 a TTL to RS232 signal converter chip, which will provide the voltage conversion to +/- 12 volts as well as providing the required signal inversion. The MAX203 is connected to the OOPic though I/O lines 22 and 23. The data transmitted by the OOPic is sent serially through the UART's transmit line located on I/O line 22. Data is received by the UART through the receive line located on I/O line 23.

Camera Control:

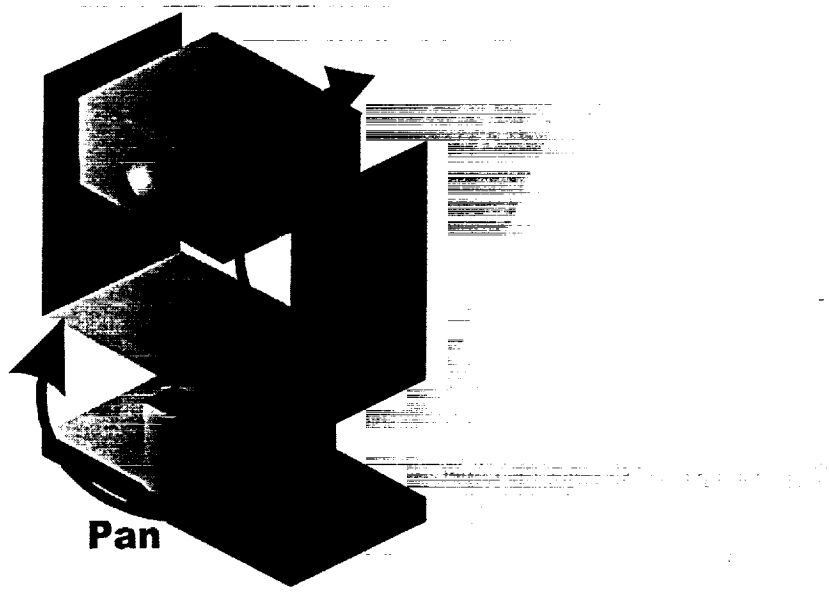

Figure 9: Camera control assembly

The camera control unit controls the tilt and pan rotation of a NTSC digital video camera (Figure 9). Two hobby servos are used to rotate the camera. The OOPic sends a Pulse Width Modulated (PWM) signal from I/O lines 31 and 30. By modulating the width or the pulse sent to the servos the servos can be precisely positioned to the desired location. The signal from line 31 controls the pan variable of the camera and the signal from line 30

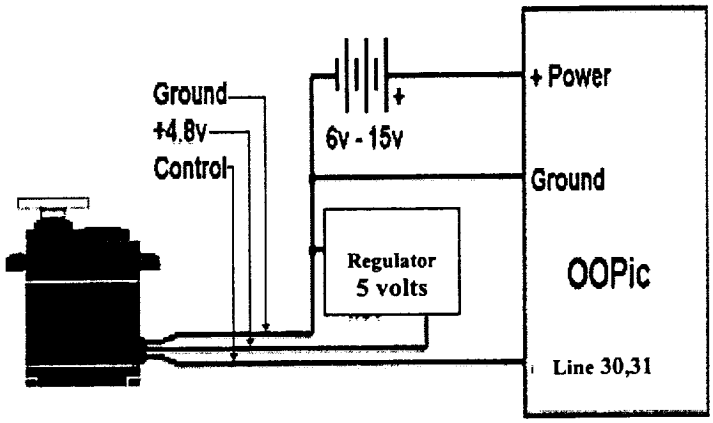

Figure 10: Servo connection diagram

controls the tilt variable. Since the OOPic can only source 0.20 amps an external driver is needed to power the servos, this is done by using an LM780 to convert the 12 volt source used by the deployment controller to a 5 volt, 1 amp source to drive the servos (Figure 10).

Deployment Control:

The deployment of the MARV plane wings is controlled from the OOPic's I/O line 15. The signal from the OOPic is TTL and can only source 0.20 amps, while the SMA's used for wing deployment call for 10 amps. Therefore there needs to be additional circuitry to provide the 10 amps needed to deploy the wings. To source the power needed to provide the 10 amps two 12-volt dry cell battery are used. The TTL signal from I/O 15 of the OOPic is used to switch a relay, which closes the loop and allows the SMA's to draw 10 amps from the batteries. LM338s are used to regulate the current flowing from the batteries so that only 5 amps go to each of the SMA's.

MARV SOFTWARE

As with any advanced flight system such as the MAP, which requires various modes of operation, communication between components, and the ability to be reprogrammed after launch, one of the core underlying systems is the software. For a system such as the MAP, software is preferred, if not necessary, to perform such functions as real-time control and data processing. For the MARV project, only a subset of the MAP software architecture was necessary. When possible, the software for MARV was designed to implement the actual mission requirements as much as possible. The subset of functionality that we chose to design and implement involves the deployment system, the video imaging system, and the core software required to schedule multiple tasks, control the timing of mode transitions, and telemeter data. The way in which our software system fits into the system level data flow can be seen from the following diagram:

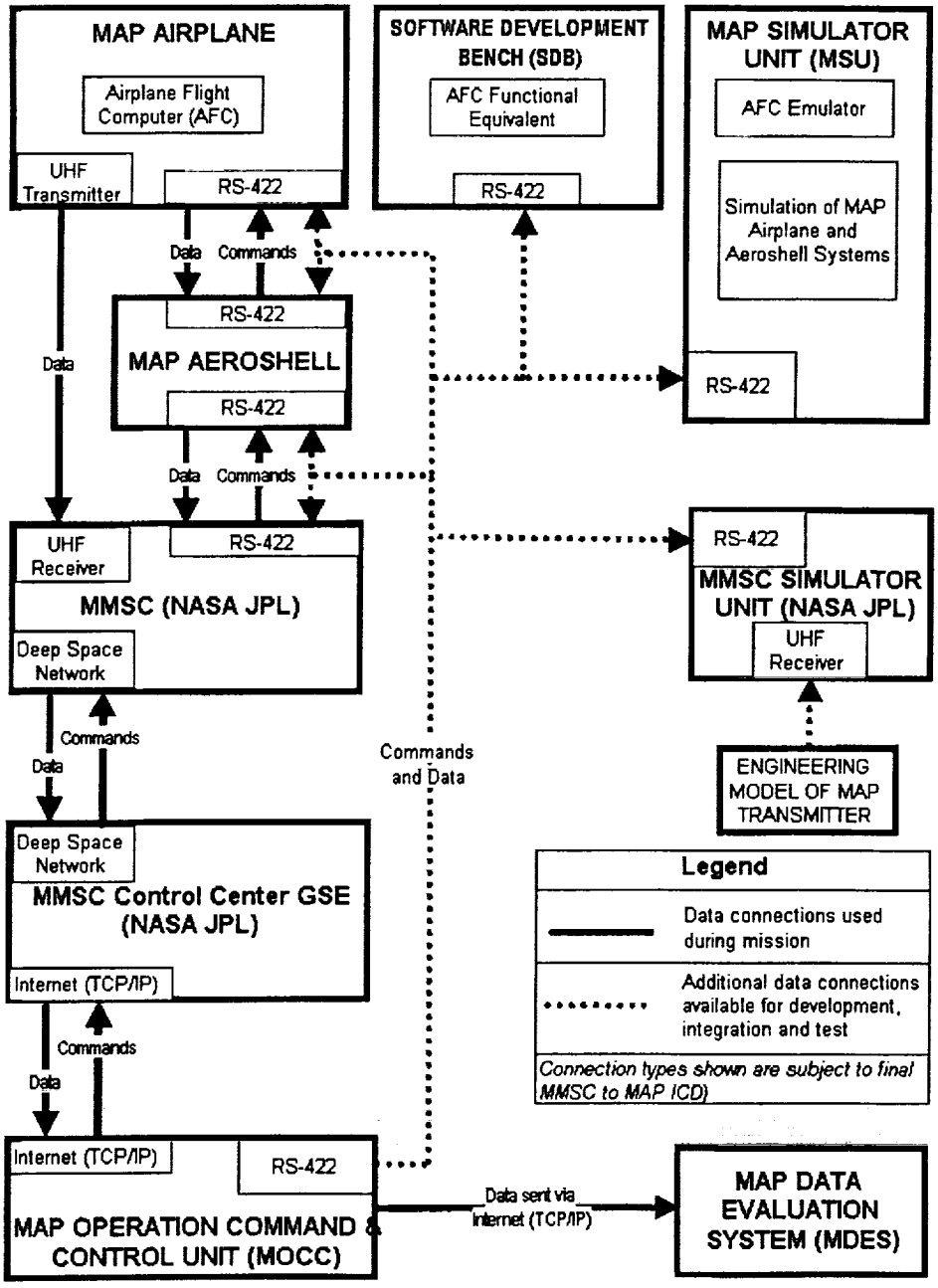

We are running the AFC software on a x86-based computer using the COTS real-time operating system VxWorks. We are connecting the AFC directly to the MOCC, which is a Unix application running on Solaris. The MDES is a Java applet, which can run on any host.

Imaging is a major focus of the MAP mission. Partly to address this important area, MARV has also focused on imaging. The Airplane Flight Computer (AFC) acquires image data (frames) and sends them via the MAP Operation Command and Control System (MOCC) to the MAP Data Evaluation System (MDES). One purpose of choosing video imaging was to explore the usefulness of a compression algorithm that only sends data that has changed since the last frame was sent.

For frame acquisition, we purchased a Hauppauge WinTV camera and framegrabber card based on the bt878. This affordable COTS solution has the benefit of available Linux drivers. Our first plan was to write a VxWorks driver for the card and acquire frames locally. When completing the driver became unfeasible, we resorted to doing the frame acquisition on a Linux x86-based computer. The frames are sent from the Linux machine to the AFC via a TCP/IP socket. In the AFC software, the frame grabber driver provides a top half interface as if the frames were acquired locally but the bottom half of the framegrabber driver actually receives the frames via the socket connection. On the AFC, a video imaging task consumes the frames by performing the change-only compression algorithm and sends the resulting data to the telemetry task for delivery to the GSE.

The idea of a change-only compression algorithm was explored by the MARV team in an attempt to reduce the amount of image data that would need to transmitted. The basic principle involved in this algorithm is that it is only necessary to transfer the data for a pixel if that pixel has changed since the last frame. The pixel is determined to be changed if the numerical difference is exceeds a predefined threshold. There is a tradeoff, however, between sending only the changed pixels and just sending the entire frame because when there are a large number of changed pixels, the amount of data that would need to be transferred would actually be greater than that for a normal full frame. This is because when a full frame is sent, it is not necessary to send the locations for each individual pixel because they are sent in order, without skipping any pixels. When sending the change-only data, however, the pixel location along with the actual image data needs to be transmitted. In our algorithm, we encode the location in 17 bits (for 320x240 pixels) for both color and grayscale modes. For the color mode we encode each of the three color components in 5 bits for a total size of 32 bits. For the grayscale mode, the lone intensity value is reduced to 7 bits for a total size of 24 bits.

The achitecture of the software was designed for the MAP mission. A subset of this achitecture has been implemented for the MARV project. The following modules have been implemented for MARV:

Application : Mission Operations : Mode Management

Application : Mission Operations : Deployment

Application : Science : Video Imaging

OS : I/O : Digital I/O

OS : I/O : Framegrabber

OS : I/O : Ethernet (instead of UHF / RS-422)

OS : Utilities : Time Tag

OS : Utilities : Task Manager

OS : VxWorks (configured)

A diagram of the core software architecture can be seen below. It illustrates the dependency hierarchy; os/utils are not dependent on application modules etc. As listed in the previous section, only some of the units on the core software architecture diagram have been implemented for MARV.

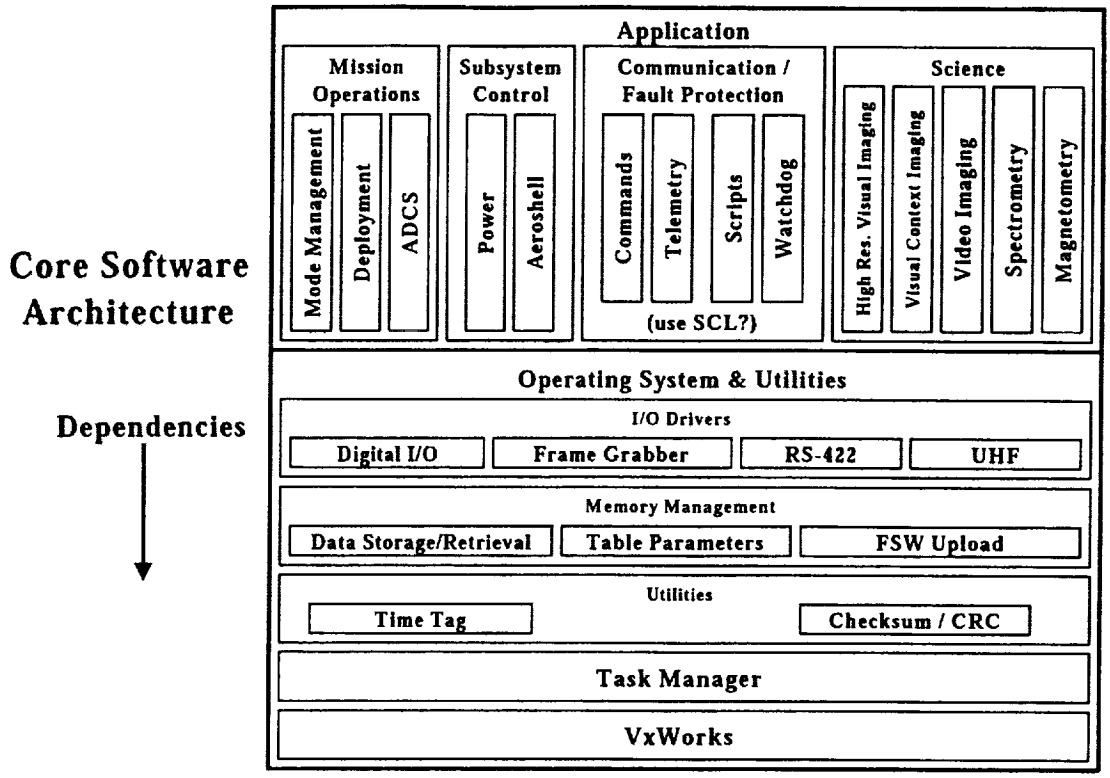

Another important figure from the detailed design of the AFC software is the task level data flow seen here:

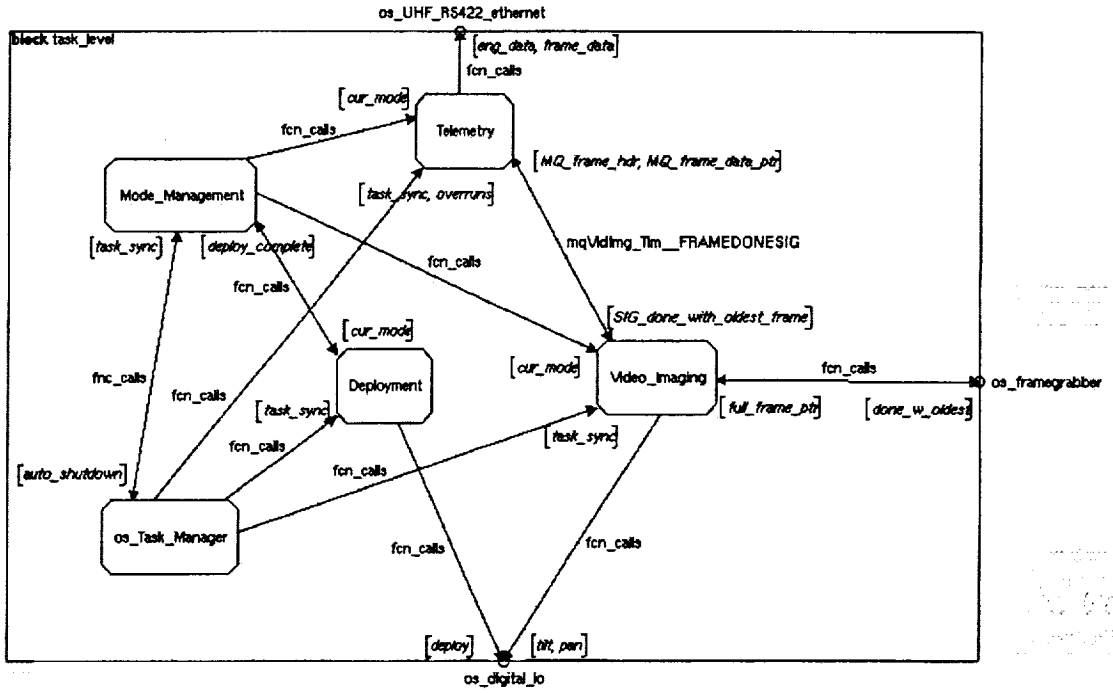

This figure illustrates the data flow and relationships between all of the MARV AFC tasks. The external interfaces to the AFC are via the ethernet, framegrabber and the digital I/O.

The mode management task controls the mode timing and transitions between the following major modes: Manual, Aeroshell Deployment, Airplane Deployment, Level Flight and Final Flight. It provides the current mode to the other three aplication tasks. The deployment task handles the timing and commanding to control the airplane deployment sequence. The telemetry task gathers data from the other tasks and sends the engineering and frame data to the Ground Support Equipment (GSE). The video imaging task, as discussed previously, receives data from the framegrabber driver, performs the change-only compression algorithm and sends the data to the telemetry task. Actually, only pointers to the large image frames are sent between the tasks. Telemetry task receives a frame header and a ponter to data. The pointer is either to compressed data or a full frame. When done transmitting a frame, the telemetry task signals the video imaging task to announce that a frame can be discarded.

We also chose to focus on the GSE side of the mission and in particular the MDES. Connecting to the GSE to send command and control data to the MMSC is the MOCC. While we did not focus on the commanding of the MAP via the ground station, another responsibility of the MOCC is sending the MAP data sets to the MDES via internet. In our system, the MOCC connects directly to the AFC via a socket connection, and passes on all the data it receives from the AFC to the MDES. In both the mission requirements and our implementation, MDES is then responsible for reconstructing the MAP science and engineering data to its original form, displaying it, as well as storing it for later retrieval.

In our implementation, the MDES is a Java applet that is accessible via the Internet. Most web browsers currently cannot view it because they only support Java 1.1.5 at the latest, while the MDES includes classes from Java 1.2. Java's appletviewer is a viable alternative, however, and can be easily installed by any user.

The applet can retrieve its input data from any of three source types, depending on the parameters it is passed. The first such method is to make a socket connection to the MOCC in which, the data is input and processed in real-time. If the MDES gets behind in reading the data, the MOCC will drop data that it is unable to write to the socket, but the system is setup the reduce the possibility of that situation occurring. While in the socket mode, the MDES writes all the data that it reads to a file on the applet server, which can be accessed and replayed using one of the other two methods. Since the second and third input methods involve reading from stored data files, they are therefore not real-time like the previous method. Playing the frames back with the same frequency as they were recorded was not accomplished, but MDES does attempt to maintain accurate timing. These two methods get an input data stream from a URL and a local file, respectively, but do not store anything. The URL method works effectively while working on a high-speed network, but generally it is preferred to store the data file locally, and use the third method.

Once a data input stream is started for each of the three methods, the subsequent execution of the applet is virtually identical, disregarding any waits associated with reading the actual data. Each packet that is sent by the AFC contains a sync pattern that the MDES locates to synchronize itself. After reading the pattern, the MDES reads in the various engineering and science data from the packet header, which it will subsequently display for the user. If an image frame is included, it will use that data to update the video image viewer, reading either a full frame or decoding the change-only data. As stated, if the applet is reading from a socket it will then store the data for each packet to a file on the applet server.

The appearance of the MDES can be seen with the following screen shot:

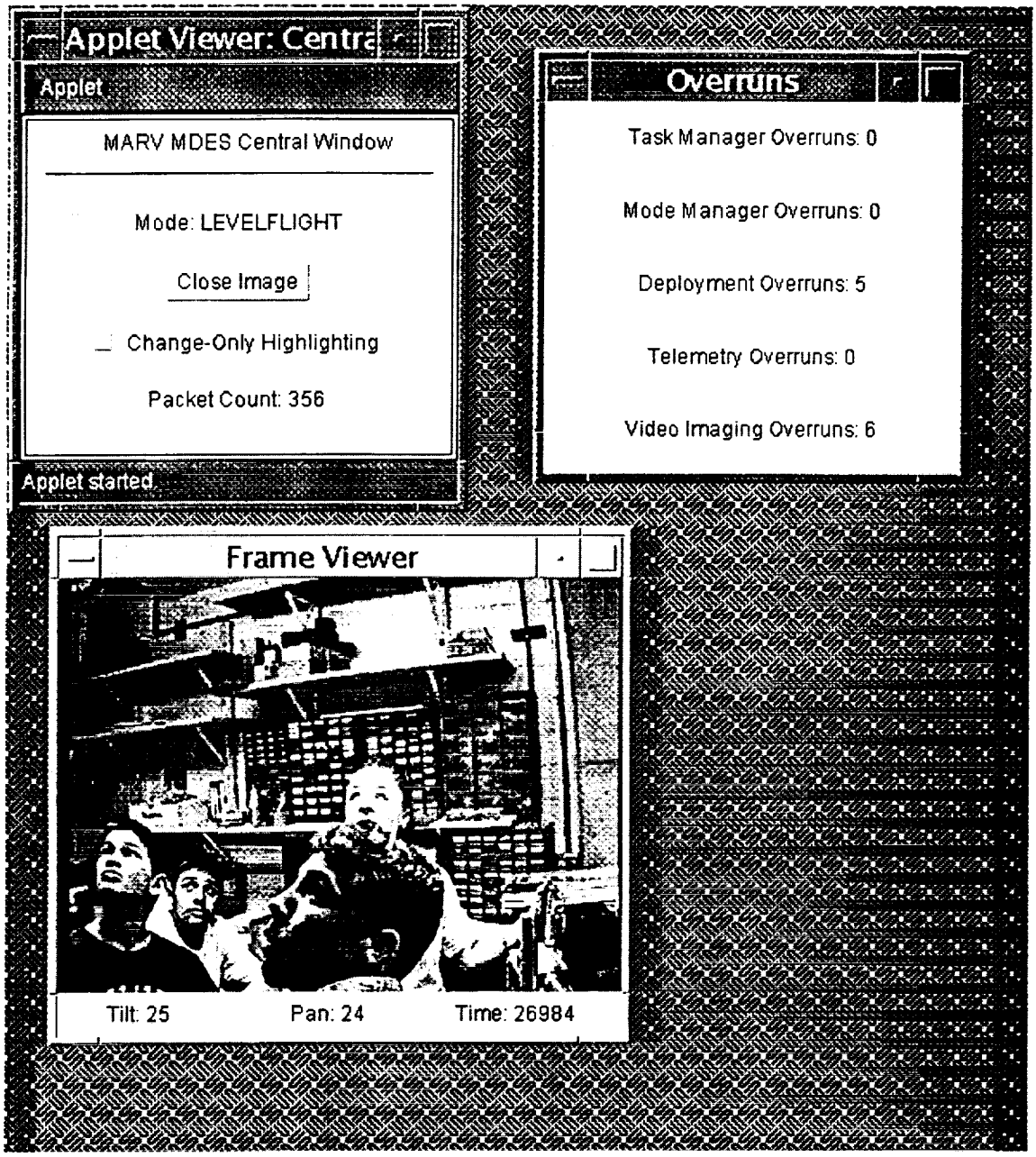

One additional feature of the MDES display that needs to be described is the "Change-Only Highlighting" checkbox. With this component, the user is allowed to highlight the pixels that were sent as change-only data. Besides being an interesting feature, this component proved value in the process of designing and implementing the pixel compression algorithm, and gave a feeling for how much data reduction was being achieved. When the right balance was achieved, only pixels for objects on the screen that were moving would be sent.

Although there are sometimes limitations in execution speed by using a Java applet, it was a fairly easy platform choice. The two obvious factors that played into the decision were the portability achieved by using a Java implementation, and the ability to run the MDES from any computer on the Internet.

The system we created is limited by various factors inherent in our design choices and our execution environment. The first such limitation is caused by the 10 Megabit Ethernet network in which the targets are

located. Due to the high amount of data that we attempt to transfer in real-time, a faster network would possibly have allowed for a higher frame rate, closer to what was included in the original requirements for the MAP. While such an increase in network bandwidth would have allowed the Linux / VxWorks / Solaris machines to perform at closer to their processing capabilities, other factors involving the displaying of the video would also have come into play. Due to limitations in Java's execution speed as well as the inherent overhead in actually sending the video data to the user's screen, it is uncertain what the peak level of data rate / frame rate would be within our system.

Structured software engineering methods were followed in the development of the MARV software. We began with a requirements definition based strongly on MAP documentation from NASA Langley. High level design was completed along with various design reviews. During implementation, modules were incrementally tested and code reviews were conducted. We used the configuration management software CVS (Concurrent Versions System), which provides an unreserved checkout mechanism that facilitated simultaneous work on the software system.

CONCLUSIONS

Wind tunnel testing was completed of a 1/4-scale model of the Mars Airplane (MARV), and the pitching moment was compared to a computer model prediction. The predicted pitching moment was found to be stable up to stall, and unstable at higher angles of attack. The wind tunnel data, however, showed static instability at every angle of attack from zero to 75 degrees. This instability is likely due to insufficient area in the horizontal stabilizers, as well as disturbed flow over the tail during testing. Further instability is due to the neglect of body lift in the predictions, as well as an aft cg position. This instability should be overcome through an increase in tail size, a forward movement of the center of gravity, and the use of separation springs to impart a downward pitching moment during aeroshell separation.

OUTREACH ACTIVITIES

The environment of the Senior Design Lab (SDL) class promoted outreach to other engineering students, industry, and the community. As students who participated in SDL, we were required to give multiple presentations pertaining to the progress of our project including a Conceptual Design Review, a Preliminary Design Review, a Critical Design Review, and a Delta Critical Design Review. These reviews were presented to other engineering students in the SDL class (approximately 50 students), faculty advisors, and the Engineering Advisory Council (EAC). The EAC consists of variety of engineers from industry that advise the College of Engineering on multiple issues regarding academics, student life, funding sources, and leadership organizations.

This spring two groups of students toured our laboratory facilities and were exposed to our design project. The first group consisted of approximately 150 high school students from disadvantaged areas in Colorado. Group number two was comprised of middle school students from both urban and rural areas. These students received a brief overview of the MARV project and a demonstration of the digital camera ability. The picture below (taken with the digital camera and captured with the MDES) shows part of the middle school group that toured our labs.

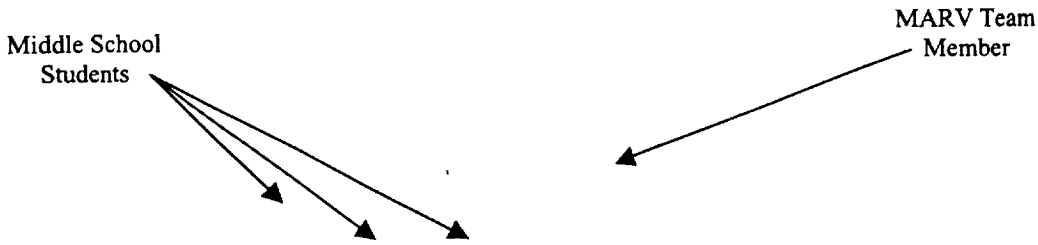

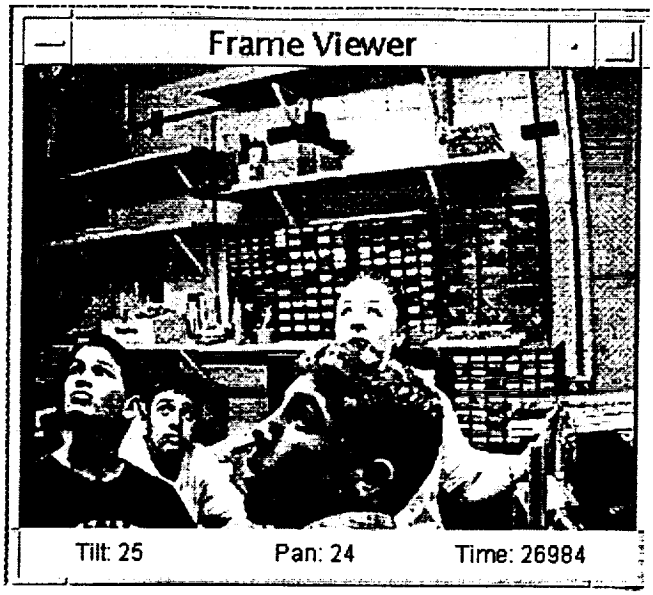

Finally, each spring during Engineering Days (E-Days) the University of Colorado Engineering Council (UCEC) sponsors a Design Expo. The MARV team attended this years expo which was held on April 29, 2000. This expo was open to all engineering design teams including chemical engineering, freshman projects, mechanical engineering, aerospace engineering, computer science, and electrical engineering. The community and industry representatives were also invited to attend the expo, and this year approximately 600 people attend, ranging from children to parents and from faculty to industry leaders.

Project Magellan: First Human Circumnavigation of the Moon

University of Maryland, College Park
Department of Aerospace Engineering Undergraduate Program

Jhason Abuan, Jorge Aviles, Ryan Dickson, Oscar Hsu, Michael Kessler, Mehdi Khoali, Daniel Maloney, Karen Mitchell, Nicholas Patregnani, Peter Pawlowski, Lisa Policastri, Jonathan Quigg, Robert Reed, Molly Simmons, Diane Thies, Paul Timko, Kevin Turner, John Van Eepoel, Rommel Zara

Advisors: Dr. David L. Akin
Dr. Mary L. Bowden

Abstract

This report summarizes a single-semester team design effort for human circumnavigation of the moon. The initial design constraints included the goal of performing this mission within a single local day to take advantage of solar power. Details are presented on the rover system, which was designed to support three humans for a 35 day mission around the moon with a 7 day contingency, traveling at an average velocity of 17.6 km/hr while stopping three hours/day to perform extravehicular surface science. The final rover design is 12 meters long by 5.2 meters in height, with a total mass of 10,000 kg. The power requirement of 35 kW for propulsion and life support is supplied by a 100 sq.m. solar array, articulated to track the sun within 30deg of the local vertical. Detailed analysis is presented in the areas of life support and habitability, power, propulsion, thermal analysis, avionics, structures and mechanisms, and systems integration. Scenarios are presented for building and deploying all systems to the lunar surface, with the goal of a complete surface navigation in 2009. The final cost of $12.2B is approximately 1/8 that of the Apollo program in constant dollars, while providing extended science investigations around the equator and including the first detailed exploration of the far side.

1 Introduction

December 2009. Two astronauts gaze across a flat white plain. Beyond, the earth hangs suspended in space like a glistening sapphire on a bed of black velvet. Much like the pioneers of the late 19th century that heeded the call of manifest destiny and opened up the uncharted regions of America's West, these astronauts take the next steps on mankind's quest to colonize the last great frontier: space.

The covered wagon of yesteryear becomes the lunar rover of the future. Project Magellan, an innovative, unprecedented mission, will take humans beyond the limits of any previous manned program. Like the explorer it is named after, our rover will circumnavigate a heavenly body. But unlike Magellan, who proved without a doubt that the Earth is round, we will circumnavigate the moon. No human being has ever set foot on the far side of the moon; what limited knowledge we currently have comes from thirty year old fly-by data. What follows is a detailed analysis of the Magellan Rover and its mission.

2 Surface Mission

2.1 Route Design

Feasibility of a lunar rover mission is a function of design constraints of an acceptable lunar route. The route (see figure 2-1) follows the following mission design requirements:

- ?? Land at lunar dawn
- ?? Remain as close to an equatorial profile as possible
- ?? Safe abort of the crew at any point enroute
- ?? Maintain visibility with the sun at all times
- ?? Daily 3-hour EVA (21 hours of driving time)
- ?? Maximum long-term[1] climbing slope of 20°
- ?? Circumnavigate the moon with a 4-day contingency

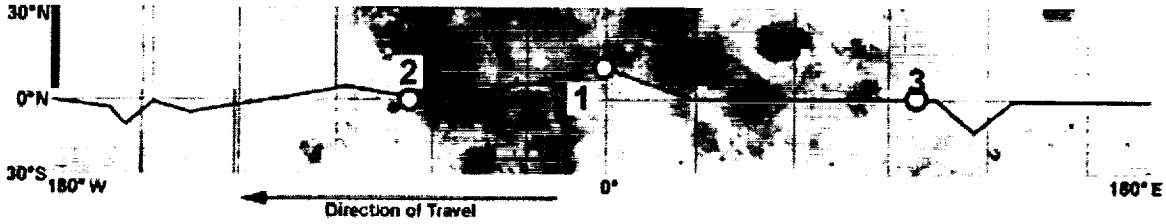

Figure 2-1: Lunar Route. Point 1: Landing at 0°W,14°N. Point 2: Entrance into highlands (1.3° c limbing slope for 150 km). Point 3: Exit from highlands (0.03° descending slope for 3000 km).

Ideally the rover should travel at 17.6 kph to minimize changes in sun elevation through the entire route. However, power design constraints to climb from the mare to the highlands (a 1.3° long-term slope) as well as short-term[2] climbing slopes within the highlands forces the rover to travel at a maximum of 13 kph while on the far side of the Moon. To accommodate for the forced slower speed, a route velocity profile has been developed (see figure 2-2).

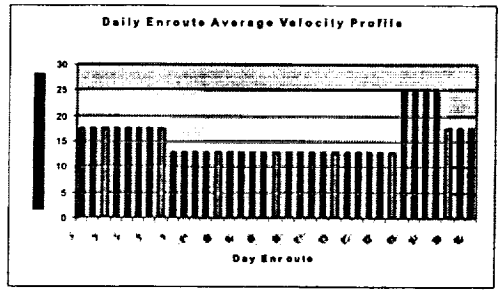

Figure 2-2: Daily enroute average velocity to meet sun elevation requirements.

A result of the route velocity profile is the daily route sun elevation profile (see figure 2-3). While the sun is directly overhead (see figure 2-4) it will prove difficult to distinguish terrain features with the naked eye. This unavoidable situation requires the rover to be able to navigate via remote sensing.

The derived mission length as a function of the velocity profile is 38 days. This allows a full circumnavigation of the moon within 35 days. An initial 2-day period is allotted for the rover crew to become acclimated to the environment as well as maneuvering the rover. A final day is allotted for the crew to prepare for launch. This route design allows a 4-day contingency to complete the mission.

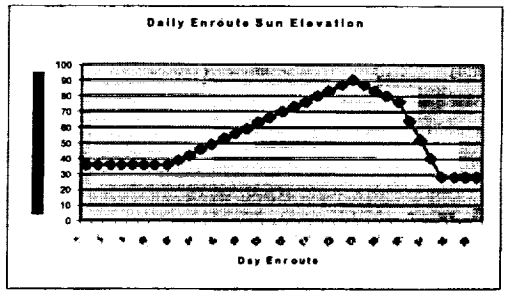

Figure 2-3: Corresponding sun elevation during each mission day.

The current route design allows periods of deviation up to 14° latitude from the equator to avoid large known obstacles. Therefore, the contingency vehicle and launch vehicle that must dock with the Command Module in orbit needs to carry enough fuel to make a 0.4 km/s plane change delta-v.

The route consequently drives requirements for systems to operate the rover (see table 1). The systems that operate the rover abide by these driven requirements and prove that the circumnavigation of the moon by the Project Magellan rover with these set design constraints is feasible.

1 Long-term climbing slope is a slope that the rover can climb with full power until the sun elevation changes to cause reduced power and force the rover to fail.

2 Short-term climbing slope is an uncharted climbing slope expected to be no greater than 45°. The rover can climb these slopes, but only for finite time.

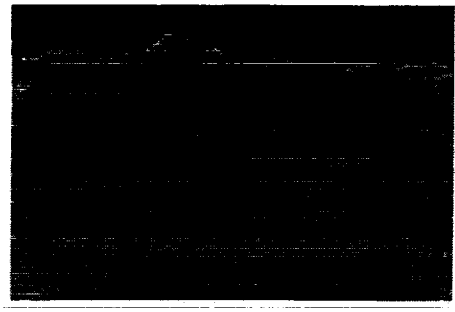

Figure 2-4: Image generated with sun elevation at 90° showing total shadow washout.

Table 1: Affected requirements, features, and systems by route design.

Derived Requirement	Driven Feature	Driven Rover System
1.3° climbing slope for 150km to enter highlands	Propulsion power	Power, Propulsion and Thermal
0.03° descending slope for 3000km to exit highlands	Regenerative braking	Power, Propulsion and Thermal
14° maximum deviation from equator enroute	Delta-V requirements to plane change	Contingency Vehicle
90° periods of sun elevation	Navigation by remote sensing	Avionics

2.2 Science

The unique advantage of Project Magellan is that it is a sustained, manned lunar mission. Never before has a manned lunar mission been capable of circumnavigating the moon. Previous lunar missions have been isolated to specific small regions near their landing site where geological sampling has been done and have only lasted for a few days. Therefore, it would only be obvious for the science during Project Magellan to focus on geological experiments.

The main purpose of geological sampling on the lunar surface is to more accurately develop a geological profile of the lunar surface. Invaluable data collected from the circumnavigation of the moon will be correlated with state-of-the-art Lunar Prospector and Clementine data. Due to equipment limitations of on-orbit remote sensing of the lunar surface, core samples will be taken at every EVA location to a depth greater than 0.5m. At six specified locations, a Lunar Surface Science Package (LSSP) will be deployed. The LSSP will be powered by a Radio-isotope Thermal Generator (RTG) so experiments can be conducted Earth-side without supervision by the rover crew. Experiments conducted by the LSSP include measurements of:

- ?? Lunar magnetic field
- ?? Suprathermal ions
- ?? Subsurface thermal temperatures
- ?? Lunar atmosphere
- ?? Gravity
- ?? Surface neutron flux
- ?? Each individual Apollo mission returned about 130 kg of lunar samples and one surface science package (isolated to a single landing site). Project Magellan will return 500 kg of core and rock samples and deploy six LSSPs about the entire lunar surface and not just a single location.

Even though in recent years, state of the art equipment has orbited the moon and done extensive surface mapping and scanning for water ice and elements, non-invasive science from orbit can only penetrate the surface so far. For example, the gamma-ray spectrometer on Lunar Prospector could only penetrate approximately 0.5 m beneath the regolith. This means that anything beneath this depth is completely undetected, and we may be missing important information about the elements on the moon. The only way to accurately determine what elements there are on the moon will be to go there on a sustained mission with Project Magellan.

3 Rover Overview

3.1 Launch Vehicle Selection

The Space Shuttle was selected as the launch vehicle because it has a payload capacity of 25000 kg, a payload bay dimension of 4.57 m diameter and 17 m length, and the assembly infrastructure is already present.

3.2 Locomotion Method

Two methods were considered: tracks and wheels. Other methods such as legs and hoppers, did not fit the mission requirements or were impractical for this environment.

Wheels have been used successfully on both Lunokhod and Apollo missions [1]. Wheels have a lower number of moving parts when compared to tracked vehicles, making maintenance easier. One primary concern with locomotion deals with conducting repairs while on the surface. It is easier to replace a wheel then it is service to a track while in an EVA suit. For these reasons, wheels were the logical choice.

3.3 Failure Mode Analyses

Two types of failure modes may occur. A Nose-In Failure (NIF) occurs when the front end of the vehicle makes contact with an obstacle. Based on the derived requirements of Mission Planning and Analysis (MP&A), the maximum slopes encountered on the route are no more than 30 degrees and maximum obstacle clearance of 1-meters. From this requirement, the maximum distance from the front end of the vehicle to the front wheels can be no greater than 1.1-meters.

The second failure mode, Hang-Up Failure (HUF), occurs when the underside of the vehicle makes contact with an obstacle. This can occur along the length of the vehicle (Longitudinal HUF) or along the width of the vehicle (Transverse HUF). To clear 1-meter obstacles, the distance between the ground and the underside of the vehicle must be greater than 1 meter. To prevent Longitudinal HUF, the distance between adjacent wheels cannot be greater than 4.8 meters; and to prevent Transverse HUF, the distance between pairs of wheels cannot exceed 4.3 meters.

Tipping will occur at 30 degrees if the center of mass is greater than 4.74 meters from the ground and sliding will occur at angles greater than 38.70 degrees assuming a coefficient of static friction of .8.

3.4 Steering Method

Two steering methods, Ackerman and Slip, were considered. Ackerman steering is used in automobiles and based on the premise that the inner tire turns more than the outer tire, the angle each tire makes is known as "Ackerman Geometry".

Slip steering, the wheels on the left side of the vehicle can run at different speeds and possibly different directions than the right side. This configuration imparts a lateral load to the wheels.

The method of choice is a modified Ackerman steering method. Ackerman steering is based on turning only one set of wheels, and the rover will be steering all wheels. A control law will have to be developed to determine the necessary angle each tire will need to steer and to determine what situations the wheels will need to be steered. High maneuverability/low speed situations will have all wheels steering. Higher speed situations may only require the front wheels to steer in order to achieve a heading change.

The turning radius of the vehicle is determined using geometry. Since the rover is using all-wheel steering, the turning radius is determined by the wheelbase between the outer set of wheels. The resulting turning radius is 7.1 meters for a single segment vehicle with a wheelbase between outer wheels of 8.25 m and a turning angle of 30 degrees.

3.5 Number of Wheels/Sizes

The number and size of wheels are constrained by several variables including wheel loading, wheel sinkage, size/shape of obstacles, and the size and shape of the launch vehicle. Based on the required obstacle clearing of 1-meter high boulders (from MP&A), the optimum diameter of each wheel is 2 meters. The 12-meter length of the rover bounds the number of wheels. Another factor taken into account is the towing resistance. Towing resistance, as defined by Dr. M.G. Bekker is the resistance in the direction opposite of the vehicle motion due to sinkage of the wheels [3]. From a graphical analysis, 4 wheels with a 4.3-meter diameter minimize the total towing resistance. However, from a practical standpoint, 4-meter wheels will increase the torque requirements on the motors. Therefore, 8 wheels at 2 meters in diameter is the best configuration.

4 Crew Systems

4.1 Crew Cabin

The driving force behind the crew cabin layout is usable floor space, because of the presence of one-sixth gravity. The design must have a clear vertical orientation, unlike the Orbiter. Areas that have high traffic should be kept accessible but out of the way. There are also comfort issues to consider; for example, keeping noisy machinery away from the beds and keeping the food and commode as far apart as possible. Taking all of this into consideration, the design has the steering controls in the front end-cap of the rover. Directly behind that is the sleeping area on one side and the food station on the other. Next to the food station is the ergometer for crew exercise and then on the end of that side is the personal hygiene station including the shower, commode and hand washing station. On the other side of the cabin next to the sleeping station is the storage area. In the storage area will be clothes, towels, personal effects, an extra space suit and spare parts for both the space suits and the mechanical units. Finally at the end of the cabin is the door to the airlock.

Due to the vibrations of driving, the interior environment is expected to be noisy. They must have protection for any noise above 85 dB but can go for 8 hours without protection if the noise is below 84 dB [5]. Types of noise that may be encountered are impulse noise, wide-band random noise, narrow band noise and tones, infrasonic, and ultrasonic noise. Taking all this into consideration, the crew is provided with two-way communication headsets that will allow them to speak with both each other and mission control. The headsets protect hearing up to 140 dB and are multi-channeled so they do not interfere with each other or any of the rover's systems. There is one window located in the navigation station, 1.5 meter long by 1.4 meter high. This window doubles as a last resort navigation window and as a viewing window. The window will be coated on the outside to protect the crew from infrared light and on the inside to reduce reflections and glare.

All navigation, steering, and communication controls are housed in the control station, as well as warning lights. In addition to these warning lights, warnings are sounded in the headsets. The navigation controls consist of a wheel, for steering, and a joystick to control speed, acceleration and braking. The driver will be able to lock in a speed, similar to an automobile cruise control.

Foods is shelf stable and does not require water reconstitution. There is enough food for three meals a day plus snacks per crewmember for 42 days (35 days of the mission and 7 contingency days). Each food locker holds 36-40 meals and weighs 6.4 kg empty and 24.5 kg full, and there is a forced air convection oven for heating food. Beverages are provided in pre-packaged, single serving containers. The crew will choose food and beverages from the basic NASA food list, provided the chosen options meet all the nutritional and caloric requirements of 11.720 MJ per person per day (for an average person of about 70 kg). Nutrition requirements can be supplemented with vitamins.

For personal hygiene a shower, commode and hand washing stations similar to ones found on the space shuttle are provided. Because of the vibrations while driving the crew will need restraints and handles to keep them still while cleaning or using the commode. Cleaning products are provided with low-sudsing, non-toxic, and non-staining properties and. Dry, wet, detergent, and biocidal wipes are also provided. Garbage is stored in two containers: one for wet trash (stored underneath the floor in airtight bags) and one for dry trash (stored in empty lockers in Velcro sealed bags). The waste from the commode is connected to a waste collection system that deals with gas, solid, and liquid waste individually. The gas is sent to filters to remove odor and bacteria, and then mixed with cabin air. Solid waste is stored and liquid waste is sent to the wastewater tank to be processed. There will be no dishwasher and no clothes washer because of their weight and water draw.

4.2 Life Support Systems

Every manned space flight mission has a need for some sort of Life Support System (LSS). Not only does a LSS must be life sustaining, it also must create a working environment that is conducive to high moral and work productivity. A number of factors, such as mission requirements, duration, number of crew, mass and cost constraints determine the type of LSS to be implemented. In this case, the driving constraints were mass and power consumption.

An open loop system capable of sustaining a crew of 3 requires an extraordinary amount of consumables, 2100 kg, mostly from water. Water can be reclaimed from a number of different sources such as urine waste, hygiene waste, and respiration/perspiration from the crew. Figure 4-1 shows the water usage per crewmember on the rover for the preferred closed-loop system.

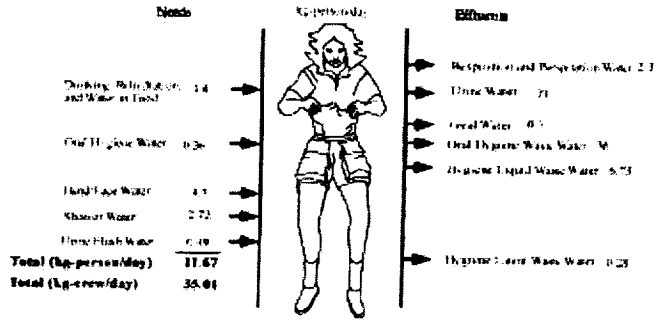

Figure 4-1: Water Usage for the Rover
Adapted From: Wiseland, P., "Designing for Human Presence in Space", NASA RP-1324. pg. 6. 1994

Water reclamation is done using a multifiltration (MF) Unibed ® for hygiene wastewater, and Vapor Phase Catalytic Ammonia Removal (VAPCAR) for urine wastewater. Both devices output potable water for the crew, eliminating the need for separate hygiene and potable water loops.

The crew cabin atmosphere is maintained at a pressure of 55 kPa (8 psi). The pressure was chosen to reduce leakage, exert less stress on the pressurized vessel structure, and to eliminate EVA pre-breathes. At 55 kPa, the O_2 concentration must be adjusted to 40% to maintain unimpaired performance and to avoid hypoxia and hyperoxia. CO_2 levels must be maintained at levels as low are reasonable achievable (ALARA), with a maximum concentration no greater than 1.25%.

A 2 Bed Molecular Sieve comprising of a bed of carbon fiber will be used to extract CO_2 from the atmosphere. O_2 and N_2 will be generated from high-pressure vessels located outside of the pressurize volume. The high pressure at which these gases will be contained at will serve as the means of controlling the associated partial pressures of each of these gases.

The expected 2009 launch date may pose concerns over radiation exposure. Figure 4-2 shows that the launch date will be around a solar minimum. At solar minimum, the solar wind strength is weaker than at solar maximum. Therefore, the solar wind is not sufficient enough to "blow" away Galac tic Cosmic Radiation (GCR). Thus, exposure to GCR will be much more profound during a solar minimum. Another type of hazardous radiation exposure are very powerful X-class solar flares (Solar Particle Events). Instead of adding additional mass to serve as radiation shielding, the interior layout places as much of the existing structure (piping, water tanks, etc.) on the ceiling. This design philosophy, along with coverage of the solar array provides sufficient shielding for the duration of the entire mission.

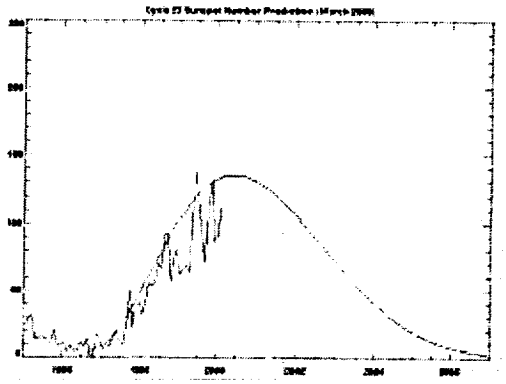

Figure 4-2: Sunspot Number Predictions
From: 2000, www.sunspotcycle.com

4.3 Interior Thermal Control System

The objective is to maintain an ideal cabin temperature of 20~21 C. The total heat generated inside the cabin is about 2000 W. This system consists of 2 condensing heat exchangers that will absorb excess heat and moisture and 2 radiators to dump the heat out. They will be placed on each side of the cabin. Whichever radiator is facing the sun will be turned off while the other radiator will be dumping heat to outer space. Two 60-cm diameter fans will be used to circulate the air around the cabin at a velocity of 0.20 m/s. Each heat exchanger is 2-m long and has eleven 2-cm pipes. Water is pumped at a temperature of 4 C and collects the excess heat from the atmosphere to reach room temperature of 20C. The mass flow rate of water is 0.3 kg/s. The size of each radiator is 6.5 m^2. We are going to use a high emissivity coating to maximize heat rejection: Zn_2TiO_4 pigment plus Potassium Silicate binder e=0.92 with an Aluminum plate of thickness 0.15cm. Two pumps of efficiency 0.7 requiring 9.3 W each are used to pump the water. The total mass of the system is 89 kg and the power requirement is 20 W.

The interior thermal control system maintains a cabin temperature of 20-21°C. The total heat generated inside the cabin is 2000 W. Two heat exchangers absorb excess heat and moisture; each is 2-m long with 11 2-cm diameter

pipes. Water pumped at 4 °C flows through the exchangers and radiators at 0.3 kg/s. Two 60-cm fans circulate cabin air at a velocity of 0.20 m/s. Two exterior radiators, one on each side, radiate waste heat to space. If the radiator on one side is receiving too much incident solar energy, it can be turned off, therefore using the other radiator to dump heat. These radiators made of aluminum are 6.5 m^2, coated with YB-71 (Zn_2TiO_4 pigment plus Potassium Silicate binder) to raise emissivity to 0.92. Two pumps (70% efficient), complete the radiator system, each drawing 9.3 W. The total mass of the interior thermal control system is 89 kg with a total power requirement of 20 W.

4.4 Fire Detection and Suppressant System

Eleven detectors are used as part of the fire detection system. It is important that they be mounted away from solar radiation to avoid false alarms and from filters to avoid smoke being absorbed before reaching the detectors. Table 2 shows a list of the detectors that are used.

Table 2: Fire Detection Systems

3 Energy (flame) Detectors	-Detects visible, infrared and ultra-violet emissions. -Detects flames at a distance of 10m -Response time less than 150 milliseconds -Location: Airlock
4 Smoke Detectors	-Detects particles 0.3 microns or larger emitted from burning materials -Detects smoke levels at concentrations of 2.5mg/m^3 -Response time less than 5 sec -Location: 2 in the crew cabin and 2 in the airlock
4 Ionization Detectors	-Detects burning particles 0.3 microns or smaller emitted from electrical fires -Location: 2 in the navigation console and 2 in the crew cabin

The rover carries 12 1-kg containers of Halon, two in the crew cabin and two in the airlock. Two bottles are manually activated and two bottles are automated and linked to an activation system within the detector. The suppressant delivery rate is 0.25lbm/sec (0.1134kg/sec) [2]. Also included are 6 cylinders of pressurized air (~0.081 kg of air in each bottle) to allow breathing for 45 minutes while fighting a fire. The Trace Contaminant Control System will remove any produced substance.

4.5 Trauma treatment [4]

-First aid kit: needles, syringes, local anesthesia, cotton, gauze, Band-Aids, ace bandages, splints, antiseptics (butadiene), ointments (eye patches), hemostatics medications (gel foam), strong pains medications (morphine), first aid for burns, gastro-intestinal medications (Lomotil)
-O_2 airways: Oropharyngeal and Nasopharyngeal airways, nasal canulas, nonrebreather mask to deliver high concentrations of O_2 and endotracheal tube for emergency situations.

4.6 Health monitoring [4]

Apply a small gadget to the index finger to control O_2 saturation. Pulse oximeter (80 beats/min), Holter monitor for heartbeats (60 to 90 beats/min), Sphygmomanometer for blood pressure (100-130mmHg systolic and 60-90mmHg diastolic), Thermometer for temperature (97.4 to 98.4 F) and for emergency situations like heart attack use Electrocardiogram and Defibrillator.

4.7 Sickness treatment [4]

Asthma reaction, allergic reaction, and anaphylactic shock: Benadryl 50mg, Cortisone IM or IV. Hypoxia (lack of Oxygen): use appropriate airway. Dehydration and to keep veins open: Dextrose-5-Water, Ringers Lactate. Symptomatic slow pulse: Atropine and Epinephrine IV. Symptomatic rapid pulse: Vagal maneuver and Adenosine. Hypotension: epinephrine 2 to 10 mg/min. Chest pain: Nitroglycerin 0.4mg. Seizure and convulsions: Valium 10mg or Dilantin 300mg. Heart attack: attach ECG monitor, pulse oximeter, blood pressure cuff, nitroglycerin 0.3mg/5min, morphine sulfate 3mg, aspirin.

4.8 Extravehicular Activity (EVA)

Only two crew members perform EVAs each day, the airlock has been sized for two unsuited astronauts, three suits, and additional space for the astronauts to move comfortably when suiting and unsuiting. Although the design only calls for room enough for the 95th percentile American male (~ 2.0 m tall), the height of the airlock is 2.5 m, for the comfort of the suited astronauts. The hatch from the airlock to the outside is sized for the comfort of the suited astronauts as well. When they exit the airlock hatch, there is a platform on which they will step. Then they proceed to walk on the platform, then down a deployable ladder to the lunar surface. This platform/ladder design is strategically sized and located to avoid contact with the rover wheels during a maximum vertical wheel deflection of .22 m while the wheels are turned inward at their maximum turning angle of 30 degrees. The ladder swings upward by means of a rope-pulley system and is latched to the horizontal stringer for storage. Due the size of this component, it must be installed in orbit.

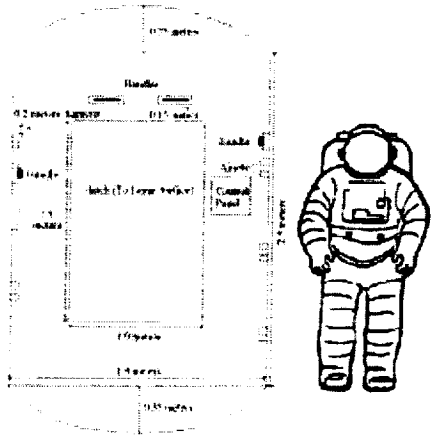

Figure 4-3: Side view of Airlock

The crew cabin pressure of 55 kPa and the airlock pressure of 27.8 kPa correspond to an R-value of approximately 1.2. Therefore, no pre-breathe is required before an EVA. The airlock will be depressurized from 55 kPa to 27.6 kPa and then from 27.6 kPa to 0 kPa. This procedure will take no less than 80 seconds for every 27.6 kPa pressure drop. The airlock will be repressurized in the same manner. The volume of the airlock will be approximately 8.1 cubic meters. The mass of oxygen needed in the airlock will be approximately 3 kg. The total amount of oxygen needed for the airlock for the entire mission will be close to 14 kilograms.

The airlock will also operate as an air shower. There will be 12 air jets throughout the airlock that will simultaneously pressurize the airlock and blast moon dust off the extravehicular mobility units (EMU). The air leaving the jets will be traveling at 20 m/s (45 m.p.h.). The dust will be collected using a circular HEPA filter 2.84 square meters with a thickness of 2 centimeters. It will hold a maximum of 1.2 kilograms and will need to be replaced twice during the mission. Figure 4-3 shows a side view of the airlock

The dimensions of the EMUs are 1.918 m high, 0.848 m wide, and 0.686 m thick, including the portable life support system [5]. Each EMU has a mass of 50 kilograms and will be stored in the airlock (3 total) [6]. A spare EMU is stowed in the crew cabin. The total mass of all the EMUs will be 200 kilograms. The EMUs carry a primary and secondary oxygen tank. The primary tank holds 0.55 kg of recyclable oxygen with a 70% efficiency rate. The secondary tank holds 1.19 kg of non-recyclable oxygen to be used in case of primary tank failure [7]. The total mass of oxygen needed for the EMUs is 20 kilograms. Potable water is also carried in the EMUs. Each astronaut is allotted 0.6 kilograms (~21 ounces) of water per EVA [6]. The total amount of water required for the EMUs for the duration of the mission will be around 42 kilograms.

Astronauts will have a variety of choices for entertainment. Some of the most popular forms of amusement are reading books, listening to music, looking out the window, and watching movies. The ergometer will also be provided as a form of entertainment, as exercise is not mandatory but highly recommended, for the mission.

5 Avionics

5.1 Communications

Having constant communication between the rover and the Deep Space Network (DSN) for the duration of the mission presents a challenge when the rover is on the far side of the moon. Different designs are analyzed to meet the 3 dB link margin while incorporating video signals as well as voice, data, and telemetry to broadcast to the DSN. This challenge is overcome by using a small constellation of satellites in orbit around the moon. The rover uploads data to a satellite in the constellation, which then relays the information around the constellation until there is a line of site with the Earth. An omni directional antenna is used on the rover to eliminate pointing errors from the rover to the constellation. The constellation, placed in a 3500 km circular orbit to keep power usage to a minimum for

broadcasting from the rover. The constellation consists of four satellites spaced 90 degrees apart, with a period of 5 hours. Figure 5-1 shows the satellite orbital positions.

Each of the four satellites in orbit consists of two 0.3-meter parabolic dishes to transmit and receive communications through the constellation. A 1-meter parabolic dish is used to transmit and receive communications from the rover, while a 0.125-meter dish communicates with a 36-meter dish in the DSN. The largest consumption of power is used for transmitting from the rover to the constellation using 8 watts. Transmitting from the constellation to the rover consumes 5 watts, while all other communications require approximately 1 watt or less.

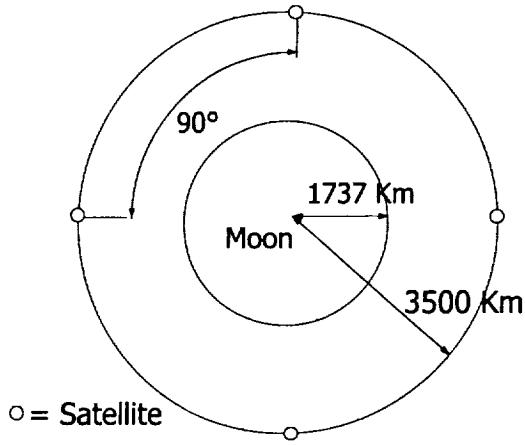

Figure 5-1: Satellite Orbital Position

Taking into account galactic and atmospheric noise, frequencies between 7.8 to 9.3 GHz are used. These frequencies leave ample room for bandwidth to incorporate the 1.2 Mbits/sec data rate required, with video being the largest consumption of the bandwidth.

5.2 Navigation Sensors

The Clementine satellite provides images to a resolution of only 500 meters. This fact, combined with the fact that the rover is only capable of navigating over a one-meter object, makes it a requirement that the rover have navigation sensors with better resolution. A synthetic aperture radar (SAR) system will be placed in orbit around the moon with the communication satellites. It will scan the surface of the moon and send the data back to earth for processing, via the satellites. This processed data provides the day-ahead route planning. The SAR system uses the RADARSAT-2 with an ultra-fine resolution of 3m x 3m. A Light Detection and Ranging (LIDAR) system will be used on the rover for near-range sensing. This system provides a one-meter resolution at a distance of 150 meters. A exterior front mounted camera system will provide the far-range sensing. The center camera will have a zoom lens with a field-of-view of 120? to 30? to resolve a one-meter object at a distance of 325 to 1300 meters. A camera will be located on either side at the front and back of the rover with a fixed field-of-view of 90? to provide a range of 650 meters. All five cameras will have two degrees of freedom and will also be used to watch the astronauts during EVAs. Figure 5-2 shows a relative camera layout

To assure that the rover's true path does not wander from the planned route, it is necessary to have an inertial navigation unit (INU) such as the OceanTools INS-06. This system drifts only about 0.08? after 21 hours of driving resulting in a change in latitude of 0.3 to 0.9 km (depending on driving speed). The system will be updated everyday during EVA using a high accuracy star tracker located on the top of the rover.

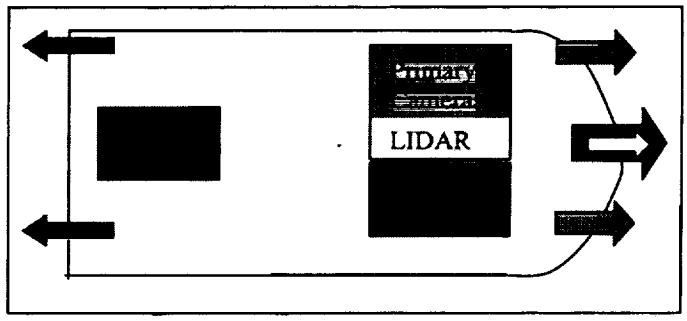

Figure 5-2: Camera Layout

Guidance during ascent and descent is provided by a radar system on the command module. At the initial landing site, there will be three radar beacons triangularly placed to guide the landing of the ascent vehicle. The rover will also carry a set of beacons in case of emergency evacuation.

5.3 Computer Design

In order to control the flow of telemetry and sensor data for the rover, a sophisticated yet simple and reliable computer processing system must be designed. Key system requirements dictate a 90% chance of mission success and a 99.9% chance of crew survival rate. To comply with these requirements the rover has six Litton LC-750EV

general computers for monitoring crew sustaining systems and navigation. Each Litton 40 MHz computer is radiation hardened, weighs 9.09 kg and has a mean-time-between-failure of 4,000 hours proven in vehicles such as RAH-66 Comanche, V-22 Osprey, and the Clementine Spacecraft. The mean-time-between-failures provides a 77.8% reliability rate for our 42-day (1008 hour) mission. Four of these computers are redundantly designated to monitor and control primary mission critical systems and thus dubbed mission critical computers (MCC). The four MCC monitor all data separately. An average of all four signals are sent back to each computer and to the display screen. If there is more than a 5% deviation the computer ceases monitoring the set function until reset. The nominal reliability for the MCC are 99.7%.

The other two computers, mission-aiding computers (MAC), augment the capabilities of the MCC. They provide extra functions such as automatic driving modes like heading hold, speed control, limited autonomous travel, and data reduction for science and mapping without excessively increasing the weight of the system to maintain reliability. The nominal reliability of the two MAC system is 95.0%, however their ability to replace damaged MCC assure a total system a reliability above 99.9%. The computers will be spaced nominally .5 m apart axially and 3.0 m laterally to reduce the chance of single incidents failing multiple computers.

Backup mission critical software is stored on EEPROM Chips, with primary software and data is stored on a 40 GB radiation hardened hard drive specially designed with no moving parts for space environment. The hard drive stores data until it is compressed and transmitted. Compression follows MPEG-4 standards, compressing audio down to 50% and video down to 8% before it is relayed back to Earth via the lunar orbiting satellites. In case of hard drive failure or communication loss, data can be written to a digital optical disk, similar to a DVD, specially designed for the lunar environment. 20 disks are carried on the rover, each disk is able to interface with science equipment and stores 2 GB of data. This disk system increases the survivability of data in the event of a communications loss.

To reduce fatigue and boredom, several driving aids can be implemented. Heading hold can be engaged to hold the rover on a nominal heading. It relies on a computer feedback loop with the gyrocompasses and is automatically disengaged when the LIDAR sensor on the rover detects a 1 m obstacle within 30 m of its direct path. A speed control function maintains a preset speed by monitoring the motor speed and the accelerometers. This mode will be disengaged when either a 1 m object is detected within 30 m directly ahead of the rover or when the motor increase rate is too high (indicative of excessive slipping). Automatic disengaging of each of these modes will cause the rover to sound an alarm and engage in braking unless the driver intervenes. An autonomous mode allows a limited preplanned course input into the computer to be executed similar to robotic control. This mode uses both heading hold and speed control and is disengaged by any of their failure criteria.

6 Power, Propulsion, Thermal

6.1 Power System

The final power system configuration is composed of solar cells, regenerative fuel cells and batteries, and is designed such that the loss of the main system allows for 24-hours of emergency life support.

As a safety factor, the solar cells must be able to produce 35 kW of power when the sun angle is at its lowest projected point in the sky of 25 degrees. By plotting the size of the solar array vs. the amount of articulation (figure 5-1) is generated.

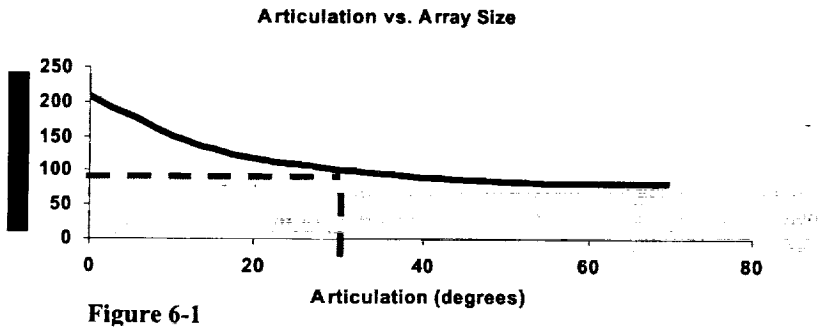

Figure 6-1

From figure 6-1 it is clear that 30 degrees of articulation is the optimum articulation, which can be realized with an area of 100 m^2. The solar cells used for the array are 32% efficient and should be developed in the near term by Spectrolab Inc. [8].

The tracking accuracy required for the array is minimal when the sun is high in the sky; the sun can be at plus or minus 35 degree from perpendicular to the solar array to produce the needed 35 kW. The solar array is actually capable of a 45 kW output maximum, which is 20% more than is needed. This allows for damage to occur to the solar array, and a decrease in efficiency due to dust while still meeting the power needs of Magellan. Tracking is accomplished using power output feedback, inertial feedback, and manual input and corrections. This allows for automation of the system without being completely dependant on computer controlled.

For energy storage a mixture of regenerative fuel cells and batteries will be used. There must be enough energy stored at all times to 24 hours of life support; however since the energy stored will also be used to provide power boosts there should actually be enough energy stored to provide 48 hours of full life support. The regenerative fuel cells that used are Unitized Regenerative Fuel Cell System (URFCS) [9]. There will be 500 cells, allowing a discharge of 12.8 kW for a maximum of 75.5 kW-hr of stored energy. The battery storage system will be composed of Li-Ion Polymer batteries that can store 0.175 kW-hr/kg. This technology is a future technology however given the development of batteries and the need for improvements in industry it is worth while to develop these batteries. The batteries will be sized such that they can provide enough power storage to run minimal life support for 17 hours. With the addition 7 hours of life support from the space suit, 24 hours of life support is provided to the astronauts. This will bring the mass of the batteries to 100 kg.

6.2 Locomotion System

Having determined that the best choice of motion is a wheeled vehicle, the dynamics and loading of such a system must be developed in order to determine how to drive those wheels. Once a model of the forces on the system is developed and analyzed, a system can be designed.

The forces developed on a wheeled vehicle under motion consist of a loading from the Lunar regolith due to the vehicle penetrating the soil, a frictional force, an acceleration force, and a loading from obstacle traversing. Cases considered in designing the system were:

- ?? Driving on a straight and level surface
- ?? Climbing up an incline
- ?? Traversing an obstacle while on an incline

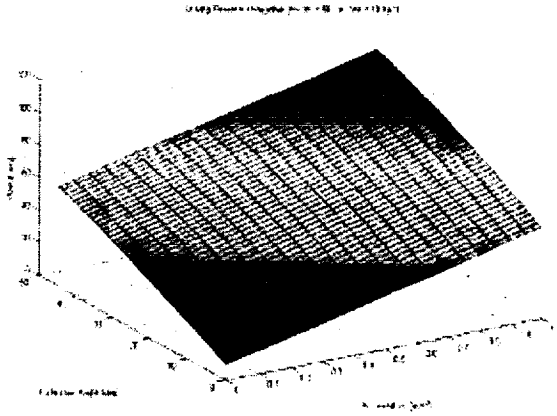

Figure 6-2: Locomotion System Power

Attached to each of these is the variation of adding acceleration or simply considering constant velocity. At first glance, the last case would appear to be the limiting case for the motors, but the motors must also be able to operate continuously if the vehicle is climbing. From a development of the soil model [3] and dynamics of a rolling wheel, figure 6-2 was generated showing how the power required by the system varies with inclination and acceleration.

From this, in order to remain within the power requirement of 28 kW for continuous operation, the maximum sustained slope was set at 10?, at an acceleration of 0.25 $^{m}/_{s}^{2}$, and the velocity was held constant at 13 kph as set from Mission Planning and Analysis.

From the analysis of climbing up a hill, a peak torque was determined for a worst-case obstacle of 1 m in height with a 45? slope. This value was 4800 N-m, and allowed sizing of the Kollmorgen Direct Drive Motors and disc brakes.

The system will make use of regenerative braking technology by having the motors act as generators. This involves a more complex control system, but will return 10W-h nominally, and approximately 90 W-h

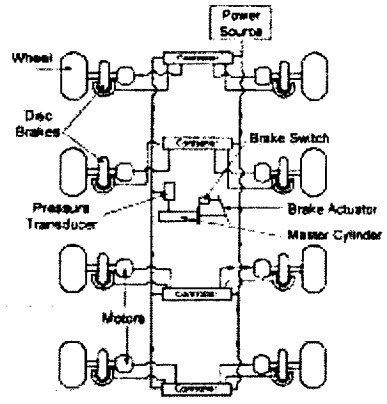

Figure 6-3: Locomotion System Schematic

when traveling down a slope. A schematic of the system is shown in figure 6-3 and a parts drawing is shown in figure 6-4. The steering mechanism was developed to articulate the wheel +/- 30?. Using a ball and socket joint at the point where the strut joins the rod, and a pin connection on the arm from the motor case that slides up and down. With that structure, the entire mass of the locomotion system, not including the tire, is 950 kg for 8 wheels.

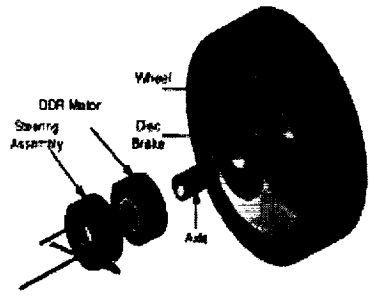

Figure 6-4: Locomotion

6.3 Exterior Thermal Control Systems (ETCS)

The challenge of designing a cooling system in an environment without an atmosphere may seem daunting at first. Common everyday solutions such as fans and air-conditioning are completely unfeasible. However, radiative transfer alone governs heat transfer in such an environment. Systems using radiative cooling are much simpler and lighter than those utilizing convection or conduction. In addition, only one equation is necessary to size such systems: $q = A?? (T_s^4 - T_a^4)$, where q is the emitted energy, A the surface area, ? is material's surface emissivity, ? the Boltzmann constant, T_s the absolute surface temperature, and T_a the absolute ambient temperature.

The ETCS for this project utilizes both active and passive thermal control. Thermal blankets, properly known as multilayer insulation (MLI), make up the passive control system. The entire surface of the rover and airlock, 63 square meters, is swathed in MLI, as are all science packages, exterior avionics, pressure tanks, and batteries. Composed of ten layers of aluminized mylar alternated with ten layers of Dacron fabric, the MLI has a protective top layer of Kapton with an emissivity of 0.02. Total surface area of MLI is 198 square meters, and the total weight of is 368 kg.

The active thermal control system encompasses two cooling methods: radiators and heat pipes. The motors, being 90% efficient, have sufficient surface area to dissipate 500 Watts of waste heat each. The fuel cells must be kept at 4 ?C during regeneration. The most logical choice for this application is a radiator. With a thermostat, the radiator system will be turned on only when needed.

Two coolant loops run through the radiator (color coded green and red). The interior separation o f the tubes is 0.1 m. The purpose of this double loop design is to add reliability to the system. If for some reason one of the internal loops suffers a puncture, the damaged loop can be sealed off and the second loop can then handle cooling load. Under normal operation, however, coolant will flow through both loops. The radiator is coated with a compound known as YB-71 (Zn_2TiO_4 pigment with potassium silicate as a binder), a coating noted for its excellent radiative properties. Use of this coating raises the emissivity of the radiators to 0.92.

Aluminum honeycomb face plating separated by 5/16" diameter aluminum tubing comprises the radiator. The feed tubes are ¼" diameter aluminum tubing. A water/glycol mix is the coolant fluid. The total amount of coolant needed here is approximately 15 liters (7.5 liters of glycol and 7.5 liters of water). The total weight of the radiator system, including pump, is 127 kg.

Heat pipes service the avionics heat sinks. Each of the five exterior cameras has a heat sink maintained at 35 ?C. The cameras utilize thermoelectric coolers to dissipate the 19-26 Watts emitted by each. The heat from these coolers is stored in heat sinks. Heat pipes are an extremely simple, yet effective means of radiating heat. The weight of the heat pipes is approximately 5 kg.

7 Structures

The primary goal of the structural design of the rover is to protect the well being of the crew while maintaining maximum functionality. The first step in designing a viable structure is to establish the safety constraints in the form of specific factors of safety for different types of structure. Identification of the loads and where they will act is the logical second step in the design process. As an external design requirement, the rover must also be able to fit in the payload bay of the space shuttle and the structural components must be less than 3000 kg.

To ensure the safety of the crew and the successful completion of the mission, all systems must be designed to provide a non-negative margin of safety for worst-case loading conditions. All systems must also incorporate the factors of safety listed in table 3.

Table 3: Factors of Safety

Factors of Safety	
Structure	F.S.
Primary Structure	2.0
Secondary Structure	1.5
Pressure Lines	4.0
Pressure Tanks	3.0

The structural design of the rover is divided into three main sections: crew cabin and airlock, loads cage, and suspension system. The crew cabin and airlock are pressure vessels designed to house the crew and their equipment. Surrounding the crew cabin and airlock is the loads cage, a rib/stringer structure designed to divert and absorb the driving loads transmitted by the suspension system. Additionally, attached to the loads cage are support struts for the solar arrays. The struts are positioned so that the solar array can articulate 30?? in both the pitch and roll axes. Finally, there is a suspension system that absorbs the driving loads of the rover. A listing of the primary structures, the source of their respective critical loading, and their margins of safety can be found in Table 4. The launch loads, although they are the most massive load on the vehicle (15.2g, 9.6g, and 15.2g respective to the x, y and z axes after incorporating the applicable factor of safety), are not listed as critical loads on the table. Instead of directly absorbing these extremely high loads, the rover will rest on a cradle (design pending) that takes a majority of the launch loads.

Table 4: Primary Structure and Associated Loads

Component	Critical loading	Source of Critical Loading	Design Factor of Safety	Margin of Safety	Mass (kg)
Crew Pressure Vessel	55.2 kPa	Internal Pressure	2	27	753
Suspension System	8000 N	Start-up Torque	2	1	163
Solar Array Struts (6)	11.375 kN	Dynamic Braking	2	1	16
Airlock	55.2 kPa	Internal Pressure	2	37	167
Pressurized Storage Tanks	20.68 MPa	Internal Pressure	3	2	Variable

7.1 Crew Cabin & Airlock

The crew cabin (figure 7-1) encompasses 63 m^3 of total volume. 51 m^3 is assigned as living space for the crew; the remaining 12 m^3 being used for storage space. The inner shell of both the crew cabin and the airlock are made of 1.25 mm of graphite/epoxy in a quasi-isotropic lay-up. Both are also covered with 18 mm of composite impact shielding to protect against micrometeoroid impacts and collisions with lunar obstacles. The impact shielding consists of alternate layers of Ensolite foam, graphite facesheet, aluminum mesh and another graphite facesheet. It is a thinner, lighter version of the shells developed and tested by the White Sands Test Facility [10].

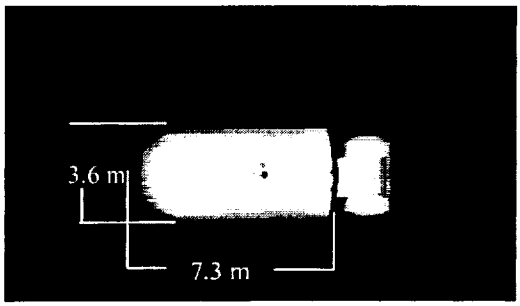

Figure 7-1: Side View of Crew Cabin

The main section of the crew cabin is cylindrical with a length of 5 m and a radius of 1.8 m. The front hemispherical section also has a radius of 1.8. The rear endcap has a radius of curvature of 3.48 m resulting in a length of 0.5 m from the intersection plane. The total length of the cabin section is 7.3 m. A navigation window of dimensions 1.4 m high by 1.5 m wide is located on the front hemisphere.

The airlock is a vertical cylinder with a total height of 3.2 m. The cylindrical section is 2.5 m in height with a radius of 0.95 m. The endcaps each have a vertical height of 0.35 m. Both the hatch into the crew cabin and the hatch to the surface are 1.5 m tall and 1 m wide.

The inside of the crew cabin is designed to promote functionality. Ribs are mounted to the interior of the crew cabin wall to provide mounting points for high strength, plastic isogrid structures. The isogrid "walls" will then be used to mount equipment and enclose storage areas. The floor is also an isogrid structure, manufactured of a low density,

high strength material. The main advantage of the isogrid design is that objects and people can be attached to the floor and still be mobile. Video footage from the Apollo missions illustrates that objects under impulse loading have a tendency to float before returning to the lunar surface. The lunar terrain will produce a vibration laden ride making attachments for people and internal structures important to prevent constant floating of objects in the crew cabin. Ensolite foam coats the inner wall of the structure to protect against accidental impacts.

The primary loading for the crew cabin and the airlock comes from the internal pressure. A stress analysis determined the maximum hoop and membrane stresses due to the internal pressure load. The maximum hoop and membrane stresses (and the corresponding factors of safety) for the crew cabin are 79.5 MPa (F.S.=28) and 76.8 MPa (29) respectively. In comparison, the numbers for the airlock are significantly less: the hoop stress is 39.9 MPa (57) and the membrane stress is 52.1 MPa (38.) The radial deflection of the shells is not a problem as the maximum deflections were 1mm for the cabin section and 0.3 mm for the airlock. Fatigue loading is not a factor for either structure given the low number of cycles and low stresses.

The maximum bending and torsion loads that the crew cabin could withstand were also calculated should one of the primary load bearing members get damaged. The maximum shear stress the crew cabin can undergo is 1.77 MPa, corresponding to a tangential load of 25.2 kN. The maximum bending stress of the cabin is 719 MPa, corresponding to a bending load of 9.2 kN.

A large percentage of the mass of the structure is attributed to the impact shielding. The crew cabin and airlock without any additional protection mass 154 kg and 34 kg respectively. However, the impact shielding will mass an estimated 580 kg. A twenty percent mass margin was also added to account for additional structure around hatched, windows, and punctures of the crew cabin from piping. The total mass of the crew cabin and airlock section then becomes 920 kg.

7.2 Ribs and Stringers

The loads cage is a rib/stringer structure designed to absorb the bending and torsion loads from the suspension system. It also has a secondary purpose in that it provides mounting points for external equipment such as radiators. Given the unfavorable behavior of graphite structures to mechanical fasteners, both the ribs and stringers are constructed of thin walled aluminum I-beams for ease of fastening. Also, for preliminary analysis, the beams are assumed to have identical cross sections that are uniform for the length of the beam. Attached to the loads cage are the struts that support the solar array. These struts have a telescoping mechanism that allows the solar array to articulate. The struts were designed using aluminum also, mainly for the fastening reasons stated above, although a graphite/aluminum hybrid beam may be introduced later to take advantage of graphite's stiffness properties.

7.3 Suspension System

Modeled the rover as an idealized block, spring, and damper system. To complete the model, need to pick spring constant and damping constant. Damping constant is not a factor as can be set to a required value by using active damping. Spring constant is chosen by the maximum strut deflection (discussed later)

Rover suspension system consists of two struts, one connected to the top of the wheel motor casing, one connected to the bottom. A spring-damper connects the top strut to the rib of the rover. To size, the spring constant, the maximum deflection of the top strut must be calculated. This depends on the angle the struts make with the horizontal when the rover is just sitting there. I prefer that the struts are parallel to the ground when the rover is just sitting there. In that case, the maximum deflection of the top strut before it hits the rover body is about 5 degrees. Put in a margin of safety and the spring constant that you need is around 52 kN/m. If you choose to orient the struts at a different angle, then you can obviously change this number.

Vertical Loads: F_{static} = 2043.75 N; $F_{dynamic}$ = 4087.5 N; F dbl = 7285 N. Looking at F_{dbl} as a design load, we find that the spring force Fs = 7668N, the reaction force, Fr = 383N, and the maximum moment in the strut is 727.7 Nm.

Horizontal Loads: Start up torque happens to be greatest load. Doing analysis shows that the reaction force, Fr = 8000 N and the maximum moment in the strut is 16000 Nm. This is the design load for the strut. Sizing the strut as

a thin walled circular cylinder yields a strut of .2 m in diameter and a thickness of 3 mm. Each strut is made out of aluminum and weighs about 6.4 kg.

The Keel Beam is the beam that runs under the Rover. Its design is driven purely by geometric considerations. If it were sized to the loads, it would be extremely this and not very big. The keel beam is also made out of aluminum and is 11.25 m in length. The flange and web thickness are 1/8 of an inch. It is .7m high and .2 m wide. It weighs, at most, 60.7 kg. Holes can be cut out of this beam to make way for cables or other accessories that need to go in that general area.

8 Final Rover Layout

The final rover layout is shown in figure 8-1 through 8-3.

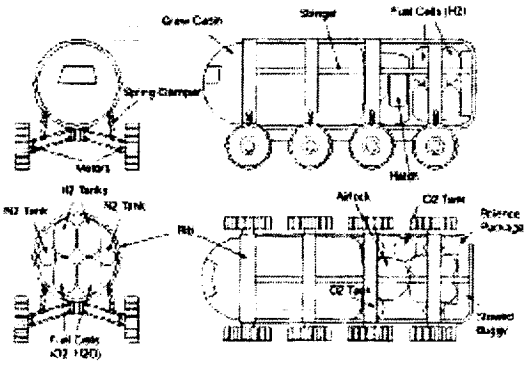

Figure 8-1: Rover Layout without Solar Arrays or Radiators

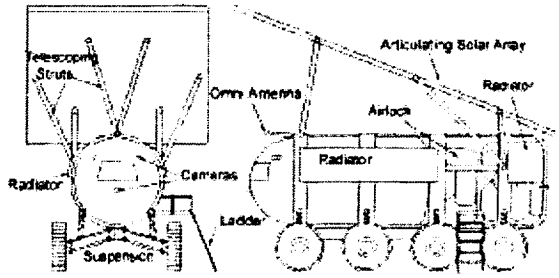

Figure 8-2: Rover Layout with Solar Arrays and Radiators

9 Support Vehicles

The centerpiece of this phase of the project is the surface rover system. However, one of the few things that it cant do is fly. Therefore, this system requires an assembly of spacecraft in support of its mission. These vehicles fall into two broad categories; near Moon and trans orbital spacecraft.

A variety of different scenarios were envisioned that were each capable of successfully completing the mission as outlined. Each scenario is based around a limited number of trans orbital transport sorties, between the Earth and the Moon, that precede the crew in order to assemble all of the mission assets in a Low Lunar parking Orbit (LLO). These plans differ in the number and configuration of the Lunar Shuttle Vehicles (LSV) used to transfer the crews from LLO to the surface, the configuration of the Lunar Cargo Lander (LCL), and the type of crew extraction method used to satisfy the external requirement that the crew enjoy an unaided means of abort to orbit anywhere along the route. Each of these configurations was compared in a trade study using the same performance envelope. The results of this parametric analysis were compared on the basis of total system mass, system costs, payload to structural mass ratio optimization and the probability of surface mission survival. Although the results of this study identified two high value scenarios, in terms of their basis for comparison, the least expensive of these cost nearly 14 billion dollars. Since these cost estimates were based on performance figures developed through the parametric analysis, and did not include any design margins or provisions for testing and development, economic concerns sent us back to the drawing board.

The outgrowth of this study led to a concept called the Unified Lunar Flight Vehicle system (ULFV). In order to satisfy the mission goals 3 LSVs and one LCL comprise this package. The LCL transports the rover system to the primary landing site followed by the crew in an LSV. The other two LSVs remain on orbit for emergency crew extraction en route. Initially, this system was based around a common descent stage for the LCL and LSV variants. Later, the ascent stages that carry the crew back to LLO was also standardized. Since the two LSVs remaining on

orbit would have the greatest delta V requirement and hence require the greatest propellant mass for both stages all of the design work was based on these performance points. Simply put, the LCL and LSV used for the primary landings would be these same craft with less than a full propellant load.

The ULFV system provides several important benefits to the overall mission. First among these are the reduced expenses realized by the common stage designs. Necessarily, previous scenarios had suffered higher non-recurring costs due to the mission specific optimization of each flight vehicle type. This savings more than offsets the increased vehicle operating costs. ULFV system also frees the rover from carrying a piggy-back flight vehicle along its surface journey, the plan that had previously been envisioned in response to the aforementioned external requirement, since it allows for an extra on orbit contingency vehicle. Serendipitously, this had the effect of reducing rover's power requirements for locomotion and associated subsystems which ultimately reduced the overall system mass. A further benefit of sizing the system to the emergency flight envelope is an additional 900 kg payload mass margin, above the specified 10000 kg, for the LCL that could be used for extra structure that can help the rover withstand specified landing loads.

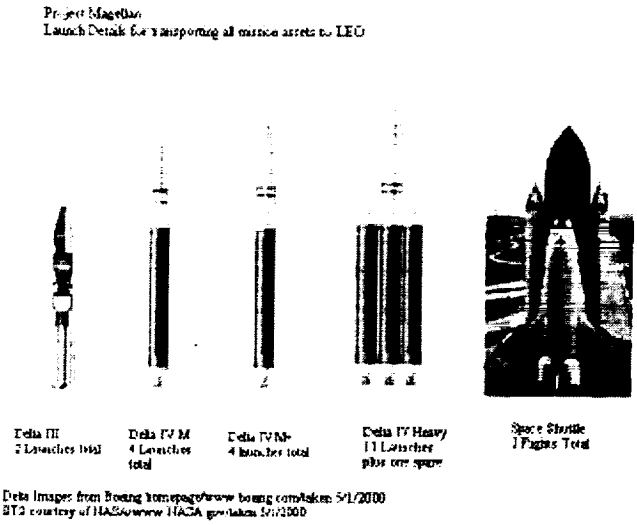

Figure 9-1: Launch Vehicles

ULFV is a modular system that is designed to be placed into Low Earth Orbit (LEO) using currently available and near future launch vehicles. The ascent stages are launched complete with full propellant loads. The components of the descent stages are packed for launch. Once on orbit, the basic platform unfolds like a carrier fighter's wings and the modular propellant tanks and landing gear subassemblies are mated to the platform. Then either an LSV ascent stage or the surface rover system is mounted to the complete platform. All of the vehicle components are placed at a rendezvous point in a LEO parking orbit. Then, a Shuttle mission is flown transporting the rover to LEO. The shuttle crew will perform minor assembly work to the rover as well as assemble the ULFV flight vehicles. As versatile as ULFV system is, it is still a near Moon flight system and just as with the rover, requires transport from Earth to Moon. This is the job of the Orbit-to-Orbit Transfer Vehicle (OOTV).

OOTV is an autonomous or remotely piloted vehicle designed to transport the ULFV system from LEO to LLO. Three different approaches to this mission have been considered. One concept involves linking all of the assembled ULFV vehicles together as one assembly, including the crew and command module (the trans orbital crew habitat), and propelling this assembly to the Moon. Only command Module would return to Earth under this plan. The other two approaches involve flying each vehicle, in a series of sorties, between the parking orbits. The difference in these approaches is one employs a reusable spacecraft with a robotic arm that refuels itself by trading empty fuel tanks for pre-charged ones launched into the parking orbit. The other utilizes one-way, expendable transfer stages that are assembled on orbit at the same time as the ULFV flight systems. Although the one-shot and expendable transfer vehicle approach saves total fuel mass consumed, the reusable OOTV concept allows for very low cost subsequent Lunar Missions.

10 Program Schedule, Costs, & Budgets

10.1 Program Schedule

Figure 10-1 shows the program development schedule.

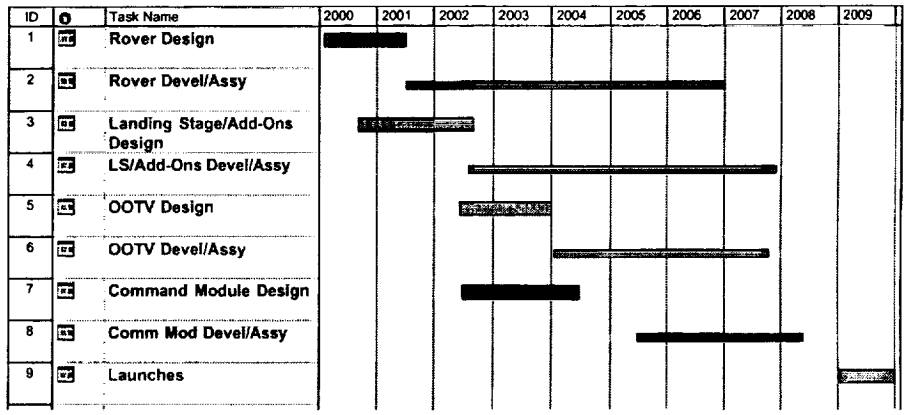

Figure 10-1: Program Schedule

10.2 Rover System Mass Breakdown

To ensure that the total mass of the rover does not exceed 10,000 kg, a 9,000 kg mass budget was created. The decision to design to a 9,000 kg rover increases the chance that the rover will meet the 10,000 kg requirement, allowing for a 10 % margin. The mass budget breakdown is illustrated below in Figure 10-2. From this current actual mass breakdown, it is clear that the 10,000-kg rover requirement will be met.

10.3 Rover System Power Budget

The power budget divides up the available power of 35 kW amongst various systems that are in need of it. It is representative of the power needed for driving the rover on a continuous route during normal daily operations, which allows for a long-term sustained climbing angle of 15 degrees. Currently, the actual total power required for each system is actually under the budget goal, totaling 31.7 kW. This budget, shown below in figure 10-3, illustrates both the goal and actual power for each system; however, it does not directly include a margin.

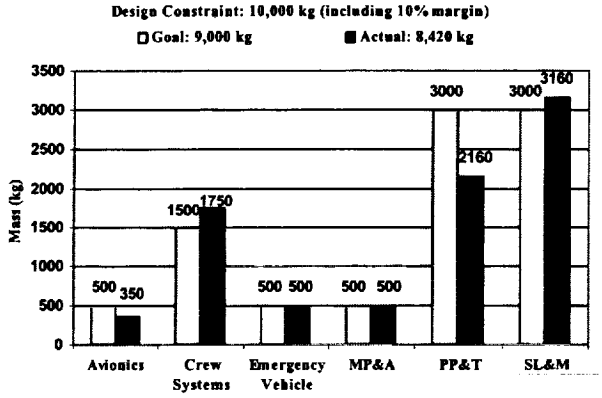

Figure 10-2: Rover Mass Budget

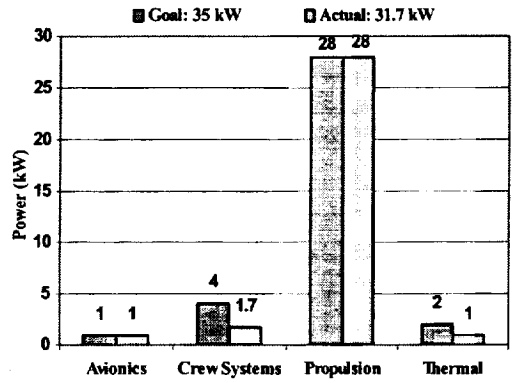

Figure 10-3: Daily Continuous Operation Power Budget

10.4 Program Cost Estimation

The cost estimating relations provided by Johnson Space Center projected the total Magellan Project cost to total $12.22 Billion. Table 6 lists the non-recurring and production costs of each of the vehicles, as well as the cost for satellites and launches. The number of each vehicle produced exceeds the number of vehicles needed for the mission for most cases. These extra vehicles were included in the cost budget to allow for pre-flight testing purposes. Additionally, the non-recurring cost of this program accounts for 65% of the total program cost and the total cost for satellites and launches accounts for another 20%. Leaving only 15% of the cost for producing the vehicles concludes that producing the additional vehicles for pre-flight testing purposes barely increases the cost

(see Figure 10-4). In fact, if only the number of vehicles needed for the mission were produced, the total program cost would only be $11.38 Billion. On another note, the projected program cost of $12.22 Billion is not all that expensive when it is compared to the Apollo Missions, which in 1967 dollars cost $23.19 Billion. In year 2000 dollars, the Apollo Missions would have totaled $97.65 Billion.

Table 6: Program Cost Estimate

Vehicle	Mass Per Unit (kg)	Non-Recurring Cost ($M)	Number Needed for Mission	Number Produced	Production Cost ($M)	Additional Costs per Item ($M)	Total Cost ($M)
Lunar Rover + Buggy	10000	$2,862.32	1	3	$663.12		$3,525.44
Landing Stage (Descent)	2338	$507.75	4	6	$134.84		$642.59
LSV Flight Cabin	2000	$1,181.09	3	5	$351.16		$1,532.26
Ascent Stage Add-on	795	$711.08	3	5	$190.67		$901.75
Orbit to Orbit Transfer Vehicle	10000	$1,129.24	1	1	$75.28		$1,204.51
Command Module	3500	$1,606.78	1	3	$330.95		$1,937.73
Satellites			4			$45.00	$180.00
Shuttle Launches			1			$400.00	$400.00
Delta Launches			19			$100.00	$1,900.00
TOTAL ($Billion)		**$8.00**			**$1.75**		**$12.22**

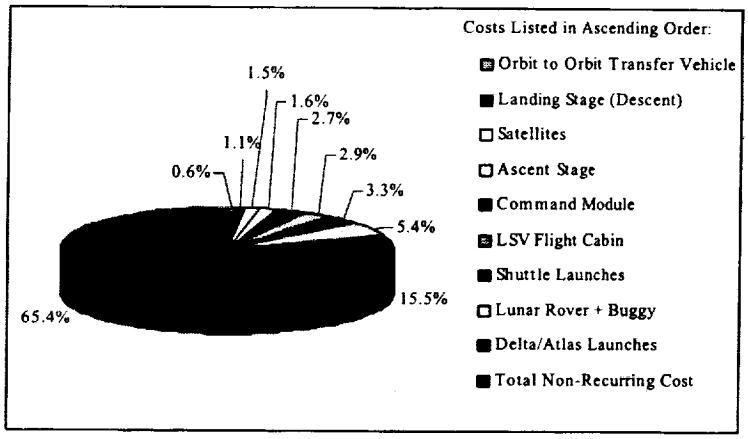

Figure 10-4: Total Program Cost Estimate

11 Outreach

As with any project it is important to provide a link to the community in which the idea was fostered in. The class held formal Preliminary and Critical Design Reviews that were open to the University community and interested outsiders. For example, over 100 invitations were extended for the Critical Design Review. The audience included University of Maryland faculty, graduate students, and undergraduates, professionals from NASA and the Naval Research Laboratories, and students from Eleanor Roosevelt High School. It was important to not only include the community of the University of Maryland but also the aerospace industry in the surrounding Washington D.C. area. The presentation provided the opportunity for the mixing of industry and education in a setting that was electrified with the need for increased planetary exploration.

12 Conclusion

Just as the Lewis and Clark expedition opened the West to settlers, the Magellan expedition will open the moon to colonization as well. And those lunar settlers will turn their eyes to the next big unknown: Mars. For in the grand

scheme of things, as momentous as this lunar circumnavigation is, it is only one step in a far more ambitious goal: the circumnavigation and colonization of Mars. And from there, the cosmos awaits.

13 References

1. Heiken, Grant, et al. Lunar Sourcebook: A User's Guide to the Moon. New York: Cambridge University Press, 1991.
2. Wiseland, P., "Designing for Human Presence in Space", NASA RP-1324, 1994.
3. Bekker, M.G., Off the Road Locomotion. Ann Arbor: University of Michigan Press, 1960.Oweiss, Zakaria, Doctor of gynecology & obstetrics, interview March 2000
5. National Aeronautics and Space Administration. "Man-Systems Integration Standards". NASA-STD-3000, Volume 1, Revision B, July 1995.
6. Dismukes, Kim. "Wardrobe for Space." NASA Facts. NASA. 12 Feb. 2000 http://www.jsc.nasa.gov/pao/factsheets/nasapubs/wardrobe.html
7. Conrad, Linda. "O2-How Much?" Space Team Online. NASA. 12 Feb. 2000 http://quest.arc.nasa.gov/space/teachers/suited/9d6o2.html.
8. "Cells Galore." *Aviation Week & Space Technology*. April 10, 2000, pg. 17
9. Burk, Kenneth A. "High Energy Density Regenerative Fuel Cell System for Terrestrial Applications." July 1999 NASA/TM-1999-209429.
10. Tapphorn, Ralph M. and Tim E. Roth. "Protective Shells for Composite Overwrapped Pressure Vessels." NasaTech Briefs. Internet. Available: http://www.nasatech.com/Briefs//Feb00/MSC22762.html (17 April 2000).
11. "NASA Apollo Mission Apollo-1 – Effects of The Apollo 204 Accident On Schedule And Cost Of The Apollo." http://www.hq.nasa.gov/office/pao/History/Apollo204/effects.html.
12. "Cost Model – GDP Deflator Inflation Calculation." http://www.jsc.nasa.gov/bu2/inflateGDP.html. 1 May 2000.

THE MARS SOCIETY OF CALTECH HUMAN EXPLORATION OF MARS ENDEAVOR

California Institute of Technology [undergraduate]
Contributors: Christopher Hirata, Nathan Brown, Derek Shannon
Faculty advisors: Jim Burke, Bruce Murray, Mark Adler

Abstract

The Mars Society of Caltech Human Exploration of Mars Endeavor (Mars SCHEME) is a detailed description of robotic and human missions necessary to establish a permanent human presence on the surface of Mars. The sequence begins in 2009 with a robotic Mars sample return mission on a larger scale than that currently planned. This is followed in 2011 by a pair of HEDS landers designed to test in-situ propellant production and other necessary technologies. Cargo for the human crews is sent in 2016 and in 2018, with the first five-member crew traveling to Mars during the 2020 opportunity. The Mars SCHEME features design redundancy; for example, the capsules for Earth ascent, Mars ascent, and Earth arrival are based upon a common design. Systems redundancy is also included to provide multiple habitats on Mars and in interplanetary space. The plan uses only chemical propulsion, starting with the Z-5 launch vehicle that can deliver up to 112,000 kg to low Earth orbit. Costs of human missions are comparable with those of the NASA Design Reference Mission 3.0. Human missions have low recurring costs, high reliability, and high scientific return. Extensive computer simulations were used to develop launch vehicles and trajectories. Further details are available at *http://mars.caltech.edu/*.

1. Overview

1.1 Statement of Design Problem

Our design problem is the creation of the safest, most cost-effective, and most easily achievable human Mars mission architecture possible. This architecture must also lead to a permanent human presence on Mars and elsewhere.

Our decision in favor of this design problem is first based on what technological decisions are currently most crucial to getting a human Mars mission off the ground. Because such a mission is still in the earliest of design stages and lacks funding, the broader mission architecture decisions are currently more important than the detailed design of individual components. Our design problem is therefore centered on fundamental mission architecture decisions that will shape details later in the design process.

Second in our selection of a design problem was context. We will be relating future human Martian exploration to current robotic Martian exploration and human spaceflight efforts, easing the transition between the two. For this reason, our primary design problem of human Mars mission design will also encompass robotic missions to occur before the first human mission, additional applications of mission hardware, evolution of hardware needed for long-term exploration and settlement, and the fiscal and political pressures that NASA and its potential partners will face in their attempts to send humans to Mars.

1.2 Robotic Predecessors to a Human Mission

At present, NASA's Mars Surveyor program sends robotic spacecraft to Mars in order to accumulate valuable scientific data. Robotic Mars spacecraft can help us send humans to the Red Planet in many ways. Those identified in this study are:

1.2.1. Communications and Navigation Infrastructure. A human Mars mission will require near-constant communication with Earth. Automated communication satellites near Mars will be necessary for occasions when direct radio contact with Earth is impossible. In addition, the mission will require good navigation, both for precision landing of vehicles and for surface rover guidance, so navigation satellites will also be needed. Dual-purpose satellites could fulfill both functions.

1.2.2. Testing Technologies in the Martian Environment. Though far more expensive than Earth-based tests, operating a technology on the surface of Mars provides the most useful data on how it functions in the Martian environment. Technologies such as in-situ propellant production, precision landings, and aerocapture should be tested with robots if they are to be included in a human mission.

1.2.3. Characterization of the Martian Environment. Before sending humans to Mars, we must better understand the environment that awaits them. Radiation levels, soil oxidants, dust damage to surfaces, and other potential hazards can be studied by robotic landers. Studies of more complex interactions between Martian soil and humans may require returning Martian samples to Earth for analysis. A network of surface meteorological stations and orbiters could survey the pressure, temperature, and wind conditions at potential landing sites.

1.2.4. Scientific Study of Mars. In addition to laying the technological groundwork for human exploration of Mars, scientific instruments on robotic Mars missions will increase our knowledge of the Red Planet. This will place the astronauts' observations in context. More important, it allows us to send the astronauts with the proper tools to answer the most intriguing questions raised by the discoveries of the next generation of robotic probes.

These objectives will be met by three classes of Mars missions. The micromissions, of which the (failed) Deep Space 2 probes were the first, are already part of the Mars exploration program. These are fast and cheap, so many can be flown. The Small Mars Landers (SMLs), such as Mars Pathfinder and Mars Polar Lander (several hundred kilograms), can carry more instruments but are still small. The largest of the robotic probes, the Intermediate-Sized Mars Landers (ISMLs), will have masses in the thousands of kilograms and will fill the technological gap between the current SMLs and the heavy machinery needed for human missions. The ISMLs will also be able to operate high-power experiments and return large samples to Earth for analysis. A possible sequence of robotic missions to Mars (excluding micromissions) leading up to a human mission is shown in Figure 1.2.1 and discussed in more detail in §4.

Figure 1.2.1. Possible Future Mars Missions

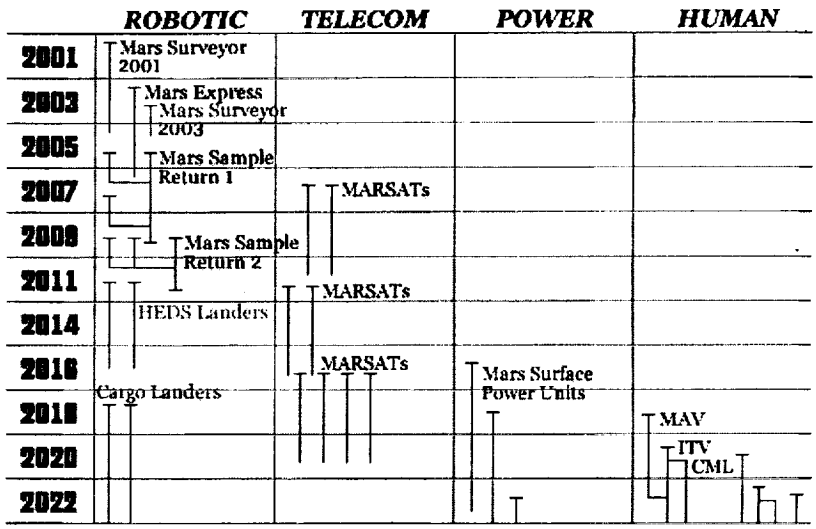

1.3 First Human Mars Mission

The first human Mars mission begins in 2016, when an unmanned Z-5 rocket lifts off from Earth. The Z-5, which can place up to 112 metric tons (112,000 kilograms) into orbit, is roughly the size of the Saturn V that once took astronauts to the Moon. Its first payload is a Mars Surface Power Unit (MSPU), launched directly to Mars. It descends to the surface using parachutes and rockets. In 2018, four more Z-5s launch directly to Mars with Large Mars Landers (LMLs) carrying a Mars Ascent Vehicle (MAV), a crew habitat, a cargo lander with two rovers and other science equipment, and a second MSPU.

Figure 1.3.1. Human Mission Sequence

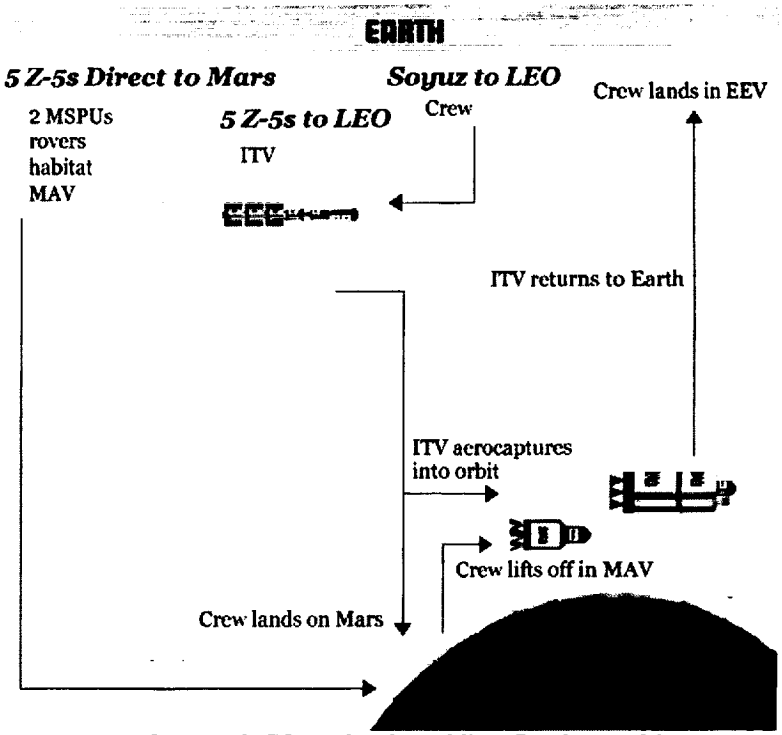

When the first MSPU lands, it generates power and deploys small rovers that will connect power cables to the habitat and MAV when they arrive. The MAV contains a small capsule on a liquid hydrogen (LH_2)/liquid oxygen (LOX) powered rocket stage. It arrives on Mars with its LH_2 tank full but its LOX tank empty. Using MSPU power, the MAV draws carbon dioxide (CO_2) from the Martian air. The MAV's array of electrolysis cells pulls an oxygen atom from each CO_2 molecule and liquefies the resulting oxygen, storing it in its LOX tank. By early 2020, the MAV propellant tanks are full.

In 2020, another set of five Z-5 launches assembles an Interplanetary Transfer Vehicle (ITV) in low Earth orbit (LEO). The ITV consists of the crew Mars lander (CML), a habitat, the Earth entry vehicle (EEV), a truss, and four LH_2/LOX rocket stages. When the ITV is complete, five astronauts travel to it in an Earth ascent vehicle (EAV) launched by a Soyuz booster.

The first three of the ITV's four LH_2/LOX stages fire to raise the ITV orbit to near Earth escape. Finally, the fourth and final stage fires, sending the ITV on a 146-day trajectory to Mars. During the trip to Mars, the ITV spins at four revolutions

per minute to provide about 1/3 of normal Earth gravity in the habitat. Upon arrival at Mars, the crew enters the Mars lander and separates from the habitat, descending to the surface. The truss is jettisoned, and the remainder of the ITV aerocaptures into Mars orbit.

The crew explores Mars for over 500 days, living in either their lander or in the habitat. At the end of their stay on Mars, the crewmembers enter the MAV and blast into Mars orbit. There they dock to the ITV and transfer into its habitat. The ITV propulsion system fires its engines to send the crew back toward Earth, where they arrive 177 days later. The crew performs a direct entry at Earth in the EEV, splashing down in the Pacific Ocean in 2023.

1.4 Subsequent Missions

A crew of five can be sent to the same site on Mars every 2.14 years using this architecture if, in each launch opportunity, six Z-5s and a Soyuz launch a MAV, an ITV, and an EEV. In addition, MSPU systems, consumables, and science payloads are replaced whenever they are consumed, break, or wear out. However, additional possibilities may be opened after the first mission. Since there will be a significant infrastructure on Mars after the first mission, it makes sense to make this primitive Mars base less dependent on Earth to reduce the cost of the Mars missions. For example, finding usable in-situ water would reduce the costs of resupply from Earth.

1.5. Methods and Validation

Three computer simulations were designed using the C programming language to calculate interplanetary trajectories and launch capability (from Earth and Mars).

1.5.1. Trajectory Program. The trajectory program analyzed mean Keplerian orbital elements of Earth and Mars and assumed a heliocentric conic section transfer orbit. Within these approximations, trajectories were calculated exactly. The program was validated by comparison to previous interplanetary probes.[1,2] Table 9.2.1 displays this validation, using C_3 as the benchmark trajectory feature. After establishing this small absolute error in C_3 for recent Mars trajectories, the program was deemed valid for calculations used in designing this mission. (Note that because the 200 km error in the Mars Climate Orbiter trajectory is small compared to the distance scale of the inner planets, Climate Orbiter was considered an acceptable reference against which to validate the trajectory program.)

Table 1.5.1.1. Validation of Trajectory Program

Probe	*Predicted C_3 [km²/s²]*	*Actual C_3 [km²/s²]*	*Absolute Error [km²/s²]*
Mars Global Surveyor	9.9846	10.0194	0.0348
Mars Climate Orbiter	10.93	11.19	0.26

It was initially desired to run the trajectory program in a faster, two-dimensional mode in which the inclination of the Mars orbit was neglected. A quick check, however, indicates that this is not a good idea; compare the parameters of the 2022 Mars mission trajectory as shown in the table below. In particular, we note that the two-dimensional assumption is optimistic, as it is in nearly all cases. (Earth departure on SAT 17 SEP 2022 and Mars arrival on SUN 26 MAR 2023 were assumed for 190 day transit time.)

Table 1.5.1.2. Comparison of 3D and 2D Trajectory Simulations in 2022 Opportunity

Simulation Type	*Earth departure C_3 [km²/s²]*	*Mars entry velocity [km/s]*	*Launch declination*
Three-dimensional	19.9	6.27	39°N
Two-dimensional	18.0	6.23	23°N

1.5.2. Launch Vehicle Program. The launch vehicle program assumed a gravity turn trajectory, thrust, and a simple model for air drag. Within these approximations, the payload capacity to low-Earth orbit (LEO) was calculated exactly. The Space Shuttle was used as a test case for the launch vehicle program, which predicted a payload capacity of 28.442 MT to LEO, as opposed to an actual 29.5 MT,[3] an error of 3.59%. Given that the error is expected to be greatest for vehicles on which the payload is a small fraction of the mass at burnout (such as the Shuttle, unlike the Z-5 launch vehicles described in §2.4), this program was considered valid for use in designing the mission architecture.

1.5.3. Aerocapture Program. The simulation program used for Mars aerocapture numerically integrates the trajectory of a spacecraft in the Martian atmosphere. A drag force proportional to atmospheric density and the square of the spacecraft velocity was assumed, as was a constant lift-to-drag ratio and an exponential atmosphere with a scale height of 11 km.

1.5.4. Cryogenic Systems. These were sized using the model of Kittel *et al*[4] with a 25% mass margin and 100% heat load margin.

2. Launch Systems

2.1. Launch Needs for Mars Exploration

Neither robots nor humans can get to Mars without a launch vehicle for Earth-to-orbit (ETO) transportation. For the current generation of Mars spacecraft, vehicles that can send roughly one metric ton of payload to Mars are sufficient, but future missions such as Mars Sample Return will need to send an order of magnitude more payload to Mars. Eventually, human missions will require at least an order of magnitude more payload still; the ITV is projected to have a mass up to 421 MT upon departure from LEO. Even if such a large spacecraft is launched in several pieces, a large launch vehicle becomes a necessity. The human Mars mission plan we have outlined requires a launch vehicle with 111 MT to LEO capacity; a smaller vehicle could be used at the expense of reduced efficiency, but current launch vehicles under the 25 MT to LEO regime would require nearly twenty launches for the ITV alone, clearly not reasonable if we wish to travel to Mars on a regular basis. Thus for the near term current launch vehicles are sufficient, whereas a human mission will require something larger.

2.2. Current Launch Vehicles

The near-term Mars missions are likely to fly on Delta II vehicles, including the upcoming 2001 Mars orbiter. Future robotic missions may require payload capacities as great as that of the Titan IVB Centaur or an Evolved Expendable Launch Vehicle. Additionally, the Ariane 5 will be upgraded in the early years of the 21st century; a cryogenic upper stage, currently under consideration,[5] would increase its payload capacity substantially. Thus for the next decade, the approximate maximum that can be delivered to Mars in a single launch is 7,500 kg. For this reason, the ISML is designed for this size.

2.3. Need for a New Launch Vehicle

There are several reasons why current launch vehicles, despite their applicability to the robotic Mars missions of the next decade, are inadequate for human missions to Mars.

2.3.1. Payload Fairing Diameter. Current launch vehicles typically have payload fairings no wider than five meters. Packaging the Mars Ascent Vehicle, for example, into such a narrow fairing is nearly impossible given the wide hydrogen tanks and rocket engines. A mission has two options for avoiding this difficulty: extensive on-orbit assembly, or a larger fairing. The latter is simpler and probably much cheaper and better in the long run; it would be expensive and dangerous for astronauts to assemble Mars landers or aeroshells on orbit.

2.3.2. Number of Launches. A 25 MT to LEO vehicle, probably typical of the heaviest rockets that would be built for commercial, military, and scientific missions, would require at least 17 launches to build the ITV in orbit. Operationally, the prospect of 17 launches just for this part of the Mars mission presents difficulties. For example, there is a high probability that one launch would fail. Additionally, some components, in particular the ITV's large cryogenic stages, are not split easily into smaller pieces because the dry mass fraction of cryogenic systems increases as they become smaller (higher surface area to volume ratio).

2.3.3. Earth Orbit Rendezvous. Rendezvous in Earth orbit is a well-tested technology, but sixteen rendezvouses add significantly to the number of failure points in the mission.

A new launch vehicle is clearly needed. It must be a large launch vehicle with a wide fairing. A compromise must be made between the capacity of the launch vehicle and its associated development costs; a good choice is probably a vehicle about equal in size to the Space Shuttle or the Saturn V, as this is the largest size with which there is operational experience.

2.4. The Z-5 Launch Vehicle

The Z-5 expendable launch vehicle consists of three stages. The third is used only on direct-to-Mars missions, not on LEO missions. The Z-5 will be launched from Kennedy Space Center. The stages are summarized in Table 2.4.1.

Table 2.4.1. Characteristics of Z-5 Booster

	First stage	*Second stage*	*Third stage*
Propellant	LOX/RP1	LOX/LH_2	LOX/LH_2
Engines	5 RD-170	4 Vulcain 2	5 RL-10D
Thrust	39.45 MN (*vac*) 36.30 MN (*sl*)	5.40 MN	1.11 MN
Specific impulse	337 s (*vac*) 309 s (*sl*)	433 s	472 s
Burn time [min:s]	02:14	04:22	06:15
Dry mass	150 MT	35 MT	10 MT
Propellant mass	1795 MT	350 MT	90 MT

Length	30 m	22 m	15 m
Diameter	11.7 m	10.5 m	8.0 m

Vacuum performance data for the RD-170 and Vulcain 2 engines are from Andrews Space and Technology.[6,7] The RL-10D is a derivative of the existing Pratt and Whitney RL-10 engines used on the Centaur and Delta III vehicles.[8]

The overall height of the Z-5, including a 10.5 × 45 m payload fairing that encloses the third stage and payload, is 97 m (318 ft), taller than the Space Shuttle but somewhat shorter than the Saturn V. The total liftoff mass for a direct-to-Mars mission is 2.48 million kg (5.48 million lb), and the liftoff thrust is 36.30 MN (8.16 million lb). The Z-5 payload capacities are calculated for a 51.6° inclination orbit. Launch trajectories were determined both for ITV assembly missions and for direct-to-Mars missions. Acceleration is kept under 6 *g* at every point in the trajectory. Table 2.4.2 shows the launch trajectory for the Z-5 on a direct-to-Mars mission at 51.6° inclination. The three-stage Z-5 can carry 44 MT to $C_3 = +14.9$ km²/s². The third stage burns for 80 seconds after second stage separation. It then coasts to the proper TMI point and burns for an additional 295 seconds to place its payload en route to Mars.

Table 2.4.2. Z-5 Direct to Mars: Sequence of Launch Events

Event	*Time [min:s]*	*h [km]*	*d [km]*	*v [km/s]*	*Notes*
Liftoff	T+00:00	0	0	0	1.47 *g* T/W
Mach 1	T+00:50	7.1	1.7	0.33	
First stage separates	T+02:30	75	99	2.72	Peak acceleration from first stage 5.5 *g*
Payload fairing separates	T+03:00	107	177	2.89	
Second stage separates	T+07:04	226	1,250	6.82	Peak acceleration from second stage 3.0 *g*
Third stage shutdown	T+08:24	228	1,820	7.48	79% propellant remains in third stage tanks

h: altitude above surface; *d*: downrange distance; *v*: ground-relative velocity

For a LEO mission, such as the ITV propulsion stages, the third stage is replaced with a Star 48/TE-M-711-8 solid motor. The payload capacity to a 360 km orbit is 112 MT. After second stage separation at T+07:04, the spacecraft coasts for 45 minutes until apogee at 360 km altitude. There the Star 48 fires for 88 seconds, providing 48 m/s of ΔV. (The Star 48 has a dry mass of 116 kg, 2,000 kg of propellant, and an I_{sp} of 292.9 seconds.[9]) Alternatively, the first stage of the Z-5 can be throttled down to 60% two minutes into launch. This ensures that acceleration remains below 4 *g* but reduces payload capacity to 109 MT.

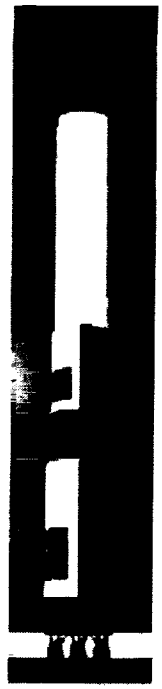

2. 5. Z-5 Design Considerations

A number of tradeoffs were considered for the Z-5 launch vehicle. It could be expendable, reusable, or mixed (like the Space Shuttle); it could be parallel or sequentially staged; and each stage could use any of several propellants.

2.5.1. Expendable or Reusable Vehicle. A large RLV would be a significantly costlier development program than a large expendable due to the complexity of recovering and refurbishing a rocket. Furthermore, reusability only pays off for systems that fly often, and these missions will only need several Z-5 flights per year. It is also possible to envision a partially reusable launch vehicle such as "Magnum" which would have liquid fly back boosters as its first stage and an expendable core vehicle as its second. This strategy was not chosen due to the potential high development costs associated with liquid fly back boosters. Thus an expendable vehicle was chosen.

2.5.2. Propellant. Hydrogen/oxygen is undoubtedly the best choice for the upper stages of the launch vehicle; it is the only current propellant that achieves I_{sp} in excess of 400 s. This prevents the heavy-lift vehicle from becoming unreasonably large. The lower stages should use a low-energy, high-density, high-thrust propellant: solid propellant (Al/NH_4ClO_4), storables (N_2H_4/N_2O_4 and derivatives), or LOX/RP1. Of these, LOX/RP1 has the highest I_{sp}, with the relatively high-thrust RD-170 rocket engine providing 337 s I_{sp} in vacuum. Although it has the operational difficulties associated with cryogenic oxygen, the other choices have worse difficulties. Since solid propellant cannot be loaded on the launch pad, explosive propellant is present during much of the launch processing, and the exhaust has a high concentration of acidic HCl, an environmental concern. Storable propellants are highly toxic and require special precautions to handle. Given these

drawbacks and the relatively advanced state of LOX/RP1 propulsion technology in Russia, LOX/RP1 was selected for the Z-5 first stage.

2.5.3. Parallel or Sequential Staging. Parallel staging, in which the first stage is composed of booster rockets strapped to the core stage, has advantages in that the core stage can be ignited on the ground, allowing a simpler ignition system and verification before launch commit. However, the core stage spends part of its burn pushing not only its own mass but that of the boosters as well, inefficient from the ΔV perspective. This can be solved with a cryogenic upper stage, as in the Mars Direct Ares or CMSM2 Janus. [10] To avoid this additional stage, a sequentially staged configuration was chosen for the Z-5.

2.6. Soyuz/EAV Launch

The crew is launched in an Earth Ascent Vehicle on the Soyuz booster from Baikonur, Kazakhstan. The Soyuz has four boosters burning kerosene and oxygen in RD-107 engines and a two-stage core. The first core stage burns kerosene and oxygen in the RD-108, very similar to the RD-107; the second stage burns kerosene and oxygen in an RD0110 engine.[11] With an escape tower, the Soyuz booster can lift the 6,850 kg mass of the Soyuz-T to LEO.[12]

The Soyuz was chosen to launch the crew because of its long history of reliable transportation to orbit and because of its launch facilities, which can already handle a crew. A capsule capable of carrying five humans to orbit within the Soyuz launch capacity will be built anyway for the MAV; modifying this capsule for Earth ascent is expected to be a minor part of total mission cost. Some modifications to the Soyuz launch system might be necessary to accommodate the EAV.

2.7. Selection of the Z-5

The selection of a launch vehicle remains a major issue for a human mission to Mars, but it probably will not be resolved until the time of program approval. This mission is baselined with the Z-5 as the launch vehicle.

3. Trajectories

3.1. Orbital Mechanics of Mars Missions

A human Mars mission will require a selection of trajectories, both for cargo vehicles (one-way) and humans (two-way). Most cargo vehicles will use either a Type I (6-9 months) or Type II (8-12 months) trajectory, each of which has a departure C_3 of 12 km²/s² and an entry velocity at Mars of 6 km/s. For human missions, several mission profiles could be considered. There are three major options to be considered: fast missions, opposition missions, and conjunction missions. These are compared in Table 3.1.2.

Table 3.1.2. Possible Profiles for Human Crews to Mars

Mission profile	*Assessment*
Fast 3 months to Mars 1 month on Mars 3 months to Earth	Short mission is desirable for initial mission, but ΔV over 50 km/s results in absurdly massive mission with present technology. **Is not currently feasible.**
Opposition 7 months to Mars 2 months on Mars 11 months to Earth	Again, short mission is desirable for initial mission, but is not much shorter than conjunction mission. ΔV is about 1.5 km/s higher than for conjunction mission. VGA is needed, so trajectory is highly variable from one launch opportunity to the next. Surface stay is a small fraction of the total mission. **Feasible, but difficult and only moderately rewarding.**
Conjunction 7 months to Mars 16 months on Mars 7 months to Earth	Long length of mission is a drawback, but most time is spent on Mars at the (relative) safety of the base and under the protection of Martian atmosphere (radiation shielding) and in Martian gravity field. **Feasible, technically easiest mission, and most rewarding.**

3.2. Interplanetary Trajectories for Humans

Since the fast mission's high ΔV prevents it from being performed with present or near-term technology, a human Mars mission must use either the opposition or conjunction profile. An opposition mission is somewhat shorter in total but requires a larger ΔV. Additionally, most of the conjunction mission is spent on Mars, whereas most of the opposition mission is in interplanetary space. The opposition mission might be appropriate for a "flags-and-footprints" mission, but it defeats the purpose of an overall Mars exploration program. For these reasons, a conjunction trajectory was chosen for the first missions.

Within the conjunction class missions, there is a choice of slower versus faster trajectories between Earth and Mars. Faster transit times reduce deep space radiation and microgravity exposure at the expense of higher ΔV, requiring a smaller spacecraft, better propulsion, or more fuel; in addition, fast trajectories raise entry velocities, making aerocapture more difficult. With an Earth departure C_3 of 20.25 km²/s², a transit time of 220 days or less can be achieved with Mars hyperbolic ap-

proach velocities no greater than 3.9 km/s in all launch opportunities from 2020 to 2033. This trajectory requires a ΔV of 1,300 m/s greater than that of the optimal Hohmann transfer. (See §1.5 for further details on the program used to compute interplanetary trajectories.) Table 3.2.1 lists trajectories for human Mars missions between 2020 and 2033.

Table 3.2.1. Details of Human Trajectories, 2020–2033

Launch	*Leg*	*Departure*	*Arrival*	*Transit time*	*Orbital elements*
2020	E→M	MON 10 AUG 2020 C_3=20.2; δ=+9°	SUN 03 JAN 2021 v=6.28	146 (568:553)	e=0.26; p=1.00; a=1.72 T=1.59; i=0.6°
	M→E	MON 25 JUL 2022 C_3=17.5; δ=–10°	WED 18 JAN 2023 v=12.67	177	e=0.23; p=0.88; a=1.39 T=1.21; i=1.7°
2022	E→M	SAT 17 SEP 2022 C_3=19.9; δ=+39°	SUN 26 MAR 2023 v=6.27	190 (526:537)	e=0.28; p=1.00; a=1.78 T=1.64; i=2.5°
	M→E	MON 02 SEP 2024 C_3=17.2; δ=+1°	FRI 07 MAR 2025 v=13.05	186	e=0.25; p=0.88; a=1.47 T=1.27; i=0.1°
2024	E→M	THU 24 OCT 2024 C_3=20.0; δ=+43°	MON 26 MAY 2025 v=6.29	214 (512:499)	e=0.27; p=0.99; a=1.70 T=1.56; i=2.5°
	M→E	SAT 10 OCT 2026 C_3=17.5; δ=+15°	MON 19 APR 2027 v=13.00	191	e=0.26; p=0.92; a=1.57 T=1.39; i=1.4°
2026	E→M	WED 02 DEC 2026 C_3=19.8; δ=+28°	SAT 10 JUL 2027 v=6.27	220 (499:486)	e=0.25; p=0.96; a=1.60 T=1.45; i=0.9°
	M→E	MON 20 NOV 2028 C_3=17.5; δ=+27°	THU 24 MAY 2029 v=13.00	185	e=0.29; p=0.94; a=1.68 T=1.50; i=2.0°
2029	E→M	THU 11 JAN 2029 C_3=19.9; δ=+4°	SUN 19 AUG 2029 v=6.20	220 (678:660)	e=0.22; p=0.94; a=1.49 T=1.34; i=1.5°
	M→E	FRI 17 JAN 2031 C_3=17.4; δ=+28°	SAT 28 JUN 2031 v=13.03	162	e=0.30; p=0.94; a=1.76 T=1.57; i=1.6°
2031	E→M	TUE 04 MAR 2031 C_3=19.8; δ=–19°	SUN 14 SEP 2031 v=6.29	194 (565:550)	e=0.20; p=0.93; a=1.41 T=1.27; i=2.4°
	M→E	FRI 01 APR 2033 C_3=16.8; δ=+7°	MON 08 AUG 2033 v=13.04	129	e=0.30; p=0.92; a=1.40 T=1.51; i=0.0°
2033	E→M	THU 12 MAY 2033 C_3=19.4; δ=–36°	TUE 11 OCT 2033 v=6.27	152 (602:586)	e=0.19; p=0.95; a=1.40 T=1.27; i=1.8°
	M→E	TUE 05 JUN 2035 C_3=17.6; δ=–19°	SUN 07 OCT 2035 v=13.03	124	e=0.26; p=0.85; a=1.46 T=1.24; i=1.6°

C_3: Jacobi constant for departure orbit [km²/s²]
δ: injection declination with respect to planet's equator
v: entry velocity [km/s] (assuming 125 km entry interface altitude and 4.93 km/s escape velocity at Mars; 122 km entry interface altitude and 11.07 km/s escape velocity at Earth)
Transit time in days; surface stays in parentheses (Earth days:Martian sols)
e: orbital eccentricity; p: perihelion [AU]; a: aphelion [AU]
T: orbital period [yr]; i: orbital inclination

3.3. Mars orbits

In this mission, the ITV travels from Earth to Mars, inserts into Mars orbit, and then returns to Earth. The Mars orbit must be accessible from the Earth-to-Mars trajectory and must bring the ITV to the proper point for trans-Earth injection.

To a first approximation, orbits around Mars follow the familiar Keplerian orbital mechanics laws. However, Mars has a gravitational quadrupole moment J_2=0.001959 [see [13]] due primarily to its equatorial bulge, causing a gradual precession of orbits. Essentially, this precession leaves the period, eccentricity, and inclination with respect to the Martian equator fixed but perturbs the nodal and apsidal axes. It is undoubtedly significant for any spacecraft that lingers in Mars orbit for an extended period of time; a spacecraft in a low-inclination, low-altitude Mars orbit would have a precession rate of about 12° per day.

The ITV will fly in a near-polar, circular orbit around Mars at 250 km altitude. The nodes regress at the rate of 11.9° per day times the cosine of the orbital inclination i. In 450 days, an orbit of inclination i=90° does not precess at all, while an inclination of i=88.07° is sufficient to cause a one-half orbit precession. By varying the inclination between 88.07° and 90°, we can adjust the "final" ITV orbit plane (that is, the ITV orbit plane after 450 days or more of Mars orbiting) to be within 2° of any direction we choose. This is useful for the trans-Earth injection maneuver.

4. Robotic Mars Missions

4.1. Mars Sample Return and ISMLs

Current plans call for a Mars Sample Return (MSR) mission, returning about a kilogram of Mars rocks, sometime in the next decade. While this mission would be a useful step in the exploration of Mars, it is not sufficient for the needs of a human Mars mission that will spend up to 600 days on the surface. A human Mars mission will require at least 10 kg from the site of the first Mars base. There are several ways to increase sample size, such as changing ascent propellants (solid, storable, or in-situ produced propellants). ISPP was rejected since cryogenic systems do not scale well to small vehicles. A single-stage storable rocket was chosen because it is a better analogue to the MAV that will carry the astronauts. (Specifically, it allows the ascent vehicle to play the active role in the rendezvous rather than the Earth return vehicle.) The general architecture (two landers which launch samples into orbit where an orbiter grabs them and returns to Earth) is very similar to that of the first MSR mission, except that all the vehicles launch in the 2009 opportunity.

The Mars sample collection systems and ascent vehicle are to be landed on Mars by an Intermediate-Sized Mars Lander (ISML), which has a mass at TMI of 7,000 kg. Upon approach to Mars, the ISML separates from its cruise stage and enters the atmosphere of Mars, protected by an aeroshell of L/D = 0.4. Parachutes and three hydrazine/nitrogen tetroxide rockets slow the ISML to a touchdown on the surface of Mars, with a useful landed payload of 2,000 kg. The ISML mass allocation is shown in Table 4.1.1. (Margins are included in the individual items.)

Table 4.1.1. Intermediate-Sized Mars Lander mass budget

Component	*Mass [kg]*
Cruise stage	800
Aeroshell, heat shield, and reaction control system for descent section	1,550
Descent parachute (20 m diameter)	175
Descent propellant (for 700 m/s ΔV with 8% residuals)	1,030
Descent propulsion system (engines, propellant tanks and feed systems; 300 s I_{sp}, 35 kN thrust at full throttle)	250
Power supply (dynamic isotope)	445
Landing system structure, communications, and information management systems	750
Payload	2,000
Total	**7,000**

The ISML would be launched on a large vehicle [see §2.2] such as an EELV or an upgraded Ariane 5. The ISML power supply will be a dynamic isotope power supply (DIPS) using Stirling power conversion technology. The mass of a 2.5 kWe DIPS using 27 kg $^{238}PuO_2$ is estimated at 350 kg;[14] here 445 kg was budgeted, some of the increase necessary to move the DIPS system some 50 m away from the ISML. (When the Mars ascent vehicle launches, the ISML and any equipment remaining on it will be destroyed. We wish to conserve the Martian ^{238}Pu isotope inventory for future use.)

The MSR lander payload consists of a sample acquisition system, spacecraft utilities, and an ascent vehicle. The ascent vehicle is capable of producing 4.8 km/s of ΔV using a 50/50 mixture of hydrazine and dimethylhydrazine ("aerozine-50") and nitrogen tetroxide oxidizer, which can yield 320 s vacuum I_{sp} (used on the Delta II second stage). It can lift an 80 kg capsule containing 10 kg of Martian samples into low Mars orbit; its total liftoff mass is 1,500 kg and it has an inert mass of 245 kg excluding the capsule but including residual propellants. The ascent vehicle has a single engine providing 9 kN thrust.

The sample acquisition system features a robotic arm of length 4 m that obtains samples of Martian regolith and rocks and loads them into the ascent vehicle. This design is simpler than a sample-collecting rover, which would require a robotic arm anyway to raise the samples to the ascent vehicle. The lack of a rover will bring a scientific loss, since only the most accessible Martian material can be acquired; however, the first MSR mission is primarily scientific, whereas the second MSR mission is intended to acquire Martian material in bulk for compatibility analysis and testing with humans and their spacecraft. This objective is met just as well by typical Martian dirt as by any specially selected sample.

4.2. HEDS Lander

Before humans travel to Mars, it will be necessary to test out the Mars surface technologies needed for human exploration on a scale larger than, for example, the currently planned MIPP. Also, certain data on the proposed base site will be needed that the second MSR mission cannot return. An oxygen generator that produces at least 500 kg of oxygen in 400 days must be tested. (The human mission will require three generators to produce 17,710 kg O_2 in the same time frame.) Radiation levels of all varieties (neutrons, gamma rays, ultraviolet, and charged particles) must be measured, since radiation levels can vary significantly with site due to sunlight, altitude, and soil composition. Weather patterns at the landing site must be monitored for a full Martian year or more to show that diurnal thermal cycling (for example) will not damage critical systems.

Concentrations of CO_2 and H_2O in the air should also be monitored since ice or dry ice may condense on a vehicle. Water content of surface and subsurface material must be measured to as great a depth as possible.

The HEDS lander will serve these needs. It uses the ISML landing system, common with the second MSR vehicle, to save development costs. Its most massive payload element is the oxygen generator and storage system. The oxygen tank has 1 m^3 volume to store 1,100 kg of liquid oxygen at 92 K. The internal temperature is maintained by 100 layers of MLI and one of four cryocoolers capable of extracting 2.5 W of heat from the interior of the tank. The tank radius is 70 cm including insulation and a vacuum jacket necessary for the MLI to work on the surface of Mars. The oxygen generation system is 399 kg and draws 2,115 W, scaled from [DRM1/p. 3–106].

Another major mass item on the HEDS lander is a 10 m surface drill with a mass of 260 kg [DRM1/p. 3–52]. Due to power constraints, this drill cannot operate when oxygen is being generated. The mass of the sample analyzer, radiation monitoring instruments, and the spacecraft material exposure system is estimated under 100 kg. These instruments, the drill, and the oxygen generator easily fit within the ISML mass budget.

5. Cargo Vehicles and the Large Mars Lander

5.1. Selection of a Permanent Base Site

After the second MSR mission and the twin HEDS landers, a site for a permanent Mars base may be selected. The following considerations are key in landing site selection:

5.1.1. Availability of Water. It is generally believed that water concentration increases toward the poles and decreases toward the equator due to the temperature gradient. Water, of course, is a key resource for a Mars base.

5.1.2. Sunlight. Some daylight during each Martian sol is probably desirable, for psychological and operational reasons; EVAs may be difficult at night.

5.1.3. Elevation. Lower elevations are desirable due to increased atmospheric density. This results in an easier task for the atmospheric compressor of an ISRU system and greater protection from radiation.

5.1.4. Temperature. To simplify vehicle design, it is desirable to choose a landing site at which the spacecraft is always operating at a temperature significantly greater than that of its surroundings. If the temperature at the base site reached 280 K, for example, a very large radiator or active cooling system (both undesirable) would be necessary to prevent spacecraft overheating. Overheating is likely to be at least as great a danger as cooling to Mars base spacecraft because of the high power consumption compared with current robotic Mars missions.

5.1.5. Agricultural Potential. Crops may be grown on Mars using either natural sunlight or artificial light. The former will obviously be easiest at the equator due to greater sunlight; the latter will be easiest in polar regions due to the colder temperatures, which reduce radiator size. Artificial lighting, which is more dependable, can operate in a limited volume (such as an inflatable habitat style module), and avoids water condensation on the roof of an inflatable greenhouse, may be desirable. In this case, the polar regions may be favored.

Once a base site is selected, it is time to deliver cargo and humans there. This will require a larger lander, the Large Mars Lander (LML), and its cargo payloads.

5.2. Large Mars Lander

The LML is a circular shelf of 3.4 m radius on three 2.7 m tall landing legs. On its underside are four 1.48 m diameter descent propellant tanks, two containing hydrazine and the other two containing nitrogen tetroxide. A pressure-fed engine consumes this propellant, providing 300 kN thrust at 300 s I_{sp}. The mass allocation for the LML is shown in Table 5.2.1.

Table 5.2.1. Large Mars Lander mass budget

Component	*Mass [kg]*
Payload	19,267
Lander structure	2,000
Descent stage propulsion system dry mass (incl. engine, propellant tanks, and feed system)	1,396
Propellant load (incl. 8% residuals)	7,511
Parachutes (2 main parachutes, 45 meter diameter, plus 2 drogues)	625
Aeroshell and reaction control system	13,001
Interplanetary power supply (inflatable solar arrays, 20 kWe at 1 AU, 7 kWe at Mars aphelion)	200
Total	**44,000**

Here the propellant tanks and the helium tanks for the propellant feed system are scaled from the Space Shuttle orbital maneuvering system[15] and the parachutes and lander structure are scaled from DRM3. The aeroshell and reaction control

system (RCS) are allocated 29.7% of the total entry mass since the RCS must provide up to 300 m/s of ΔV in orbital maneuvers using hydrazine/nitrogen tetroxide bipropellant with 315 s I_{sp}.

The LML descent sequence is as follows:

5.2.1. Mars Aerocapture. Several minutes before Mars arrival, the LML separates from its interplanetary power supply. The LML enters the Martian atmosphere at 125 km altitude at up to 6,300 m/s. The entry flight path angle must be between 9.8° and 12.4° to capture into orbit around Mars without exceeding the 3.2 *g* deceleration limit. To capture into a 160 km circular orbit, the LML would first capture into an elliptical orbit and then aerobrake until the apoares fell to 160 km. Then an engine firing of under 100 m/s, depending on the entry parameters, would place it into this low Mars orbit. The entry corridor is 48 km deep. The LML aeroshell is based upon an ellipsled configuration specified by Lockheed Martin.[16] It has a lift-to-drag ratio of 0.4 and (with this heavy payload) has an estimated ballistic coefficient of 300 kg/m².

5.2.2. Mars Descent. After a final checkout of LML systems, its reaction control system retrofires to send the lander down toward the surface of Mars. At 8 km altitude, terminal velocity is 650 m/s, and the parachute deployment sequence begins. At 1 km altitude, the LML's velocity has dropped to 100 m/s if one of the parachutes has opened and 70 m/s if both have opened. In the former case, the LML separates from its parachute and ignites the single bipropellant engine on its underside, slowing itself to a halt 30 m above the Martian surface. It may then hover for up to 150 seconds in some cases before it must touch down on a smooth landing site. On some missions the LML will need a larger payload than the 19,267 kg listed above. This can be achieved by removing propellant from the descent stage and accepting a reduced hover time, leaving the lander's total entry mass unchanged. For example, the 22,696 kg MAV can be landed on Mars with 45 s of hover time.

5.3. MSPU Lander

The minimum power requirement will be 100 kW for 600 days, the duration of a crew surface stay. Three usable energy sources can be imported from Earth: wind, solar, and nuclear fission. Wind power has many moving parts at risk of malfunctioning in the Martian environment, and the extremely limited flux of sunlight on Mars is prohibitive to solar power.

A 160 kWe MSPU requires a nuclear reactor that can run for seven years, a radiation shield, a power conversion system, a radiator, and power conditioning equipment, for a total mass of 9,738 kg.[17] The radiation shield leaves an acceptable radiation dose (below 5 rem/yr) at a distance of 2.8 km. The MSPU will land roughly this distance from the proposed Mars base site and will be targeted into a crater for additional shielding, making the crew's exposure to MSPU radiation negligible.

After separation from the LML interplanetary power supply, power is provided by fuel cells. The mass and performance are taken from the STS fuel cells,[18] but some changes may be necessary to improve their lifetime. The total mass budget for the fuel cell system, including the five fuel cells generating at least 6 kWe each, is 1,844 kg dry. 2,000 kg reactants can run one fuel cell for 40 days, which will keep the MSPU alive during approach, landing, and deployment.

Once the LML/MSPU payload has landed, its radiators are deployed, and power can be produced. Five small rovers connect it to other payloads; each rover has a total mass of 1,200 kg, of which 704 kg [see [19]] is devoted to the power cable that is rolled off a spool on the back of the rover. Thus the total payload mass of the MSPU's LML (including 320 kg for communications, as in [DRM3/§A4.0], and a 500 kg power distribution system) is 20,402 kg plus rover deployment ramps.

In the dusty Martian environment, a direct metal surface contact like a conventional electrical outlet is not a good way to connect the power rover to a base element. Two schemes avoid the need for a metal surface contact: the metallic connector, which uses a heater to solder two connectors together, and the inductive connector, which uses neighboring coils to transfer alternating current by magnetic induction. The final selection must await a thorough engineering analysis of both options.

5.4. Cargo Payloads

Two cargo payloads will be sent directly to Mars on Z-5s in 2018. One of these payloads will be a backup habitat derived from the CML [see §6.3] for the first crew. In addition, the scientific exploration of Mars will require a long range mobility capability on the surface. Two 5 MT rovers [DRM3/§A2.2.1] are allocated in the first cargo payload, with a total mass of 10 MT. The remainder of the capacity on this first LML will be dedicated to scientific equipment. There is also the capability for additional cargo landers in 2020 and in subsequent opportunities.

5.5. Mars Ascent Vehicle

The mass of the MAV payload is 22,506 kg, broken down in Table 5.5.1.

Table 5.5.1. MAV payload mass budget

Component	*Mass [kg]*
Food for 5 people, 600 days	6,600
MAV capsule [§6.8]	3,100
Dry MAV stage	5,338
Liquid hydrogen in MAV (kept cold by MAV stage cryocoolers, powered by interplanetary	3,152

power supply in transit to Mars)	
Oxygen generators (4)	4,156
Dynamic isotope power supply and radiator	350
Total	**22,696**

The food is intended to be the primary food supply for the crewmembers during their stay on the Martian surface. The dry MAV stage includes a 4.45 m diameter liquid hydrogen tank, a 3.10 m diameter liquid oxygen tank, and four RL-10D engines burning hydrogen/oxygen bipropellant. The RL-10D is a possible future variant of the current RL-10 Pratt-Whitney rocket engines providing 222 kN thrust and 472 s I_{sp} with a mass of 378 kg.[20] The dynamic isotope power supply is the same as that used on the ISML [see §4.1], except that it needs no deployment system. At Mars landing, the MAV hydrogen tank is full but the oxygen tank is empty. The MAV oxygen generators use the same basic process as the HEDS lander oxygen generator but are larger, draw more power, and have a higher output rate.

Table 5.5.2. MAV oxygen generator and storage systems

Component	*Mass [kg]*	*Power [W]*
Atmospheric compressor/CO_2 extractor	115	658
Zirconia cell electrolyzer ($2\ CO_2 \rightarrow 2CO + O_2$)	600	17,838
Oxygen liquefier	116	1,120
Margin (25% mass, 25% power)	208	4,904
Total	**1,039**	**24,520**

The output rate of a MAV oxygen generator is 15 kg O_2 per day, more than sufficient to produce the required 17,710 kg of liquid oxygen in a 400 day time span. The system masses and powers have been scaled from [DRM1/p. 3–106].

Upon separation from the interplanetary power supply, the hydrogen begins to boil off. With a heat of vaporization of 445 J/g, and a capability to boil off up to 200 kg of liquid hydrogen without loss of functionality of the ascent stage, the MAV can handle up to 89 MJ of heat transfer into the hydrogen tank. Since the expected heating rate is 50 W, the MAV will be able to sit on Mars without power for up to 20 days before hydrogen boiloff becomes problematic.

The MAV is then plugged into the MSPU lander, providing power to run the high-power MAV systems, specifically the oxygen generators and the cryocoolers in the hydrogen tank. Three of the four oxygen generators must operate for sufficient oxygen to be produced. Together, they consume 73,560 W power. After 400 days, the MAV is fully fueled for ascent into orbit. This information is transmitted to Earth, allowing the next phase of the Mars mission to begin.

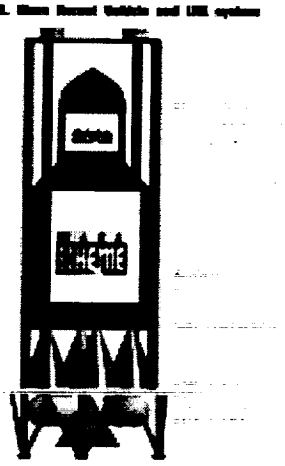

6. ITV and First Human Mission Design

6.1. Interplanetary Transfer Vehicle Habitat

The ITV is the vehicle in which the crew travels from low Earth orbit to the vicinity of Mars and in which the crew makes the return transit to Earth. Although unneeded items can be jettisoned in the EEV, there is no capability for extensive EVA in interplanetary space. Such a capability was deemed unnecessary because there are no spacecraft systems outside the pressurized compartments that the astronauts could conceivably repair.

6.1.1. Structural and Thermal Systems. The basic structure of the ITV is a rounded cylindrical inflatable habitat 8 meters in diameter and 8.5 meters long, with 300 m³ of internal volume. The mass estimate for this component was taken from the TransHab derived habitat proposed for Mars exploration [DRM3/§A3.1] at 1,039 kg structure and 500 kg thermal control systems. Here we increase the thermal control system's mass budget to 1,000 kg, allowing redundancy for many components, and introduce an additional 25% margin on structural and thermal systems, bringing the total mass budget for this item to 2,549 kg.

6.1.2. Life Support Systems. A life support system for six people (this mission would have five) is estimated as having a mass of 3,796 kg, a power requirement of 5,831 W, and a volume of 19.13 m³.[21] This includes complete recycling of oxygen and water, meaning that only food and power are required as inputs to run the life support system indefinitely. While this mass budget does include spares, it may still be prudent to send two such life support systems due to the lack of in-space experience with extensive recycling of consumables. The 3,796 kg figure was taken unadjusted; the performance reduction (five astronauts versus six) serves as margin. Additionally, food should be sent with the astronauts; the mass of food needed is

taken from a TransHab derived module mass budget [DRM3/§A3.1] as 2.2 kg per person per day, or 11 kg/day for a crew of five. The ITV (including the crew Mars lander) will carry 1,000 days of food (enough for the entire mission) through launch and TMI; 800 days of food at MOI; and 200 days at TEI. Adequate consumables are present at each mission phase. To make the ITV lighter during launch, five metric tons of food are launched with the crew Mars lander.

6.1.3. Crew Accommodations. This item includes health care equipment and other crew systems. A mass of 2,356 kg is estimated from a TransHab derived module [DRM3/§A3.1] crew accommodations item, removing food (which we include in the life support category) and adding a 25% margin.

6.1.4. Communications and Information Management. This item is again taken from [DRM3/§A3.1] with a 25% margin, yielding a total mass of 400 kg.

6.1.5. Electrical Power. The power requirement for an ITV-type habitat was estimated at 29,400 W [DRM1/p. 3–93], but the life support power requirement has been reduced in more recent studies from 12 to 6 kW, so a power supply need only provide 24 kWe to the habitat. During the return trip to Earth, therefore, a 30 kWe power supply has been baselined to provide margin. In addition, the cryogenic tanks in the TEI stage must remain chilled, yielding a power requirement of 40 kWe prior to TEI. The most promising power source is a combination of solar and battery power, avoiding the complications of a nuclear reactor or the large quantity of ^{238}Pu (roughly 400 kg) for an isotope power supply. The solar arrays provide the power except during eclipse periods, when the battery is used. It is later recharged from the solar arrays.

The solar arrays will be of the type projected for the (now cancelled) Space Technology 4/Champollion mission. These would provide a power density of 100 W/kg and about 55 W/m² at 1 AU from the Sun,[22] or 35 W/kg at Mars aphelion. The post-TEI array system would have a mass of 857 kg and an area of 1,500 m². The array for Mars orbit should provide 80 kWe at Mars aphelion to adequately charge the batteries during the sunlit portion (at least 62%) of the ITV's orbit; it would have an area of 4,100 m² and a mass of 2,286 kg. Before MOI, power is to be provided from the ITV-CML truss; see §6.4.

The battery will have to endure at least 10,000 charging cycles; nickel-metal hydride batteries with a specific energy of 55 W-hr/kg can survive only 3,000 cycles.[23] However, some improvement in battery technology can be expected; for this study, a 40 W-hr/kg rechargeable battery that can survive 10,000 cycles is assumed. The batteries must provide up to 42 minutes of power at 40 kWe, corresponding to a mass of 700 kg. Dividing into fourteen units of 50 kg (2 kW-hr energy storage each) and adding two spare units, the total battery mass is 800 kg. Half of these are to be jettisoned just before TEI along with the Mars orbit solar arrays; this reduces the TEI mass but still leaves a backup power source during the trans-Earth cruise.

Additionally, power will be needed for up to several days after MOI while the ITV aerobrakes. It is not desirable to drag a solar array through the Martian atmosphere, so a non-regenerative fuel cell consuming hydrogen and oxygen was selected to power this phase. It is comprised of nine fuel cells using the existing STS fuel cells as a mass and performance estimate,[24] although they would need an improved in-space lifetime. Six fuel cells are needed to produce 37 kWe power; together they consume 300 kg/day of hydrogen and oxygen reactant. If reactants for five days are supplied, the total mass of the fuel cell reactants is 1,500 kg, and their tankage has a mass of 422 kg. The fuel cells themselves total 1,041 kg.

Power must be distributed to the components and radiated away after it is used. Power distribution mass was taken as 550 kg, double the value given in [DRM3/§A3.1] since there is a higher power requirement along with a TEI stage that also requires power; the radiator was scaled from [DRM1/p. 3–96] to a 93 m² area and a 507 kg mass. In total, the power system has a mass of 2,314 kg at TEI, with an additional mass of 5,649 kg to be inserted into Mars orbit.

6.1.6. Earth Entry Vehicle and Return Payload. The Earth entry vehicle is described in greater detail in §6.9; it has an unloaded mass of 3500 kg. The crew has a mass of 500 kg (80 kg per crew member and five 20 kg pressure suits). The samples returned to Earth from Mars have a mass of 500 kg, and there is an additional 100 kg of scientific equipment.

6.1.7. Reaction Control System. This system was designed to provide 80 m/s of ΔV during each of the three legs of the mission (trans-Mars, Mars orbital, and trans-Earth.) It uses hydrazine resistojets with 320 s I_{sp} and thus requires 8,000 kg propellant with a 2,000 kg dry mass. Of this dry mass, 1,000 kg holds propellants which will be used prior to TEI, so this part of the RCS is to be jettisoned along with the Mars orbital power systems just before TEI.

6.1.8. Solar Storm Shelter. This device protects the crew from radiation from solar particle events. It must provide 10 g/cm² of shielding to the crew during a major flare in addition to that available from onboard equipment. This is described further in §8.1, but here we merely note that a 2.6 m diameter sphere using LiH shielding is 2,346 kg.

6.1.9. Atmospheric Repressurization System. The EEV may need to be repressurized several times, for example, if the EEV is used as an airlock through which to jettison unneeded items. If this is to be done three times, 100 kg of air will be expended. The mass of this air and its cryogenic storage systems was estimated at 250 kg. Additionally, the ITV/EEV complex contains 300 kg of air budgeted under this mass item.

Table 6.1.1. ITV mass budgets at major mission stages

	Mass [kg]			
Component	*at launch*	*at TMI*	*at MOI*	*at TEI*
Structural and thermal systems	2,549	2,549	2,549	2,549

Life support (includes consumables)	13,592	13,592	16,392	9,792
Crew accommodations	2,356	2,356	2,356	2,356
Communications and info management	400	400	400	400
Electrical power supply	7,963	7,963	7,963	2,314
EEV and return payload	3,600	4,100	4,100	4,600
Reaction control system	10,000	10,000	4,449	1,816
Solar storm shelter	2,346	2,346	2,346	2,346
Atmospheric repressurization system	550	550	550	550
Total	**43,356**	**43,856**	**41,105**	**26,723**

6.2. ITV Main Propulsion System

The ITV is propelled by a hydrogen/oxygen stage that is required to deliver a ΔV of 300 m/s post-MOI and at least 3,080 m/s at TEI. The stage contains 5,450 kg of usable hydrogen and 32,700 kg of usable oxygen; its dry mass is 6,739 kg distributed according to Table 6.2.1.

Table 6.2.1. Inert mass of ITV main propulsion

Component	*Mass [kg]*
Residual propellants (2%)	763
Propulsion engines (3 RL-10D, common engine with MAV, 222 kN thrust, 472 s I_{sp} [25])	1,134
Liquid hydrogen tank (100 layers MLI plus 4 cryocoolers; 5.49 m diameter including insulation; draws 3,563 W power)	1,870
Liquid oxygen tank (with 35 layers MLI plus 4 cryocoolers; 3.84 m diameter including insulation; draws 1,246 W power)	435
Propellant feeds and stage structure	1,189
Margin (25%)	1,348
Total	**6,739**

If a 2% margin is applied to this stage's I_{sp} (that is, I_{sp} = 462.6 s is assumed rather than the specified 472 s), the propulsion system burns 5,503 kg of its 38,150 kg propellant providing the 300 m/s post-MOI ΔV to the ITV. This leaves up to 3,089 m/s for the TEI burn. The ITV main propulsion stage, including the rocket engines, is 7 m in diameter and 14 m long.

6.3. Crew Mars Lander

The Crew Mars Lander (CML) is the vehicle in which the astronauts will descend to the surface of Mars. On the surface, they will live in either this CML or in the habitat (derived from the CML) that landed in 2018. They move the food landed in the MAV into this habitat and connect it to the MSPU's power grid. It is then the analogue of the habitat module in the Mars Direct plan. It is essentially a Large Mars Lander (LML), similar to those described in §5, but with a different payload and without the solar arrays in interplanetary space. Thus the Mars entry mass is 43,800 kg. The CML payload contains the following elements:

6.3.1. Structural and Thermal Systems. The estimate in §6.1.1 applies; the TransHab derivatives from which the ITV structural/thermal unit was scaled [DRM3/§A3.1] operate on Mars as well as in interplanetary space. Thus we retain the 2,549 kg mass estimate.

6.3.2. Life Support. The crew Mars lander should be able to land on Mars and keep the crew alive for 30 days; in addition, it should operate much longer if power and consumables are available. Thus we provide the 3,796 kg life support system from the ITV, which requires only food as input [see §6.1.2]. As a backup, an open-loop life support system, of mass 1,000 kg, is included in the crew Mars lander as well as 420 kg of hydrogen peroxide for oxygen generation, sufficient for 30 days. Additionally, food sufficient for 45 days (495 kg) is provided, so the crew will be able to survive in the CML for up to 30 days in all cases. (Water is produced in sufficient quantity for crew survival by the fuel cells; see §6.3.5.) This yields a total mass of 5,711 kg. An additional 5 MT of food is present in the CML at launch, since there was not room in the ITV.

6.3.3. Crew Accommodations. 2,356 kg; see §6.1.3.

6.3.4. Communications and Information Management. 400 kg; see §6.1.4.

6.3.5. Electrical Power Supply. The electrical power supply for the crew Mars lander is the fuel cell system from the MSPU [see §5.3]. It has a mass of 1,844 kg dry, with 4,507 kg reactants. The reactants can supply three fuel cells (18 kWe power generation) for 30 days. Loss of any one of the cryogenic reactant tanks still allows the crew to survive for 20 days. The production rate of water from the fuel cells is 150 kg/day, sufficient to meet the crew's needs. A 500 kg power distribution and rejection system has been budgeted.

6.3.6. Crew and EVA Systems. The crew has a mass of 500 kg, including pressure suits [see §6.1.6]. The Reference Mission allotment for EVA systems [DRM3/§A3.2.4] was used here: 195 kg for the airlock and 940 kg for the EVA suits (including one spare since we have a crew of five). Thus the total mass for this item is 1,635 kg. (At launch and TMI, the crew is not in the CML, leaving 1,135 kg.)

6.3.7. Atmospheric Repressurization System. Like the ITV [§6.1.9], the crew Mars lander contains 300 kg air. It also carries two 1/3 scale versions of the MAV oxygen generators, each with a mass of 346 kg, drawing 8,173 W power, and producing 5 kg/day of O_2 (sufficient to make up for the CML's lack of oxygen recycling). It is not feasible to run the oxygen generators until the crew Mars lander is electrically connected to the MSPU. Also, a buffer gas generation system will be needed on the crew Mars lander if it is to serve as a long-term habitation unit on Mars. The buffer gas is a mixture of nitrogen and argon, minor constituents of the Martian atmosphere; it is added to oxygen in habitation modules to reduce the danger of fire. The two generators each produce 1 kg of buffer gases per day. Mass and power are scaled from [DRM1/p. 3–105] with a 50% mass and power margin for a total mass of 219 kg and power consumption of 699 W. Additionally, there are four 63 kg / 44 W cryogenic tanks for storing up to 0.78 m^3 of buffer gas or oxygen each. These are identical to those from the HEDS lander [see §4.5]. This brings the total mass allocation for atmospheric pressurization to 1,682 kg.

Table 6.3.1. CML mass budgets at major mission stages

	Mass [kg]	
Component	*at TMI*	*at Mars arrival*
Structural and thermal systems	2,549	2,549
Life support (including consumables except for H_2O)	5,711	5,711
Crew accommodations	2,356	2,356
Communications and info management	400	400
Electrical power supply (including H_2O production)	6,851	6,851
Crew and EVA systems	1,135	1,635
Atmospheric repressurization system	1,682	1,682
Total	**20,684**	**21,184**

6.4. ITV-CML Tunnel and Truss

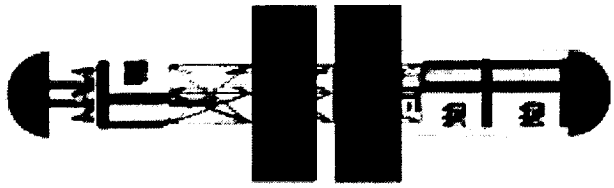

Figure 6.4.1. ITV with Solar Arrays Deployed

The ITV and CML will be connected in transit to Mars by a 30 m tunnel encased in an equilateral-triangle shaped truss with 7 m side length and three segments. During launch and TMI, the truss is collapsed to a 10 meter length. One of the three segments supports compression of the truss during these events. After TMI, the other two 10 m segments will deploy. Figure 6.4.1 shows the appearance of the ITV on the way to Mars; the CML is shown at left inside its aeroshell, with the truss and solar panels to the right, followed by the EEV within the truss, and the ITV habitat and propulsion system within their aeroshell.

The tunnel itself will need to be collapsed to 10 m length for launch and deployed to 30 m post-TMI. An inflatable tunnel was suggested by James Cameron, and will be portrayed in his upcoming Mars TV miniseries and IMAX 3D movie; since we have a 10 m initial length to work with, however, the inflatable tunnel will have this initial length.

The three sides of two of the truss segments will be covered with triple-junction ($GaInP_2$/GaAs/Ge) solar cell arrays,[26] which will convert sunlight into power with at least 21% efficiency. After truss deployment, the arrays on the two sides of the truss facing away from the Sun are deployed. Because only 400 m^2 of solar arrays are needed here, sufficient power can be produced even if one of the four deploying solar arrays fails to open.

If the tunnel cannot be used to connect the CML and the ITV habitat, the mission proceeds nominally but without rotating the ITV as described in §7.2. As a result, the crew will land on Mars after living in microgravity for approximately six months.

The solar panels and their backing/deployment system are estimated at 2,400 kg, three times the panels themselves. The aluminum 2024 T3 alloy primary segment (the one that holds compression during launch and TMI) of the truss will have a mass of 2,045 kg, and the remaining two segments, which do not have to hold nearly this load, will total 2,045 kg. The inflatable tunnel of radius 1 m has a mass of 1,500 kg, scaled from the TransHab-derived module study [DRM3/§A3.1] by surface area with a factor of 3 margin accounting for the differences in configuration between TransHab and the tunnel. A 700 kg docking module for the EAV is located at the CML end of the tube. This gives the ITV-CML tunnel and truss an 8,690 kg mass.

6.5. TMI Stages

The ITV/CML combination will use four stacked hydrogen/oxygen stages to inject to Mars. The first three are modified versions of the Z-5 third stage, fitted with cryocoolers to keep the hydrogen and oxygen propellants cold, solar arrays to power the cryocoolers, a reaction control system providing 150 m/s of ΔV, and insulation to reduce the heat load on the cryocoolers. The fourth stage duplicates the ITV main propulsion system, with a 3 MT adapter that attaches to the CML aeroshell and a 6 MT reaction control system (similar to that on the large TMI stages) for rendezvous with the other components.

Table 6.5.1. Mass budget for first three TMI stages

Component	*Mass [kg]*
Liquid hydrogen tank structure (189 m³, 7.12 m diameter), purge bag, MLI (100 layers/39 W heat leakage rate), and cryocoolers (5; 6,755 W power)	3,457
Liquid oxygen tank structure (70 m³, 5.10 m diameter), foam insulation, MLI (40 layers/96 W heat leakage rate), and cryocoolers (5; 2,477 W power)	831
Primary propulsion system (5 RL-10D engines, common with MAV and ITV main propulsion system)	1,889
Propellant feeds, stage structure, communications and information management system	3,090
Solar arrays (118 m² area, 40 kWe at 1 AU, scaled from DS1/SCARLET)	952
Regenerative fuel cell (for power during eclipse; provides at least 10 kWe continuous in LEO)	694
Radiator	200
Reaction control system dry mass (25% of propellant)	1,327
Margin (25%)	3,110
Total dry mass	**15,550**
Residual hydrogen (2% of tank capacity)	265
Residual oxygen (2% of tank capacity)	1,591
Total mass after firing	**17,406**
Usable hydrogen (12857 kg capacity)	12,755
Usable oxygen (77143 kg capacity)	76,530
Total mass before firing	**106,691**
Reaction control propellant, N_2H_4/N_2O_4 (expended prior to firing; can provide 150 m/s ΔV at 315 s I_{sp} using bipropellant thrusters)	5,309
Total mass at launch	**112,000**

It is frequently suggested that either nuclear thermal rockets (NTR) or solar electric propulsion (SEP) systems be used for TMI instead of conventional chemical rockets. NTR would reduce the number of Z-5 launches needed for the ITV by one and replacement of the Z-5 upper stage with an NTR system would increase the Z-5's trans-Mars delivery capability from 44 to 50 MT. It was determined that this performance gain does not balance out the political difficulties associated with nuclear systems or the need to develop a special new test facility required for NTR engines.

SEP is another possible TMI technology, whether it is used for the entire TMI process or augmented by a chemical "kick" stage.[27] While SEP provides a high specific impulse, a human mission would require an SEP system to be at least two orders of magnitude larger than the kilowatt-scale SEP systems used today on communications satellites and Deep Space One, thus presenting a major development risk. Additionally, since solar arrays do not produce power in Earth's shadow, an SEP spacecraft must either turn its propulsion system on and off once each orbit, discharge/recharge batteries or regenerative fuel cells once each orbit, or fly in an orbit with continuous sunlight. The first option involves running the SEP system and its associated hardware through of order 1,000 on-off cycles, which is undesirable from the standpoint of reliability. The second option greatly increases the mass and unreliability associated with the power system. The third option could involve restricting launches to the solstices, when a 51.6 degree inclination LEO can be in continuous sunlight, or it could involve launching into a (nearly) sun-synchronous orbit. The former idea is operationally undesirable, as it places a large burden on the launch facilities; the latter idea requires launching of the Z-5 from Vandenberg or another site with access to sun-synchronous orbit. Additionally, it adds another 300 m/s to the ΔV required to reach orbit, reducing the booster's payload capacity. Finally, the crew of the Mars mission must either spend months traversing the Van Allen Belts or ride a larger rocket (such as Proton) when their EAV is launched.

The costs of large SEP systems are not known at present, but given their complexity they will undoubtedly be more expensive to produce than chemical stages, although they might cost less to launch. One method of reducing overall costs

would be to reuse the SEP system, but depending on the specific configuration, even one reuse may require tens of thousands of hours of thrusting. SEP system lifetimes would have to be extended to make this option feasible. For these reasons, SEP was not used for the TMI scheme in this Mars mission.

6.6. LEO Assembly and the EAV

The complex of the ITV, CML, and four propulsion stages is launched in five pieces.

Table 6.6.1. Sequence of ITV/CML Assembly Launches

Launch	*Payload*	*Mass [MT]*
Z-5 #1	Trans-Mars Injection Stage 4	54
	Crew Mars Lander	49
	ITV-CML tunnel and truss	9
Z-5 #2	ITV habitat	44
	ITV main propulsion system	45
	ITV aeroshell	19
Z-5 #3	Trans-Mars Injection Stage 3	112
Z-5 #4	Trans-Mars Injection Stage 2	112
Z-5 #5	Trans-Mars Injection Stage 1	112

Each component is launched northeast from KSC into 51.6° inclination, 360 km altitude orbits. The orbit nodes precess backward by 5.1° per day, so launch windows to this orbit are 23 hours 36 minutes apart. Because the TMI stages have cryogenic coolers, scheduling of these launches is not critical; they need only occur well in advance of the TMI window.

Finally, several days before departure to Mars, the crew is launched on a Soyuz booster in the EAV. Because of the degrading physiological effects of the space environment, it is desirable not to extend the crew's stay in LEO unnecessarily. Launching the crew on a Z-5 with the CML (for example) would have to occur well before the TMI window because a delay close to the TMI window would force a mission abort. (The Z-5 is a large and complicated launch vehicle, and launch delays are to be expected.)

For this reason, a reliable means of sending the crew to the orbiting ITV/CML/TMI system is necessary. The only system currently capable of carrying a crew of five to the ITV is the Space Shuttle, but experience has shown that it too is susceptible to long delays. Thus a new vehicle will be needed. Fortunately, it does not need all capabilities of the STS; in fact, it should be as simple as possible to reduce the likelihood of a launch delay. An EAV was therefore designed to carry the crew into orbit and to the ITV/CML. It will launch on the Soyuz booster, which at present has been man-rated; humans frequently use it to travel to *Mir* with relatively few delays. The continued production of Soyuz vehicles is considered very likely, both because it has found a commercial role in launching communications satellites and because it will launch Progress and Soyuz spacecraft throughout the ISS program.

Trans-Mars injection uses the three large cryogenic stages and the copy of the ITV main propulsion system for a total ΔV capability of 4342 m/s. The ΔV necessary to reach Mars (C_3=20.25 km^2/s^2) from the 360 km assembly orbit is 4103 m/s.

6.7. Mars Arrival and Landing; Surface Operations

When the ITV arrives at Mars, the ITV/EEV complex separates from the CML, and the two aerocapture into Mars orbit separately. The CML follows the LML aerocapture and landing procedure described in §5.2, while the ITV and EEV capture into low Mars orbit at altitude 250 km. This orbit is nearly polar – its inclination varies between 88.07° and 90° [see §3.3]. The truss and tunnel are jettisoned.

During the crew's surface stay of 553 sols on the first mission [see Table 3.2.1], the crew will have access to the contents of the cargo payload landed in 2018, namely the two rovers and the scientific equipment. Possible examples of scientific equipment include greenhouses to test crop raising in the Martian soil, drills to excavate samples of subsurface materials, and automated rovers to collect samples from nearby locations.

6.8. Mars Ascent and the MAV Capsule

At the conclusion of the crew's surface stay, the MAV lifts off into a 250 km orbit and docks with the ITV and EEV. The MAV's crew capsule stands 4.5 m high and is 3 m wide; its mass budget is detailed in Table 6.8.1.

Table 6.8.1. MAV capsule mass budget

Component	*Mass [kg]*
Structure	700

Thermal control and life support systems	300
Consumables	40
Power, distribution, and rejection systems	600
Communications and information management	200
EVA systems	493
Reaction control system (600 kg propellant, 500 m/s ΔV)	767
Total landed mass	**3,100**
Crew	400
Mars rocks	500
Total mass at Mars ascent	**4,000**

6.9. Trans-Earth Injection, Earth Return, and the Earth Entry Vehicle

After docking of the MAV, the crew transfers its rock samples to the EEV. The MAV is then jettisoned, and the ITV's main propulsion system fires to place the crew on a trans-Earth trajectory. Upon arrival at Earth, the crew enters the EEV, separates from the ITV habitat, and aerobrakes at Earth for a direct splashdown. The Earth Entry Vehicle is derived from the MAV crew capsule; it also measures 3 m in diameter and 4.5 m in height.

Table 6.9.1. EEV mass budget

Component	*Mass [kg]*
Structure	700
Thermal control and life support systems	300
Consumables	40
Rechargeable batteries and power distribution	300
Communications and information management	100
Reaction control system (245 kg propellant, 170 m/s ΔV)	445
Aeroshell and descent system	1,290
Additional margin	325
Total unloaded mass	**3,500**
Crew and pressure suits	500
Mars rocks and scientific payload	600
Total mass at Earth entry	**4,600**

7. Crew Health Issues

7.1. Radiation

The majority of the crew's radiation dose during the first several human missions will be acquired in interplanetary space. Although the Martian atmosphere is much thinner than Earth's, it still provides reasonable shielding. At altitude 4 km, the atmosphere provides the equivalent of at least 11 g/cm² shielding in the vertical direction. For a surface stay in 2020–2022 similar to that called for in §3.2, Simonsen and Nealy estimate a dose equivalent in the blood forming organs of no more than 19.0 rem from GCR.[28] Solar flares are unlikely considering the fact that this mission occurs shortly after solar minimum, but subsequent missions at solar maximum can expect comparable dose equivalents from solar particle events.

Since GCR is continuous, a shelter for this type of radiation is not feasible. Shielding must be available throughout the entire interplanetary transfer vehicle. A TransHab-derived habitat would have about 5-8 g/cm² with included equipment, with typical atomic number between that of polyethylene and aluminum; the crew's dose equivalent would be about 65 rem/yr at solar minimum.[29] The missions listed in Table 3.2.1 all spend of order 1 year in transit between planets. As a result, the crew's maximum total dose from GCR over the course of the mission is about 100 rem.

On the other hand, a variety of shielding materials may be used for solar particle events; those with high atomic numbers are inadvisable because of the secondary radiation produced when particles collide with these large atomic nuclei. By contrast, when a particle strikes a low-Z material such as hydrogen, little of this secondary radiation is produced. Since hydrogen has the lowest atomic number, it would appear to be the logical choice, but logistical difficulties prevent it from being a useful shielding material. Only the liquid form of hydrogen is dense enough to provide appreciable shielding, and although the crew has an ample supply of LH_2 in the ITV's main propulsion system, the rotation of the structure [see §7.2 below] means that this tank cannot shield the crew in the case of a solar flare. But it is relatively easy to create a solar flare shield from

polyethylene. A shelter of polyethylene can provide 10 g/cm² of shielding to the crew in addition to the habitat's own shielding. For this reason, the ITV includes a polyethylene sphere 2.6 m in diameter as a solar flare shelter.

An additional concern on the Martian surface is neutron radiation produced from interactions of cosmic and solar radiation with the Martian regolith. The severity of this radiation is not known exactly, but our calculations based on a Langley Research Center model of the neutron flux[30] and our own neutron propagation code (validated by experiments using a ^{252}Cf fast neutron source) suggest that the total dose equivalent to a Mars crew from these neutrons is roughly equal to the direct GCR dose for the surface phase of the mission.

7.2. Artificial Gravity

The ITV-CML complex totals 62 m in length. The center of mass lies 20 m from the lowest level of the ITV habitat, providing a 20 m baseline for artificial gravity. The system rotates around a point in the central section of the truss. At three revolutions per minute, the crew experiences a centripetal acceleration of 2 m/s², somewhat higher than lunar gravity. At 4 rpm, the crew's acceleration is 3.5 m/s², slightly below Martian gravity. Revolution rates greater than 4 rpm will likely have disorienting effects on the astronauts. During this rotation, the complex is oriented so that the truss's solar panels face the Sun at all times. The truss is jettisoned at MOI, so artificial gravity is unavailable for the return trip. The astronauts will travel to Earth in microgravity since medical facilities will be available upon arrival.

8. Summary

8.1. Cost Estimates

Cost estimates of the human missions were constructed using the NASA Spacecraft/Vehicle Level Cost Model.[31] A learning curve of 85% (*ie*, the cost of producing twice as many items is only 1.85 times as much) was assumed. Both optimistic and conservative estimates were applied to the results of the cost model, as listed in Table 8.1.1. All values are in 1999 US dollars.

Table 8.1.1. SVLCM Cost Estimates of Mission Components

	Three missions		*Five missions*	
Component	*Optimistic*	*Conservative*	*Optimistic*	*Conservative*
Z-5 Launchers	$11,442,000,000	$19,616,000,000	$13,559,000,000	$23,244,000,000
Habitats	$17,570,000,000	$43,925,000,000	$19,379,000,000	$48,448,000,000
Aeroshells	$2,575,000,000	$7,724,000,000	$2,776,000,000	$8,328,000,000
Propulsion Stages	$4,319,000,000	$10,798,000,000	$4,726,000,000	$11,815,000,000

The estimates also assumed one pre-landed habitat per mission sequence, one ITV and one MAV per human crew, and two MSPUs and rover landers for the three-mission sequence or three each for the five-mission sequence. Estimates of the MSPU and rover costs were derived from [DRM1/p. 3–128], approximating the cost of two MSPUs and rover landers as 11% of the $55 billion overall cost and scaling linearly upward for the five-mission sequence. The costs of Soyuz launch vehicles for the crew was estimated at $18,000,000 per booster in each set of estimates.[32] Finally, the cost of mission support was estimated using the Mission Operations Cost Model.[33]

Table 8.1.2. Other Cost Estimates of Mission Components

	Three missions		*Five missions*	
Component	*Optimistic*	*Conservative*	*Optimistic*	*Conservative*
Surface Support	$3,025,000,000	$9,075,000,000	$4,538,000,000	$13,613,000,000
Soyuz Launchers	$54,000,000	$54,000,000	$90,000,000	$90,000,000
Mission Support	$738,000,000	$1,549,000,000	$822,000,000	$1,736,000,000

The results of these models are compared with optimistic estimates of the NASA Design Reference Mission 3 [see [34]] in Table 8.1.3.

Table 8.1.3. Total Cost Estimates

	Mars SCHEME Optimistic	*Mars SCHEME Conservative*	*NASA DRM3 Optimistic*
Three Missions	$39,724,000,000	$92,742,000,000	$40,320,000,000
Five Missions	$45,890,000,000	$107,274,000,000	$46,729,000,000

From this we conclude that the total costs are comparable to those of DRM3. We also see that the recurring costs are relatively low; each individual mission has a cost of $3 billion to $7 billion after the initial development of components.

8.2. Risk

A number of factors contribute to the reduced risk of the Mars SCHEME. First, each stage of the mission contains redundant crew life support systems. On the Martian surface, the first crew has available the CML in which it landed, as well as the 2018 habitat. (The MAV was not designed as a long-term habitat.) Subsequent crews will have the same two options as well as the CMLs of previous crews. In interplanetary space, the ITV habitat is equipped with two fully redundant life support systems [see §6.1.2], and the CML is also available on the way to Mars.

Second, new technologies are tested in the Martian environment before they are used by the crew. The HEDS landers [see §4.2] each contain a smaller version of the oxygen generators to be carried by the MAV, as well as radiation and materials exposure experiments. The descent and landing system on the crew Mars lander is identical to that used by the other LMLs, which are first tested in 2016 by the MSPU.

Third, a perfect (error below 1 km) surface rendezvous is not a requirement for crew safety. The CML has sufficient power and consumables [see §6.3.2] to support the crew for up to 30 days, enough time to drive the pressurized rover from the base to the crew's landing site by teleoperation and to return to the base.

Fourth, all LOX/LH_2 propulsion stages have engine-out capabilities. The TMI stages of the ITV each need three of five engines, the ITV's main propulsion stage requires two of three engines, and the MAV requires two of four engines. Although the LML descent stage uses only a single engine, it uses hydrazine/nitrogen tetroxide, a highly reliable bipropellant. In addition, the crew launches on a Soyuz rocket, which is already man-rated and has an extensive history of reliability. An escape tower is provided for the Soyuz launch.

Fifth, electrical power systems were also designed to reduce risk. The Mars SCHEME does not rely on retractable-redeployable solar arrays; retraction of such an array would be a major risk element due to the possibility of a failed retraction just hours before an aerocapture, which would be catastrophic to the mission. Also, there are two MSPUs provided for the crew on the Mars surface, providing redundancy in case of failure of one.

8.3. Conclusion and Recommendations

Clearly, the high reliability and low recurring costs of the Mars SCHEME make it a very feasible sequence of Martian exploratory missions. The plentiful infrastructure it establishes on the surface of Mars also make it a good predecessor to a fully staffed base on the Red Planet.

9. Outreach

As the leaders of the Mars Society of Caltech/JPL, we are at the forefront of space advocacy and public outreach on behalf of Mars exploration. We have had tremendous outreach success in politics, education, and in getting the general public excited about Mars. Highlights of our outreach efforts include:

- Production of an educational activity for 4th-6th grade students in which students pretend to be the first Mars explorers and use math and reasoning skills to save their Mars base's greenhouse. We have visited six schools with the activity and distributed it through our high school science teachers, our web page and via the Mars Society quarterly CD-ROM. We have visited nearly a dozen schools from elementary to college to promote Mars exploration.
- Meetings with major politicians, including face-to-face encounters earlier this year with President Bill Clinton and all four major presidential candidates – Bush, Gore, McCain, and Bradley, before the latter two exited the race. We have met with four members of Congress (Waters, Rohrabacher, Rogan, Calvert) and ten congressional offices (the above and Royce, Sanchez, Pomeroy, Conrad [Senator], Waxman, and Kuykendall).
- Consulting for James Cameron's upcoming Mars movies. Chris calculated his trajectories and we provided feedback on the architecture he will be depicting in his projects during a visit to his office.
- Creation and regular updating of our chapter web site, which features the outreach materials we have designed available for download by other Mars Society chapters or other space advocacy groups, information on our technical projects, Mars, and Mars missions, education materials, and photos from our activities.
- As of this writing, we have gathered 1,998 names and E-mails for our own chapter's mailing list and that of the national Mars Society.

A detailed listing of our events is available at our website, http://mars.caltech.edu/.

10. Acknowledgements

The authors would like to thank all who suggested improvements and modifications to the Caltech Mars Society Missions 1.0 and 2.0. We would especially like to thank our faculty advisors, Jim Burke, Bruce Murray, and Mark Adler for their

input and encouragement. We also wish to thank others who have supplied us with much-needed information, most notably C.R. Joyner of Pratt-Whitney and John Connolly of NASA Johnson Space Center. We would like to thank the Lunar and Planetary Institute and the HEDS-UP program for giving us the opportunity to participate in the 2000 HEDS-UP Forum. Caltech's Digital Media Center provided us with guidance, equipment, and software for the graphics in our presentation. Finally, we would like to recognize the contribution of David Berry of NASA Jet Propulsion Laboratory, who graciously provided the name of this mission plan.

11. References

[1] Jet Propulsion Laboratory. *Mars Global Surveyor Mission Plan, Final Version, Rev. B (542-405).* http://mars.jpl.nasa.gov/mgs/pdf/405.pdf. 1996, p. 3-9.
[2] Jet Propulsion Laboratory. "Mars Surveyor 98 Launch Vehicle." http://mars.jpl.nasa.gov/msp98/delta2.html. 1999.
[3] Wiesel, W.E. *Spaceflight Dynamics.* (The McGraw-Hill Companies, Inc., 1997). p. 206.
[4] Kittel, P. *et al.* "Cryocoolers for Human and Robotic Missions to Mars." (Received by personal communication from Plachta, D./NASA Glenn Research Center)
[5] Arianespace. "Arianespace, Launcher Family, Ariane 5." http://www.arianespace.com/launcher_5_evolving2.html.
[6] Andrews Space and Technology. "Zenit-Specifications." http://www.spaceandtech.com/spacedata/elvs/zenit_specs.shtml.
[7] Andrews Space and Technology. "Vulcain-Specifications." http://www.spaceandtech.com/spacedata/engines/vulcain_specs.shtml.
[8] Joyner, C. Russell (Pratt-Whitney). Personal communication, 1998.
[9] Thiokol. "STAR Performance & Summary Chart." http://www.thiokol.com/StarPerf.htm.
[10] Hirata, Christopher *et al.* "A New Plan for Sending Humans to Mars: The Caltech Mars Society Mission 2.0." 1999. http://mars.caltech.edu/chris_its/mars/cmsm2r.html.
[11] Starsem. "Starsem." http://www.starsem.com/web_in/family.htm.
[12] Newkirk, Dennis. *Almanac of Soviet Manned Spaceflight.* (Gulf Publishing Co., 1990).
[13] Lang, Kenneth R. *Astrophysical Data: Planets and Stars.* (Springer-Verlag, 1992). p. 49.
[14] Cataldo, Robert. "Considerations for Mars Surface Power Systems: From Robotic to Human Outposts." Presentation at the American Astronautical Society National Conference and 46th Annual Meeting.
[15] NASA Human Spaceflight. "HSF – The Shuttle." http://spaceflight.nasa.gov/shuttle/reference/shutref/orbiter/oms/.
[16] Lockheed Martin Space Mission Systems & Services. "Aeroheating Analysis for Mars TransHab Vehicles, Volume I – Methodology and Results." LMSMSS-32724, February 1998.
[17] Cataldo, Robert. "Considerations for Mars Surface Power Systems: From Robotic to Human Outposts." Presentation at the American Astronautical Society National Conference and 46th Annual Meeting.
[18] NASA Human Spaceflight. "HSF – The Shuttle." http://spaceflight.nasa.gov/shuttle/reference/shutref/orbiter/eps/pwrplants.html.
[19] Cataldo, Robert. "Considerations for Mars Surface Power Systems: From Robotic to Human Outposts." Presentation at the American Astronautical Society National Conference and 46th Annual Meeting.
[20] Joyner, C.R. (Pratt-Whitney). Personal communication, 1998.
[21] Connolly, John (NASA JSC). Personal communication, 1998.
[22] Muirhead, Brian (NASA JPL). "Champollion/DS4 Mission Overview." Presentation, June 1997. http://cism.jpl.nasa.gov/randp/docs/muirhead.pdf.
[23] Cornell University, student design team. "Extravehicular Activity Suit Systems Design: How to Walk, Talk, and Breathe on Mars." http://cass.jsc.nasa.gov/lpi/HEDS-UP/cornell.pdf. 1999, p. 13
[24] NASA Human Spaceflight. "HSF – The Shuttle." http://spaceflight.nasa.gov/shuttle/reference/shutref/orbiter/eps/pwrplants.html.
[25] Joyner, C.R. (Pratt-Whitney). Personal communication, 1998.
[26] Hughes Spectrolab. "GaInP2/GaAs/Ge Triple Junction Solar Cells." http://www.spectrolab.com/DataSheets/TJCell/TJCells.html.
[27] Gefert, L. *et al.* "Options for the Human Exploration of Mars Using Solar Electric Propulsion," Space Technology and Applications International Forum 1999, American Institute of Physics Conference Proceedings 458, El-Geuk, M. ed. 1999, p. 1275.
[28] Simonsen, Lisa C. and John E. Nealy. "Mars Surface Radiation Exposure for Solar Maximum Conditions and 1989 Solar Particle Events." NASA TP-3300, February 1993.
[29] Wilson, J.W. *et al.* "Galactic and Solar Cosmic Ray Shielding in Deep Space." NASA TP-3682, pp. 22. December 1999.
[30] Wilson, J. W. *et al.* "Mars Surface Ionizing Radiation Environment: Need for Validation." *MARS 2001 Workshop*, Houston, Texas. October 2-4, 1999.
[31] NASA Johnson Space Center. "Cost Models - Spacecraft/Vehicle Level Cost Model." http://www.jsc.nasa.gov/bu2/SVLCM.html.
[32] NASA Johnson Space Center. "Launch Vehicle Cost and Performance Data - International." http://www.jsc.nasa.gov/bu2/ELV_INTL.html.
[33] NASA Johnson Space Center. "Cost Models - Mission Operations Cost Model." http://www.jsc.nasa.gov/bu2/MOCM.html.
[34] Hirata, Christopher *et al.* "A New Plan for Sending Humans to Mars: The Caltech Mars Society Mission 2.0." 1999. http://mars.caltech.edu/chris_its/mars/cmsm2r.html.

Lunar Interferometric Radio Array
L.I.R.A.

EMBRY-RIDDLE
AERONAUTICAL UNIVERSITY

Undergraduate Student Team

John Abbott
Shane Pixton
Christopher J. Roberts – Team Leader

Dr. Mahmut Reyhanoglu – Faculty Advisor

Abstract

The Lunar Interferometric Radio Array (LIRA) is a performance driven design, with emphasis on utilizing the unique attributes of the far-side of the moon as a platform for radio astronomy. LIRA consists of three independent Lunar Telescope Units (LTUs), autonomously landed on the moon, and a communications relay satellite orbiting at libration point two (L2). Each LTU deploys a large inflatable spheroid, whose underside has been impregnated with a reflective coating. The spheroid is then gradually hardened into a shell by the sun's ultraviolet radiation.

LIRA achieves broadband capabilities by operating each LTU independently (tuned to offset frequencies), or provides high resolution observations as a three-element interferometer. The interferometer is functional with as few as two elements, yet will achieve greater resolution with additional elements. Thus, LIRA delivers both redundancy and the possibility for future expansion. Data processing, including interferometric synthesis, occurs at an earth-based ground station, eliminating the need for complex onboard data manipulation.

Definitions and Constants

CEI – Connected Element Interferometry

GN – Ground Network

HPBW – Half-Power Beamwidth

IBS – Inflatable Balloon-like Structure

ISM – Interstellar Medium

k – Boltzman's constant, 1.38×10^{-23} J/K

L2 – Libration point two

LIRA – Lunar Interferometric Radio Array

LPDA – Log Periodic Dipole Array

LTU – Lunar Telescope Unit

OFW – Operational Frequency Window (defined as 150 – 330 MHz)

RTG – Radioisotope Thermoelectric Generator

S – flux density, in Jansky (1 Jy = 10^{-26} Watts/(m^2 Hz))

SNR – Signal-to-Noise Ratio

T – Temperature, in Kelvin unless noted otherwise

VLBI – Very Long Baseline Interferometry

η – Antenna efficiency

λ– Wavelength

σ = feed spacing factor

τ = feed scale factor

Mission Introduction

In the electromagnetic spectrum, radio photons have the lowest energy. Therefore, they are emitted in larger numbers for the same energy radiated. This imparts a fundamental advantage to radio astronomy in the detection of distant objects, which is essential to understanding the nature and origin of the universe.

As radio spectra are extended to longer wavelengths, many tend to show radical changes, suggesting that different mechanisms are dominant in different parts of the spectrum[3]. The three important mechanisms of radio emission are blackbody radiation, plasma thermal emission and synchrotron radiation. The first two mechanisms are attributed to Planck's radiation law, which states that all objects at temperatures above absolute zero radiate energy in the form of electromagnetic waves. However, synchrotron radiation is a non-thermal emission (not due to temperature), and originates from relativistic electrons moving in the presence of a magnetic field of a star.

Manmade broadcast prohibits broadband terrestrial observations at frequencies from a few kilohertz to hundreds of gigahertz. Additionally, the earth's highly dynamic ionosphere and the presence of water vapor affect the propagation of radio signals, inhibiting high-resolution observations at particular frequencies internationally allotted to radio astronomy.

Engineering Considerations on the Lunar Far-Side

In order to effectively engineer an astronomical system on the lunar far-side, it is important that the nature of its environment be understood. The moon's weak gravitational constant ($g_{moon} \sim 1.6$ m/s^2) and lack of atmosphere (and hence weather-imposed loading such as wind, rain, etc.) allow for innovative approaches to structural design not possible on the earth. However, the magnetic field of the moon is variable and weak, and does not provide protection from the solar radiation during the lunar day,[4] inducing structural degradation. Micrometeorites also impact the surface at cosmic velocities due to the lack of a lunar atmosphere. The above factors are likely to serve as the fundamental limitations to the mission longevity.

Lunar equatorial temperatures range from 100 K to 385 K (-170 °C to 110 °C). The cold nighttime temperatures allow the cooling of many systems without the use of cryogenics, as the LIRA will be operational only during the lunar night.

The lunar regolith is fine grained, cohesive and has a low thermal diffusivity[5]. These properties indicate that thermal control problems could arise as a result of excessive regolith blown by rocket exhaust onto structures during descent to the surface. Also, the low diffusivity prohibits efficient thermal control by conduction to the surface.

The motion of the moon can be predicted more easily than the motion of the earth due to characteristics associated with the lack of an atmosphere and oceanic tides. Although the moon does experience solid body tides due to the gravitational attraction of the earth, the main tidal bulge is fixed. This makes the moon an ideal location for an interferometer. Additionally, lunar seismographs indicate that the moon experiences only a few hundred

quakes yearly, with the majority of their magnitudes within the earth's seismic background noise level[4].

Mission Drivers

The lunar far-side offers two primary advantages over the earth as a site for astronomical observations in the radio spectrum. First, the lunar-far side is the only place in the solar system perpetually shielded from manmade broadcast, as the moon rotates about the earth at the same rate it rotates about its own axis. Secondly, the moon does not have an appreciable atmosphere or ionosphere to adversely affect incoming signals[4].

The LIRA shall be sensitive to frequencies ranging from 150 MHz to 330 MHz, defined as the Operational Frequency Window (OFW). This enables observation at frequencies allocated to the observation of pulsars (150.05 to 150.03 MHz) and deuterium (at 327.38 MHz), in addition to continuum thermal and non-thermal emission at frequencies never before reliably observed on earth due to manmade broadcast.

The LIRA design is driven by the following objectives:

- To provide sensitivity from 150 to 330 MHz
- To achieve high angular resolution
- To provide instantaneous 30 MHz bandwidth broadband capabilities

Approach

The LIRA project was approached in a top-down fashion, seeking scientific performance while being limited by current or near-future technologies. After researching previously proposed lunar observatories, it was determined that a simple antenna (such as a dipole) array would require significant onsite processing and too vast an area to be viable. Alternately, a very large aperture dish could be supported in a crater, similar to Arecibo. However, deployment without a human presence seems unlikely.

Telescopes in an array, known as elements, receive radiation from a distant source with a time delay due to the distance between them, known as the baseline. The time delay can be accounted for if the baseline and the orientation of the source with respect to the baseline are well known. As the source drifts through the reception pattern, the amplitude of the superimposed signal varies periodically as the constituent signals interfere. The true brightness distribution of a source may be obtained as the Fourier transform of this signal, yielding higher resolution than from any single element.

There are two broad categories of radio interferometry: Very Long Baseline Interferometry (VLBI), and Connected Element Interferometry (CEI). VLBI utilizes independent array elements, which is desirable to allow for future expansion or the failure of an element.

A lunar-based VLBI array, with medium sized apertures, can achieve high angular resolution, or by tuning the elements to offset frequency ranges, broadband observations of a given source are possible. The LIRA shall operate in this manner.

The next phase in the LIRA mission was to identify the number of elements and the aperture size required for acceptable scientific results within the limits of feasibility. The LTU was designed around a Titan IV or Ariane V class launch vehicle, with attention given to the physical dimensions and mass budget to accommodate three units on a single launch.

Subsystem designs for the LTU and relay satellite were given secondary importance to the scientific performance due to the complex and detailed nature of subsystem design. However, significant, yet somewhat generalized, consideration was given to subsystems directly related to the performance and longevity of the mission.

LIRA Mission Outline

LIRA is an unmanned mission that consists of three Lunar Telescope Units (LTUs) and a communications relay satellite. The LTU is a semi-autonomous spacecraft, with a deployable telescope aperture. Each LTU will land at a predetermined destination near the equator on the far-side of the moon. Near-equatorial placement allows observations of sources in both the northern and southern skies. Because interferometers are largely self-calibrating, deviations from the desired landing site may be accounted for by observing a known source. However, the surface curvature of the moon imposes a maximum LTU separation of 10 km for interferometric purposes[4]. Upon landing, the LTUs establish a communications link with the ground network via the communications relay satellite.

A relay satellite is necessary because the lunar far-side is never in view of the earth. A suitable orbit for the satellite lies at libration point two (L2). This orbit remains in constant line of sight with the lunar far-side and the surface of the earth. The communications relay satellite requires two antennas and three independent transceivers to relay the telescope data in real-time. Additionally, ground controllers may uplink commands, such as steering position to the LTUs.

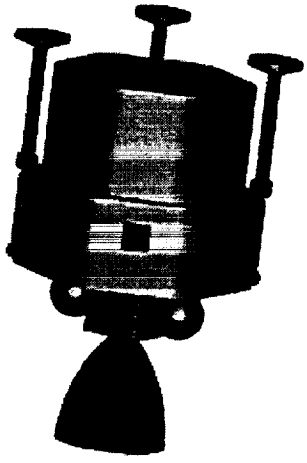

Figure 1: LTU in packed configuration

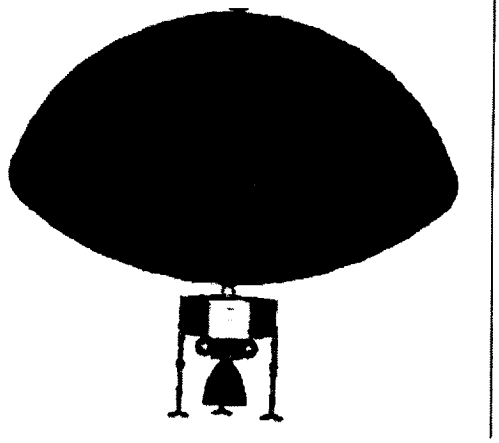

Figure 2: LTU with IBS fully deployed

Telescope Design

The moon's weaker gravitational attraction and its lack of an atmosphere enable the deployment of a large Inflatable Balloon-like Structure (IBS), which may serve as a telescope aperture by impregnating the underside with a metallic coating.

The IBS is compactly stored atop the LTUs in transit to the moon. Once on the surface, deployment of each IBS is delayed to allow the cloud of lunar regolith stirred by the LTU engine exhaust to settle, to avoid increased thermal absorption. After approximately 48 hours, the IBS is inflated with helium gas. It is desirable that the IBS harden into a shell structure to reduce maintenance associated with diffusion and temperature induced pressure variations. This is achieved by manufacturing a cross-linking chemical agent, activated by exposure to ultra-violet solar radiation, into the IBS material.

A control loop, involving pressure regulators and a calibration source, ensures that the dish takes its proper geometry as the lunar day progresses. Since the IBS will be in solar exposure for 336 continuous hours (the duration of one lunar day), the hardening process can be gradual. Off-axis steering from the sun, and the introduction of a catalyst gas may also be used to encourage homogeneous hardening. Once the shell is cured, the helium gas is vented, and a thorough calibration is performed.

A high-performance synthetic material will be required to realize the IBS. However, the capabilities of current materials suggest that such a suitable material could be produced should an initiative to develop it be taken.

Surface errors are less critical for the longer wavelength signals for which the LIRA is designed. Additionally, minor structural deviants, such as wrinkles from packing, may be accounted for by identifying critical points for each instrument, and correcting for them electronically. These initial errors, combined with structural degradation over time, result in an attenuation of the signal. It can be seen below that a surface error greater than 10 cm will significantly impact the telescope gain.

Graph 1 : Surface Error Losses

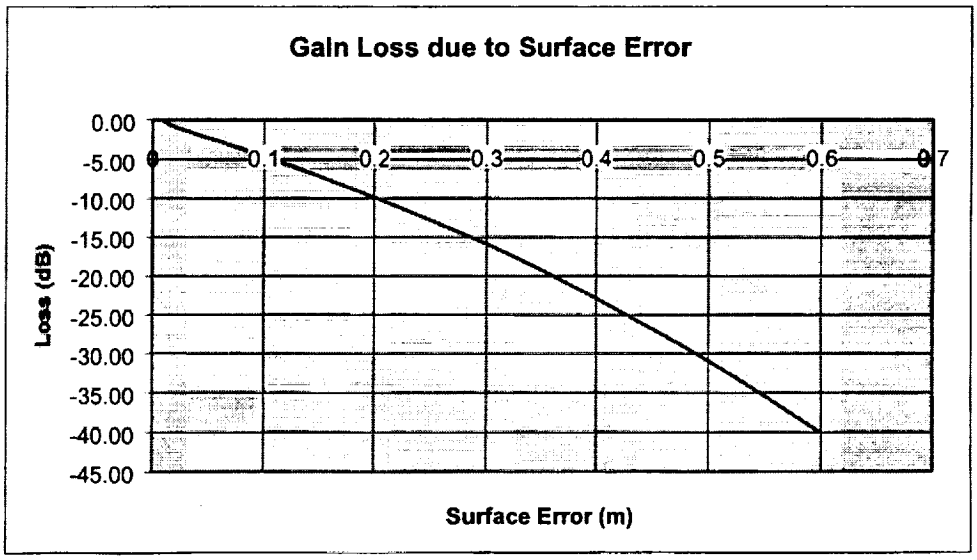

The aperture of the telescope must be on the order of several wavelengths to avoid diffraction. An aperture of 20 meters will allow acceptable resolution for signals within the OFW.

An important feature of telescope design is the focal length to diameter ratio (f/D). Side level radiation introduces noise to the signal, but is attenuated by a high f/D ratio. However, a low f/D ratio increases cross-polarization performance, which is important because sources are generally random emitters. A f/D ratio of 0.5 is a satisfactory compromise to these factors, which yields a focal distance of 10 m.

The height of the dish determines its shape and can be calculated by the following equation:

$$H = \frac{D}{16\frac{f}{D}}$$

where H is the height of the dish from the base to the top of the rim, D is the aperture and f is the focal distance.

With a dish diameter of twenty meters and a f/D ratio of 0.5, the dish height is found to be 2.5 m.

Gain is a multiplication factor by which the dish performs better than an isotropic receiver or transmitter given by:

$$Gain = \frac{4\pi\eta A}{\lambda^2}$$

where A = 314 m^2 is the area of aperture, η = 0.65 (typical[9]).

Table 1. Telescope gain as a function of wavelength (150 to 300 MHz)

Gain (dB)	Wavelength (m)	Frequency (MHz)
28.07	2.00	150
29.41	1.71	175
30.57	1.50	200
31.59	1.33	225
32.50	1.20	250
33.33	1.09	275
34.09	1.00	300

The feed receives the reflected signal from the dish. Each LTU will utilize two log periodic dipole arrays (LPDAs), oriented perpendicularly to provide reception for randomly polarized signals. The LPDAs are located at the focal point of the dish, 10 meters above the base and within the IBS. An individual LPDA consists of ten separate antennas, which are sized for different frequency sensitivities. With optimal scale and spacing factors ($\tau = 0.917$ and $\sigma = 0.169$, respectively) it will yield an additional 9 dB gain. The feed is 2.21 m in length. Below is a chart showing the length and spacing between each feed element. Additionally, the angle of the feed can be defined, and is equal to 38.88°.

Table 2. Feed element characteristics

Feed Element	Length (m)	Spacing Distance (m)
L1	1	0.34
L2	0.92	0.31
L3	0.84	0.28
L4	0.77	0.26
L5	0.71	0.24
L6	0.65	0.22
L7	0.59	0.20
L8	0.55	0.18
L9	0.50	0.17
L10	0.46	--

To help account for all polarizations, the two LPDA feeds can themselves be circularly polarized electronically. This is accomplished by sending one of the pre-amplified LPDA signals through a phase shifter. Switches placed in the circuit of each LPDA permit each signal to be observed individually, thereby allowing observation of all polarizations.

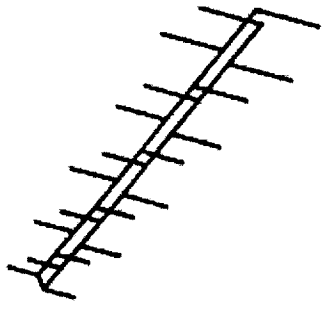

Figure 3: A single LDPA feed

Once a signal enters the feeds, it is sent to a receiver. The LTU receiver has the responsibility to amplify the incoming signal, change the polarity of the feeds, and to integrate and output a signal to the data relay transmitter. This process is handled by the following circuitry:

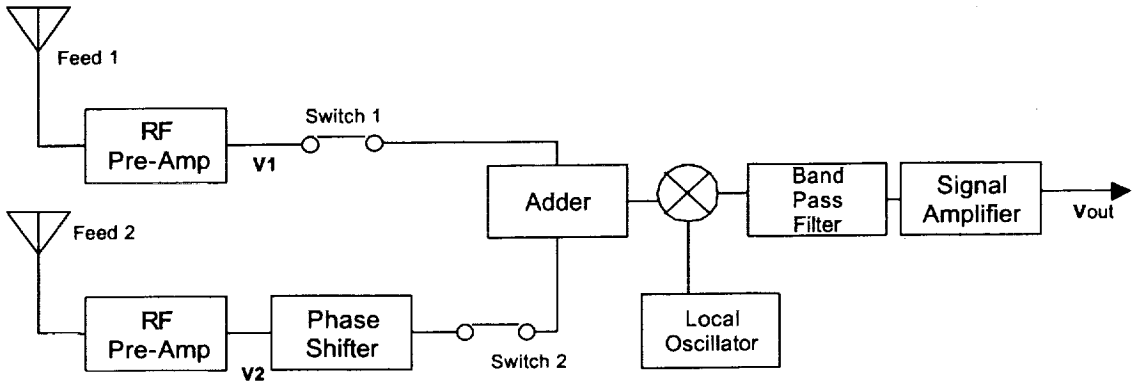

Figure 4 : Phase Switching Receiver Schematic

The incoming signal from Feed 2 can be phase shifted from –90 to 90 degrees to cover all polarizations. The switches will allow each feed to be selected individually, providing an even greater range. The final signal voltage can then be sent to an amplitude modulator to be transmitted to the relay satellite.

To conduct successful interferometry, the three LTUs must be spaced far enough apart to create helpful diffraction gratings which eliminate sideband noise. The baseline will also increase the resolution of the system. However, the baseline will be limited to a 10 km maximum due to the curvature of the moon[4]. The incoming direction of the wave plane can be found by analyzing the diffraction patterns and phase shifts between elements for a given frequency. The resolution is calculated by:

$$\frac{57.3^{o}}{d_{\lambda}}$$

where d_{λ} is the distance between elements in wavelengths.

The resolution and the directivity of the antenna dictate the amount of elements needed in an array to achieve specific results. The following spreadsheet compares baseline separation to maximum resolution (in degrees) for two elements at 150 MHz:

Table 3. Angular resolution between two elements at 150 MHz

Angular Resolution

λ= wavelength (m)

D = Dish Diameter (m)

L = distance between LTUs

R = Resolution (deg)

n= number of elements

Input: Distance Between LTUs, in Wavelength

n	L (m)	λ	Aperture	Resolution
3	100	2	20	0.382
	250			0.153
	500			0.076
	750			0.051
	1000			0.038
	1250			0.031
	1500			0.025
	2000			0.019

For multiple elements, the resolution can be calculated by dividing the above resolution by (n-1), where n is the number of elements. Thus, the three-element LIRA, operating at 300 MHz and at the maximum baseline of 10 km, is capable of 3.44 arcsec resolution.

Mechanical control of the LTU aperture is very important to conduct successful interferometry. The LIRA is movable up to 15 degrees off vertical and able to rotate 180 degrees about the vertical (thereby allowing +/- 15 degrees off vertical in all directions). This is accomplished by mounting the support plate of the IBS to a rotational swivel and a curved track. A simple gear, pulley and chain assembly will drive the IBS. Additionally, motion in right ascension can be achieved by meridian-transit scanning. However, the rate of right ascension is quite slow (~2.6×10^{-6} rad/s), due to the moon's long rotational period.

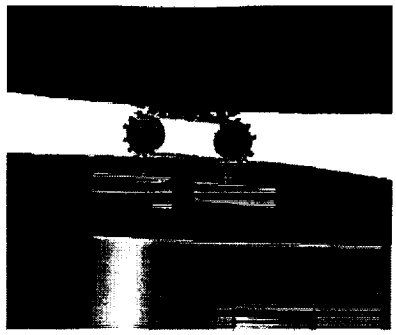

Figure 5: Drive steering mechanism

Case Study – CASSIOPEIA A:

In order to understand the broadband performance of the telescope, a well known source, such as Cassiopeia A will be examined in a case study.

First, the minimum detected temperature is calculated by

$$\frac{Ks\ T_{sys}}{(Bw\ t)^{1/2}}$$

where Ks is a receiver constant, t is the output time constant and Bw is the bandwidth.

The output time constant will be taken as one second for integration. Ks will be assumed to be 2 using a phase-switching interferometer[3]. The maximum bandwidth will be 10 MHz and the system temperature for the telescope is 100 K, the lunar nighttime temperature. This provides a minimal detectable temperature of 0.06325 K, which leads to the minimum detectable flux density given by:

$$S_{min} = \frac{2\ k\ T_{min}}{A_e}$$

$$S_{min} = 0.55618\ Jy$$

With this knowledge in hand, a Cassiopeia A may be used as a calibration source. It is situated 11,000 light years from the moon and has a flux density of 11,600 Jy at 178 MHz. The signal to noise ratio can now be calculated as:

$$SNR = S_{cass}/S_{min}$$

$$SNR = 43.19\ dB.$$

The Half-Power Beamwidth (HPBW) of the telescope and the source's subtended solid angle must be known. The HPBW telescope is 0.08587 ster, and Cassiopeia A subtends a solid angle of 1.66×10^{-6} ster. This provides a multiplication factor of 51179, which is used to measure the temperature of Cassiopeia A at a particular frequency. To accomplish this, the temperature factor is multiplied by the temperature increase in the antenna at that frequency. In other words, if the antenna temperature changes by 0.1 K while focused on Cassiopeia A at 178 MHz, then it can be deduced that the apparent brightness temperature of Cassiopeia A at 178 MHz is 5172.9 K.

Astronomical data from the telescope receiver will be handled by analog processing, due to limitations imposed by the performance of space certified computers. Data from the receiver will be combined with coherence data, important for the interferometric synthesis, modulated and transmitted to the relay satellite in real-time for processing and analysis at an earth based ground station. The achievable bandwidth is limited by the telescope electronics taken to be 10 MHz. As each LTU is capable of 10 MHz bandwidth, operating individually, a maximum instantaneous bandwidth of 30 MHz within the OFW can be obtained.

Communications Link Budget

The communications link budget must account for three independent channels from each LTU to the relay satellite then to the ground network. The link budget calculations were done with a spreadsheet, where inputs are given in dark gray boxes, and outputs given in yellow (or light-gray). The parameters of frequency and transmitter power are based on small deep space mission transceivers in the Ka band[6] (~30 GHz). Optimization of the Signal to Noise Ratio (SNR) can be achieved by modifying the input parameters. Calculations for the link budget from the ground station to the LTU are not included, as the LTU to ground station link is the limiting performer.

The LTU communications dish has a 1 m aperture and is placed on top of the IBS. The dishes of the LTU must be able to track the position of the 1.5 m dish of the relay satellite. The receiver temperature is kept at 303 K (30 °C), the presumed temperature inside the relay satellite. Results are listed in Table 4.

The satellite relay dish positioned towards the ground network has a diameter of 1 meter, and broadcasts to a ground network. The NASA Deep Space Network receiver temperature and aperture are used for this calculation, found in Table 5.

Both calculations are based on the maximum 10 MHz analog bandwidth (introducing the most noise), and thus are link minimum performances.

Table 4. LTU to relay satellite communications link budget

LTU-Satellite Communications Link

Ka-band communications:

Carrier Frequency (GHz) = 30.0 Lambda = 0.01 m

Transmitter Power = 5.0 W

LTU

Inputs	
Dish Aperture =	1
Antenna efficiency =	0.7
Effective Area =	0.55
Gain =	69087.23
Gain (dB) =	48.39

Satellite

Inputs	
Dish Aperture =	1.5
Antenna efficiency =	0.7
Effective Area =	1.24
Gain =	155446.27
Gain (dB) =	51.92

Free Space Loss (FSL)

Input	
Distance between LTU and Satellite =	67500000
FSL =	7.19E+21
FSL (dB) =	218.57

Incidental Losses (Li, in DECIMAL)

Input	
Li =	1.2

Receiver Noise (Nr)

Inputs	
Temperature of receiver (K) =	303
Bandwidth (MHz) =	10
Nr =	4.18E-14
Nr (dB) =	-133.78

Signal to Noise (SNR)

SNR =	148.67
SNR(dB)=	21.72

Table 5: Relay satellite to GN communications link budget

Satellite-Ground Network Communications Link

Ka-band communications:

Carrier Frequency (GHz) =	30.0	Input	
Transmitter Power =	5.0 W	Lambda =	0.01 m

Satellite

Inputs	
Dish Aperture =	0.5
Antenna efficiency =	0.7
Effective Area =	0.14
Gain =	17271.81
Gain (dB) =	42.37

Ground Network (Using NASA DSN)

Inputs	
Dish Aperture =	34
Antenna efficiency =	0.41
Effective Area =	372.25
Gain =	4.68E+07
Gain (dB) =	76.70

Free Space Loss (FSL)

Input	
Distance between Satellite and GN =	4.49E+08
FSL =	3.18E+23
FSL (dB) =	235.03

Incidental Losses (Li, in DECIMAL)

Input	
Li =	1.2

Receiver Noise (Nr)

Inputs	
Temperature of receiver (K) =	28.8
Bandwidth (MHz) =	50
Nr =	1.99E-14
Nr (dB) =	-137.02

Signal to Noise (SNR)

SNR =	531.87
SNR(dB)=	27.26

Electrical Power and Thermal Control

The LTU electrical power subsystem must be operational for 336 continuous hours in absence of the sun. This, in addition to the logistical problems associated with the deployment of solar array panels beyond the IBS, suggests that a Radioisotope Thermoelectric Generator (RTG) be used.

Due to the geometry of the IBS, the electronics and main structural components of the LTUs are constantly shielded from solar radiation. Since the moon has no atmosphere, and the surface is a poor conductor of heat, the LTUs remain essentially at the lunar nighttime temperature of 100 K, and the region of space in the shadow of the IBS may be used as a heat sink. (If the periods of time when the sun is close to the horizon are neglected, and the lunar albedo received by the LTU is not significant.) Space radiators, modulated by louvers, control the thermal environment of the LTU, which is always in an excess of thermal energy generated by the RTG[9].

Mission Lifetime

Micrometeoroid flux measurements indicate 300 impacts per square meter per year, with average diameters of 10 microns[4]. At this flux, the upper structure of the IBS will incur over 94,000 such impacts per year. Additionally, craters 100 microns in diameter will form at the rate of about 150 per year.

The LTU dish will be the only structure directly exposed to the sun. The thermal control of such a large area would ideally be achieved through the use of thermal coatings, to avoid complexities associated with active controls. Due to the solar ultraviolet radiation, the degradation of these coatings is exponential in nature[9]. The upper limit for functional performance of thermal coatings is 44,000 hours[9]. This corresponds to a continuous exposure time of five years. Since only half of the time is spent in exposure, the upper limit of mission lifetime is 10 years. A more realistic approximation would be a maximum exposure time of 22,000 hours (allowing for thermal coatings of a lesser performance and micrometeoroid impacts), corresponding to a maximum five-year mission lifetime.

The mission is scheduled to launch in the year 2005, or any consecutive period less than 2.5 years before the solar activity minimum. This will minimize the solar wind flux and ultimate thermal degradation of the IBS.

Conclusions and Recommendations

The LIRA design may be expanded to include a scientific impact study to determine more specific mission objectives and their relevance to science. From this point, the LIRA concept could be modified to meet those objectives. This would also enable a more detailed subsystem analysis and reasonable cost estimates to be performed.

Due to the scientific nature of the LIRA mission, the only likely sources of funding will be governmental. LIRA was designed with an emphasis on as-simple-as-possible design principles to address the NASA initiative of "faster, cheaper, better" missions. However,

the inherent complexities of a lunar-based interferometer seem to disqualify LIRA from this philosophy, unless international sources can help defray the costs.

The invasion of restricted frequencies by the communications industry seriously threatens the future of radio astronomy,[3] and already prevents very broadband observations. In the future, the lunar far-side may become the only suitable place from which to conduct observations. In such a case, the costs of a LIRA-class mission would be justified.

A possible political motivation for an international lunar-based interferometer, aside from sharing industrial technologies, could be stimulated by the Search for Extra-Terrestrial Intelligence (SETI). Current large-scale SETI projects presume that an extra-terrestrial civilization is intentionally broadcasting on significant frequencies[7]. However, our civilization itself does not continuously broadcast at these frequencies. Instead, our broadcast occurs all along the radio spectrum, *except* at those significant radio astronomy frequencies.

Outreach

LIRA team members have maintained an Internet site since early October, from which progress reports, presentation slides and pictures are accessible. The site will remain active as part of a showcase of Embry-Riddle Engineering Physics design projects, and also as a HEDS-UP resource.

In September, members presented preliminary design concepts to Engineering Physics freshmen as guest lecturers in the PS109 course. Team members were also present to give a project summary and show Pro/Engineer models (contained in this report) to prospective students at the Fall Open House. The results of the first semester were presented to colleagues in the senior design course in December. The final presentation occurred in the Miller Auditorium on April 12, before an audience of 150 students, professors and the general public.

A LIRA project summary, and a photo of team members, appeared on the cover of the Spring 2000 Engineering Physics Newsletter, distributed to over 300 Engineering Physics students professors and alumni. Embry-Riddle's campus newspaper, The Avion, also has a forthcoming article about the LIRA project and the HEDS-UP forum.

Each outreach activity was designed to increase awareness and understanding of the basic principles of radio astronomy, the drivers for a lunar far-side based observatory, the lunar environment and the LIRA design, with levels of complexity adjusted for the audience.

Acknowledgments

The LIRA team would like to thank the following members of the Embry-Riddle faculty: Professor Charles Bishop, Dr. David Cameron, Dr. James Cunningham, Dr. Peter Erdman, Dr. Robert Fleck, Dr. Al Helfrick, Dr. John Olivero, Professor Elliot Palmer and especially Dr. Mahmut Reyhanoglu for his time and effort put into the design courses.

We would also like to thank Dr. Mike Duke of the Lunar and Planetary Institute for giving us the opportunity to participate in the 2000 Human Exploration and Development of Space – University Partners symposium.

Christopher Roberts: I would like to thank my parents Tom and Carmel Roberts for making any sacrifice to allow me to pursue my dreams, and Ms. Judith Bush for her dedication to all students.

Shane Pixton: I wish to thank my family (John, Cathy, Lundy, and Erin) for all their support in my education. I would also like to thank all my friends for being there, especially Celine Aubouin.

John Abbott: I wish to thank my mother and father Pam and John Abbott for their years of support.

References

[1] Campbell, Bruce A. (1996). *Introduction to Space Sciences and Spacecraft Applications*. Gulf Publishing Company.

[2] Johnson, Richard C. (1993). *Antenna Engineering Handbook,* 3rd Edition. McGraw-Hill, Inc.

[3] Kraus, John D. (1966). *Radio Astronomy*. McGraw-Hill, Inc.

[4] NASA Conference Publication #2489 (1986). *Future Astronomical Observatories on the Moon*. Houston, TX. January 10.

[5] NASA Conference Publication #3039 (1988). *A Lunar Far-Side Very Low Frequency Array*. Albuquerque, NM. February 18-19.

[6] Noreen, G.K., A. L. Riley and V. M. Pollmeier. *Small Deep Space Mission Telecommunications*. Jet Propulsion Laboratory, California Institute of Technology. Pasadena, California.

[7] The SETI Institute (1997). *Ask Dr. SETI*. http://www.setileague.org/askdr/waterhol.htm

[8] Stutzman, Warren L. (1998). *Antenna Theory and Design,* 2nd Edition. John Wiley & Sons, Inc.

[9] Wertz, James R. (1999). *Space Mission Analysis and Design,* 3rd Edition. W.J. Larson and Microcosm, Inc.

[10] Wolff, Shirley (1999). *Deep Space Network*. http://deepspace.jpl.nasa.gov/dsn/index.html

MAEV
*M*artian *A*irborne *E*xploration *V*ehicle

Wichita State University
Department of Aerospace Engineering

HEDS-UP Forum
May 2000

Manager:
Ravi Malla
MAEV Team Members:
Soo Han Loo
Loy Yik Liew
Ng Seet Wai
Dean Edmonston
Truong Dinh
Nishanka Mahathalagalage

Martian Exploration Parachute
Chuong Dinh
Roberto Medina-Fernandez
Jaime Gavino-Nadal

Faculty Advisor:
Dr. M. Gawad Nagati

Abstract:

A conceptual approach was taken to design an airborne exploration vehicle capable of operating in the Martian atmosphere. To complete the design, a modular Carriage and Track system capable of deploying and retrieving the aircraft was also developed. Known as the Martian Airborne Exploration Vehicle, it is a solar powered wing body design with a span of 30.5 meters and a chord of 1.2 meters. With a full payload of 30 N, it weighs 300 N on Mars and has 4 propellers, which are capable of generating enough thrust to reach a maximum velocity of 67 m/s at a maximum altitude of 500 meters. The maximum radius of operation at the equator is 1000 kilometers. A 60-meter long Carriage and Track system fastened to the ground will be able to deploy the MAEV using a rocket assisted takeoff process, and then retrieve it using a resistance pulley mechanism.

TABLE OF CONTENTS

LIST OF TABLES

LIST OF FIGURES

1. Introduction

The success of human presence on Mars will critically rely on several factors. Among the most important ones is the ability for humans to have exploration capability on the planet. The prospect of successful missions to Mars has raised more questions than answers, in relation to what we need to know about our neighboring planet. With this in mind, a concept of an up-close, yet long range, exploration vehicle was conceived.

Due to the adverse geological construction of the planet, the range of surveillance should not be limited by the unpredictability of the terrain. An airborne craft will be suitable in meeting the demands of such missions. With a plan for the future, several considerations were taken into account, and after making logical assumptions, a conceptual aircraft was designed. Also, due to the unavailability and the difficulty in construction of a landing strip, a concept of a landing and takeoff track system was developed.

2. Initial Assumptions

The following assumptions made were critical in conceiving the MAEV design.

- § Forecasting successful space travel in the next 20-30 years
- § Capability of mass transportation of parts and components
- § Long term human habitation
- § Light scale manufacturing capability on Mars
- § Availability of engineers to assemble and maintain the aircraft system
- § Reliability of current planetary data and their accuracy
- § Ability of forecasting of Martian weather
- § Availability of lightweight avionics and laser precise telemetry equipment
- § Dependability of stability augmentation and guidance system for aircraft

3. Approach

To create such an exploration aircraft system, several factors involving atmospheric differences between Earth and Mars were taken into consideration. The lesser gravity and considerably lower atmospheric density on Mars were the key components. To produce a feasible design, fundamental aspects of aircraft theory were assessed. These key categories include:

Aerodynamics:	Finding an aerodynamically capable and suitable airfoil configuration for the aircraft wing.
Power (Source/Supply):	Utilizing solar or forms of reusable power sources.
Propulsion:	Designing highly efficient propellers to provide thrust and solid rockets for assisted take-off.
Structures:	Using ultra light, yet strong materials to construct the aircraft.
Control & Avionics:	Application of highly accurate control and telemetry systems for maneuvering, landing and take off.

Focusing on each category, the fundamentals were addressed, and concepts meeting the criteria were developed. Analyses of individual components were completed to evaluate the feasibility of the final design.

4. Description

The current stage of the MAEV design consists of two major components: the aircraft itself, and the takeoff & landing track system. The aircraft has a wing body configuration with a span of 30.5 meters and a chord of 1.2 meters. The resulting aspect ratio is 25.42 with a wing area of 36.59 square meters. The aircraft itself consists of a solar array, 4 double blade propellers, lightweight electric engines (off-the-shelf motors), a rechargeable battery pack, avionics, control systems and predetermined weight room for payload. A detailed list of these components including the aerodynamic specifications, weight and dimensions of the aircraft are shown in Table 1.

Table 1. Component details of the MAEV

Components	Sub-components	Mars		Dimensions (m)
		Newtons	Kilograms	
Wing (structure)	Wing Skin			2.3×10^{-5} thick
	Circular Spar			0.1 dia., 30.5m length
	Airfoil Rib			
	Truss Member Rib			
	Prop Engine Supports			
	sub-total	104.4	28.0	30.5m x 1.2m
Engines & Prop (4)		37.2	10.0	1.4 m dia. Prop
Solar Array		98.1	26.3	17.5 m^2
Battery Pack		22.4	6.0	Variable (small)
Payload		29.8	8.0	Variable
Avionics		7.5	2.0	Variable (small)
Total Weight		**300.0**	**80.5**	**36.6 m^2**

The overall weight of 300 N includes secondary parts such as wiring and fasteners, which are assumed to be insignificant compared to their primary components. An exterior view of the wing body is shown below in Figure 1.

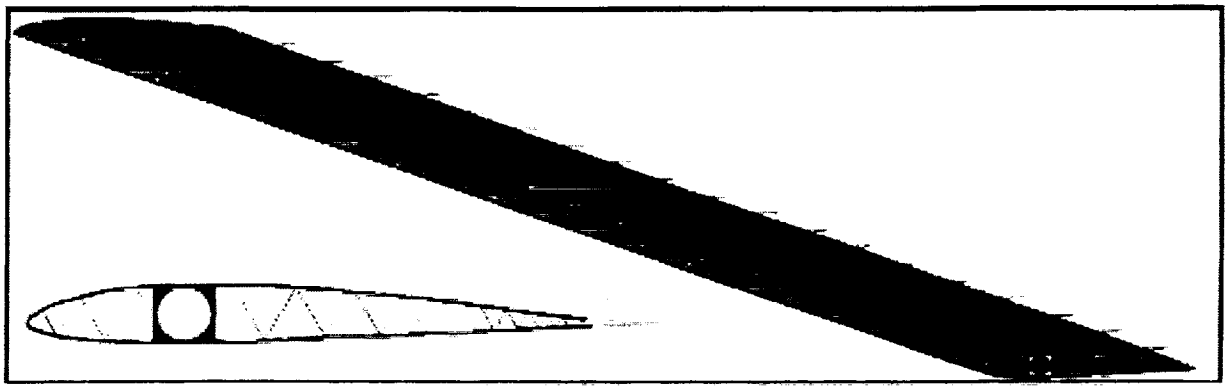

Figure 1. Exterior view of the wing body design

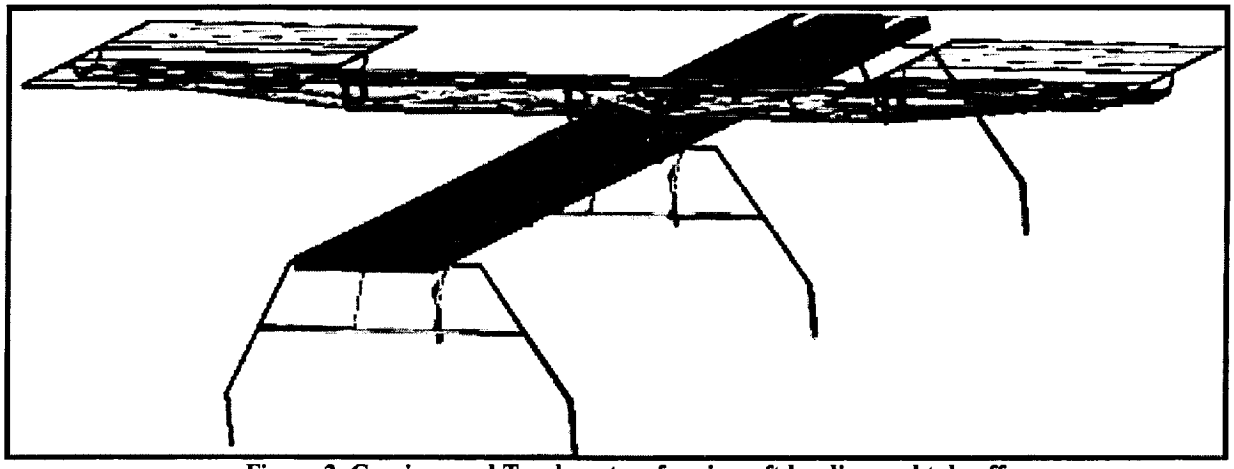

Figure 2. Carriage and Track system for aircraft landing and takeoff

For the takeoff and landing process, a track and carriage system as shown in Figure 2 was developed. Designed to be lightweight yet structurally stable, it is constructed mostly of Aluminum 6061 –T6. The specific dimensions and its details are shown below in Table 2.

Table 2. Component details of the Carriage and Track system

Components	Sub-components	Mars		Dimensions (m)
		Newtons	Kilograms	
Carriage	Carriage support	98.5	26.5	6 x 0.5 x 0.15
	wing supports			1.5 x 1.5 x 0.1
	wheel support			0.5 x 0.15
Track System	Main track module	58.0	15.6	0.75 x 0.1 x 3.0
	Main support			
	Outrigger support			
	Ground Support			
Total Weight		**156.5**	**42.0**	

4.1. AIRFOIL SELECTION

To obtain a suitable airfoil, the atmospheric data conditions of Mars were collected and analyzed. The key factors were the air density, the gravity and the air viscosity. Table 3 and 4 below lists these values.

The MH62 airfoil selected for the wing has a maximum lift coefficient, C_{Lmax} of 1.111 and parasite drag coefficient, C_{do} of 0.01332. It also has low moment coefficient, which is suitable for flying wing design. The trailing edge reflex of the airfoil tends to drive the pitching moment to be zero, allowing an aircraft configuration without a tail.

Table 3. Martian Atmospheric Data

Air density of Mars @ altitude 500 m	:	$\rho = 0.0144$ kg/m^3
Air density of Mars @ Sea Level	:	$\rho = 0.0150$ kg/m^3
Air viscosity of Mars	:	$\mu = 1.08 \times 10^{-5}$ N.s/m^2
Gravity of Mars	:	$g = 3.7278$ kg.m/s^2
Speed of Sound on Mars	:	$a = 200$ m/s

Table 4. Density Gradient Formula for Mars

For $h < 7000$

$T = -31 - 0.000998 * h$

$P = 0.699 * e^{-0.0009 * h}$

$R = p / (0.1921 * (T + 273.1))$

Where :

R = Density (kg/m^3)
P = Pressure (Pa)
T = Temperature (°C)

The MAEV is designed to have a maximum cruising velocity of 66m/s and a possible minimum velocity of 28 m/s. The operating Reynolds Number is around 100,000. The best lift to drag ratio cruising velocity for the current aircraft configuration is at 42 m/s. During takeoff conditions, with a full payload of 30N, the stall speed at sea level is 31.4 m/s and, during landing, the stall speed is 30 m/s, assuming that the payload has been jettisoned. The rate of climb of the MAEV at the maximum velocity of 67 m/s is 0.5 m/s and the best rate f climb of 2 m/s occurs at a velocity of 60 m/s. These values are, however, based on steady flight conditions.

4.2. PROPELLER DESIGN

To provide the thrust required for the MAEV, a highly efficient propeller is needed. The design chosen for this purpose, is a GM-15 airfoil, which has a low Reynolds number and high lift coefficient with moderately low drag coefficient. It has a maximum lift coefficient of 1.32 at an angle of attack of 16 degrees and a low Reynolds's number of 40000. The propeller is designed using detailed steps involving basic aerodynamic principles. Applying known values of the Martian atmosphere, a program was written.

Section	r, m	dr, m	Twist angle degree
1	0.03048	0.06096	89.989
2	0.09144	0.06096	79.241
3	0.1524	0.06096	68.116
4	0.21336	0.06096	59.064
5	0.27432	0.06096	51.903
6	0.33528	0.06096	46.232
7	0.39624	0.06096	41.763
8	0.4572	0.06096	38.154
9	0.51816	0.06096	35.175
10	0.542544	0.06096	34.144

Table 5. The r and β values for each segments

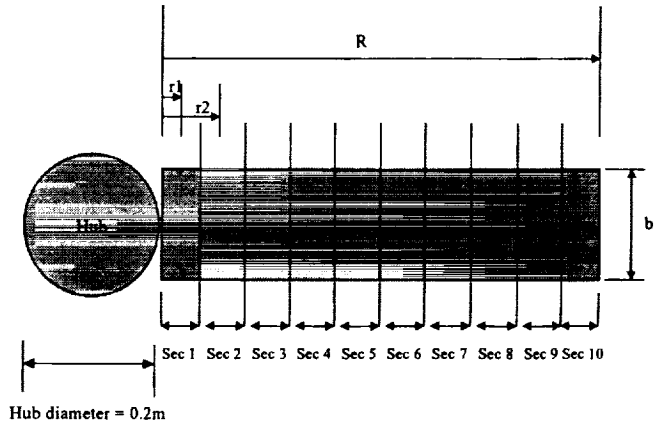

Figure 3. Configurations of a propeller blade

The radius of the propeller was divided into 10 equal length segments to find the best twist angle/geometric pitch angle from tip to root of the propeller. The gradient of the C_L versus α graph for GM 15 airfoil is $a_o = 0.1415$. The radius of the propeller is r = 0.6096m. The number of propeller blades is defined as B = 2. The chord length of the entire airfoil for the propeller is b = 0.1m with a hub radius of 0.1 m.

The thrust required for the aircraft was obtained. The angle of attack where the highest C_L/C_D value during cruise velocity was determined. The speed range of the MAEV was obtained and a speed was selected. A reasonable value for the revolution per seconds, n, was chosen. A trial and error method was conducted to estimate the twist angle, β, for all ten segments of the propeller blade based on the selected MAEV flying cruise speed. The effective pitch angle, ϕ, and the angle of attack, α, were calculated. The C_L and C_D values for lift and drag coefficients were taken from graphs for GM-15 airfoil. The values of the induced angle, θ, was determined and used to find ϕ_o. By limiting the tip speed of the propeller to 200 m/s, the relative velocity, V_R, was calculated. The thrust and torque was then determined. These steps were repeated for each of the ten segments. The r-values and the angle of twist values are shown in Table 5.

The next steps involved calculating the thrust and torque required at cruise speed. With the thrust found for one propeller, the total thrust produced by four propellers was determined. By applying a tip loss factor, 2% of the propeller length is deducted from the tip segment to calculate the actual thrust each propeller can produce. With the total thrust produced by 4 propellers (varying n to achieve the required thrust), the thrust produced can be matched to the thrust required. With this, the different velocity's power requirement to run the propellers was calculated. The propeller efficiency, P_{output}, P_{input}, and the efficiency, η, was then calculated. Additionally, the aspect ratio was calculated. The best performance of GM-15 airfoil is at the angle of attack of 9 degrees. The total thrust produce by 4 propellers at

different velocity was shown in Figure 4 and 5. Due to the need in changing the rps of the propeller to increase the free stream velocity, a gear mechanism for calculation purpose is required. The power required and the efficiencies to run 4 propellers at various velocities are shown in Figure 6 and 7.

The Aspect Ratio for the propeller is 12.2. The changes of thrust produced and required, power required and efficiency of the propeller can be seen in Figure 4, 5, 6 and 7, below. As shown in Figure 4, with a motor speed control system (for calculation purpose only), the propellers were only capable of cruising at the speed where the thrust required and thrust available intersect. The available cruising speed as shown in Figure 4 are 45m/s, 67m/s and 50 m/s. If avionics control systems are used to control the power input to the propellers, the cruising speed would be from 31m/s to 67m/s. The power required ranges from 502.866 W to 1366.4 W. This is mainly due to the capability of the control system in changing the revolution per second of the propellers. This can be seen in Figure 5. As a result, the propeller drawing with actual twist angle and its configuration is shown in Figure 8.

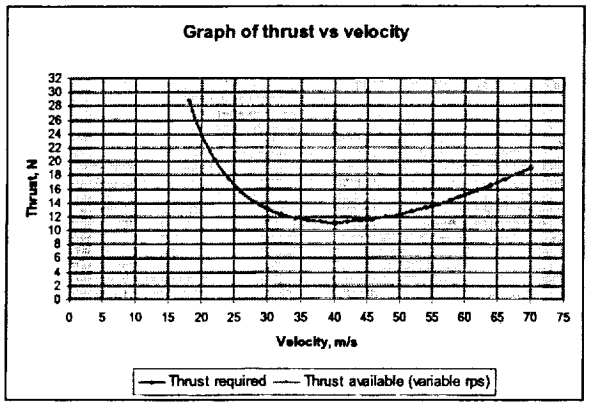

Figure 4. Graph of T_{ave} and T_{req} vs. V (MSC)

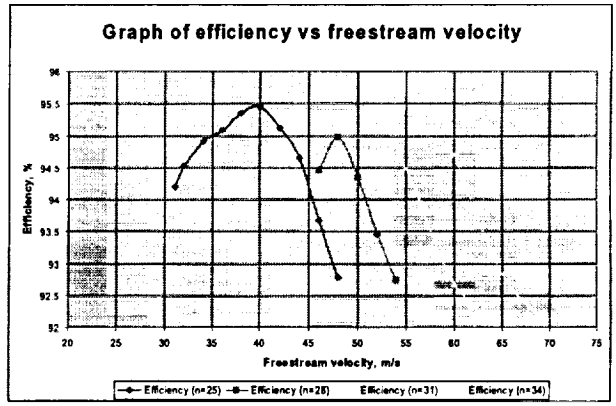

Figure 5. Graph of T_{ave} and T_{req} vs. V (a.c.s)

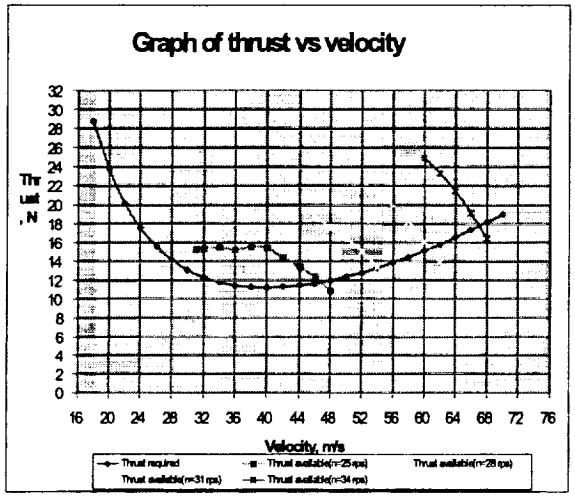

Figure 6. Graph of η_{prop} versus V

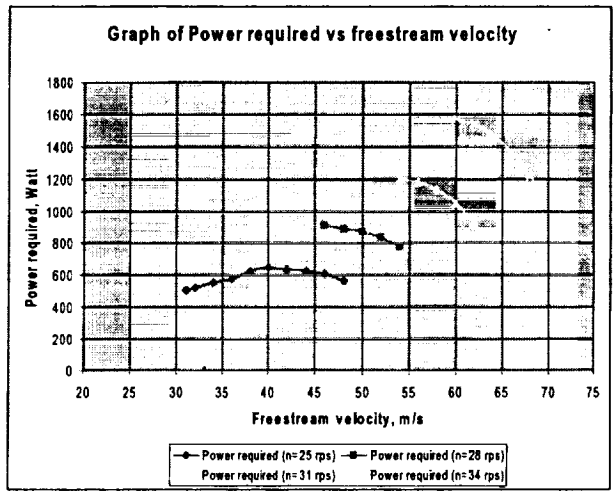

Figure 7. Graph of P_{req} vs V

The results show that the effective pitch angle is increasing from tip to root of the propeller. The n generated by this double blade propeller is reasonable as it provides an average of about 3500rpm rotation with the tip velocity (maximum tip speed = 130.245 m/s) not exceeding the speed of sound in Mars. Due to the low average operating Reynolds number of the propellers (Re # = 7611.278 to 12598.072), the GM-15 airfoil (Re # = 40,000) used for these calculations are not very accurate. The reason other airfoils were not chosen is because the GM-15 airfoil is the only low Reynolds number airfoil available with accurate data. Modifications on the airfoil, n, size, twist angle will help improve the efficiency of the propeller.

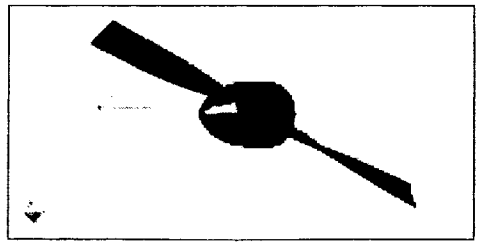

Figure 8.CAD Drawing of Designed Propeller

4.3. POWER

To meet the power requirement for the MAEV, two types of power sources were selected. One is a photovoltaic solar array, which utilizes solar energy in the form of photons converting light into electrical energy. The second power source is a rechargeable battery pack with a high energy density. These batteries can also be dedicated as backup power during solar array malfunctions. This precaution is taken due to the harshness of the Martian atmosphere.

4.3.1. Solar Array

Mars has lower light intensity of 0.4306 compared to 1.0 on Earth. The solar cells that are used on the MAEV are the dual-junction Gallium-indium-phosphorous/Gallium-Arsenide with Germanium substrate or $GaInP_2/GaAs/Ge$. The particular solar cell has an intensity (power per surface area) of $266W/m^2$ and mass per surface area of $1.51kg/m^2$ with efficiency currently stands at 21.5%. The solar array can survive 10-15 years of mission environment as claimed by Hughes Spectrolab.

The power requirement from the electric motor ranges from 560~1500 Watts depending on the speed and rpm of the propeller The maximum power output from the solar array is 2000W. This covers an area of $17.5m^2$ on top of the $36.6m^2$ wing area. The weight of the solar array is 26.3kg or 98.1N in Mars. (Note that the solar array area can be increased to generate more power, however, increasing the area in turn would pay a heavy weight penalty). The excess power from the solar array is directed to other electric components in the aircraft such as avionics and payload equipment (example, spectrometer, imaging instrument, communication devices, micro probes etc.).

4.3.2. Rechargeable Battery Pack

A rechargeable Silver-Zinc battery pack is the second types of power source selected for the MAEV. The aircraft is designed to carry 6 cells of this type, which weigh 1kg each, in parallel configuration instead of a series for a fail-safe reason. Silver-Zinc has a high power density and a discharge rate of 176W.hr/kg and 320A.hr respectively. It is a rugged, leak proof and spill proof design, which can operate in very cold temperatures ($+70^0C$ to -21^0C) and can be packaged in the most severe requirements. The recharge time is 8 hours with and the life span is 200 charges.

The power generated by the solar array is heavily dependent on the angle of the sun with respect to the aircraft's upper surface and the latitude of operation. Table 6 shows the variance in performance with respect to the power produced at a given operation time frame. These values are based on a zero degree Martian latitude operation.

Table 6. Variable cruise velocity with respect to power generated by solar array

Flight time in hours	Power produced at particular time frame(Watts)	Minimum power required with respect to velocity(Watts)	Cruise velocity (m/s)	Distance traveled(km)
0800-0900	911	673	46	165.6
0900-1000	1332	1260	58	208.8
1000-1600	1831	1520	66	1,425.6
1600-1700	1177	931	52	187.2

(Note: This situation only refers for 0-degree latitude)

4.4. RANGE OF OPERATION

Relying on just the Solar Array, the MAEV has a flight distance of 2000 km and a flight time of 9 hours at 0-degree latitude. The maximum distance capable at a latitude range of 0 to 60 is shown in Table 7 below. It also shows the maximum flight time possible for each 10-degree increment. The maximum range of the aircraft is deduced from a best cruise velocity combination, which is dependent on the time of day. An example is shown in Table 6 above.

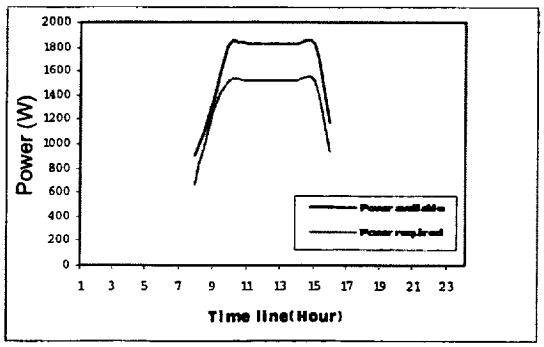

Figure 9. Power Available vs. Required

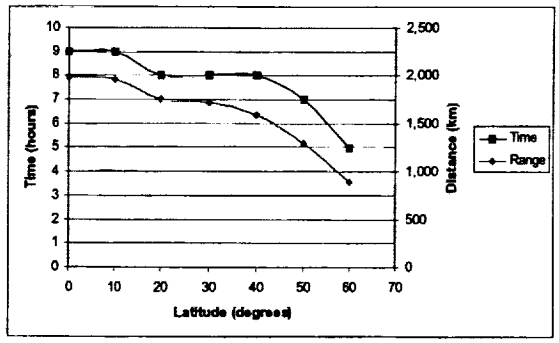

Figure 10. Operation hours & distance traveled

Increasing the cruise velocity will greatly improve the range, therefore, batteries can be used as a supplemental power source to maintain a cruise speed of 66m/s during the entire flight. Maintaining a cruise speed of 66m/s requires constant power of 1520W. Thus, the rechargeable Silver-Zinc batteries can compensate the deficiency in power at certain flight time frames. Table 7 summarizes the battery usage in attempting to maintain the 66m/s cruise speed.

Table 7. Batteries integration to maintain highest cruise velocity

Cruise velocity(m/s)	Power required w.r.t. velocity(W)	Power demand to maintain 66m/s (W)	Batteries required	Power supplied by batteries (W)
52 @ 0800	931	589	4	704
58 @ 0900	1260	260	2	352
66 @ 1000	1520	0	Not required	0

(Note: This situation only refers for 0-degree latitude)

By utilizing the battery pack in sequence with the solar array, an increase of 79-km flight distance can be achieved. Also, the MAEV will be able to operate anywhere within –60 to +60 degrees of latitude on the Martian atmosphere as long as the solar exposure is equal on both hemispheres.

4.5. Design of Carriage and Track System

A system for taking-off and landing the MAEV on the Martian surface is proposed here. Due to the harsh geological environment on the Martian surface, runways are unrealistic during early exploration. A take-off and landing apparatus has been proposed which can adapt to the terrain on which it is erected. The system consists of two main systems: a track and a carriage system. Each main system consists of several subsystems that are described below.

4.5.1. Carriage System

The carriage system is a detachable landing gear for use during departure and landing. The system has three subsystems, the wing supports, the carriage supports, and the wheel supports. The aircraft is designed to take-off and land in the same direction.

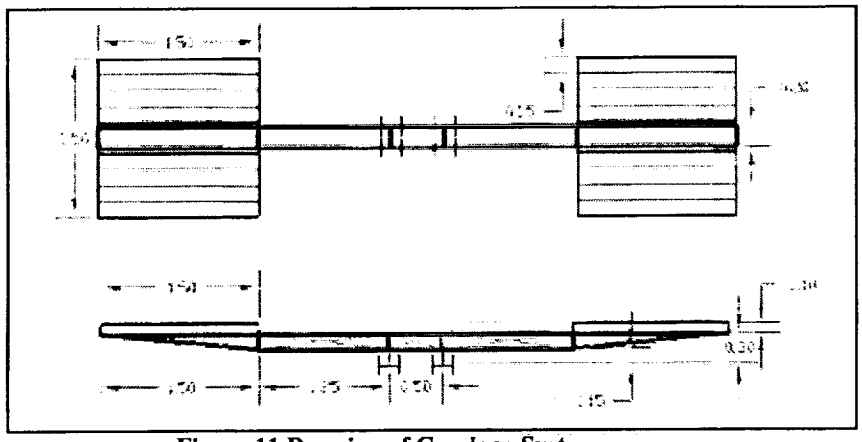

Figure 11 Drawing of Carriage System

4.5.2. Carriage Subsystems

Carriage Wheel System

The wheel system is designed to translate the carriage system to one direction. The wheel system is confined by the track and provides unidirectional travel during take-off and landing. A dual track monorail has been proposed for stability and resistance to bending loads.

Carriage Wing Support System

The wing support system is designed to restrain the aircraft during acceleration and deceleration associated with T-O and landing, respectively. To restrain the aircraft, the wing supports are fitted with end caps that are free to rotate 90° and lock into place. To secure the vehicle to the supports, magnets have been purposed. Magnetic force can be used to secure the aircraft during take-off until the vehicle has attained a velocity to induce lift. During landing, magnets can be used to secure and align the vehicle with the supports. Magnets will be carried on the wing support subsystem and metal strips placed on the exterior of the vehicle.

Carriage Support System

The carriage supports provide structural rigidity for the wing supports. The carriage support is a truss frame that resists bending loads due to the weight of the vehicle on the wing supports.

4.5.3. Track System

The track system is a portable, adjustable runway for the MAEV vehicle. The track system is designed to support the carriage system and the aircraft during take-off and landing. Additionally, the system must be easily transported, erected, and maintained on the Martian surface by a two person's crew. The track system consists of two subsystems, the main track, which houses the carriage wheel subsystem and the track support system.

The length of the overall track will need to be 50+ meters long. To provide this length, the track is designed to be modular, connecting several tracks together for the required length. Special consideration was also given to non-structural problems including ease of transport and set-up, ground restraints, module interfacing, and dust contamination control. The maximum overall dimensions of the system are 1.6-m high, 1.95-m wide and 3.0-m long. The maximum dimensions are for fully extended supports.

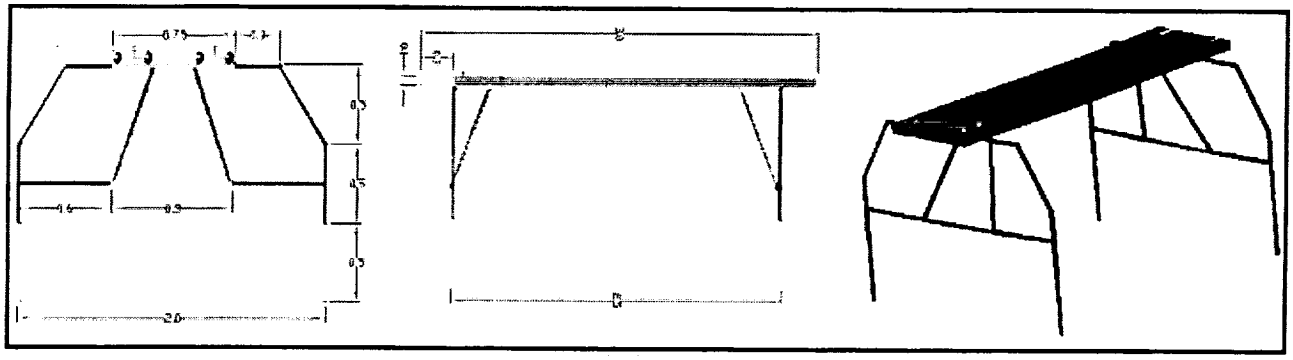

Figure 12. Detailed Drawing of Track System

4.5.4. Track Subsystems

Several logistic problems concerning the feasibility of the track system have been identified. These include transportation of the modular tracks, ability to assembly the system under harsh conditions, securing the system to the ground, and dust contamination of the wheel track wells.

Transportation of the module track system involves two aspects, transportation from earth and ease of transportation by crew. Since the weight and volume are critical attempts were made to produce a system that was volumetrically small and light in weight. To reduce the volume the system would take up during transport, the support legs of the track are collapsible, similar to the support legs found on folding tables.

In addition to transport to the planet, ease of transportation on the ground was considered. The track is designed for two persons to handle with ease. The width of the wheel track housing was limited to a width of 1 m for this purpose.

The set-up of the track system on Mars is designed to be completed by a two-person crew. Special consideration is given to the adverse terrain feature on Mars and the design of the track reflects this. The support legs of the track system are extendable in two axes to allow for modifications due to terrain. This will relieve the crew of moving large masses of soil or rocks to accommodate the track. The track supports are made of three different sized thin walled rectangular elements. The main support connects the track support to the wheel track. Outrigger supports are connected to the main supports and extend out and down from the main supports. The ground supports are adjustable legs perpendicular to the ground. Table 8 lists the track support names and their dimensions. The range of extension for the supports is 0.6 m parallel to the ground and 0.5 m perpendicular to the ground.

Table 8 Track Support Names and Dimensions

Support Name	Height x Width (cm)	Wall Thickness (cm)
Main	2.5 x 2.5	0.1
Outriggers	2.3 x 2.3	0.1
Ground	2.1 x 2.1	0.1

Track Ground Restraints

High winds are expected on the Martian surface. To restrain the track system from moving during high winds, ground restraints will be required. Adequate types of restraining mechanisms have not been investigated. However, a support structure, sufficiently driven deep into the Martian soil should secure the apparatus.

Modular Track Interface Feature

An interface has been designed to connect the modular track sections. The system consists of a male-female joining. The system works by fitting the end of one track into the supporting structure of another track. Each track contains a male and female connection.

Dust Contamination

Martian dust contamination will be a control problem for any sensitive apparatus operating on the surface. Dust control has been proposed to reduce the amount of dust that may enter the wells. The system consists of brushes that run the length of the opening of the carriage wheel structure. The brushes create a seal, restricting dust movement into the wells. As the wheel structure moves along the track, brushes will scrap dust way from the structure, further reducing contamination. One type of dust control will not be sufficient, however, and regular blowing of the track to displace dust may be required.

4.5.5. Design Limits

Carriage System

The carriage system has been designed to sustain a maximum landing load of four times the vehicle weight at a 60° glide path and a maximum deflection of 5cm.

Track System

The track system is designed to withstand a maximum 4G landing. The maximum deflection of the system is slightly less than the carriage system at 3 cm. The maximum deflection was decreased from the carriage system requirements to reduce cyclic vibration in the track while the carriage system is moving.

4.5.6. Factor of Safety for the Carriage and Track Systems

A large factor of safety was used to design the two systems. Normally, for an unmanned flight vehicle, a relatively low factor of safety between 1.0 and 1.2 is acceptable. However, due the extraordinary conditions that the system is to be used in and the distance from traditional repair facilities, a larger than normal factor of safety equal to 4 was used.

4.5.7. Material Selection for Carriage and Track Systems

The materials considered for the construction of the carriage and track systems consist of traditional aluminum alloy. The materials need to be light in weight, have good strength properties in bending, a minimum deflection under high loading, and desirable, a low cost. Aluminum alloy was found to closest meet these goals for both systems. Special consideration was made for the wheels of the carriage system. The wheels in the wheel carriage system could be made of polyurethane similar to the wheels found on commercial rollerblades™.

Material Properties

Table 9 is a list of the material properties for aluminum 6061-T6 used in this investigation.

Table 9 Material Properties for Carriage

Material	Density (Mg/m^3)	Young's Modulus (GPa)	Yield Strength (MPa)		
			Tension	Comp	Shear
6061-T6	2.71	68.9	255	255	131

4.5.8. Load Cases

Three load cases were examined to determine the configuration and cross-sectional element design of both the carriage and track systems. The load cases consisted of one 1G-load scenario and two 4G-load scenarios. The 1G load simulates the flight vehicle a rest. The 4G-load case examines a maximum landing scenario as described above. Two types of applied loads, a normal landing and a side-loading case were used. Normal landing loads are experienced when both wing supports are loaded at the same time. Side loading is experienced when one wing support is loaded before the other.

The weight component perpendicular (-y-axis) to the direction of travel was used. Loads parallel to the direction of travel (z-axis) were not considered. Any loads associated with the x-axis were not considered in this investigation.

The actual applied loads varied between the carriage analysis and the track analysis. For the carriage analysis, only the vehicle weight was used. For the track analysis, the vehicle weight and the weight of the carriage was used. For the 1G-load cases, the entire vehicle weight was used since the vehicle is at rest.

4.6. Structural Analysis of the Wing

Accurate analysis of half of the MAEV wing body was done using MSC NASTRAN. A Finite Element Model (FEM) of half of the wing was constructed using rectangular bar-element for the ribs, membrane-element for the wing skin and plate-element for the circular spar. The wing section was then subjected to 2g loading to investigate its behavior under static and flight conditions. The materials used for the wing are Mylar Type A and Kevlar 149. Figure 13 shows the right half-span of FEM wing.

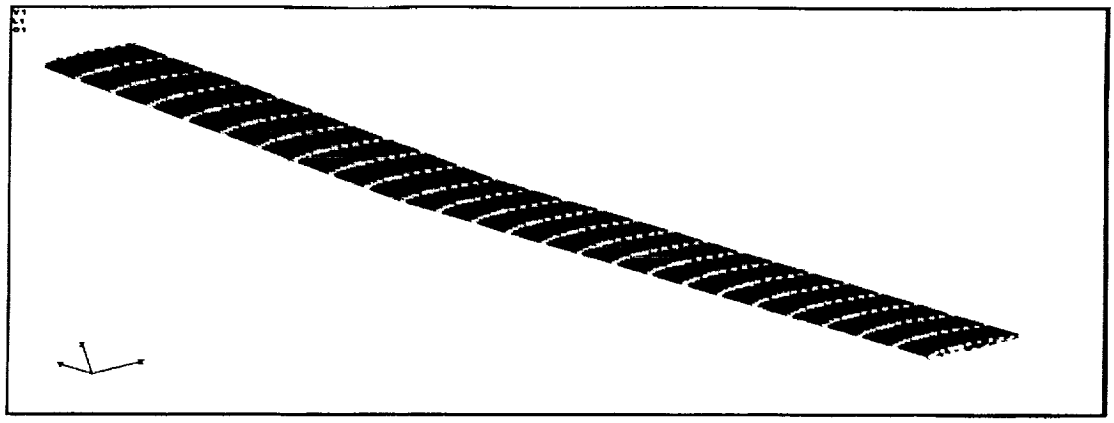

Figure 13. Right half span of FEM wing

4.6.1. Model

The wing has 6-degree dihedral on the 15th spar from the center as shown above. The main circular spar has diameter of 0.1 m from root to tip. It has two separate sections where the top and bottom wall thickness of 0.0012 m with 6 plies lay-up angle of [90/0/90]s2. Both sidewalls of the circular spar have a thickness of 0.004 m with 2 plies lay-up angle of [90/90]. The ribs are modeled as bar-elements, and have rectangular cross sections. They are placed 0.61 m apart of each other. The entire wing skin is made of a membrane-element and they carry only tensional load. Two types of material are used to construct of the wing. They are Mylar Type A and Kevlar 149. Two types of loading cases were considered and the behavior was analyzed using the Finite Element Method.

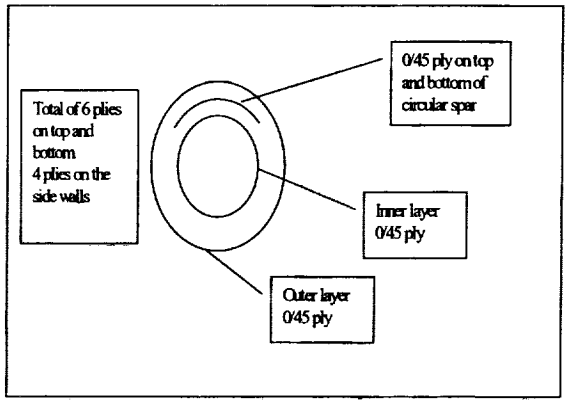

Figure 14. Main circular spar cross section

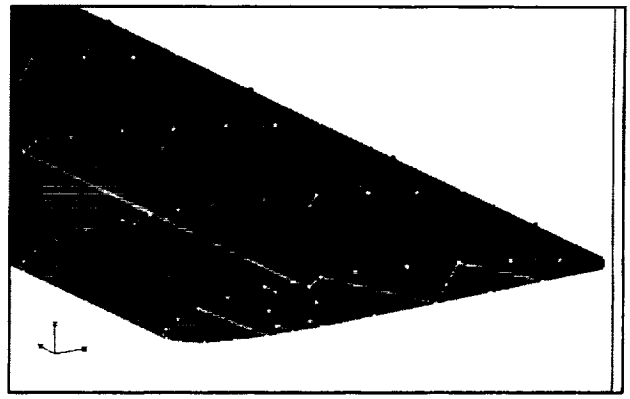

Figure 15. Cross-section of the wing

4.6.2. On Ground Case

For the On Ground Case, the aircraft is sitting still on ground and no aerodynamic force applies to it. The entire weight of the aircraft will be pointing downwards except for the landing gear and payload weight. The payload will be carried by the landing gear. The total downward force is 236 N. This causes reaction force of 236 N upward to fulfill the 'zero sum rule'. Figure 16 and 17 below show the wing loading and the deflection respectively, for half of the wing.

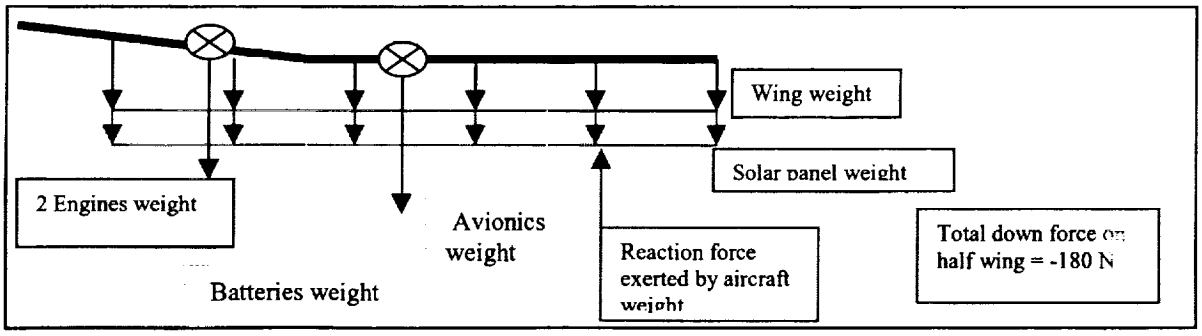

Figure 16. Load for On Ground Case (half wing shown)

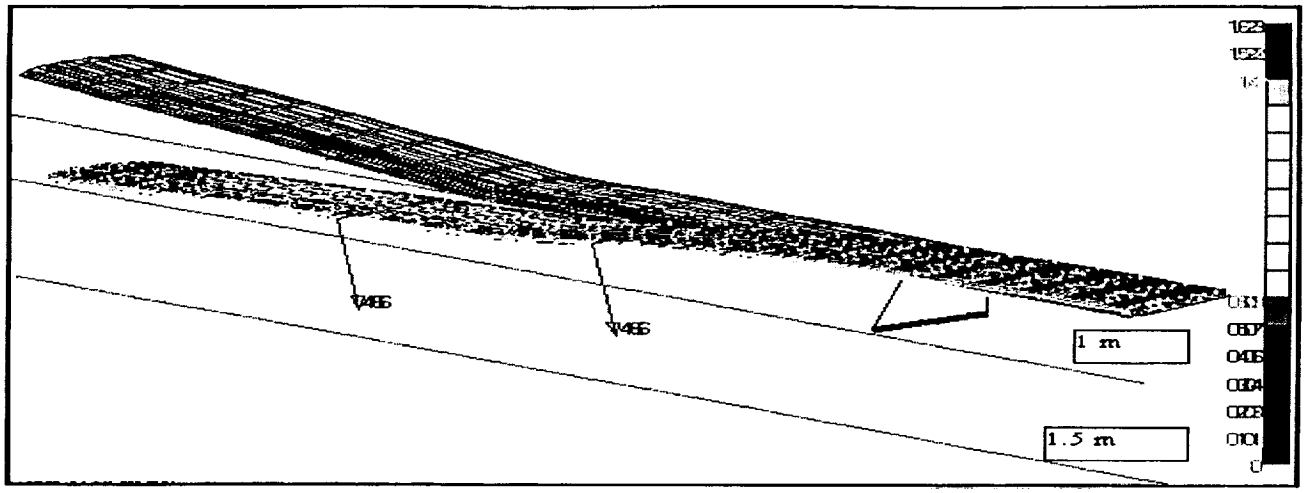

Figure 17. Deformation of wing On Ground Case

The wing deflection was calculated to be 0.68 meters downwards, which is small enough for the tip of the propeller blades to clear the ground by at least 1.0 meters. Stress analyses were done for the main circular spar, the ribs, the upper and lower skin and the leading edge using the same methods. The smallest margin of safety occurred on the bar-elements at 120%. The margins of safety for the other components were, however much higher.

4.6.3. In Flight Case

For the in flight case analysis, ideal and normal flying conditions were assumed. With the wing loading of 117 Newtons per half wing, the tip deflection was calculated to be 0.32 meters. Similar stress analyses were done for the in flight case and the smallest margin of safety occurred on the bar-elements at 200%. The other components resulted in much higher margins of safety.

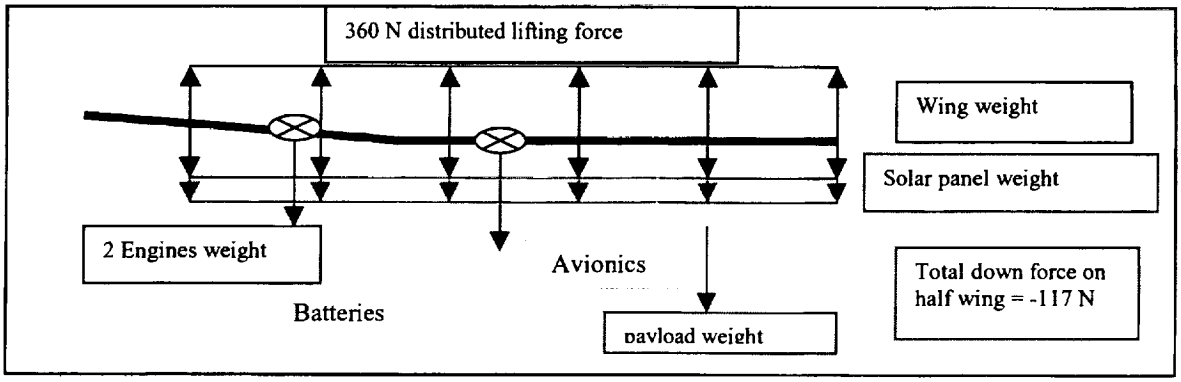

Figure 18. Loading for In Flight Case (half of wing shown)

4.7. STRUCTURAL ANALYSIS OF CARRIAGE AND TRACK SYSTEM

MSC NASTRAN software is utilized to analyze the structural models for the carriage system and the track system under the different load cases described above.

4.7.1. Analysis of Carriage System

The carriage models are constructed using solid, thin walled circular beam elements. Eight constraints are applied to simulate the carriage wheels. Loads are applied to the peripheral of the wing supports at 24 nodal point per wing support.

4.7.2. Four G NASTRAN Analysis of Carriage Support

Side Loading

The 4G-side loading yielded the largest elements stresses and deflections. This load scenario was used to determine the geometry of the structure and the element thickness'. The vector weight component of the vehicle was divided into 24 nodes and applied to the right wing support. The nodal loads are 43.3 Newton's each.

The individual elements of the carriage system are separated into five different material properties; each associated with a subsystem. In NASTRAN, a material property identifies an element material and cross-sectional

geometry. For the truss subsystem, two material properties were used to increase the options for individual element sizing. The wheel support subsystem contains one material property and the wing support subsystem contains two material properties. Table 10 lists the material properties, the subsystem they are associated to, and the element geometry.

Table 10. Material Property Definition

Property Name	Subsystem	Geometry	Radius(cm)	Thickness(cm)
Truss	Truss	Thin-walled circle	1.0	0.2
TrussA	Truss	Thin-walled circle	0.5	0.2
Wheel	Wheel	Thin-walled circle	1.5	0.1
Wing Support	Wing Support	Thin-walled circle	2.0	0.2
Stringer	Wing Support	Solid circle	0.1	N/A

The analysis of the carriage system with the defined material properties yields an acceptable deflection of 5.0 cm. The maximum combined element stress is 144 MPa. The combined stress is defined as a combination of the bending stress and the axial stress. The largest stresses were experienced in the elements of the wheel subsystem. Bending stress largely influences the maximum combined stress. The wheel support elements are nearest the constraints and furthest from the applied loads, experiencing the largest reaction moments.

The maximum allowable deflection was the limiting factor in the design consideration of the carriage system. In meeting the maximum deflection criteria, the allowable yield stress for aluminum 6061-T6 were easily satisfied. The largest stress in an element was 144 MPa, just over half the allowable yield stress for the material. With the structural geometry given, the total mass of the structure was calculated to be 26.45 kg.

Normal Landing

A 4G normal landing load case was analyzed to confirm that deflections and element stress did not exceed design limits. The maximum deflection for this scenario is 2.13cm and the maximum combined stress is 78.05 MPa. All elements meet the allowable yield strength for aluminum 6061-T6.

4.7.3. One G NASTRAN Analysis of Carriage Support

A 1G NASTRAN analysis of the carriage system to simulate the vehicle at rest on the carriage system was conducted. This investigation identified the deflection and stress of the carriage system due the weight of the vehicle only. The carriage system deflection is 0.75 cm and the maximum combined stress is 27.1 MPa. All elements meet the allowable yield stress for the material.

4.7.4. Results of carriage Analysis

Table 11 is a reference table listing the results of the structural analysis for the carriage system. The three load case scenarios are listed with the maximum deflection and element stresses. All design limits are satisfied for the load cases investigated.

Table 11. Results of Carriage System Analysis

Load Case	Deflection (cm)	Maximum Combined Stresses (MPa)
4G-Side Loading	5.1	144
4G-Normal Landing	2.1	78.5
1G-Normal Landing	0.75	27.1

4.8. Analysis of Track System

The same load cases for the carriage system were used to investigate the track system. These load cases consisted of a 4G landing case and a 1G wing weight only case. For the 4G-load case, side loading and normal landing scenarios were investigated. NASTRAN was used to examine the structure for maximum combined stress in the supports and principal (Von Mises) and shear stresses in the plate elements of the track.

4.8.1. 4 G Hard Landing

Side-loading

Similar to the carriage system analysis, the 4G side-loading scenario yielded the highest element stresses and largest deflection. This load scenario was used to satisfy the design requirements. The NASTRAN analysis of the track system contains two different types of element properties. The track supports, as described above, are thinned-walled rectangular beam elements. The main track is modeled as thin plates. The analysis of the track system identified the maximum required thickness for both the beam elements and the plate elements.

Similar to the carriage system, the maximum allowable deflection was the limiting factor in the design of the track system. The largest element stresses were experienced in the track supports. The maximum combined stress is 113.1 MPa.

The maximum Von Mises stress is 96.1 MPa. The maximum shear stress is 34.6 MPa for the main track. All elements in the analysis meet maximum allowable stresses for the material.

The total deflection for the track system for a 4G side loading case is 2.8 cm. The total mass for the apparatus is 15.56 kg.

Normal Landing

A 1G normal landing analysis was conducted to simulate the weight of the vehicle and the carriage on the track at rest. The maximum deflection is 1.3 cm. The maximum combined stress for the support subsystem is 61.0 MPa. The maximum Von Mises and shear stresses are 39.1 and 14.1 MPa, respectively. All elements meet maximum allowable material strengths for aluminum 6061-T6.

4.8.2. 1G Normal Landing

A 1G, vehicle and carriage mass only analysis was performed to identify the maximum deflection of the system while at rest. The maximum deflection of the apparatus while at rest is 0.47 cm. All structural elements maintained a substantial factor of safety for allowable stress values.

4.9. Results of Track System Analysis

The result of the track analysis is presented in Table 12. The maximum deflections and stresses of each load case scenario are presented. The design limits are satisfied for all load cases.

Table 12. Results Track System Analysis

Load Case	Deflection (cm)	Maximum Element Stresses (MPa)		
		Von Mises	Shear	Combined
4G-Side Loading	2.8	96.1	34.6	113.1
4G-Normal Landing	1.3	39.1	14.1	61.0
1G-Normal Landing	0.47	14.2	5.1	22.2

4.10. Take Off Analysis

To enable the MAEV to takeoff safely in a short track distance, the carriage system can be designed to accommodate two progressive rockets for additional thrust. Selecting a form of solid rocket booster that can provide progressive thrust, the takeoff process can be initiated with a small thrust vector to avoid structural damages to the aircraft and the Carriage. A quick analysis was done using rocket boosters composed of Polysulfide Aluminum and Ammonium Perchlorate (PS/AL/AP) grains weighing 22 Newtons each. Initially, each rocket booster can generate about 296.42 N of thrust, which increases progressively over time. As required from performance, the aircraft needs the lift-off velocity at 36.3 m/s to be airborne. At the time of 19.05 second, the maximum thrust is 1779.0 N, which gives the aircraft a velocity of 37.36 m/s. This velocity is slightly greater than required velocity, which intends to ensure the aircraft to generate enough lift. The resulting take-off distance is approximately 30 meters. To simplify the calculations, the drag and friction on the track are ignored and the total combined weight of the MAEV and the Carriage is 400 N. The linear dimension of each booster will be at least 0.5 meters. The inner and outer cross sectional diameter for the grain will need to be approximately 0.015 and 0.09 meters respectively to accommodate enough grain volume for a successful takeoff.

These boosters can be attached to the Carriage system instead of the aircraft, which eliminates excess weight of the boosters after they are used up, and will also avoid possibilities of exhaust blast damage to the wing. The thrust output of the rockets can be varied to satisfy any type of take off requirements.

4.11. Landing Simulation

From the principle of work and energy, the average horizontal acceleration of the MAEV is $3.96 m/s^2$ during touchdown. The MAEV, which moves along with the carriage on the landing track applies a load factor of 1.11g.

The horizontal g-forces after impact is 2.13g, which slowly decreases with the spring force. The kinetic friction of the track also provides resistance. The combined effect of the spring and the spool mechanism halt the MAEV in just 60-meter. This is assuming that the landing speed of the MAEV is 10% of the stall velocity (30m/s) or 33m/s ($1.10V_{stall}$). Figure 19 (a to d) shows the sequence of the MAEV landing on the carriage and track system.

Figure 19(a) shows the setup before the aircraft comes into contact with the carriage. The fundamental mechanisms include a spring, spools and an inelastic wire. It also shows the carriage rushing to make contact with the

wire, assuming a landing approach from the right. Side view of the spools shown in the right, indicates the wire in tension both at top (colored in orange) and bottom (colored in blue) of the spool. The spring is shown in static equilibrium.

Figure 19(b) shows the moment after the carriage comes in contact with the wire. The wire is designed to feed out turning both the top and bottom spools. The wire, which is connected to the spring, causes it to compress. Recall that the spring is designed to provide resistance force during the MAEV landing process.

Figure 19(c) shows the stage when the MAEV is brought to a complete stop. The wire is fed by the top spool is relaxed. The bottom spool, however, remains locked, storing the kinetic energy as potential energy in the spring.

Figure 19(d) shows the release of the stored potential energy from the spring as the top and bottom spool wind in. The force of the spring is also designed to assist in "pushing" the carriage back towards the takeoff position, which is at the right end of the track diagram shown below. The purpose of this design is to allow the aircraft to take off and land in the same direction.

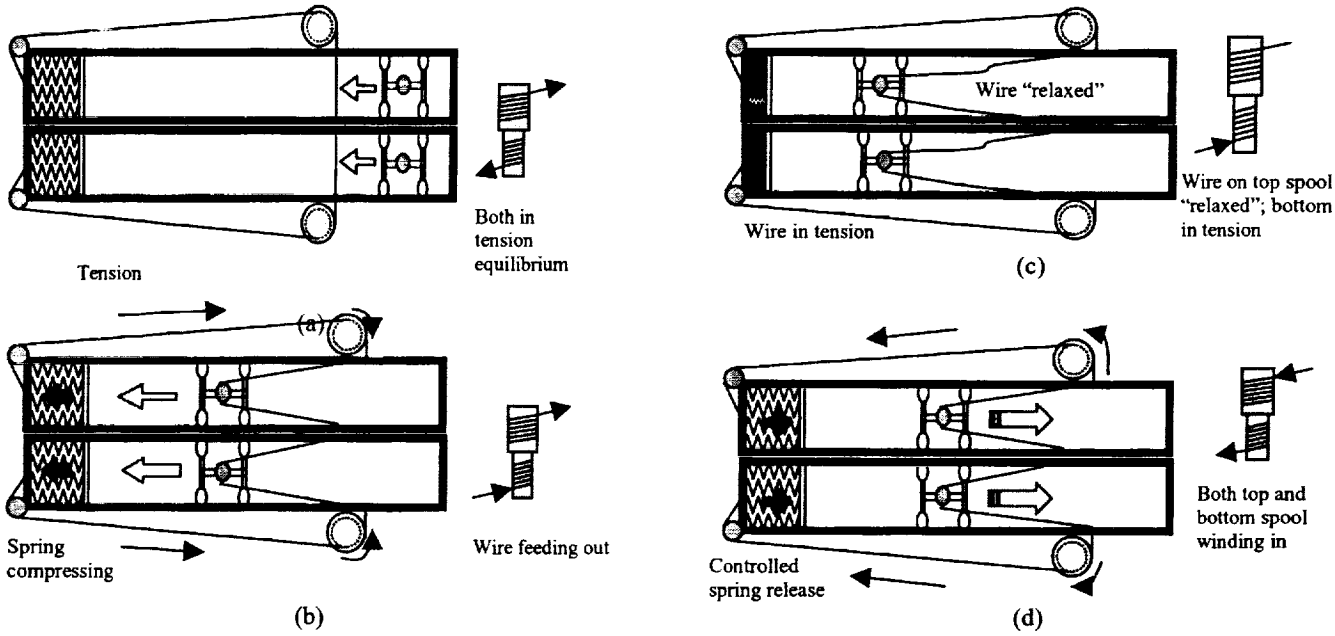

Figure 19. Process of landing using spring and spools mechanism with wire

4.12. MARS EXPLORATION PARACHUTE

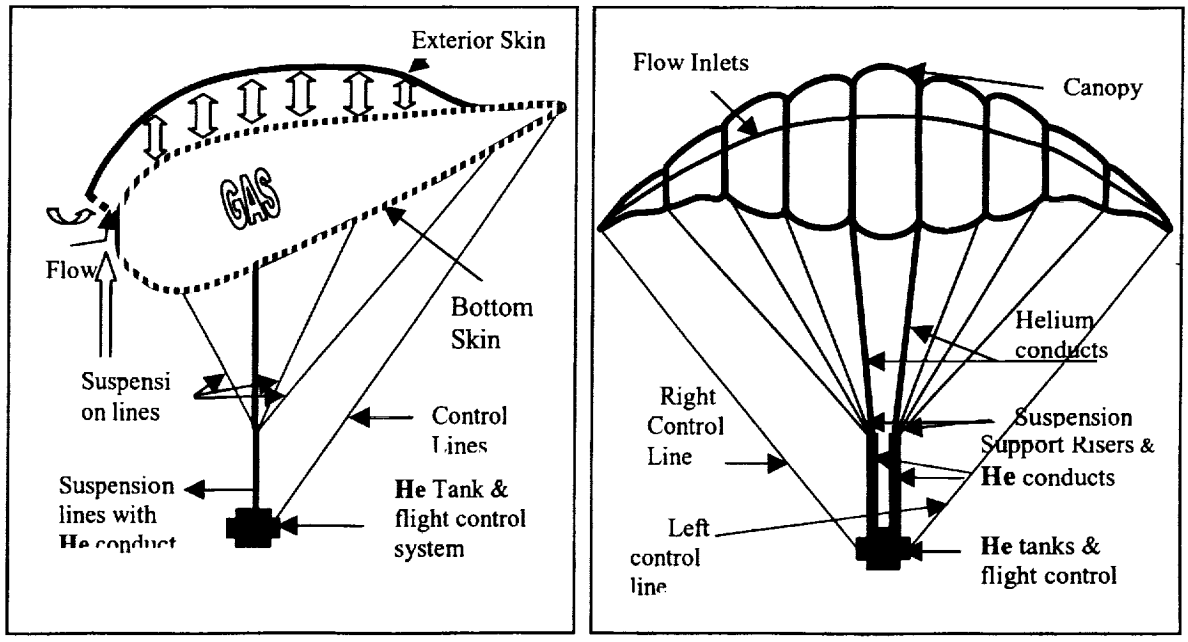

Figure 20. View of the parachute payload

The *Mars Exploration Parachute* is the combination of an aerostatic balloon (filled with a lifting gas, such as helium or hydrogen) in combination with a ram-air or gliding parachute. As a balloon, it is able to ascend and descend at specific rates depending on the controllable amount of gas flowing in and out of the envelope. As a gliding parachute, it meets all the design criteria to be classified as a wing of variable shape with specific aerodynamic characteristics.

The canopy is made of three skins, an upper skin and a double lower skin. The upper skin preserves pressurization inside when it is descending by means of several flow inlets located at the nose of the parachute. The inner skin preserves the wing-like shape of the parachute when gas is pumped in. A set of lines cascade from the top to a small payload located at the bottom, consisting of a guidance and automatic control, a small digital camera, and all necessary electrical and telecommunications devices. Figure 20 of the parachute show the front and profile views of the structure.

The *Mars Exploration Parachute* is intended to function in two different ways:

a) To be released from high altitude and glide to the surface. The more important issues involved this case are the opening peak force of the parachute when it deploys, the rate of descent, and the landing velocity conditioned by the buoyant force of Helium.

b) To be released from a lower altitude and land it by means of airbags and retrorockets. In this case, the parachute deploys automatically on the ground and Helium provides the necessary lifting force. Once the system has acquired the desired altitude, the Helium supply is stopped and the parachute starts its descent, releasing gas and obeying the basic aerodynamic laws.

In any case, when a specific spot is sighted via digital camera, the canopy is directed towards that location with an automatic system that drives the control lines, which deflect part of the canopy just as a regular flap of a rigid wing. Since the motion of the system is expected to be slow, only static stability is of concern, achieved through the length of the control lines supporting the payload.

Since the atmosphere is so frigid and thin, a large quantity of Helium is necessary to lift the payload, and therefore extraordinary wing dimensions are expected. A brief study was performed based on several calculations. Table 13 below lists the major specifications of the parachute payload.

Table 13. Parachute design specifications

NACA-4415	
C_L max	1.1
C_L with flaps	2.5
$C_{d,o}$	0.015
Reynolds number	$5x10^5$
Mach number	04-0.6
Weight of system	15 N
Wing span, b	28
Wing chord, c	11
Wing average height	1.5
Wing volume	460 m^3
Wing area	308 m^2
Wing aspect ratio	2.54
Wing loading	0.048
Flight path angle	15 °
Lift to Drag ratio, L/D	~4

5. Conclusions

The optimal configuration for the MAEV was determined. The flying wing configuration is a span of 30.5 meters and a chord length of 1.2 meters. Four propellers driven by electric motors power the aircraft. A solar array on the upper surface of the wing and six rechargeable batteries supply power for the motors and all systems. The MAEV will be able to accomplish its mission objectives over a nine-hour flight time and maximum range of 1000 km. The optimum cruise velocity of the aircraft is 66m/s at a maximum altitude of 500 m.

The modular track and carriage system will assist the MAEV with take-off and landing. The overall length of the track is 60m. Two solid rocket boosters mounted to the carriage and the resistance pulley mechanism will assist the aircraft in the take-off and landing process respectively. The track and carriage systems have been designed to be ergonomically suitable for a two-man crew.

6. Recommendations

For future academic research on the report presented, several recommendations have been proposed. A process of modularizing the entire aircraft, carriage and track system needs to be developed for transportation to and on the Martian planet. To further improve the performance of the MAEV, several areas can be researched.

These include:

- Design a better, more suitable propeller with lower Reynolds numbers
- Conduct a thorough stress analysis during takeoff and landing condition
- Use of alternative materials to construct the Track & Carriage and some components of the aircraft.
- Develop avionics and control systems appropriate for a wing body design
- Research on higher efficiency solar arrays and batteries
- Additional loads applied to the Track and Carriage system need to be considered
- Find alternative methods to assist in the takeoff and landing process of the MAEV
- Do a cost analysis and a feasibility study to recommend further development on this design

By following these recommendations, the overall functionality and the possible reality of the Martian Airborne Exploration Vehicle and the Carriage & Track system can be greatly improved.

7. Outreach

In April of this year, the Wichita State University College of Engineering held its annual Open House. The MAEV group participated in this event. The daylong event allowed varies engineering disciplines to present their semesters work. The event is attended heavily by both the industry and local elementary schools. Presenting to local industry engineers allowed the MAEV group to refine their technical presentation. Presenting to the school groups allowed the MAEV group to garnish the interest of the next generation.

Future plans for the MAEV project consist of presenting the model and a brief description of our work to Wichita's newest science learning center, Exploration Place. Exploration Place is an interactive learning environment for children of all ages. It is our hope that the MAEV project will be awarded a place on permanent display, so that children and grown-ups alike can come to understand the possibilities in the new frontier.

8. Bibliography

Allen, David H. and Walter E. Haisler, "Introduction to Aerospace Analysis", John Wiley and Sons, 1985

Hibbeler, R.C, "Statics and Mechanics of Materials", Simon & Schuster, 1993.

Lacy, Thomas E. Jr., "Aerospace Engineering Flight Structures Class", Wichita State University, 1998-99, Wichita KS

Boresi, Schmidt, and Sidebottom, "Advanced Mechanics of Materials", 5th Edition, John Wiley and Sons, 1932.

Bruhn, E.F., "Analysis and Design of Flight Vehicle Structure," Jacobs Publishing, Inc., 1973.

Dommasch, Daniel O., Sherby, Sydney S. and Connolly, F. Thomas, "Airplane Aerodynamics", 4th edition, Pitman Publishing Corporation, NY, 1967.

Durand, W. F, "Aerodynamic Theory", vol. I, Durand Reprinting Committee, Galcit, 1943.

Michael A. Dornhem, "Aviation Week & Space Technology, AeroVironment Pushes Limits of Solar Flight", May 1998.

Fishbane, Gasiorowicz, "Physics for Scientists and Engineers", 2nd ed. New Jersey: Prentice Hall, 1996.

R. C. Hibbeler, "Engineering Mechanics, Dynamics", 7th ed. New Jersey: Prentice Hall, 1995.

John D. Anderson, "Introduction to Flight", 3rd ed. New York: McGraw Hill, 1989.

Fishbane, P. M., "Physics for Scientists and Engineers", Prentice Hall, 2nd ed, 1996, pp. 12-614.

Chenming Hue and R.M.White, Solar Cells From Basic To Advanced Systems, McGraw-Hill, New York, 1983.

H.S.Rauschenbach, Solar Cell Array Design Handbook, Van Nostrand Reinhold, New York,1980.

K.Zweibel, Basic Photovoltaic Principles and Methods, Van Nostrand Reinhold, New York,1984.

Martin A.Green, Solar Cells;Operating Principles, Technology and System Application, Prentice Hall, New Jersey,1982.

Robert G.Seippel, Photovoltaics, Reston, Prentice Hall, Virginia, 1983.

Anthony J.Colozza, "Preliminary Design of a long-Endurance Mars Aircraft," NASA CR 185243, http://powerweb.lerc.nasa.gov/psi/DOC/mppaper.html

Anonymous, "Flexible Thin Film Solar Cells," NASA SBIR./STTR

http://sbir.gsfc.nasa.gov/SBIR/successes/ss/3-027text.html

Dale Burger, "Mars Microrover Power Subsystem," Mars Pathfinder Microrover http://192.88.114.52/Mars/roverpwr/power.html

Anonymous, "Pathfinder Leading the Way In Solar Flight," Pathfinder Fact Sheet http://www.dfrc.nasa.gov/PAO/PAIS/HTML/FS-034-DFRC.html

Geoffrey A.Landis, "Solar Cell Selection For Mars," Solar Cell Selection for Mars http://powerweb.lerc.nasa.gov/pvsee/publications/wcpec2/cells4mars.html

Anonymous, "Solar Cell Efficiency Records," Photovoltaics Special Research Center http://www.pv.unsw.edu.au/eff/eff_tab1.html

Kirk Flittie and Bob Curtin, "Pathfinder Solar-Powered Aircraft Flight Performance," AIAA-98-4446

Anonymous, "New World-Record Efficiency in Thin-Film Solar Cell," National Center for Photovoltaics" Anonymous, "Function and Performance of Lithium/Thionyl Chloride Cells," Function and Performance of Lithium/Thionyl Chloride Cells http://www.batteryeng.com/func_perf.htm

Anonymous, "Lithium/Thionyl Chloride Batteries," Application Overview- Lithium/ Thionyl Chloride Batteries http://sonnenschein-lithium.de/Applicat/applltc/overview/Overview.htm

Anonymous, "Rechargeable Solid State Battery," SBIR/STTR http://sbir.gsfc.nasa.gov/SBIR/successes/ss/105text.html

Brown, C.D., Spacecraft Propulsion, AIAA, 1996, pp. 9-212.

Hill, P. and Peterson, C., Mechanics and Thermodynamics of Propulsion, 2nd ed., Addison-Wesley, 1992, pp.469-612.

Sutton, G. P., Rocket Propulsion Elements, John Wiley & Son, 3rd ed., 1963, pp. 310 – 386

McGettrick, Mike, "AE660N Finite Element Modeling Class", Wichita State University, Jan - May 2000

Smith, Bert, "AE653 Introduction to Composite", Wichita State University, Sept.- Dec. 1999.

KNECHT: THE MARS MINING SOLUTION
Colorado School of Mines

Team Members:
James Gross
Phil Tyler
Abby Bazin
Kieth Crowe
Brent Pounds
Wes Marlatt

Faculty:
Bob Knecht
Barbara McKinney

To: HEDS-UP Forum
From: Team CRATER
Date: May 4 2000

Subject: Abstract of Mars Mining Project Final Report

The engineering problem presented in this report is that of a Mars mining vehicle. We feel that our design has met or exceeded most, if not all, of the criteria set forth by NASA and ourselves. We believe that this design is the best out of all those considered. We have come to this conclusion through discussions and interactions with mentors and others in the field. We never completely ruled out any design, but rather took parts and ideas from all of our previous designs. Our final design is loosely based on an earth-based dragline and is composed of six subsystems:

The frame will house the mechanical and computer subsystems, providing them protection from the 100+ degree temperature range and highly windy atmosphere, which would jam our machine with sand. It is also the support for the boom.

The mechanical subsystem consists of two motors, two spools of cable, and a dual clutch unit. The function of this system is to rotate the boom and retract/release cables of the bucket. By using only two motors to operate our entire system, we reduced the number of moving parts, increasing its reliability.

The boom will be a triangular tube that is six meters long. Its function is to support the cabling and the bucket and protect the pulleys from sand thrown by windstorms. Low wind resistance will be obtained by keeping the boom slender.

The bucket, having dimensions of 20 cm x20 cm x 30 cm, will collect regolith from the surface of Mars. There will be three cables in our design, functioning to retract the bucket and as a cantilever support system for the boom. The cables are strong, yet thin and lightweight. The bucket is unique in its design because it makes the machine highly efficient by carrying more regolith than needed to meet the requirement. Another feature of the bucket is its recessed top, which allows it to flip over large rocks when caught. Due to the buckets size it could flip over once per hour, dumping its load, and still meet its quota of regolith.

The computer will be a matchbox-sized pc that will control the functions of the entire system. It will be protected from the atmosphere and any radiation encountered on Mars. It was designed and developed at Stanford university and is perfectly suited for our system because if its lightweight and compact size.

Our sorting system will be capable of separating fine material from regolith greater than 1 mm by running it through several different sorting mechanisms. These systems will last 500 days with minimal clogging problems and are reliable because the rotating drum is self-cleaning.

This mining system design is reliable because it is made of durable materials and has few moving parts and is, therefore, less prone to breakdown or malfunction. It is simple and easily constructed, limiting the chances of error during operation. It is also highly efficient because it is capable of gathering more regolith than necessary.

Introduction

In early September Mike Duke gave us the goal of designing a lightweight, efficient, semi-autonomous, long lasting, mining vehicle for use on Mars. The purpose of such a system would be to extract water from the regolith for the purposes of using it as both water and components of rocket propellant for possible future manned missions to Mars. While mining here on Earth is relatively simple we were faced with many problems that are not present on here. The constraints placed on us are shown in the table, Table I, below:

Table I
Restrictions Given by Mike Duke

Requirement	Rationale
Excavate granular material from surface down 10 cm-12 cm	Collect regolith to be brought to the reactor and sorted.
Avoid surface rocks	Reduce hazards to excavator.
Discard rocks greater than 1 mm in diameter.	There is more water in finer grained materials. Heating of large fragments with little water should be avoided.
Transport material from excavation site to furnace. Maximum distance of 20 m.	Get regolith to water extraction location.
Deliver soil to furnace input hopper	So soil can be sorted and water extracted.
Operate 8 hrs a day under Mars ambient environmental conditions.	Operates only from the equivalent of 8 a.m. to 4 p.m., when maximum sunlight is available.
Operate continuously for 500 days.	Mission duration.
Operate semi-autonomously.	No real time communication available, instructions from earth can be provide only once a day.
Provide Sufficient power for excavation and transportation.	Power is required to operate systems.
Have a total mass of less than 20 kg.	Suitable for testing on Mars on a small exploration mission, later, this could be scaled up for human exploration missions.
Be capable of delivering mass of the system in soil to the reactor in one hour's time.	Meet total water requirements.

While working on satisfying these requirements our team placed other restrictions on our mining vehicle to complement the specifications we were given. The following table, Table II, contains those restrictions.

Table II
Restrictions Stated by Team C.R.A.T.E.R.

Restrictions	Rationale
Low number of moving parts.	Aids in reducing wear and tear and thus maintenance needed on the mining system.
Simplify design as much as possible.	Reduces probability of mechanical breakdowns.
Provide for redundant systems.	Allows the mining system to continue to function even if it suffers minor failures.
Take a new approach.	Former rovers have had difficulty functioning in space environments; a new approach seemed logical.

We feel that we have met the most important of these criteria. While our system does not comply with some of the requirements, we believe we have found suitable ways around these problems and our system provides sufficient benefits that will have clear merit. We have looked at many other design options and believe this one to be by far the best of those we considered. The other designs are discussed below.

Approach

Our solution to the problem evolved many times over the course of two semesters. We considered many designs before finally designing on our dragline, Knecht. As the designs changed, they became less and less complex. Past designs include:

- Vacuum system on Mars
- Drilling Rig with continuous feed auger system
- Scraper
- Excavator with a conveyer belt
- Excavator with a combine
- Multi-Vehicle system
- Dragline

As a group, we first divided up the research between members. Topics for research included, but were not limited to materials, power systems, propulsion, Mars surface conditions and climate, previous Mars missions, guidance systems, Earth mining vehicles, and robotics. We came up with several interesting ideas, but chose only one based on a decision making process, outlined

in Table III and IV. We never completely ruled out any system, but rather took parts and ideas from all, and combined the best aspects to form the best solution to the problem.

- Our first idea was a point drilling system, with two different continuous feed systems. This provided a simple solution to gathering and feeding dirt to the filtration system as well as a tried and true earth extraction system. However, there were numerous problems with this system. The first continuous feed system was a gravity fed system that would not work because of height and size constraints and wind problems. The second, an auger system, was rigid, and thus not very mobile in a rocky environment.

- Our second design dealing with excavation was the scraper system. This system was simple and extremely low maintenance. Unfortunately this system would have low mobility and would be highly likely to entrench itself and become stuck.

- The third design solution we posed was that of a vacuum system that would suck dirt from the surface. This system was simple, but ultimately, it was decided against because of the ineffectiveness of a vacuum at low atmosphere pressure.

- For a fourth idea, we considered using a combine excavation system with vehicular transport to and from the furnace. The downfall of the combine system was the wasted energy moving to and from the furnace, the tendency to entrench itself, and required high speed to operate, all making the design prone to mechanical failure.

Table III
Decision Matrix of Transportation

Designs	Cost	Durability	Efficiency	Flaws	Total
Gravity Feed	9	7	4	Wind (-6)	13
Auger Feed	7	6	7	Rocks (-2)	18
Vehicle Hopper	8	6	3	Maint. (-3)	14
Multi-Vehicle	6	5	6	Maint. (-4)	13
Vacuum	8	6	5	Atmo. (-8)	11
None*	10	10	10	None	30

Table IV
Decision Matrix of Excavation

Designs	Cost	Durability	Efficiency	Flaws	Total
Drill	5	5	6	Maint. (-3)	13
Broom	8	6	7	Wear (-4)	17
Scraper	9	7	4	Wear (-3)	17
Auger	7	6	7	Wear (-2)	18
Vacuum	8	6	5	Atmo. (-8)	11
Drag Line*	9	8	9	Wind (-3)	23

* (We selected a Drag Line, which requires no extra transportation beyond that during collection.)
Both tables are on a scale of 1 to 10, 10 being the best and 1 the worst.

Results

After considering these decision matrices we chose a final design using a dragline because no transportation is needed, and the system is very durable, christening it Knecht. We feel that Knecht is the best design based on our decision matrices. We considered many options and altered our design several times.

Technical Analysis

Our excavating machine is based on a dragline. It is composed of six subsystems, including a 6 m boom, a soil collection bucket, a control system, a mechanical system, and a regolith sorting system, which are all supported by the frame. The unit operates by first excavating the soil with the bucket, which is dropped from a cable hung from the boom. The bucket then takes the soil to the sorting system where the sorter removes the desired soil (<1 mm) from the unwanted soil and drops it into the furnace.

The frame and boom support the other systems, hold up the bucket, and protect the control and mechanical systems. They comprise the backbone of the unit. The mechanical system drives the unit and provides the necessary motion to collect the soil. It moves the bucket to and from the sorter and rotates the body of the soil to find new excavation sites. It is the muscle of the unit. The control system is the brain of the unit because it controls the mechanical system. It controls when the motors of the mechanical system operate and, therefore, controls the actions of the entire unit. The bucket is the arm of the unit since the system is designed to move the bucket, without which the other systems have no purpose. The sorting system sorts and channels the work of the bucket to the furnace and is the final part of the operation.

Our unit, Knecht, is efficient as well as durable. It is capable of surviving 500 days of labor under harsh Martian conditions per specifications by NASA. Unlike other systems, especially those consisting of a vehicle, our system has very few moving parts which makes it is far less likely to break or wear down.

The Frame

The frame of our mining system is one of the simpler parts of Knecht. It is a turret that sits on top of the sorting system, which in turn sits on top of the reactor. The design is a structural ring with a diameter of 1.0 m and two A-frames connecting the boom to the ring, illustrated in Figure 1. Instead of the boom being supported by the ring, the structure will be hanging off of the boom. Originally we did have the boom supported on the ring, but found that hanging the ring from the boom and providing direct support to the boom from the reactor was by far a superior solution.

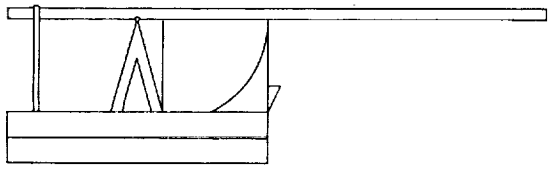

***Figure 1:** Schematic of Boom Mounted on Tower*

There will be a tri-pod coming up from the interior of the reactor and connecting to the boom at a central pivot point that will provide the support for Knecht's boom. This solution will cause a drastic reduction in the friction due to movement. By adopting this system we reduce the friction points from the entire ring to just the central pivot point and the front edge of the ring. There will be another circular ring with a geared interior attached to the reactor, which will rotate the turret. Sealed bearings will be used to reduce the friction of the upper ring on the lower ring at the friction point.

While initially we had a full cylindrical enclosure the size of the ring diameter for the housing of Knecht's mechanical and control systems, but we found that there was an abundance of extra space in the turret. Because of this, we shrunk our enclosure in order to reduce weight and wind drag. In our final design the front half of the ring will be closed and will house the mechanical components and control system. The walls will be constructed out of carbon composite or a similar material. This material will be used for almost all of our structural components due to its extremely high strength and low density.

The Boom Subsystem

The design of the boom is lightweight and sturdy enough to provide support for the bucket, while allowing for the collapse of the boom for transport and storage.

We had many different and varying concepts on what our boom would be like. At first we were using a pendulum effect to swing our bucket the 20.0 m stated in the requirements but then modified our concept eliminating the pendulum due to the many complications involved with this system such as wind effects and the complexity of computer programming. We opted to collect only to the end of the boom and move the reactor system to another position on the Mars surface to facilitate further regolith collection. After running tests with the bucket, we determined that a boom of 6.0 m would be the best length to maximize our efficiency. In this concept our boom will have a reach of about 6.0 m away from the reactor and movement of the reactor and deeper digging will compensate for the shorter reach.

We then looked at the need for a method of collapsing our boom for transport and storage. Our first idea to fulfill this need was to use a folding boom that would fold back over the reactor and then be extended by tightening the cable for the bucket, pictured in Figure 2. This worked theoretically, however, when the boom reached the vertical it would fall the remainder of the way to horizontal and thus would probably break.

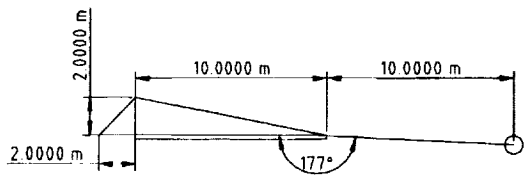

Figure 2: *Front View of Boom to Illustrate Operations*

The next concept for extending the boom was to telescope it and allowing for the modification of a method of extension best suited to our needs. We looked at the systems used for the extension of fire ladders, but found it too complicated for realistic application in this situation. We also looked at using a tubular balloon and filling it with expanding foam, but this had too many potential failures as well. Our final solution was that of a compressed spring with a catch that would give the inner boom enough force to slide out to the end of the outer boom and lock in place with a spring loaded pin. We were not given a size constraint, but you could conceivably collapse the boom using this method to whatever size necessary.

After research into the materials available, we found that there are many feasible and equally viable materials with which to construct the boom. Our first design incorporated magnesium alloy into the construction, however after further research it seems that the best material would be a carbon composite material. The carbon composite material will provide equal or greater strength while having a lower density, thus weighing less.

The boom construction will be that of telescoping triangular tube, we have only incorporated two pieces into the current design, illustrated in Figure 3; however, in the final design it would be feasible to have several. The outer tube has sides that measure 5.0 cm wide and 0.5 cm thick, while the inner tube has a measurement of just less than 4.0 cm on a side and 0.5 cm thick. The inner tube would be extendable by the process outlined above. The outer tube would extend back over the reactor and provide the top, central support for the mining system, and will have a total length of 4.0 m with 3.0 m extending from the turret. The inner boom's length would equal the distance that the outer boom extends out from the reactor, 3.0 m. The total boom length will be 7.0 m, with 6.0 m extending from the reactor. The cable would be run inside the tube and run out a slot in the bottom of the tube at the tip with a sealed pulley to guide the cable. At this length and using this construction and the constant of 1570 kg/m^3 as carbon composite's density the weight of the boom alone would be approximately 8.24 kg. The pulley will weigh approximately 2.3 g. The rod will have a weight of about 246.6 g. The pulley will be made out of magnesium alloy and, using 1800 kg/m^3 as its density, the pulley would have a weight of approximately 2.3 g. Using these weight approximations we find that this subsystem will weigh approximately 8.48 kg.

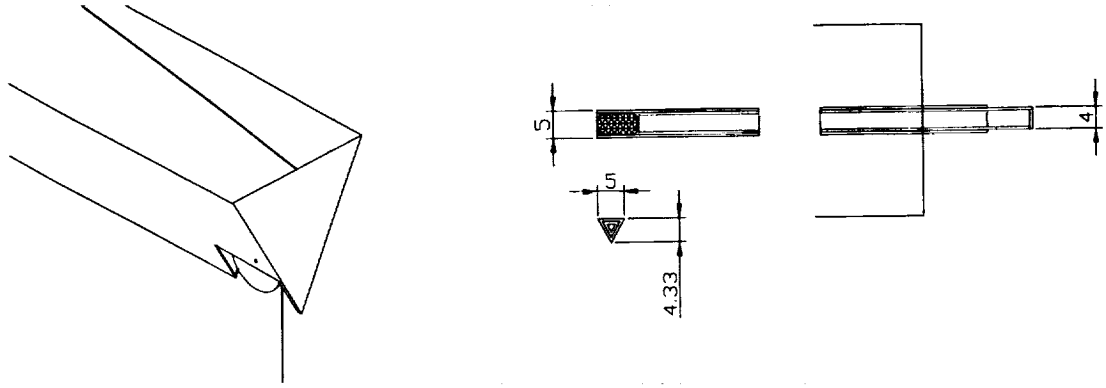

***Figure 3:** Drawing of Telescoping Boom with Cable Pulley*

Using these dimensions will minimize the weight of our system thus aiding in fulfilling our weight restraint of 20 kg. The material chosen will be both lightweight, helping fulfill the

requirement of our weight restraint, and strong. The material will also be highly resistant to temperature changes and should exhibit no problems coping with the atmosphere on Mars, including high winds and the temperature extremes ranging from –113° C to 23° C. Triangular tubular construction adds to its strength and also helps reduce weight and wind resistance. The tubular construction will also function as a protective element for the cable that extends to the end for bucket support.

The construction of this piece of our mining system is fairly simple and straightforward, since it is essentially two or more telescoping triangular tubes with the cable running through the center and a slot at the end to accommodate a sealed pulley. The pulley will be attached with sealed bearings to the walls of the tube and the cable will be run over the top of them. The cantilever support will have a small rod, 2.0 m long and roughly 1.0 cm in diameter, extending up from the base of the boom where it is attached to the main structure. A cable, approximately 8.6 m long, will be attached from the end of the boom to this rod and then run down to the main structure and attached about 1.0 m back from the base of the rod at the other end of the boom. The boom will be incorporated into the frame so that it will remain in a fixed horizontal position to the ground. The material for the cable will be Kevlar cable and will be covered in more depth in the subsystem analysis of the cables and bucket.

The Mechanical Subsystem

The mechanical system consists of two motors, two spools for the cable and a dual clutch unit. The system is the main force that moves the miner; it drags the bucket in by winding up the cable and also rotates the vehicle. This system has been split into two different parts: the first is the top assembly where one motor is dedicated to one spool. The spool will be used to wind up the top cable. This extends through the boom and to the bucket. The spool is approximately 5.2 cm long and has an inside diameter of 0.32 cm. The outside diameter is 4.0 cm.

The second part is the bottom assembly. This assembly, shown in Figure 4, is more complex than the top but still very similar. The motors will be identical except that the bottom will have dual drive shafts. On the ends of the shafts there will be twisted splines, illustrated in Figure 5, that act as one way clutches by allowing only the ratchet gear to engage the spool or the rotation gear. The splines do this by forcing the gear towards or away from the motor. These clutches will allow the motor to do two functions separately. This is accomplished by changing the direction that the motor is spinning. This clutching allows the bottom motor to turn the vehicle on its base and also wind the cable.

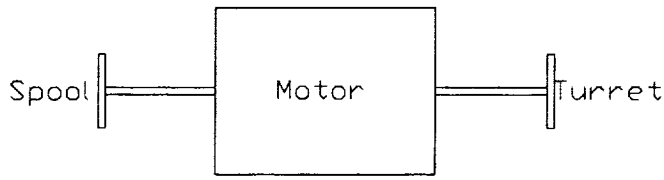

***Figure 4:** Example of Motor Assembly*

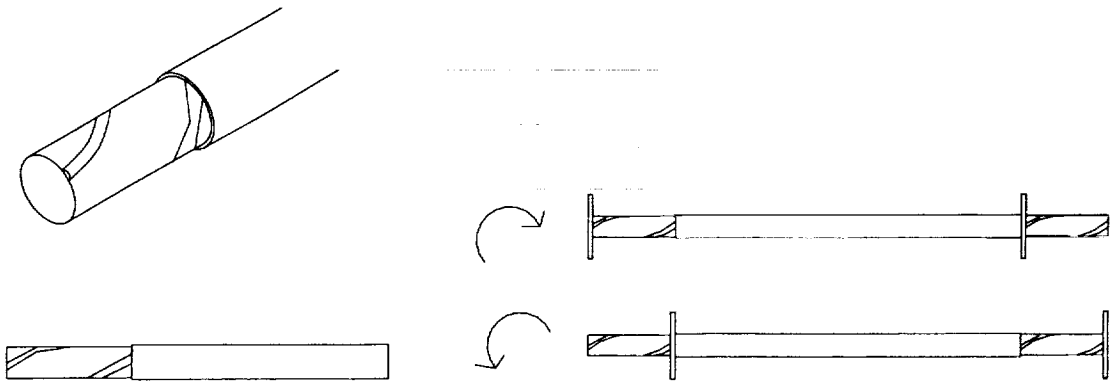

***Figure 5:** Illustration of Spline Gear Design to Serve as a Clutch Mechanism*

Both motors are brush-less to reduce friction, allowing them to operate at less than top speed, and hold one position. Their entire mass of motor and spools will be approximately 2.0 kg. The motors will have a maximum power usage of 150 W. The spools and clutches will be made out of a magnesium alloy with a density of 1.8 g/cm^3.

The top assembly will be mounted in line with the base of the boom to provide a straight pull on the cable. The bottom assembly will be in a vertical position. The spool will be above the motor as there needs to be a direct connection with the rotational gearing of the vehicle.

The design of the mechanical system was made to reduce the number of moving parts and to keep the power consumption to a minimum. Using the two separate motors and having the bottom assembly perform two functions achieves this. The clutch was designed to keep friction to a minimum by not using parts that would wear out over time such as a spring or a pure ratchet design. We believe that the design discussed in this report has fit these specifications well.

The Control System

The purpose of this computer is to control the entirety or our mining device. Specifically, it will run the motors that control the rotation of the boom and release and gather the cables. This computer will be what allows the device to mine the Regolith.

A tiny fully functional computer vehicle with dimensions measuring only 2.8 in x 1.8 in x .8 in will control the entire mining. It includes VGA, LCD, 10 Mb/s Ethernet, and a 340-MB disk; it is sufficient for a full version of Windows 98, Unix, or Linux. The total power consumption is only 2.0 W at 0.4 A with a peak power consumption of up to four watts at 0.4 A. We selected this PC, pictured in Figure 6, not only because of its power but its mass; coming in at only 70 g it is light enough to be readily used in our project.

The only protection the PC will have from the severe conditions on Mars will be the casing in which it is stored. The casing was designed out of the same materials as the rest of the frame with one small variation, the addition of insulation to the insides of the case and a heat sink machine patterned on the material. This should be enough to protect the PC from the severe temperature swings expected on the surface of Mars.

***Figure 6:** Picture of the Stanford PC Recommend for the Mining System*

While on Mars the computer will be subject to a constant barrage of cosmic radiation, this will cause the computer to crash if left unshielded. One of the better ways of stopping radiation in a lightweight manner is to use lightweight gasses such as hydrogen, boron, and lithium. Lightweight atoms can shatter the nuclei of heavy elements, in cosmic rays without producing additional hazardous recoil products like neutrons. Out of these three gases we chose to use boron because it is the most stable of the three and therefore less likely to accidentally catch fire and/or explode during launch and landing (NASA).

This computer system will be able to communicate with NASA by linking to communications equipment on the furnace. The link will consist of a simple LAN connection linking the furnace's computer and the mining device's computer with a connecting wire. This will allow for any program errors or glitches to be repaired while on the mission.

We believe this viable design is superb in quality because it meets or exceeds all expectations for use on Mars. The extremely low mass of it allows for other systems to have more leeway in their design and structure. Also the low power draw will allow others to run with more power at more efficient levels rather than be forced to limit their ability due to power restraints. This will aid in the betterment of the entire team and project.

The Bucket and Cables

This subsystem includes the soil collection bucket as well as the supporting cables. More specifically, the bucket's purpose is to gather Martian regolith, while the purpose of the cables is to carry the bucket to and from the sorter.

The bucket, made of magnesium alloy, will have a volume of approximately 3077 cm^3. The longest side will be the angled bottom, with a length of 30.0 cm, where a blade will act as a scoop, shown in Figure 7. The top will have a length of 20.0 cm allowing a 10.0 cm open space to provide for a flipping mechanism to prevent the bucket from getting caught. The height of the bucket will be 10.0 cm and the width will be 20.0 cm. It will be making six trips to the reactor per hour. We chose to use magnesium alloy for the bucket's construction because of its strength, durability, lightweight, and resistance to temperature extremes.

We chose to make the cables of Kevlar because like magnesium alloy it is lightweight and strong, but is also flexible. Because of Kevlar's strength, the cables can only be 0.32 cm in diameter. The length of the cables will depend on the height of the reactor.

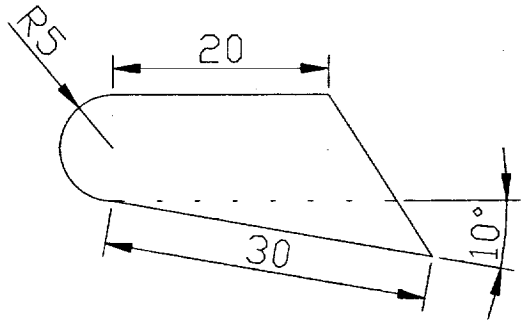

Figure 7: *Drawing of Bucket Proposed for the Mining System*

This design fits the specifications well because it is strong and lightweight. It is durable enough to perform its task for the time required. Also, the bucket transports enough soil per load so that it could spill its contents twice per hour and still meet the soil collection requirements. The construction of this design is rather simple. The bucket is to be built of magnesium alloy sheets with a 0.2 cm thickness. The location of the cables will allow the bucket to flip over any large rocks or obstacles it may encounter.

The Sorting Subsystem

The sorting system consists of a bin at the top of the sorting system, an initial sorting grate, and a trommel sorting system. The bucket is small enough that it cannot pick up materials larger than the sorting system can accommodate. The bucket dumps its load of regolith directly into the bin on top of the sorting system, represented in Figure 8. Once in the bin, the regolith will fall onto a grate, sized 30 cm^2, covered with Kevlar slats. The slats that do the initial sorting are 3.0 mm thick. All materials larger than 6.0 cm in diameter will slide over the grate and into a waste chute. All materials smaller than 6.0 cm in diameter will fall through the grate and into a trommel sorting system with a 25^0 downward from horizontal.

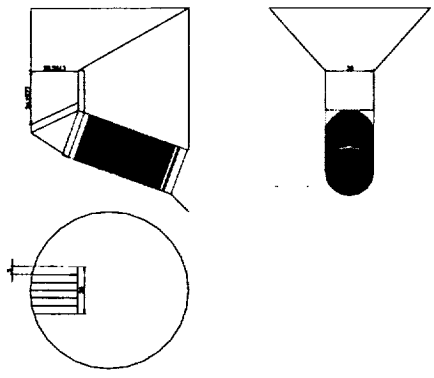

Figure 8: *Schematic Representation of the Sorting System for the Mining Unit*

The trommel system is made up of a perforated cylinder in which regolith is sorted. The cylinder rotates about its center axis and has two baffles, 6.5 cm tall, that spiral around the inside of the 30 cm diameter cylinder twice before reaching the bottom end. There are also four, 6.5 cm tall baffles that run straight down the cylinder, spaced at 90 degrees. The baffles stir, break up, and prevent the regolith from sliding straight through the cylinder. The perforations are 1.0 mm diameter holes, which allow the usable regolith to fall through into a bin where the reactor can access it as needed. The materials between 1.0 cm and 6.0 cm in diameter are dumped out the end of the cylinder into the waste chute.

The slats that do the initial sorting and the perforated cylinder will be made of Kevlar, due to its high strength and flexibility. The rest of the sorting system will be made of carbon fiber sheets and honeycomb structures. Kevlar is strong enough to stop bullets when used in vests, and will be strong enough to last 500 days.

This sorting system is very reliable because it is a self-cleaning trommel system. Every time the cylinder rotates, it dumps any material that may be clogging it back into the bottom of the cylinder where it can be resorted. Another thing that makes this system reliable is that it has only two moving parts, the rotating perforated cylinder and the small electric motor that drives it through a drive wheel system. The motor's power requirement is less than 100 W. A lot of earth-based research has gone into this system and the components have high reputations for reliability and longevity.

Future Recommendations

We have several different possibilities for the continuation of this design, contingent on funding. Among the loftier of these options, would be to see our completed design travel to Mars to perform its desired function. However, in the more immediate future, we hope to continue testing on the various subsystems, focusing on the bucket and mechanical subsystems. Ultimately we would like to build a full-scale, working prototype out of appropriate materials. We feel that this design has the potential for many uses including possible lunar excavation as well as the Martian surface.

Outreach

During the process of building and designing our miner we have had a good amount of publicity. Articles have been published in local Denver area newspapers, ranging from explanations of the entire project, to specific articles concerning our success at the school's Design (EPICS) competition. We have also had a few publications in hometown newspapers as well. Abby Bazin has had an article concerning all of her achievements with the Design (EPICS) department printed in The Plaindealer, the paper in Ouray, Co. Brent Pounds was mentioned on one occasion in his local paper, The Pueblo Chieftain. All of the members in our group are very talkative when people ask about our project. Many teachers at our school already know of our endeavors and our upcoming trip to Houston, as well as all of our friends and acquaintances. Our parents are very proud of our achievements, and have been telling anyone and everyone they possibly can. Our group has also been working with various engineers from Lockheed Martin who have visited the campus on a regular basis, assisting us with our questions, and providing comments of their own. The Trapper Mining Company in Craig, Co has been a big help in our

design based on an Earth dragline. They have been kind enough to allow one of our group members to tour the facilities and ask questions. Many other people from the local area know about our project and are spreading word of our accomplishments around from the final open house presentation we gave in mid December, and our recent presentation to CSM students and faculty.

Conclusion

The overall design of our regolith collection system is very similar to that of a dragline used here on earth. The entire system consists of a bucket attached to a boom by two cables that drag the bucket along the ground collecting regolith. Once the bucket has filled and completes its trip back to the base of the furnace it is raised up by one of the cables and dumped into the sorting system. The sorting system, which discards all materials larger than 1.0 mm in diameter, dumps discarded material near the area from which it was mined. The entire regolith collection system is mounted on a turret on top of the furnace.

We have spent significant time researching and developing this design, which has very few moving parts making it far superior because of its reliability. With fewer moving parts our design is much less likely to break down or fail in any way during the 500-day mission. Since the entire system is stationary most of the time, there is almost no chance of it getting stuck which has been the downfall for many earlier Martian exploratory rovers. In comparison to other designs we believe our design is superior in all parts of the design.

In closing, this design has many benefits over other designs and, in our opinion, is the clear choice. Thank you for reading this design project report; we hope you are as enthusiastic about it as we are.

Bibliography

Stanford University. Stanford Wearable Computing Library., wearables.standford.edu (10/2/99)

NASA. Radiation Shielding from Mars or Moon Dirt?, science.nasa.gov/newhome/headlines/msad20jul98 1.htm, (10/2/99).

MatWeb, www.matweb.com, Copyright 1997-1999 by Automation Creations Inc., Reference for Magnesium Alloy Specifications.

Specialty Steel and Forge Solutions, www.steelforge.com, Specialty Steel and Forge, 26 Law Dr., Fairfield, NJ 07004, Reference for Magnesium Alloy.

Pascal: A Mars Climate Network Mission, Author—David Catling, www.mgcm.arc.nasa/gov/mgcm/micromet/pascal.html, Space and Science Division, NASA Ames Research Center, Reference for Mars Climate Conditions.

Dr. Tim Ohno, Colorado School of Mines Physics Department, Reference for boom length and structure.

Lake Electric Motors, www.jwa.com/electric/images/cad/175dc.html, Copyright 1999, 1509 Rapids Dr. Racine, WI 53404 (12/6/99)

Bill Marlatt, Farmer/Inventor, Longmont, CO

GoldenGravel Company, Stew and Reggie Golden, Longmont, CO

Drexel University, Department of Materials Engineering, arvind.coe.drexel.edu/MATE200/kevlar.html, Copyright 1997,Drexel University, Philadelphia,PA (9/13/99)

A Comparison of Preliminary Design Concepts for Liquid, Solid and Hybrid Propelled Mars Ascent Vehicles Using In-Situ Propellants

Rowan University

Jordan Conley, Devon Lefler and Steve Shaw
Faculty Advisor: Anthony Marchese

Department of Mechanical Engineering
Rowan University
201 Mullica Hill Rd.
Glassboro, NJ 08028-1701

ABSTRACT

With a mission to Mars no longer merely an idea of science fiction, it is not too early to determine the technology requirements that will ultimately make it possible for humans to establish a long term outpost on Mars. One key aspect is the development of a reliable, reusable launch vehicle to shuttle astronauts between the Mars surface and low Martian orbit. This preliminary design study serves to provide an in depth comparison of liquid, solid, and hybrid propulsion concepts for a long-term In-Situ Mars Ascent Vehicle (IMAV) which relies only on propellants which can be harvested from the Mars atmosphere or soil. Because of the low Δv, a Single Stage to Orbit (SSTO) launch vehicle can be used to carry the crew plus cargo from the Martian surface back to the command module. Theoretical chemical equilibrium calculations have been performed to determine the optimum in-situ propellant combination for each propulsion type. The approach we took in performing a comparison of the possible design configurations contained several steps. First, we identified a baseline configuration against which we compared our design. The baseline configuration we chose was the Mars Ascent Vehicle (MAV) outlined in the current Mars Reference Mission. The second step was the addition of several constraints not specified in the baseline configuration, but which have been deemed important for this analysis. One significant constraint was that only non-hydrogen containing fuels were considered. Finally, we compared three different design alternatives to the baseline configuration. The areas of comparison wereperformance, safety, and feasibility. Based on these evaluation criteria, we have recommended a liquid propulsion system using CO/O_2propellants as the most favorable configuration for the development of a long-term, Mars ascent vehicle.

INTRODUCTION

Currently the Space Exploration Initiative (SEI) offers an ambitious plan that includes the human exploration of Mars. A manned mission to Mars will impose huge burdens on financial and technological resources. One technology that may relive some of these burdens is In-Situ Resource Utilization (ISRU) technology. ISRU is the use of materials at the site of an interplanetary mission for the production of rocket propellant or life support products. With the ability to reduce Earth launch mass and decrease cost due to a reduction in the number of required launches, in-situ propellants are being recognized as the most viable option for sending humans to Mars [1].

ISRU also holds the key to establishing permanent outposts on the moon and Mars. Development of such an outpost will require maximizing the resources available on the surface

and/or within the atmosphere of these bodies. Data from previous unmanned Mars missions has shown that a wealth of resources are available on the surface of Mars that are suitable for use as chemical energy sources for sustained, long-term manned presence on Mars. One critical chemical energy requirement that must be addressed is a rocket propulsion system since human explorers will have to be periodically transported from the surface of Mars to low Martian orbit.

In this investigation we analyzed a variety of possible in-situ propellant combinations for the development of a long-term In-Situ Mars Ascent Vehicle (IMAV). The propellant combinations were then configured into the appropriate rocket propulsion class: solid, liquid or hybrid. An optimum in-situ propellant combination choice was then chosen for each of the three propulsion classes. Each of the three candidate propulsion systems were then compared against the baseline Mars Ascent Vehicle detailed in the current Mars Reference Mission [1]. The evaluation criteria consisted of areas such as performance, safety, and feasibility.

APPROACH

We began by identifying a baseline configuration against which to compare new design configurations for the IMAV. We chose the Mars Ascent Vehicle (MAV) [1] as our baseline using the published results of the engine analysis as a comparison for our design. Next, we recognized several mission constraints not specified in the baseline configuration. As described below, a key constraint was that our launch vehicle would utilize a hydrogen-free propulsion system. These constraints provide a guideline for the evaluation criteria, which included performance, vehicle size, and weight. Finally we compared three different propulsion alternatives (i.e., solid, liquid or hybrid) using a theoretical chemical equilibrium computer code [2]. The raw materials necessary to produce propellant for each of the three propulsion system alternatives for the IMAV are available from resources within the atmosphere or soil of Mars.

BASELINE CONFIGURATION

To compare the performance of our three alternative IMAV propulsion systems, the Mars Ascent Vehicle (MAV) [1] was chosen as a baseline. The MAV consists of a single common descent stage that delivers all hardware systems to the surface of Mars including the habitats, ascent vehicle, propellant production plant, and other surface cargo. As outlined in the Mars Reference Mission [1], the lander consists of four subsystems. These subsystems include a structure which contains payload and all other elements, a parachute to assist in the slow down of descent, a propulsion system to slow the lander prior to landing, and a surface mobility system.

The MAV allows the crew from the surface to launch back into orbit to rendezvous with the Earth Return Vehicle (ERV). This vehicle consists of the crew ascent capsule and the ascent propulsion system. The vehicle will use propellant made by the propellant production

plant that was delivered by the surface lander. The crew is returned to orbit via the capsule using the ascent propulsion system fuelled by propellants derived from Martian atmosphere and soil. The MAV utilizes LOX/CH_4 produced by the propellant production plant on the surface of Mars. The use of methane was made possible by the transportation of hydrogen from Earth. Producing the fuel on Mars benefits the mission by allowing more equipment to Mars [3]. The current MAV vehicle was used as a baseline against which we compared our alternative IMAV designs.

ADDITIONAL CONSTRAINTS

We have determined important variables that help define characteristics of an optimum IMAV system. For instance, the velocity needed to ascend to a low Martian orbit is related to the ratio of the mass of the propellant to the overall mass of the vehicle:

$$\ln R = \frac{U_{esc} + g_{mars} t_B}{g_o I_{sp}}$$

$$\frac{M_p}{M_o} = 1 - \frac{1}{R}$$

So to conserve mass, it is important to minimize propellant, which is relative to the minimum velocity need to escape Mars' gravitational force near the surface. For our theoretical missions, we allow for the mass of four astronauts and an additional amount for equipment and Martian test samples.

The attention towards having a SSTO also addresses the mass conservation issue. The addition of multiple fuel tanks simply increases the mass. Another benefit of a SSTO is the simplification of the ascent stage, which offers savings in controls and additional nozzles/plumbing.

The overall dry mass of the IMAV must be minimized since it will most-likely be manufactured on earth and transported to Low Earth Orbit (LEO) using whatever earth-to-LEO launch system that will be in use in the future. Specifically, to avoid assembly of the vehicle in LEO, the weight of the empty vehicle must be less than the maximum payload capacity of the most powerful LEO launch vehicle available. As a first approach, the current Space Shuttle fleet has been chosen as the system for launching the fully assembled IMAV into LEO.

Since the current Space Shuttle fleet has been chosen as the launching platform, an additional constraint that cant be overlooked is the size of the IMAV. Specifically, the IMAV must fit inside the current Space Shuttle cargo bay under the assumption that one of current fleet will be carrying the vehicle. Only one launch from Earth will be necessary to transport the complete IMAV to lower Earth orbit. Thus, the IMAV must comfortably fit into a 15-ft wide x 15-ft high x 60-ft long volume. This constraint is significant to the analysis since it impacts the size of the fuel and oxidizer tanks.

As seen from the analysis of the Martian atmosphere, there is a sparse amount of available hydrogen most commonly used high performance liquid fuels, such as hydrogen and hydrocarbons.

For repeated launches from the Mars surface, it is not cost effective or reasonable to continually transport hydrogen from Earth to manufacture these high performance fuels. Therefore hydrogen was eliminated as an element in the in-situ propellants compared in this study.

MARS ENVIRONMENT

In order to produce in-situ propellants, we need to know what resources are available. Previous unmanned missions have provided invaluable information regarding the surface and atmosphere of Mars such as NASA's Viking missions and the Mars Pathfinder.

Mars has a very thin atmosphere [4], only about 1% as dense as on Earth [5], consisting of mainly carbon dioxide and some other common gases as shown in Table 1.

Gas	Concentration (%)
Carbon Dioxide	95.32
Nitrogen	2.7
Argon	1.6
Oxygen	0.13
Carbon Monoxide	0.07
Water Vapor	0.03
Neon	0.00025

Table 1. Martian atmospheric constituents [1].

The Martian atmosphere contains less than 1% of the water vapor found in our air, but even this amount can condense forming clouds very high in the atmosphere. At the Viking Lander 2 site, a thin layer of winter frost covered the ground each winter. There is geographical evidence that in the past, in a higher-pressure environment, water flowed on the planet surface [5].

As discussed in the previous section, due to the sparse amount of available hydrogen in the Mars atmosphere, most commonly used high performance liquid fuels (e.g. molecular hydrogen and hydrocarbons) were eliminated as possible in-situ propellants.

The Martian surface is reported to be a type of iron-rich clay that contains a highly oxidizing substance that releases oxygen when wet. Silicon Dioxide and ferric oxide are the main constituents of the soil as shown in Table 2.

Composition of Martian Samples	Weight % (Approx.)
Silicon Dioxide (SiO_2)	44
Ferric Oxide (Fe_2O_3)	19
Sulfite (SO_3)	8.5
Magnesium Oxide (MgO)	8.4
Aluminum Oxide (Al_2O_3)	5.5
Calcium Oxide (CaO)	5.3
Titanium Dioxide (TiO_2)	0.9
Chlorine (Cl)	0.75
Potassium Oxide (K_20)	<0.3

Table 2. Typical constituents in Martian Soil [6].

From experiments carried aboard the Viking Landers, iron-rich smectite clays, magnesium sulfate, iron oxides, and reactive oxidizing agents of unknown chemistry were found on the Martian surface [5]. Smectites are unique materials which have the property of expanding when they contact water, and contracting when dry. Other soil components include silicate minerals, oxides (mostly iron), and some calcium carbonate [5]. The surface contains no organic molecules that were detectable at the parts-per-billion level .

Carbon dioxide, the major component of the atmosphere, freezes at each polar cap covering each hemisphere with snow that evaporates in the

spring. The ice caps appear to have a layered structure forming alternating layers of ice with varying concentrations of dark dust [4].

This layering process may also be a result of the wide range of climates Mars experiences due to its orbit. The seasonal changes in the volume of the polar caps are responsible for changing the global atmospheric pressure approximately 25% [4].

The presence of carbon dioxide provides a variety of possible propellant configurations. Options incorporating the plentiful supply of available carbon dioxide include producing methane as the fuel and oxygen as the oxidizer, or producing carbon monoxide as the fuel and oxygen as the oxidizer. If methane and oxygen were to be used it would be necessary to bring some payload from Earth. While the use of carbon monoxide and oxygen would require no Earth recourses, and could be completely manufactured on Mars using the most abundant and readily available Martian resource, carbon dioxide.

The average temperature on the surface is -64° C with a range from -140° C at the winter pole, to 27° C on the day side during summer [4].

Mars' significantly elliptical orbit has a major influence on its climate. One of which is the variation of about 30 C at the subsolar point between aphelion, when Mars is at the point farthest from the Sun, and perihelion, when Mars is at the point in its orbit where it is closest to the Sun [4].

The average pressure on the surface of Mars is only about 0.00069 atm. Although it varies greatly with altitude from almost 0.00888 atm in the deepest basins, to about 0.000987 atm at the top of Olympus Mons, the largest mountain in the Solar System rising 24 km above the surrounding plain [5]. On occasion the entire planet can undergo very strong winds and vast dust storms for months.

Environmental effects due to climate and extreme surface conditions are important to consider for propellant storage, production, and performance purposes. For example with solid rocket fuel the following relationship demonstrates how burning rate and chamber pressure are extremely sensitive to the initial temperature:

$$\Pi_r = \frac{1}{r}\frac{\partial \dot{r}}{\partial T_i}\Big|_{P_c}$$

where Π_r is the sensitivity coefficient of burning rate and is measured in terms of [% change / °C].

Energy expended to store the fuel and oxidizer can be minimized. Any necessary precautions can be taken to protect equipment from extreme or hazardous environmental conditions.

Mars' thin atmosphere produces a small greenhouse effect but it is only enough to raise the surface temperature by 5°C, much less than what we see on Earth.

The research has exposed a variety of elements from Martian atmosphere and soil that

are applicable for use as raw materials for rocket propellants. Possible compounds that could undergo some chemical processes and be stored as propellants for the IMAV for launching astronauts from the surface of Mars to orbit are:

- Magnesium and Carbon Dioxide
- Aluminum and Oxygen
- Carbon Monoxide and Oxygen
- Aluminum and Carbon Dioxide
- Magnesium and Carbon Dioxide
- Aluminum, Carbon Monoxide and Oxygen
- Magnesium, Carbon Monoxide and Oxygen

As shown in Figure 1, these propellants can be incorporated into a variety of solid, liquid and/or hybrid rocket propulsion systems.

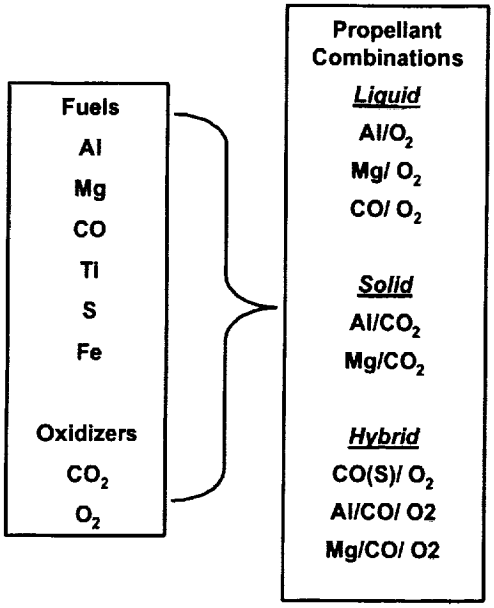

Figure 1. Raw materials for IMAV propulsion systems.

RESULTS

Theoretical Propellant Performance

To theoretically determine the performance and other design parameters of the candidate propulsion systems shown in Fig. 1, the NASA Chemical Equilibrium Computer Code (CEC) was used [2]. Different in-situ fuel and oxidizer combinations for each propellant type were modeled, simulated, and analyzed.

Figure 1 shows the different combinations that were investigated. Evaluation of rocket performance was based on the following criteria, specific impulse and the density of the oxidize/fuel mixture: I_{sp}, ρI_{sp}, and ρI_{sp}^2.

While I_{sp} is a suitable parameter to evaluate rocket performance, we also chose to consider ρI_{sp} and ρI_{sp}^2 because the ultimate criteria of the performance of a rocket propellant are flight parameters which reflect the effects of both specific impulse and propellant density [4]. The parameters ρI_{sp} and ρI_{sp}^2 can be derived from the rocket equation:

$$M_{pl} = \frac{\rho_p V_p}{e^{\left(\Delta v / g_o I_{sp}\right)} - 1} - M_{dry}$$

By expanding the exponential term and incorporating an infinite series expansion, the above equation reduces to the following linear relationship:

$$M_{pl} \propto \rho_p I_{sp}^n$$

where the variable n is related to the mission value of Δv. In a study by Zurawski and Green [7], an evaluation of several propellant combination performances demonstrated a linear relationship between delivered payload mass and ρI_{sp}^2 which can be seen in Figure 2. For the present study, since Δv is approximately the same as the mission

outlined in the study by Zurawski and Green [7], *n* is also approximately 2. Therefore, the highest performing propellant combination will likely correspond with the propellant combination with the maximum value of $\rho I_{sp}^{\ 2}$.

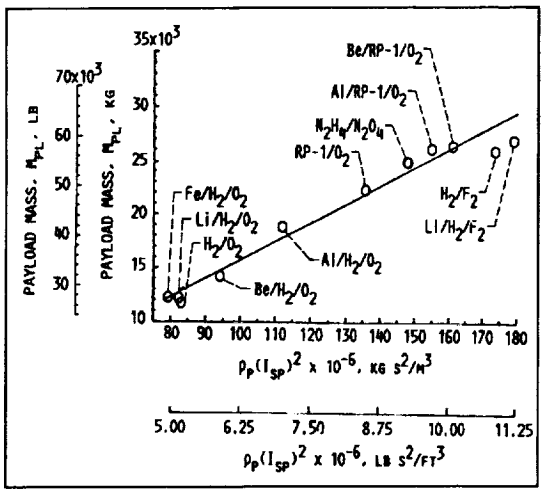

Figure 2. Delivered payload vs. $\rho I_{sp}^{\ 2}$ [5].

The above relationship makes it possible to use $\rho I_{sp}^{\ 2}$ as the preliminary criteria for the evaluation of the performance of rocket propulsion combinations. Accordingly, we calculated I_{sp}, ρI_{sp}, and $\rho I_{sp}^{\ 2}$ over a range of oxidizer/fuel ratios to simultaneously determine the optimum ratio.

Generally speaking, the optimum oxidizer to fuel ratio (O/F) is near the stoichiometric ratio. Therefore, we determined the stoichiometric value for each propellant combination and then used the NASA CEC code to calculate propellant performance at O/F ratios below and above the stoichiometric ratio. For example, for the CO/O_2 liquid propellant combination:

$$CO + \frac{1}{2}O_2 \rightarrow CO_2$$

$$O/F_{Ratio} = \frac{\dot{m}_{O2}}{\dot{m}_{CO}} = \left(\frac{n_{O2}}{n_{CO}}\right)\left(\frac{MW_{O2}}{MW_{CO}}\right)$$

$$r = O/F = \left(\frac{0.5}{1}\right)\left(\frac{32}{28}\right) = 0.57$$

The overall propellant density of each propellant combination is calculated as follows:

$$\rho_{mix} = \frac{1+r}{\frac{r}{\rho_{ox}} + \frac{1-ML}{\rho_f} + \frac{ML}{\rho_m}}$$

where ML corresponds to the metal loading in cases where metal particles are used in conjunction with liquid or solid fuel.

With the main focus of this report to determine what type of propellant and propulsion system is optimal for the IMAV, we narrowed down the assessment to the best performing configuration by choosing one propellant combination for each class of rocket propulsion: liquid, solid, and hybrid. When analyzing the potential liquid propellant combinations, we considered cost, safety, and performance of propellant combinations.

We had three liquid propellant combinations which to choose from:

- Aluminum and LOX,
- Magnesium and LOX, and
- LCO and LOX.

These in-situ propellants were compared against methane and LOX, which is the propellant combination used in the baseline MAV. The first two liquid propellants mentioned are metallized liquid propellants where the metals are

suspended in fine particulate form as a slurry or gel in the LOX oxidizer [8]. These two metallized propellants offer higher specific impulse and greater performance over the other liquid propellant combinations. Although the two metallized liquid propellants would provide a performance advantage, production of the fuel would be much more complex due to the process involving extraction of the metal particles from the surface of Mars. The two metallized propellants also have not been proven to be a safe or reliable fuel alternative since the fuel and oxidizer are mixed in a slurry potentially posing a explosion hazard. Therefore, although their performance is superior to LCO/LOX, we ruled out the metallized propellants as a possible liquid propellant for this mission.

The liquid propellants LCO/LOX and the baseline propellant methane/LOX have been compared thoroughly [5]. The methane/LOX combination was found to be a better performer with respect to LCO/LOX, but in order to produce the methane, 5.8 tons of liquid hydrogen would be needed to be transferred from Earth to Mars adding to payload cost [6]. Conversely, all the elements for the LCO/LOX propellant could easily be found on the surface of Mars therefore eliminating the cost of transporting 5.8 tons of hydrogen to Mars. Also the refining process to create methane is much more complex than the production of LCO and the energy required to produce methane would be 27% greater than producing LCO [6]. Based on cost, complexity, and safety, the LCO/LOX combination was the best choice for a liquid propellant.

Unlike the liquid rocket evaluation, the solid and hybrid choice for optimum propellant was based solely on performance. Thus, for each of the solid and hybrid propellants listed in Fig. 1, the top performer in terms of ρI_{sp}^2 was chosen as the candidate propellant combination for IMAV. In terms of this performance parameter, $Al/CO_{(S)}/O_2$ was chosen as a candidate hybrid propellant combination and $Al/CO_{2(S)}$ was chosen as a candidate solid propellant combination. Figure 3 is a plot of ρI_{sp}^2 vs. O/F for each of the identified propellant combinations.

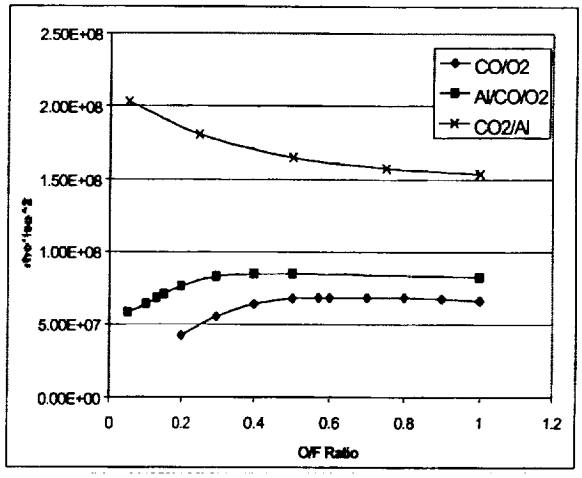

Figure 3. Calculated ρI_{sp}^2 vs. O/F ratio for liquid, hybrid and solid in-situ propellant candidates.

Having identified the top candidate propellant combination for each of the three rocket propulsion classes, we performed a more detailed analysis of each propulsion system and its corresponding candidate propellant.

Preliminary Design Configurations

Liquid Rocket Design

For the analysis of the liquid propellant operation, we used MS Excel to perform iterative design calculations taking into consideration all the factors affecting the performance of the CO/O_2 propellant. These calculations included vehicle payload, propellant characteristics, cargo bay size, and nozzle performance characteristics.

One assumption that we feel will help reduce costs and any additional need for testing is the use of a modified space shuttle main engine (SSME). By integrating a current main engine into the IMAV design, we set constraints that define the amount of thrust the IMAV can obtain. The current ratio of the area of the exhaust plane to the throat area of the nozzle on the SSME nozzle is 77.5.

$$\frac{A_e}{A_t} = 77.5 = \frac{\Gamma^2}{\left(\frac{P_e}{P_c}\right)^{1/\gamma} C_F^o}$$

$$Thrust = C_F P_C A_T$$

We are able to calculate important parameters, C_f and the pressure of the chamber, which are the variable that define the thrust of the vehicle. From the calculation of thrust, we compare it to our overall weight of the IMAV. The ratio of the thrust over the weight must be greater than unity in oder for the vehicle to get off the surface of Mars. Once again, we used the NASA CEC code to calculate theoretical values for important parameters such as pressure ratios, temperature of the chamber, and molecular weight of the products. Using these parameters we extracted the remaining design variables including fuel, size of tanks, and the theoretical propellant performance from the spreadsheet.

The example Excel calculations are included in Appendix I for the chosen liquid propellant of CO/O_2. For comparison, the baseline spreadsheet of the reference mission is in Appendix II. The calculations examine how a methane/oxygen propellant might perform ($CH_4/O2$). The sheets illustrate that, while a large quantity of CO (compared to methane) is required to lift the IMAV into a low Mars orbit, there is a sufficient thrust to weight ratio and a reasonable propellant performance. The storage tank of the oxidizer was assumed to be spherical and the storage tank of CO needed to be cylindrical because of the large volume needed. Based on the theoretical size, will take up a majority of the avalable space in the cargo bay.

Solid Rocket Design

Next, we analyzed the solid rocket motor by calculating the ratio of the exposed solid burn area over the area of the throat using the following equation for equilibrium pressure in a solid rocket motor:

$$\frac{A_B}{A_t} = \frac{P_c^{1-n}}{\rho_p C^* a}$$

In this equation, P_c is the chamber pressure, n is the pressure exponent, ρ_p is the density of the propellant, C^* is the characteristic velocity (a measure of thermodynamic propellant performance) and a is the temperature coefficient. As in most rocket propulsion design studies, a

nominal chamber pressure of 1000 PSIA was chosen. Once an approximate burn area ratio is calculated, the size of the fuel tanks can be determined.

To solve the equation we calculated the propellant density, and extracted C^* from the NASA CEC code. Since our optimum solid fuel is $Al/CO_2(S)$, we assumed a pressure exponent according to similar solid fuels containing aluminum [9]. To determine a temperature exponent, we assumed a burning rate, $\dot{r}$ for the solid fuel and extracted a temperature exponent using:

$$a = \frac{\dot{r}}{P_c^n}$$

We calculated a burn area over throat area ratio of 156.4, which is comparable to other solid rocket engine designs [10]. Assuming a throat area similar to the SSME, the approximate initial burn area is 15 m^2. From this, we determined the approximate size of the rocket chamber assuming a cylindrical design. Figure 4 illustrates how the geometric shape of chamber depends upon the temperature exponent characteristic of the specific propellant.

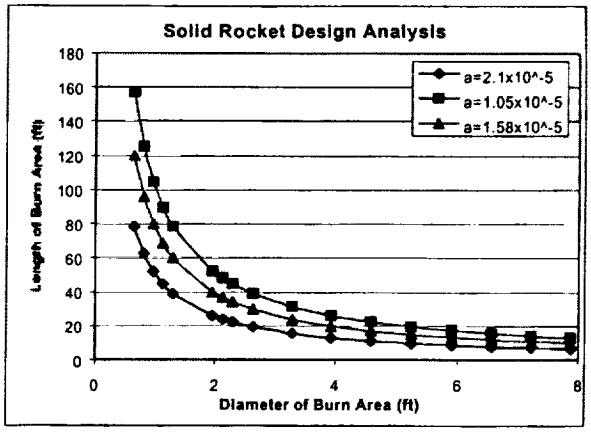

Figure 4. Length vs. diameter for Al/CO_2 solid rocket propellant motor.

The appropriate length and diameter of the burn area were determined to be 20 ft by 2 ft respectively assuming a temperature exponent equal to 2.1 x 10^{-5}. After including the overall diameter of the fuel, insulation, and the wall thickness, the tank diameter is approximately 7 ft and the length of the rocket is approximately 30 ft, which satisfies size constraints.

Hybrid Rocket Design Analysis

Analysis of the hybrid rocket design is somewhat difficult due to the lack of information and testing available on hybrid propellants. Orbitec is conducting a series of tests with various hybrid fuels that are applicable for Mars-based vehicle [12]. A shown in Figure 5, the group published the following graph comparing some of the fuels they tested. The focus of the paper was analyzing data for solid CO and oxygen. While there is no aluminum doping in the fuel, we assumed it be an accurate starting point based on the data for $Al/CH_{4(S)}$ fuel, which is also included in the figure. The graph contains

a plot of the average fuel regression rate, $\dot{r}$ as a function of the average oxidizer mass flux, G_o. Through a logarithmic derivation of the standard empirical fuel burning rate formula, we were able to that if we estimate a data line representing Al/CO/O_2 on Figure 5 and extract a slope, we can determine an approximate temperature and pressure exponent from the graph.

$$\dot{r} = aG_o^n$$
$$\log \dot{r} = \log a + n \log G_o$$
$$y = b + mx$$

Calculating the burn area allows us to approximately determine rocket chamber size according to the following equation:

$$A_b = \frac{\dot{m}}{aG_o^n \rho_f}$$

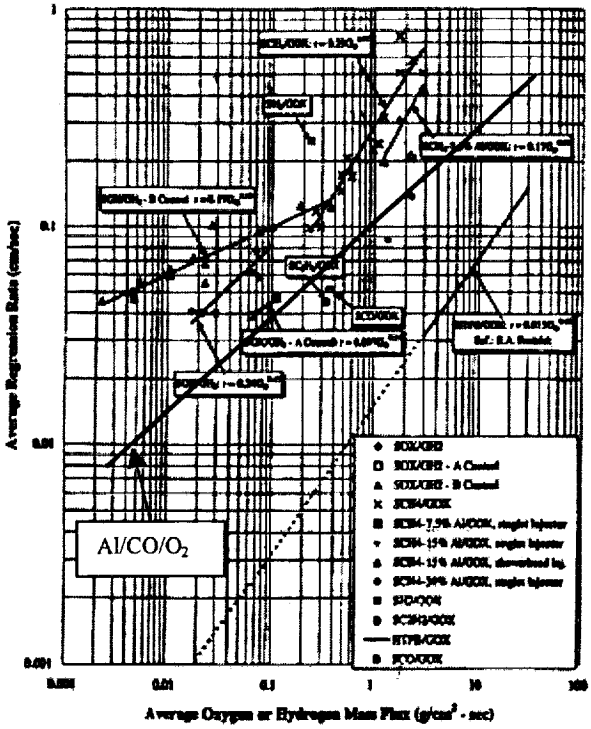

Figure 5. Fuel regression rate for hybrid rocket propellant combinations [12].

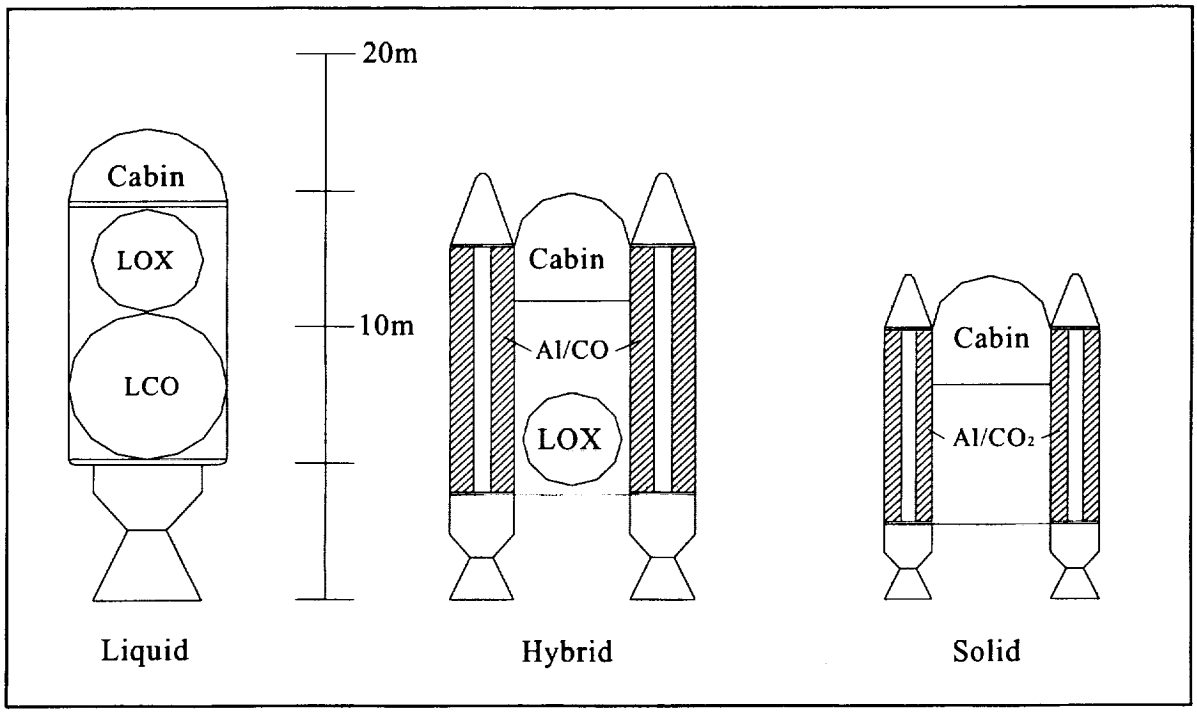

Figure 6. Approximate sizes of the MAV for each system according to the design calculations.

The approximate burn area is a function of average regression rate, $\dot{r}$, which we already know is a function of the mass flux rate, the temperature, pressure exponents, fuel density, and the fuel mass flow rate.

The calculations yield a burn area of around 25 m^2. Based on this calculation, it is possible to determine the size of the remaining solid rocket motor components. Following the same formula of the solid rocket design, we determined an overall tank diameter of 10 ft. In addition to the rocket chamber there must also be an oxidizer tank upstream resulting in an overall length of the rocket is an estimated 50 ft. In Figure 6, the scaled illustration shows the size comparison of all three different systems. This contrast is related to certain rocket design specifications such as the density of the propellant, the engine layout for each system, and the overall performance of the propellant.

CONCLUSIONS AND RECOMMENDATIONS

After thorough analysis of several in-situ propellants, we chose three candidate fuel/ oxidizer combinations, one from each rocket propulsion class. We then compared the performance, cost, and feasibility of the hybrid, solid, and liquid IMAV design configurations.

Liquid CO/O_2, the recommended choice for a liquid propulsion system is a capable fuel oxidizer combination for the IMAV. Although the theoretical performance is lower than the candidate hybrid fuel ($Al/CO/O_2$) and the solid fuel (CO_2/Al), the liquid CO/O_2 still offers many benefits. Derived from the abundant supply of CO_2 in the Martian atmosphere CO/O_2 is a safe and storable liquid in-situ propellant. CO/O_2 would also be easy to manufacture in a propellant production plant on Mars using presently available technology. The production has a minimal impact on the Martian environment and the testability of CO and O_2 make it possible to determine any uncertainties associated with this fuel choice. The design configuration demonstrates the large size of fuel tanks due to the quantity of required fuel to lift the IMAV into Martian orbit. While this requires that much of the space in the shuttle cargo bay would be occupied it does not eliminate CO/O_2 as an effectively performing fuel source. Finally, and perhaps most significantly, development of a reliable, safe CO/O_2 engine can be readily achieved using today's technology. Indeed, neither the SSME derivative engine (shown in Figure 7) described in this report nor the pair of RL-10 derivatives described in the Mars reference mission would require a quantum leap in technology.

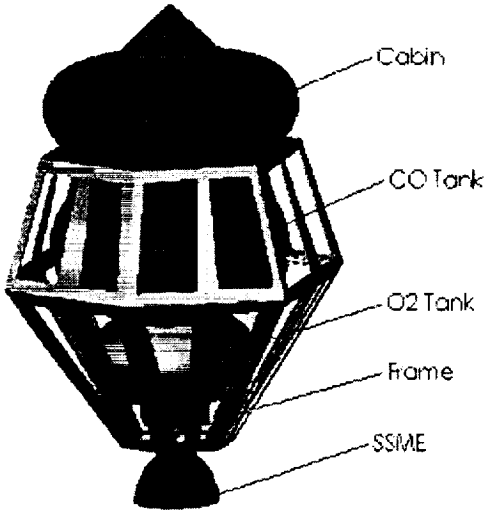

Figure 7. SolidWorks© illustration of CO/O_2 Mars Ascent Vehicle.

The recommended solid fuel choice, Al/CO_2, proved to be the best performing fuel of the three we examined. The tank size was very compact due to the density of the fuel, which in turn reduced the total weight of the IMAV design configuration. However, with solid propellant, there are severe political, economic, and safety drawbacks[11]. While proving to be extremely compact and simple, at the same time, solid fuel poses the greatest associated risk factor. With no known method, the need for technological advances in the mining of the aluminum metal from the Martian soil inflates the cost of the mission. The propellant production method must be extremely refined due to solid fuel's sensitivity to cracks and bubbles [9]. The use of solid Al/CO_2 also imposes more detrimental environmental effects to the Martian environment. Mining for the metal will create surface disturbances whose effects are undeterminable. Solid propellants' safety risk is widely known due to the uncontrollability of the rocket motor and the inability to throttle the engine or abort the launch once it has been fired. Finally, no data exists to verify that the Al/CO_2 combination would be ignitable and burn with a burning rate high enough for the development of a feasible rocket engine.

The recommended hybrid propellant Al/CO/O_2, performed slightly better than the recommended liquid propellant. Although it did not perform as well as the solid, the hybrid is a safer design because it is controllable. Unfortunately, comparatively little testing has been done with hybrid rocket motors in general, which delays mission time in order to conduct more thorough research and experimentation. Similar political and economic pressures of the solid are also associated with the hybrid design because of the need for the development of advance metal mining techniques to extract the aluminum metals from the soil. As stated before this will increase mission expenses, and possibly cause environmental damage to the Martian surface. The design for the hybrid shows the need for large oxidizer tanks and an extended rocket chamber for the solid CO/Al fuel mixture.

After significant consideration we have chosen the CO/O_2 liquid rocket engine as the optimum design configuration for the IMAV. The design offers a relatively high performance, the safety of a liquid engine, and the possibility of rapid development time due to the reliance on current and proven technology.

This paper is the culmination of a one-semester class on the fundamentals of rocket propulsion. The class helped us gain an extensive knowledge in the field of rocket propulsion, which we applied to the research and analysis conducted for this project.

Over the past year a separate group of students, as part of their Senior Engineering Clinic project, have built a hybrid rocket motor and test stand as shown in Figure 8. The work they have done provides a stepping stone for future effort into this project. The lack of test data on hybrid rocket engines was very limiting to this study, but by using the available test stand we can help develop the required data. A future project will be conducted to developing a hybrid rocket using Al/CO/O_2, our choice propellant, and verify our calculations with experimental data.

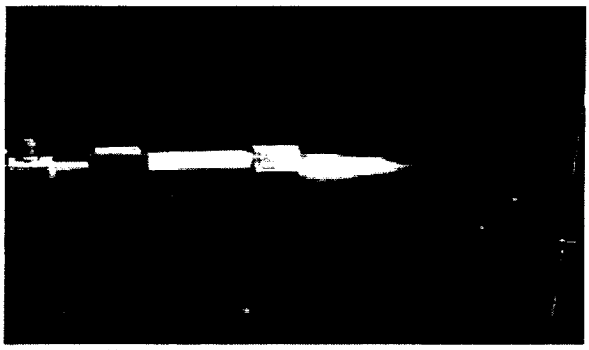

Figure 8. Test firing of hybrid rocket motor built by Rowan University students. The burning propellant is a Al/Epoxy/GOX mixture.

The research community has realized that in-situ propellants are the most viable option for a manned mission to Mars, but little research has gone into the harvesting of the elements to produce the propellants. It is evident that metallized propellants provide more energy but more research can be done on how to remotely obtain the metals from the Martian soil. A future study in the development of liquid carbon monoxide and oxygen from the Martian environment would allow us to more clearly illustrate the time and costs associated with our suggested fuel source.

OUTREACH

As engineers it is our duty not only to innovate but also to educate. With that in mind we looked to inform faculty members, our peers, the public, and the media regarding the scope of this project and the human exploration of Mars. Through presentations at local elementary schools we hope to inspire further interest in children to investigate the world around them and beyond.

Poster presentations on campus, such as the annual STEM (Science Technology Engineering Math) Symposium at Rowan University, provide outreach to students and faculty from a variety of studies. A distinguished campus-wide event, participation in the symposium exposed the project to hundreds of students, faculty, and guests.

As part of the Mechanical Engineering Department policy the design project was subject to a mid-semester design review. For the review a presentation was given to professors and students, who had the opportunity to question, critique, and evaluate the project team's progress. The development of a web page has allowed the project to be exposed to any interested party with

access to the Internet. The web page provides important information on the project and the HEDS-UP Forum.

As part of a continuing cooperative relationship between Rowan University and our local newspaper, the Gloucester County Times, publicity for the project and the team's participation in the HEDS-UP Forum is already underway. Upon return from Houston final interviews with the team will take place and an article will be released.

APPENDICES

I. Baseline Spreadsheet for CO/O_2 Propellant

II. Baseline Spreadsheet for CH_4/O_2 Propellant

REFERENCES

(1) Hoffman, Steven J. *NASA Mars Reference Mission.* http://www.sn.jsc.nasa.gov/marsref/contents.html

(2) Gordon, Sanford and Bonnie McBride. NASA Chemical Equilibrium Code: NASA Glenn Research Center Cleveland, OH 44135
References:
NASA SP-273, 1971
NASA RP-1311, PART I, 1994
NASA RP-1311, PART II, 1996

(3) AMERISAR America Search And Rescue. SPACE SHUTTLE DIAGRAMS http://www.amerisar.org/shutdiag.htm

(4) Arnett, Bill. Mars. March 9, 2000.http://www.anu.edu.au/Physics/nineplanets/mars.html

(5) Sherlock, Sean. *What is the Martian Soil Composition*?. February 8, 1997. http://www.madsci.org

(6) Clapp, M. "Comparison of Mars-Production Methane and Carbon Monoxide," AIAA-91-2442, 1991

(7) Green, J., and Zurawski, R., "An Evaluation of Metallized Propellants Based on Vehicle Performance," AIAA-87-1773, 1987.

(8) Goodall, Kirk. *Mars Surveyor 2001 Lander*. February 1, 2000.

(9) Sutton, George P., *Rocket Propulsion Elements: An Introduction to the Engineering of Rockets.* 6th edition, John Wiley & Sons, New York, 1992.

(10) Marchese, Anthony J. *Introduction to Rocket Propulsion Notes.* Rowan University. Spring 2000.

(11) Henry, G., Humble R., and Larson, W., *Space Propulsion Analysis and Design.* McGraw-Hill, New York, 1995.

(12) Rice, Eric E. and others. *Initial Test Firing Results For Solid CO/GOX Cryogenic Hybrid Rocket Engine For Mars ISRU Propulsion Applications.* Fifth International Microgravity Combustion Workshop. Glenn Research Center, May 1999.

Technical papers found on NASA technical paper server:

Wadel, Mary F., *Benefits of In Situ Propellant Utilization for a Mars Sample Return Mission,* January 24, 2000.
http://techreports.larc.nasa.gov/ntrs/hget.cgi?lerc?2723/1=... /TM-107267.html

Linne, Diane L., *Experimental Evaluation of the Ignition Process of Carbon Monoxide and Oxygen in a Rocket Engine,* January 24, 2000.
http://techreports.larc.nasa.gov/ntrs/hget.cgi?lerc?2367/1=... /TM-107267.html

Landis, Geoffrey A., *Effect of Inert Propellant Injection on Mars Ascent Vehicle Performance,* January 24, 2000.
http://techreports.larc.nasa.gov/ntrs/hget.cgi?lerc?2566/1=... /TM-107267.html

Wadel, Mary F., *Propulsion Systems Using In Situ Propellants for a Mars Ascent Vehicle,* January 24, 2000.
http://techreports.larc.nasa.gov/ntrs/hget.cgi?lerc?2321/1=... /TM-107267.html

Appendix I. Baseline Spreadsheet for CO/C_2 Propellant

Mission Parameters				**Vehicle Envelope: Space Shuttle Cargo Bay**			
Delta V	4500	m/s		Diameter	4.572	m	
Ambient Pressure	0.101526	psia		Length	18.288	m	
Isp	303	s		Volume	300.23	m^3	
g o [m/s^2]	9.8	m/s^2		Ms, Max	22727	kg	
g mars [in/s^2]	3.72	m/s^2		Mass SSME	2900	kg	
tb	120	s					
ML	2000	lbs					
Ms	22727	kg					
				Propellant Characterics			
Mission Calculations				Fuel	CO		
Max g's	37.5			Fuel Density	806	kg/m^3	
R	5.28			Oxidizer	O_2		
Final Vehicle Mass	22727			Oxidizer Density	1140	kg/m^3	
Initial Vehicle Mass	120222.56			O/F opt	0.5		CEC
Mp	97495.56	kg		Tc	3439	K	CEC
Mdot	812.46	kg/s		C*	1379	m/s	CEC
Mdot,ox	270.82	kg/s		MW	37.529	g/mol	CEC
Mdot,f	541.64	kg/s		little gamma	1.1235		CEC
Weight	1224638.4	N		big gamma	0.63		
Thrust	2413542.37	N					
Thrust/Weight	1.97			**Nozzle and Performance Characteristics**			
				Pc	6894000	1000	psia
Vehicle Calculations				Pc/Pa	9849.69		
Total Vehicle Mass	124963.10	kg		Pe/Pc, adapted	0.000101526		
Vehicle Dry Mass	22727	kg		Ae/At, actual	76.28		
Mox	32498.52	kg		Ae/At, adapted	77.5		
Mf	64997.04	kg		Pe/Pc, actual	0.0012908		CEC
Vox	28.57	m^3		Cfo	1.96		CEC
Vf	80.64	m^3		CF,sea level	2.154		
Dia, ox sphere	3.79	m		At	0.162	m^2	
Dia, fu cylinder	4.13	m		Ae	12.397	m^2	
Length of fuel cylinder	6	m		dia t	0.513	m	
Engine Mass	2900	kg		dia e	4.48	m	
Tank Mat'l Density	2800	kg/m^3		Thrust	2413542.371	N	
Tank Wall Thickness	0.00635	m		Isp	303.1274372	s	
Ox tank mass	401.87	kg					
Fuel Tank mass	478.66	kg					
Passengers(4)	260	kg					
Passenger Equipment	100	kg					
Surface Samples	100	kg					
Experimental Data	200	kg					
Navigational Equipment	300	kg					

Appendix II. - Baseline Spreadsheet for Reference Mission

Mission Parameters				**Vehicle Envelope: Space Shuttle Cargo Bay**			
Delta V	4500	m/s		Diameter	4.57	m	
Ambient Pressure	0.101526	psia		Length	18.28	m	
Isp	406	s		Volume	300.23	m^3	
g o [m/s^2]	9.8	m/s^2		Ms, Max	22727	kg	
g mars [in/s^2]	3.72	m/s^2		Mass –RL-10 (2)	300	kg	
tb	120	s					
ML		lbs					
Ms	22727	kg					
				Propellant Characterics			
Mission Calculations				Fuel	CH4		
Max g's	37.5			Fuel Density	717	kg/m^3	
R	3.46			Oxidizer	O_2		
Final Vehicle Mass	22727			Oxidizer Density	1140	kg/m^3	
Initial Vehicle Mass	78786.56			O/F opt	3.4		CEC
Mp	56059.56	kg		Tc	3543	K	CEC
Mdot	467.16	kg/s		C*	1859.1	m/s	CEC
Mdot,ox	360.98	kg/s		MW	21.21	g/mol	CEC
Mdot,f	106.17	kg/s		little gamma	1.128		CEC
Weight	817580.30	N		big gamma	0.63		
Thrust	1859241.2	N					
Thrust/Weight	2.27			**Nozzle and Performance Characteristics**			
				Pc	6894000	1000	psia
				Pc/Pa	9849.69		
Vehicle Calculations				Pe/Pc, adapted	0.000101526		
Total Vehicle Mass	83426.56	kg		Ae/At, actual	69.63		
Vehicle Dry Mass	22727	kg		Ae/At, adapted	77.5		
Mox	43318.75	kg		Pe/Pc, actual	0.001392		CEC
Mf	12740.81	kg		Cfo	1.96		CEC
Vox	37.99	kg		CF,sea level	2.140		
Vf	17.76	kg		At	0.125	m^2	
Dia, ox sphere	4.17	kg		Ae	8.772	m^2	
Dia, fu sphere	3.23	kg		dia t	0.4519	m	
Engine Mass	300	kg		dia e	3.7710	m	
Tank Mat'l Density	2800	kg		Thrust	1859241.19	N	
Tank Wall Thickness	0.00635	kg		Isp	406.10	s	
Ox tank mass	486.66	kg					
Fuel Tank mass	293.32	kg					
Passengers(4)	260	kg					
Passenger Equipment	100	kg					
Surface Samples	100	kg					
Experimental Data	200	kg					
Navigational Equipment	300	kg					

PENNSTATE

SCALING THE MARTIAN WALLS OF TIME

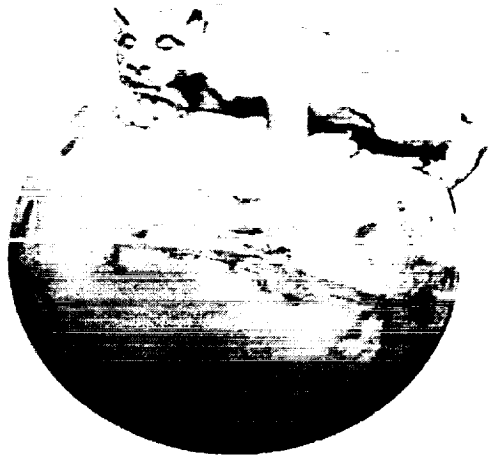

Faculty Contact:
Dr. Wojciech Klimkiewicz
Sr. Research Associate
Applied Research Laboratory
Penn State University
P.O. Box 30
State College, PA 16804
Telephone: (814)863-4149
Fax: (814)863-1396
E-mail: wxk10@psu.edu

Administrative Contact:
Robert Killoren
Assistant Vice President for Research
Office of Sponsored Programs
110 Technology Center
200 Innovation Blvd.
University Park, PA 16802-7000
Telephone: (814)865-1372
Fax: (814)865-1008
E-mail: osp@psu.edu

PENNSTATE

TEAM MEMBERS:

CLASS OF SPRING 2000 EE497D AND ME497C

Alysha Holmes, ajh169@psu.edu - Student Team Leader

Nikki Thornton, nlt112@psu.edu
Joseph Yagloski, jxy136@psu.edu
Joe Fledderman, jpf137@psu.edu
Gregg O'Marr, glo101@psu.edu
Ben Weber, bmw131@psu.edu
Chris Carlins, cxc428@psu.edu
Shubh Krishna, sxk264@psu.edu
Kevin Sloan, kfs113@psu.edu
Taite Merriman, tam245@psu.edu
David Borowski, dmb275@psu.edu
Michael Schrader, mas412@psu.edu
Mike Jordan, mxj123@psu.edu
Jean Hsu, jsh181@psu.edu
Chad Laufer, crl120@psu.edu
Christian Feisel, cld169@psu.edu
Michael W. Graham, mwg129@psu.edu
Brian Sosnowchik, bds179@psu.edu

PENN STATE FACULTY ADVISORS

Dr. Wojciech Klimkiewicz, Instructor, wxk10@psu.edu,
Dr. James Pawelczyk, Advisor, http://www.psu.edu/ur/archives/intercom_1998/May7/shuttle.html
Evan Pugh Professor Alex Wolszczan, Advisor http://www.astro.psu.edu/users/alex/
Professor Bohdan Kulakowski, Advisor, http://www.me.psu.edu/faculty/
Dr. Charles L. Lloyd, Advisor , The Applied Research Laboratory
Dr. Timothy F. Miller, Advisor, The Applied Research Laboratory
Dr. David C. Swanson, Advisor, The Applied Research Laboratory

1. SUMMARY

On Earth, when scientists want to investigate planetary history they take a core sample, with deeper fragments corresponding to older materials. In essence, descending through sedimentary layers is like going back in time. But creating a robot capable of taking samples more than a few meters below the planetary surface is still beyond the current available technology. The **cliffhanger** idea takes advantage of the natural surface features of Mars to explore the history of the planet without digging. So interesting and difficult questions can be answered not with the brute force of a drill, but with creative mission design.

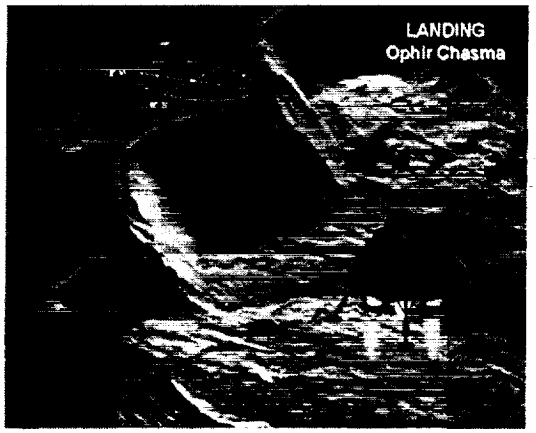

Figure 1. Landing near the cliff in Ophir Chasm.

Penn State University HEDS-UP team has designed a novel Mars mission approach. A main Lander with a Rover and a Cliffhanger (Figure 2) will land near cliffs of Valles Mariners (Figure 1). Especially design canon (gas, guided munitions or rocket) will deploy a long rope into the canyon. The rover will carry the cliffhanger to the edge of Valles Marineris following the rope, attach the cliffhanger to the rope. The Cliffhanger will then climb a 2 km down the rope and will allow the team to study sedimentary layers of rock on the side of the cliff. Samples and high-resolution images will be taken and delivered to the Lander for further investigation (***optical multispectral imaging microscope***, ***spectrometry***) and sending the results to Earth.

The robot has been designed to have the capability for locomotion at any angle (including somewhat uphill slopes) but maximum effective motion will be achieved at descent angles from 70-85 degrees.

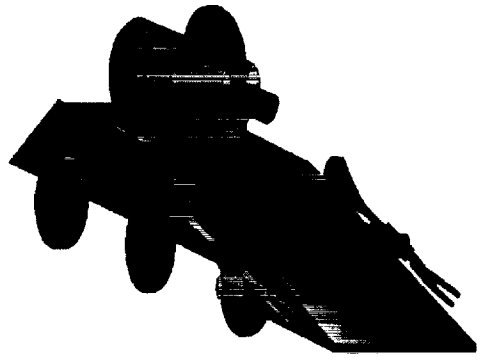

Figure 2. Rover and Cliffhanger.

After the mission of rope-climbing is completed, the Rover am Lander will embark on another long-term mission to provide meteorological and geological data over a long period of time (***long-term Mars Observatory***), and perform acoustic and seismic experiments on the surface of Mars in preparation for human arrival.

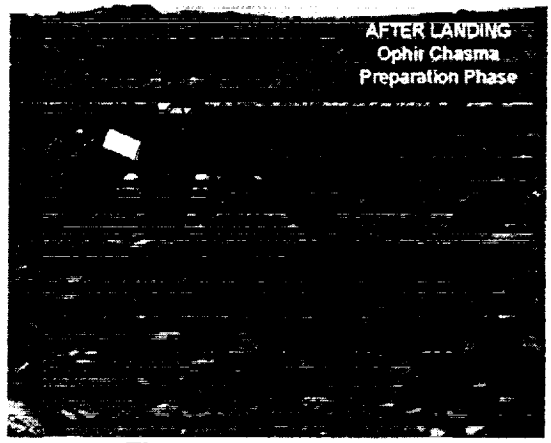

Figure 3. Lander and Rover

2. INTRODUCTION

As scientific observations of Mars create a greater understanding of the planet, and appease basic inquisitions, the unanswered questions remaining continue to become more difficult to investigate. These more elusive answers will require future missions to escape from the constraints imposed by the successes and failures of missions past and embrace more unconventional

yet thought-out ideas. Until exploration evolves from sending landers and rovers designed for disposable data collection, to attacking more adventurous robotic goals and beginning manned exploration of the planet, many scientific problems will remain unsolved.

This mission design will serve as an excellent first step in this evolutionary process. By using three specialized modules—a lander, a rover and a cliffhanger—it will be possible to take advantage of the natural features of the Martian surface to enhance understanding of the geologic and biologic history of the planet as well as pave the way for future manned missions.

Primary Science Objective:

The primary objective of the mission is to investigate of sedimentary layers of the walls of the Valles Marineris canyon system. The cliffhanger module will utilize a climbing rope launched by and attached to the lander to descend along the side of the cliff, taking samples and measurements at regular intervals. The rover will then return the samples to the lander for more exhaustive experimentation. This system will not only allow scientists and engineers to thoroughly examine Martian surface and subsurface materials, but will also answer questions about the origin and geology of Mars as well as the history and future of the solar system. And, while the large doses of solar and cosmic radiation on the planetary surface may make detection of life there problematic, deeper sedimentary layers will shed some light on the issue of the possible evolution of life on the planet.

Secondary Science Objective:

The secondary objective of the mission involves the maintenance of a long-term observatory on the Martian surface. Past undertakings, including the Viking and Pathfinder missions, centered on modules whose usefulness ended after a few months. For this mission, the lander and rover modules have been specifically designed to survive the harsh conditions of the planet for years while continuing to take scientifically useful measurements indefinitely. No mission yet has provided the long-term characterization of the Martian environment that will be a crucial element in the design of manned missions.

3. Our Approach

Students enrolled in the cross-referenced EE/ME 497 class at the Pennsylvania State University completed the work reported. Participating students had little to no prior knowledge on the subjects of Mars exploration or robotics. Thus, in order to attain the proper background knowledge of the subject, the students began work on general science tasks.

3.1 Science of Mars

Science tasks, including the search for life, the climate of the planet, and geology and planetary structure, focused on specific areas of interest in the study of Mars.

These science tasks accomplished two main objectives. First, by investigating the known scientific facts and theories of Mars, the students were able to understand better what remains unknown about the planet. These gaps in knowledge were key in mission definition decisions.

Secondly, the study of the Martian environment provides a deeper understanding of the obstacles facing manned or robotic missions to the planet. For example, the simple fact that Mars lacks a strong magnetic field makes the use of any kind of compass on the planetary surface impossible. Also, an understanding of the composition and properties of the soil of the planet is crucial to the design of solar arrays that will overcome the problem of dust deposition that will ultimately plague any mission requiring solar power for an extended period.

After the completion (reports [1] to [13], see references) and presentation of the general science tasks, students moved on to a series of robotics design tasks.

3.2 Robotics State of the Art

These projects (reports [14] to [22], see references) focused on specific aspects of robotics design such as locomotion, control, sensing and actuation, with an eye towards adapting recent advances in these areas for use on the Martian surface. The team was thus able to gain a basic understanding of the current state of robotics design. They also studied the past successful and not so successful robotic mission to Mars.

Once the students had acquired the requisite background knowledge it became necessary to choose specific mission objectives to focus design efforts.

3.3. Important Possible Future Mars Missions

At first, the team participated in a simple brainstorming session that produced more than 25 possible mission objectives for consideration. Since caves would provide an ideal shelter for the first manned missions to the planet one such idea included a search for subterranean caves and lava tubes with a ground penetrating radar device. Other ideas focused on in-situ resource production of propellants or volatile metals such as lithium, which could be burned as an efficient fuel source.

3.3 Mission Selection Criteria

In the final analysis, the criteria that were used to choose the mission objectives were pared down to a few, based on how well the mission will support the following:

- Attempting an innovative mission never proposed before.
- Uncovering the history of geology and biology on Mars
- Public involvement and interest
- Preparation for future human missions to Mars
- Enhancing scientific knowledge and advocate technologic advances in general (outside of the Martian environment).

First, in conjunction with the work done on the general science tasks, the team wanted to choose a mission that would sate scientific curiosity by investigating questions that have up to this point been unapproachable.

Questions about the geologic and biologic history of Mars have heretofore been very difficult to answer because of the lack of diversity in the depths of sample measurements. Past missions took measurements and samples at a variety of locations on the planet—but all the data collected were from the Martian surface.

On Earth, when scientists want to investigate planetary history they take a core sample with deeper fragments corresponding to older materials. In essence, descending through sedimentary layers is like going back in time.

But creating a robot capable of taking samples more than a few meters below the planetary surface is still beyond the current available technology. The cliffhanger idea takes advantage of the natural surface features of Mars to explore the history of the planet without need of digging. So interesting and difficult questions can be answered not with the brute force of a drill, but with creative mission design.

The next criterion used to decide between possible mission objectives focused on the need for public involvement and interest. When the Mars Pathfinder mission touched down on July 4, 1997, for example, the associated web sites received an average of about 50 million hits a day during the first three days. The team wanted to choose a mission that would rekindle and sustain this kind of excitement—and the cliffhanger mission seemed the perfect vehicle for this.

The mission also needed to be part of an evolution towards a more extensive investigation of Mars. It is imperative to increase preparation for future missions—manned and unmanned. For this reason, the team decided upon the ***secondary mission objective of a long-term observatory.***

Planning for future missions will depend upon precise characterization of the Martian environment. Unfortunately, past attempts to provide this characterization have failed in their limited duration.

The long-term observatory will focus on furthering theories of Martian geology and climate, which are currently based on a limited amount of surface data. Characterizing the atmospheric turbulence at the surface of the planet and better understanding the size and nature of the dust particles present in the air will help evaluate current climate models which focus on the importance of dust in seasonal changes. These investigations could also lead to more accurate prediction and categorization of damaging Martian dust storms, which could potentially endanger a manned mission.

The final criterion the team considered centered upon the prospective missions' ability to enhance scientific knowledge and advocate technologic advances outside of the Martian environment. This interdisciplinary cooperation is an area often overlooked in mission planning which is assuming greater importance in these times of strict budgetary constraints.

The team believed that the primary cliffhanger mission would serve as an excellent catalyst to future development in a potentially exciting area of robotics design. Robots similar to the one used on Mars could be employed, for example, in the investigation of volcanoes and possible landslide and avalanche hazards. Since the robot will handle well in difficult terrain, it might be of interest to the military to obtain a tactical advantage in mountainous and urban areas. It will also serve as a relatively low-cost pioneer to chasms, valleys, craters and volcanoes on Mars and

other planetary environments before more sophisticated and specialized robotics can be created and utilized in space.

Several of the experiments placed on the lander will also provide useful insight into earthbound phenomena. The climate studies, for instance, will give meteorologists a look at the physics of weather and climate on a world that, in many ways, is different from our own. By comparing these variances, it will be possible to achieve a deeper understanding of how weather works here on earth.

Once the team settled upon the primary and secondary mission objectives, students returned to their design tasks with very specific goals in mind. Students were separated into three groups—lander, rover and cliffhanger—with representatives from the different design tasks divided evenly amongst the three new groups. In this way, the team was able to provide expertise in all areas.

3.4 Robotic Experiments

Because of relatively small financial support for the project, we were not able to build any advanced system or subsystem of the robot. Most of the work in the prototyping focused on building some simple model of the robot using wood, plastic, and paper and other creative materials. The importance of modeling, for the HEDS-UP team, was to determine usability, tolerances, and to visualize the developed concepts and ideas. Examples that demonstrated robotic scenarios of the mission are shown in Figure 4A and Figure 4B.

Figure 4B. Mockup of Rover and Cliffhanger on the cliff.

Also, some robotic experiments were performed using LEGO robotics. This includes experiments like command the robot to drive a certain distance, stop for a given amount of time, go in reverse, and spin, and building and controlling catapult that launched a ball. Another robot was also built that drove on two motors and had a rotating arm that was activated by the third motor.

A different team of students took a training lesson on how to use the tools available at the Penn State Learning Factory and how to use a rapid prototyping machine that layers paper upon paper to the design specifications. Each student from Modeling Team attained an access to the facility after completing a four-hour safety course. This safety course allows the certified student access to power tools and some machining equipment.

Figure 4B. Robotics Experiments

4. INVESTIGATION RESULTS

4.1 The Primary Mission

The primary mission is to explore and collect data and samples from the canyon walls of the Valles Marineris, and to do this all three robotic modules must work together. From the engineering system design point of view, all three units should be built using ***modular approach*** for easy modification, low cost and affordable upgrades. The digital electronics should be ***reprogrammable*** to enable software upgrades and remote corrections to potential problems during the mission. All three units should communicate with each other using modern ***spread-spectrum (low-power) digital communication*** technology with easy access by everyone to anyone resources during the mission.

The Lander

In order for this mission to be a success the lander must touch down within 1000 to 2000 m

of the edge of the cliff. This will be accomplished by using jet propulsion to control the landing. We are assuming that by the time the proposed ***robotic rope-climbing mission*** can be designed, the precision of landing on Mars will improve significantly compared with today's technology (Figure 1).

The Lander module will serve as the power source and communications base for the mission. It will be constantly connected via a wire cable to the cliffhanger and rover during the primary mission.

Rope Launch

The first step of the primary mission will be to launch a rope over the edge of the canyon. The rope must be deployed in a fashion that will allow at least two kilometers of rope to hang over the side of the cliff. This requires a ballistic, parabolic, path. Obtaining the correct path requires an equation that includes gravity, initial velocity, mass of object, angle or launch, and the distance to the cliff. The gravity of Mars is known, the mass of object is the end piece plus the integrated weight of the rope as it is pulled out, and the initial velocity and angle of launch will be derived from the equation when it is solved. The only part of the equation that will not be known is the distance to the cliff.

There are two ways to acquire the distance to the cliff. The first and most expensive would be to include a targeting and tracking system with the Lander, much like a military weapons system would have. An alternative would be to use a satellite photo with the Lander and cliff in the same image. The difficulty with the second choice is the current imaging systems, on satellites orbiting Mars, do not have a resolution high enough to image the Lander. Once the distance to the cliff is obtained the ballistic equation can be solved for the initial velocity and angle of launch.

Figure 5. Firing the rope.

The firing system will include a rope drum, containing 2-3km of 4mm rope wrapped around a center cylinder, for an almost frictionless release. Another 4-5km of rope will be wound around a flywheel wench. The center of the rope drum will contain the firing mechanism.

There are two ways to launch the rope. The first is to use a rocket with the rope attached. The rocket would be able to have programmable flight characteristics. Foreseeable difficulties with using a rocket are: using explosive fuels to propel the rocket and the flight will only be a few kilometers and the air pressure is $1/100^{th}$ of Earth's which could lead to flight control problems. The second way to launch the rope is to use pressurized gas. The gas would be kept in a tank and then released into a compression chamber to be pressurized for launching. Possible difficulties using pressurized gas are being able generate enough pressure to launch the weight and rope several kilometers, and the large force applied on the lander during the launch.

In order for the cliffhanger to be able to efficiently climb up and down the cliff using the rope the rope should be anchored to the cliff and to the lander. To anchor the weighted end we have thought to use a spike firing system, much like the piton guns used by mountain climbers. The pitons would initially be inside the weighted end, attached to a pressure pins. Once the weighted end touched down on the cliff face the pressure pin would be triggered, releasing the piton securing the launched end of the rope to the cliff.

Table 1. Rope Specifications for Different Ropes

Diameter	4mm	3mm	2mm
Length	7km	7km	7km
Mass	10kg	6kg	4kg
Breaking Strength	3.2kN	1.8kN	0.85kN

After the Lander fires the rope it deploys the rover with the cliffhanger to begin stage two of the primary mission.

The Rover

The Rover's primary mission is to deploy itself from the Lander via ramp system and transport the Cliffhanger to the edge of Valles Marineris (see Figure 2). The rover and cliffhanger will always be attached to the lander via a rope with a communication / power cable inside. This cable will be carried on the rover in a spool and be

laid down as it travels. This connection will ensure that the rover and cliffhanger have enough power to complete the mission. Additionally, long distance wireless communication requires a significant amount of power and is unreliable. A direct connection to the lander would eliminate these problems. Estimations for the mass of 4km of this cable are on the order of 6 to 10 kg, which is a reasonable size for the 50 kg rover.

Rover Navigation

Multiple methods of navigation will guide the Rover to the edge of the canyon. The rope launched by the Lander will ***have encoded marks*** along the rope for rover and cliffhanger to know its actual position on the line. Also the rope will have a ***transponder*** encased inside of the end weight. A transponder is activated for transmission by reception of a predetermined signal sent by the Rover. Periodically, the Rover will use this navigation method to determine the distance and direction it should travel. In conjunction with the transponder signals, a ***laser obstacle detection*** system is used to prevent collisions, enabling the Rover to navigate around rocks, cracks, and other obstacles. In addition, a ***camera*** will capture images to send back to the Lander and Earth. These images will update NASA scientists on the progress of the Rover's travels, as well as aid in navigation. This camera will also be used to locate the rope at the cliff edge. An ***odometer*** will use wheel rotations to calculate the approximate distance traveled. This information will also be used to control the winch that will unroll the Lander-Rover power line.

Future navigation methods on Mars may (and probably will) include the ***Global Position Satellite System.***

Using the camera images and human control, the rope will be located and made accessible to the Rover's mechanical arm. While the arm rotates from the front position to the rear position, the Rover will drive under the path of the rope, thus laying the rope directly over the Cliffhanger. As the arm rotates to the rear position, the axle clamps that previously locked the Cliffhanger in place are released. The Rover's camera and the Cliffhanger clamp sensors will assure that the rope is in place. Next, the Cliffhanger is activated and the drive wheels will roll it off the front ramp of the Rover. Once the Cliffhanger is at least one meter away from the Rover, the mechanical arm will rotate back to the front position and serve as a pivot point for the rope. The Rover-Cliffhanger power line winch motor will release a length of power line equal to the distance traveled by the Cliffhanger. Rotation in the drive wheels (before reaching the canyon edge) and rope tick mark counters or number shimmies (during the descent) will calculate the length of power line to release. As the Cliffhanger shimmies down the rope, the correct amount of power line is released from the winch.

The Cliffhanger

The Cliffhanger robot is an innovative style of robot that is designed to work in the vertical world. While past missions to Mars in the past have been very successful in exploring the surface of Mars, they were unable to go below the surface, where the history of the planet lies. Although it would be neither practical nor monetarily feasible to drill two kilometers into the surface of Mars to collect data, we are still left with another option. Just as scientists have been able to study the history of this planet by analyzing the walls of the Grand Canyon, the Valles Marineres on Mars opens up a window that allows scientists to peer into its history. Once on Mars, the Lander (which we are assuming will land within one or two kilometers of the cliff edge) will deploy a rope over the edge of the cliff. For this mission we are using climbing rope, made of nylon that is four millimeters in diameter. Climbing rope is ideal because of its extreme strength (such climbing rope can bear a force of more than 3 kN), durability, ability to withstand large amounts of friction, and light weight (approximately 9.8 g/m). Once this rope has been deployed, the Cliffhanger will "ride piggyback" on top of the Rover to the cliff. At this point the Rover will place the rope into the clamps of the Cliffhanger, where it will proceed to climb down the rope approximately two kilometers, collecting data at certain points.

Cliffhanger design

The Cliffhanger's design provides a maximum amount of protection and mobility, while at the same time ensuring that all of the experiments are easily accessible. The primary section of the Cliffhanger is an octagonal prism shaped chamber (see Figure 6), which houses the experiments. Each face of this chamber is 10 cm wide, with a length of 30 cm. This inner component is encased in an outer cylinder, which has a large opening facing the cliff face, allowing the equipment to have access to the wall. The cylinder will be 31 cm in diameter and 37 cm in length. This outer shell will have a window that will expose the cliff face measuring 20 cm in length, and 12 cm across. Two clamps stick out

from the ends constituting the Cliffhanger's system of grasping the rope. A key feature of the entire system is that it is 'C' shaped, in that it has a wedge cut out of it. Since the Cliffhanger does not start off attached to the rope, it must have a system for taking in the rope. As mentioned before, the Rover feeds the rope into the Cliffhanger. This is done by laying the rope into the opening of the Cliffhanger. Measures are taken to prevent the rope from falling out of the clamps (this will be discussed later).

Climbing Mechanism

The movement of the Cliffhanger up and down the rope is very difficult considering that it is hanging a large distance above the valley floor. As discussed earlier, there are two clamps located on the ends of the outer cylinder (the design of the clamps will be discussed later). The top clamp will be encased in a cylinder 10 cm long, and 6 cm in diameter. The bottom clamp consists of two components: a clamp and a pump. When compressed, this telescoping component is 20 cm in length, and 7cm in diameter. The ten centimeters nearest the body are dedicated for a hydraulic pump. The second ten centimeters will be the telescoping section containing the second clamp. The second clamp will slide in and out of the shell as it is either pushed or pulled by the pump. These three components allow for the climbing of the Cliffhanger robot. As the Cliffhanger descends, the top clamp will hold onto the rope when the robot is in the compressed position. The bottom clamp will release, suspending the weight of the entire robot by the top clamp. The pump will push the bottom clamp down, and the Cliffhanger will then be in its expanded position. Once in the expanded position, the bottom clamp will grasp the rope, and the top clamp will release the rope. Although the top clamp will not have a firm grip on the rope, it will not allow the robot to fall off of the rope. The pump will lower the main body down, and the Cliffhanger will return to its compressed position. When the Cliffhanger is ascending the rope, the process simply reverses itself as the pump hoists the robot up the rope.

The process outlined above works well assuming that the cliff face remains a sheer face for the entire two kilometers that the Cliffhanger will descend. However, should the cliff face jut out at any point, the Cliffhanger will need to overcome this obstacle. For this reason there will be a total of six wheels on the robot. There will be two main drive wheels, forty centimeters in diameter each located in the center. Four smaller, neutral wheels will be placed on the outer corners forming a base. These smaller wheels will not only provide a good base, but they will also help to guide the robot while it is driving. This system allows the Cliffhanger to be adaptable to both the vertical and the horizontal worlds.

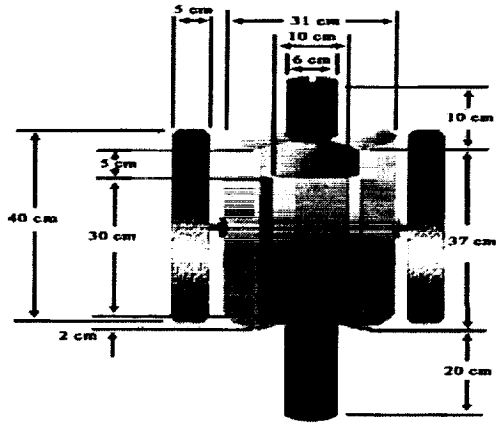

Figure 6. Cliffhanger diagram

Certainly the most crucial aspect of the Cliffhanger is the clamp. The clamps are completely responsible for ensuring the safety of the Cliffhanger. For this reason the clamps must be designed in a manner that will allow for minimal errors. The method that works best is one that requires only two quick surges of power; one to lock the clamp, and one to unlock it. The main challenge with a system is that it requires a constant stream of power to hold the clamp in either a locked or an unlocked position. The continuous, uninterrupted stream of power is required. This will not only cause increased power consumption, but will hold a greater chance for error. A loss of power, if even for only a mere fraction of a second, could result in the robot slipping off of the rope. The design of the clamps is actually a very simplistic one. They are cylinders with an opening for the rope to enter (see figure below for clamp design). The rope falls down the funnel-like opening into a semi-circle cradle, which is reinforced against the outer wall of the clamp so as to stabilize it in place. Across from the cradle is the face of the clamp.

Approximately seven millimeters across and three to four centimeters long, they consist of a flat metal face with tiny metal jags that stick into the rope and prevent slipping. A sliding door

covers the remaining opening, preventing the rope from escaping the grasp of the clamp.

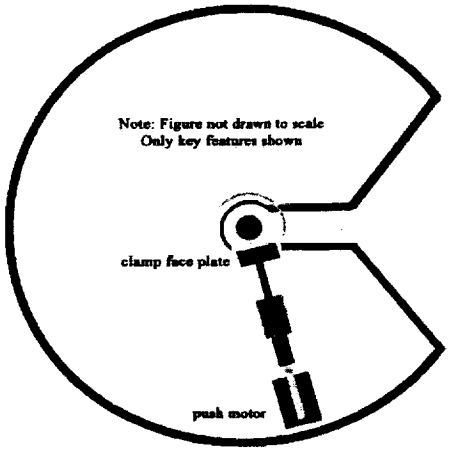

Figure 7. Cliffhanger rope catching mechanism.

The jagged metal plate that serves to grasp the rope must be pushed into and pulled away from the rope during the clamping process. For simplicity, the clamping face has only two positions to lock into, clamped (pressing the rope) and unclamped (releasing the rope). The locking process will model that used to retract the ink well on certain ball point pens. From the unclamped position, a force pushing the clamping face in will lock it in the clamped position when released. When pressure is reapplied in the exact same manner, the clamping face returns to the unclamped position when the force is removed.

There are two different types of mechanisms that perform such an action. The first type involves a geared turn cylinder with slots moving along a cylindrical grooved track, being pushed by a teethed cylinder. When it is pushed initially below the level of the grooves and released a spring forces it upward, causing the geared turn cylinder to turn with respect to the push-button and the outer track. Once the push button is pressed again, the spring causes the turn cylinder to turn once more, realigning its slots with the grooves on the track, allowing it to retract. A much simpler version of this locking system involves steel bearing on a heart shaped track. When the push button is pressed, the steal bearing is moved clockwise along that track into one of the two bulbous regions at the top of the heart shape. When the push button is released, a spring forces the ball into a recessed position in one of the two drop points of the heart. These points represent the clamped and unclamped positions, depending on the orientation of the heart shaped track. Either of these two methods allows the clamping process to be performed using minimal power, requiring only a push motor to quickly activate the clamping mechanism. Not only is this system more efficient, it is also safer, as the mechanical devices lock the clamp into place, preventing any slipping due to a power surge.

Once the rope has been placed in the opening of the Cliffhanger by the Rover, this opening must, for obvious reasons, be closed off. The solution to this is a rather simple one. Angled tracks will be placed on the cup, which holds the rope. In these tracks will be a curved piece of metal (represented by the gray bars in the figures above and below). When the Cliffhanger is on its "back", with the opening facing upward, the metal curves will fall back, leaving the full opening exposed. Once the robot is in a more upright position, gravity will pull the metal piece across the opening, thus blocking it. Placing these at certain intervals along the Cliffhanger will prevent the possibility of it losing the rope.

As outlined earlier, there are two separate shells. The outer shell has only one window that exposes the cliff face. The octagonal inner shell contains several experiments. For this reason the inner shell must be able to rotate with respect to the outer shell, allowing the different experiments to face the window. Also, there is the possibility that the entire Cliffhanger could twist away from the cliff face while climbing. Due to this possibility the outer shell must be able to rotate with respect to the clamps.

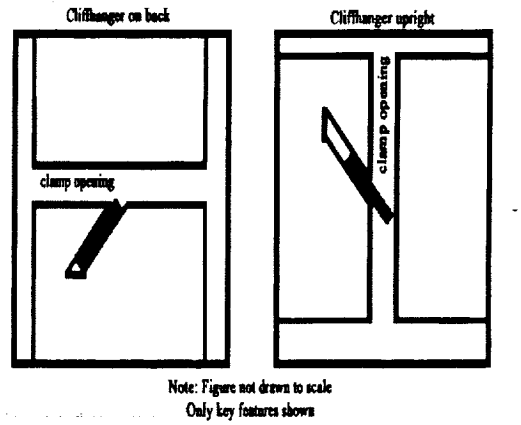

Figure 8. Cliffhanger rope trap mechanisms.

As shown in the figure 9, both shells were designed to be independent of each other, and have

the ability to rotate with respect to the clamps. 'C' shaped bearing tracks are then placed in three locations, between the clamps and the outer shell, between the clamps and the inner shell, and between the inner and outer shells.

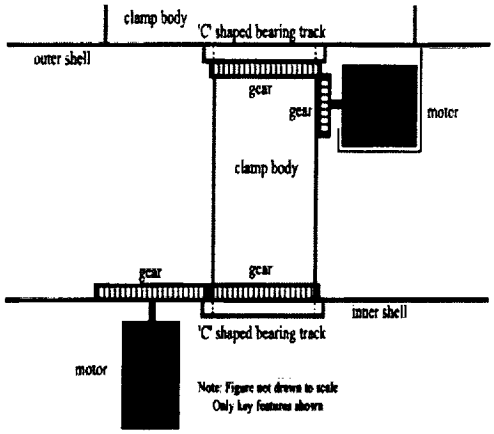

Figure 9 Cliffhanger gear mechanism.

Also, there are two different motors controlling separate gears. These gears will rotate the inner and outer shells with respect to the top clamp. Since the top clamp will remain stationary with respect to the rope, the inner and outer shells will turn with respect to the rope. These gears are illustrated in the figure 9.

Cliffhanger instruments

The Cliffhanger will only be involved in the primary mission. It has numerous experiments to perform as it scales down the canyon wall. A high-resolution, wide-angle camera will be built into one of the Cliffhanger's faces. This will be able to take detailed close-up pictures of the walls of Valles. The clamps will be able to move the Cliffhanger the same distance as the wide-angle lens' focus. The camera will release the shutter once every time the cliffhanger moves. This will enable us to compile a complete work-up of the wall.

Soil Samples and Ultrasonic Drill

An ultrasonic drill will be built into another side of the Cliffhanger. This drill will be able to bore a half-inch hole in the rock or soil on the wall. The hollow drill will also extract the sample. A vacuum chamber will suck the sample back into a small tube, where a filter will stop the sample (see Figure 10). Once the sample has been collected, the revolver will rotate, exposing a new tube. This method will enable the Cliffhanger to collect numerous samples which will be taken back to the Lander for analysis. The ultrasonic drill has only a minimal kickback, therefore precautions for anchoring the Cliffhanger to the cliff face before drilling are not necessary.

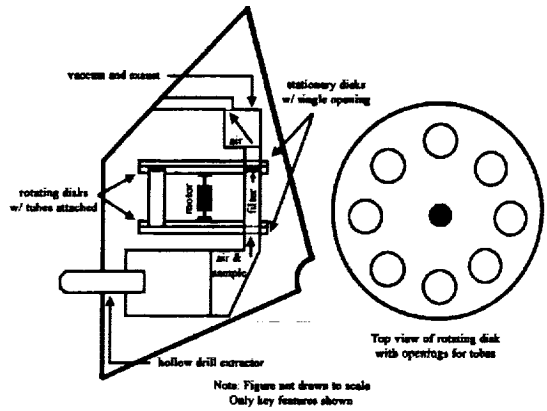

Figure 10. Cliffhanger ultrasonic drill and sample collector.

A third geological instrument may also be included. The Alpha Proton X-Ray Spectrometer, or APX. This instrument is able to determine the chemical make up of the surface. Every time the cliffhanger moves, the APX will look at the wall. A composite of the data gathered during the Cliffhanger's mission could help us to better understand the geological history of Mars.

Miscellaneous environmental experiments will also be built into the cliffhanger. These include pressure, temperature, and wind sensors. This will enable us to learn about the climatic conditions inside the canyon. It is possible that the canyon would be the most likely place to start a human settlement. The atmospheric pressure could be great enough at the bottom to grow plants. The environmental instruments will help us figure that out.

4.2 The Secondary Mission

The secondary mission is to have a repertoire of experiments that will be long lasting and continue to provide valuable Martian data over an extended period of time.

After the Mars Cliffhanger robotic team has performed their primary mission, the Lander will begin its secondary mission as a long-term observatory. We would like this secondary

mission to last in excess of a decade. The goal of this mission would be to provide extensive information about the Marian climate and weather patterns, to give insight into the frequent dust storms and how to best prepare for them, and to act as a set of eyes and ears on the Marian surface. Throughout the secondary mission, the Lander will continue to provide power for the Rover's secondary mission. The detailed analysis of data provided by the Lander's secondary mission, would allow future Mars missions to be well prepared for the hostile Martian environment.

The lander will also attempt to improve our overall model of the Martian climate and internal geologic structure with its measurements. The thin Martian atmosphere, for example, necessarily leads to large temperature gradients. Spatially, the sun's rays rapidly heat the surface of the planet without much direct effect on the temperature of the lower atmosphere. Temporarily, the heat stored in the ground during the day is rapidly dissipated at night. By measuring the differential heating of the planet and the surface wind turbulence over an extended period of time, meteorologists can get a better idea of the exact magnitude of these gradient—improving their understanding of the effects of this thin atmosphere. This improved modeling ability should lead to more accurate forecasts of what has heretofore been deemed the "unpredictable" Martian weather.

Lander Meteorological Instruments

Several meteorological instruments will be included on the Lander:

Temperature:

Two thermometers, separated by at least 0.75 vertical meters with the bottom sensor at about 0.1 meters elevation, will be used to record daily and seasonal temperature gradients. Taking temperature measurements during dust storms will be a useful aid in recording the temperature drop due to the obstruction of sunlight.

Pressure:

Barometers will be used to determine pressure readings—especially useful if it can be used to predict the commencement of dust storms. Also, Doppler radar could be deployed in predicting when and how dust storms accumulate, and how quickly they move across the landscape.

Wind speed:

An anemometer will be used to measure wind velocity and frequency, daily average wind speeds, and the speed during dust storms. Knowing how fast and when winds pick up (if there are similar daily occurrences) will inform future robotic missions when to retract or tilt solar panels to reduce dust accumulation.

The design of these ground-based weather sensors requires the proper mixture of sensitivity and durability. A mechanical anemometer, for example, would need to be impracticably large due to the reduced atmospheric density and would be far too sensitive to the shocks of lift-off and landing. One possible alternative is an active ultrasonic anemometer, which contains no moving parts but requires significant power (>30 [W]) and is somewhat expensive. The design that seems to offer the best durability with the lowest cost and power requirements is an anemometer which uses the small pressure changes around a vertically-orientated cylinder to estimate wind speed and direction. This design; [38] uses existing static flow sensor technology that could be adapted to the Martian environment with the inclusion of a larger diaphragm for pressure measurements, for example. With no moving parts and a low overhead requirement, this anemometer design seems the perfect fit for the mission.

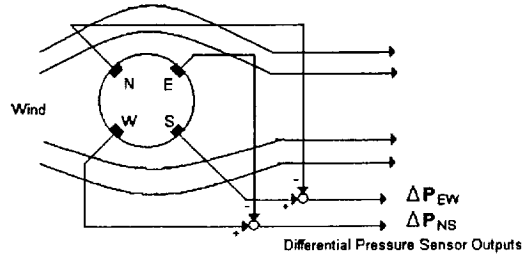

Figure 11. Differential Pressure Anemometer

The corresponding (see [38]) orthogonal components of the wind vector (voltage) are:

$$U_{NS} = \mathbf{sgn}(\Delta P_{NS}) * \mathbf{sqrt}(2\,|\,P_{NS}\,|/\rho)$$

$$U_{EW} = \mathbf{sgn}(\Delta P_{EW}) * \mathbf{sqrt}(2\,|\,P_{EW}\,|/\rho)$$

Other characteristics of the Martian environment will require the long-term study provided by this secondary mission.

Solar Radiation:

Measuring different aspects of sunlight could make solar power a more efficient source on Mars. Right now, the use of solar energy to power

a long-term mission on Mars remains problematic. By knowing precise solar measurements, solar power could be made more viable for necessarily lengthy future missions. By measuring the frequency, amount and the angle of incidence of direct sunlight, it will be possible to better characterize the sun's energy reaching the surface of the planet. Tracking and examining these data over the course of several years could lead to improved solar panel designs.

The direct study of sunlight on the surface of the planet, however, poses a problem—the sun's position varies both seasonally and daily. This variance can be overcome if mechanical mountings are used on the instrumentation required for observation, but these mountings must necessarily contain large numbers of sensitive moving parts. Another solution, which has a wide variety of possible applications, is to employ arrays of fiber-optic cables and optical switching networks. The cables are low cost and lightweight—so they can be oriented in any required direction. For the example of direct sunlight study, tracking the sun's position and choosing the correct input to spectroscopes or photometers can be as simple as determining which cable contains the highest light intensity.

Soil and deposit Layers Sample Analysis:

The samples returned from the canyon wall can also be tested with a minimum of sensitive moving parts using this technology. It may be possible to take measurements of several samples with the same instrument without moving the samples using this idea. Companies such as Ocean Optics have already proved the viability of miniature spectrometers using fiber optics. Advances in the still young field of optical switching methods will continue to improve the capability of this new technology for exploration. Another important instrument integrated with the above optical technology will be an ***optical multispectral imaging microscope***. The microscopic optical images of samples will be recorded and transmitted to Earth for more detailed analysis.

Dust:

Dust deposition also can lead to decreased solar panel efficiency over the course of a lengthy surface stay. By learning more about the Martian dust, future missions will also be better prepared to handle dust storms. Instruments will measure dust composition, electrical charge of dust particles, and dust deposition rate. This will gain insight into how these tiny particles affect the sensitive instruments of robots sent to survey Mars. Further study of the electrical properties of the dust can lead to the development of more effective electrostatic methods for removal.

But it is not merely the effect of dust upon solar panels that makes the characterization of dust particles scientifically interesting. Current Martian climate models emphasize the importance of dust in the planet's seasonal changes. The type and size of these dust particles, however, has yet to be investigated fully. A combination of lasers and optical sensors can take measurements of the number and size of the dust specks. Measuring backscattering, for example, can provide a mean particle size. This instrument would operate in much the same way as environmental protection sensors currently placed on industrial smokestacks.

Cosmic Radiation:

The Earth's atmosphere acts as a shield against many types of radiation that would be harmful to life and instrumentation. The less dense Martian atmosphere does not filter out many of these harmful rays. Robots and their components that work well on Earth are not protected on Mars from UV and cosmic rays. Instruments will be used to measure UV and cosmic ray indices, as well as the effects on components due to solar storms. Small samples of materials under consideration for use in future missions will be brought from Earth and will be exposed to the elements. These materials can include metals, silicon, circuit components, and solar panel material—anything of interest that may be used on future missions. At appropriate intervals, these materials will be examined by the microscopes and spectrometers within the Lander for corrosion, durability, permeability to dust and cosmic radiation, and robustness. By examining these materials over a long-term mission, the materials best suited for future missions can be used. A similar experiment may be conducted with a small quilt of different types of solar panels. They too can be examined to see which materials hold up best to the Martian environment, dust repulsion, as well as the best power generation and efficiency.

Sound and Infra-sound:

The rover will also play a large part in this secondary mission by deploying a large infrasound microphone—a microbarograph. The microphone requires noise-reduction hoses extending ~100 [m] in multiple directions that will be arranged by the rover. This instrument will collect data from the detonation of small charges placed a safe distance from the lander. The data recorded will give a

better understanding of the subsurface composition of the planet. It will provide the detection method of micrometeorites collision with the Martian surface, their intensity and statistical data. This may be a very important factor for designing future human habitats on Mars. But these data will not only be of use in increasing our understanding of Mars. Measurements in another environment much different from our own will challenge the current understanding of the mechanics of wave propagation. These propagation theories are used today in many areas from seismology to troop detection to counter proliferation efforts.

Mars Internet:

The Lander will also contain a multimedia center. This will include CCD cameras for both telescopic and panoramic views. Microphones will provide an audio component to record Martian sounds—the large infrasound array will also serve to help calibrate these microphones. Live video and audio feeds can be relayed back to Earth and will be made available for the general public. The purpose of this equipment serves three functions. First, the Lander can serve as a **"pair of eyes"** to monitor and control the Rover during its primary and secondary missions. It will aid in navigation along the Martian terrain and will help guide the Rover to the correct position in dropping off samples collected by the Cliffhanger. Second, it will nicely complement the meteorological instruments aboard the Lander in monitoring the environment and landscape. Seeing the dust storms in action will enhance the non-visual data collected. Finally, but still importantly, the cameras and microphones will serve to spark interest and maintain confidence in the public. As important as scientific data and discoveries found on Mars may be to all of humanity, the general public does not always see it this way. ***By allowing anyone to go on to the internet and view Martian landscapes, watch a dust storm, see weather maps complete with highs and lows and upcoming dust storms; people will know their tax dollars are going somewhere.*** Even with the space program's high success rate, the recent failed Mars missions have made people wonder why we spend billions on sending a robot to Mars. By setting up cameras on the Lander, and allowing "real-time" access to Mars, we can answer those questions, increase awareness, and increase funding for future missions.

Rover Secondary Mission:

The rover will play a large role in the secondary mission. Using power generated either by its own solar panels or batteries recharged through a docking bay in the lander, it will have its own array of scientific instruments.

Wind, Weather and Acoustic Experiments:

The rover's meteorological and acoustic payload will supplement the data collected by the lander. Mobile wind, temperature and pressure measuring devices will provide a second data point at each sample instant. Perhaps more importantly, however, the rover will carry a small whistle, which it will use in simple acoustics experiments involving the lander. Measurements of sound propagation at specific frequencies over known distances are very useful in determining wind turbulence and temperature differentials. The detailed studies of high frequency sound propagation in the terrestrial environment combined with the measurements taken in these simple experiments will provide a far more accurate characterization of the lower Martian atmosphere than has heretofore been possible.

Seismic Experiment:

Another possible and important function of the rover during long-term observation of Mars would be to help perform some geological seismic experiments. The rover will deploy seismic sensors in predetermined and recorded positions around the landing site. It will then position a detonation charge with the remotely controlled mechanism. The Lander will trigger the detonation, and the travelling waves will be recorded by lander instruments as well as by distributed seismic sensors. Data than can be collected by Rover and transferred to Lander for delivery to Earth's scientists for analysis. The seismic experiment analysis results can provide a valuable information about the structure of the Martian subsurface layers.

Though the long-term observatory has been deemed the "secondary" objective, its objectives are every bit as important to furthering the scientific understanding of Mars and paving the way for further exploration. In fact, even a complete failure of the primary objective would not render the entire mission useless, as would happen with so many other missions.

4.3 Power Requirements

It is estimated that total power required for the mission will be in excess of 1 kW for primary and secondary mission. The danger of frequent dust storms on Mars that can lasts for

months and preventing the sun illumination reaching the solar panels, as well as deterioration of solar panels due to dust depositions, will require a backup power system to be present. For this purpose we propose to use a Radioisotope Thermoelectric Generators (RTGs) in the mission - see below.

Power Production

Any electronics package launched from Earth must be equipped with its own power supply. The primary source for power supplies in near earth vicinity is the sun. In order to harness the sun's energy solar panels must be used. Solar panels are only as efficient as the amount of direct sunlight they receive and the conversion efficiency of the panel material. The amount of power provided by the sun can be derived from the Stefan-Boltzmann law:

$$F = (4\pi R_s^2)\sigma T^4$$

where σ is the Stefan-Boltzmann constant equal to $5.67*10^{26}$ $Wm^{-2}K^{-4}$ and R_s is the radius of the sun. Which then leads to intensity I at distance R from sun.

$$I = F/(4\pi R^2)$$

It can be calculated that in near Earth vicinity solar panels will receive $1400Wm^2$, but as can be seen in equation (2) the sun's intensity falls off by an inverse square relationship. This means that as solar panel travels outward from earth and away from the sun it's available power will decrease by at least R^{-2}.

Our planned mission is for a long-term observation post on Mars' surface. According to equation (2) Mars receives $595Wm^{-2}$ of energy from the sun, which is approximately 43% of the intensity that is received at Earth. By using the intensity at Earth and Mars, X being the solar panel size in m^2, one can see that a solar panel would have to be $2.35m^2$ on Mars to produce the same amount of power a $1m^2$ panel would in near Earth vicinity. This means that a solar panel has to be 235% larger on Mars. Once you apply the up to 18% efficiency of a solar panel, you find that it would take a panel of approximately $9.4m^2$ to provide 1kW of power, even during the periods of maximum solar intensity.

$$596Wm^{-2} * X = 1400Wm^{-2}$$

In addition to the lowered available intensity and efficiency of current panels, solar panels can only produce energy when the sun is within line of sight, meaning that batteries must be included to provide power when it is dark. As the distance from the sun increases during winter season on Mars, the second power supply must be used to produce power alternative to the solar panels, especially since our mission is expected to last a decade or more in unknown and unpredictable conditions.

Radioisotope Thermoelectric Generators:

Since as early as 1961 NASA has used Radioisotope Thermoelectric Generators (RTGs) to power satellites. They have been successfully been used on 25 missions, including two to Mars, seven to the Moon, and ten around Earth. Pioneer 10 / 11 and Voyager 1 / 2 contain RTGs that are still operating, after 28 years in one case.

RTGs have no moving parts and produce heat, which is converted to electrical power. The heat is a byproduct Pu^{238} alpha decay. As the plutonium decays alpha particles will be ejected, and the RTG uses the alpha particles to heat a piece a metal. The heated metal is attached to another metal that is kept at a lower temperature, in most cases the ambient of space. A current is induced between the two metals through the Seebeck Effect.

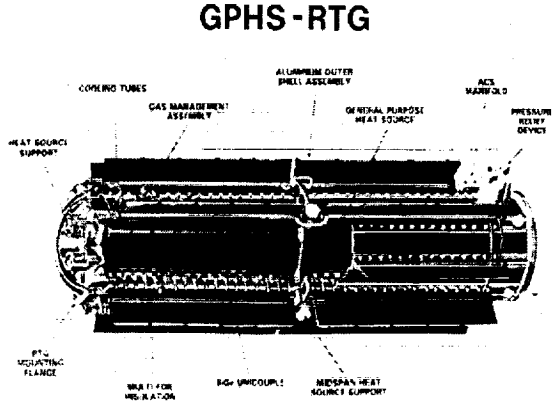

Figure 12. Radioisotope Thermoelectric Generators

RTGs use 11 kilograms of plutonium dioxide, which means that 30% of the total mass of the fuel, 3.3kg, is actually oxygen. The system is divided into 18 modules each of which contain 4

plutonium pellets. The plutonium is refined to a ceramic state that is fracture resistant. Other safety measures included are a graphite foam shell for heat resistance and iridium cladding on each pellet. The cladding is used to keep the plutonium encapsulated after an impact. The safety features designed for RTGs have worked on two occasions already.

Power provided by an RGT is available for 87.7 year, do to the half-life of Pu^{238}, with approximately 96% of the initial power at year 5. The conversion ratio for power from plutonium is 1W from .0027kg of Pu^{238}. Previous missions containing RTGs:

Table 2. Examples of existing RTGs

Satellite	# of RTGs	Weight	Initial Power	Power after X yrs
Ulysses	1	56kg	283W	223W after 9yrs
Cassini	3	168kg	850W	628W after 11yrs

RTGs are a viable energy source for sustained missions at distances from the sun greater than Earth's. They are built with multiple safety features, to insure plutonium containment should a launch or Earth flyby fail. They contain no moving parts, which reduces the possibility of a mechanical failure, such as unfurling a solar panel. RTG efficiency decreases, 4% over 5 years from decay, over time far slower than a solar panel's does from dust accumulation, 1% over 3-4 days. The only negative factor of the RTG is its mass, 56kg, but this can but rectified by replacing other redundant systems.

4.4 Site Selection

Some students of our team were assigned the task of choosing a suitable landing site for the mission. This group searched for landing sites adjacent to the large canyon systems that would best facilitate successful completion of the primary mission objective. The site, therefore, must be relatively clear of large boulders and other obstacles that could interfere with the rover's ability to transport the cliffhanger robot to the canyon edge. This clearing also needed to be large enough to overcome the lack of precision in landing.

Perhaps the most important requirement for the mission, however, is the slope of the canyon. The cliffhanger robot was designed for

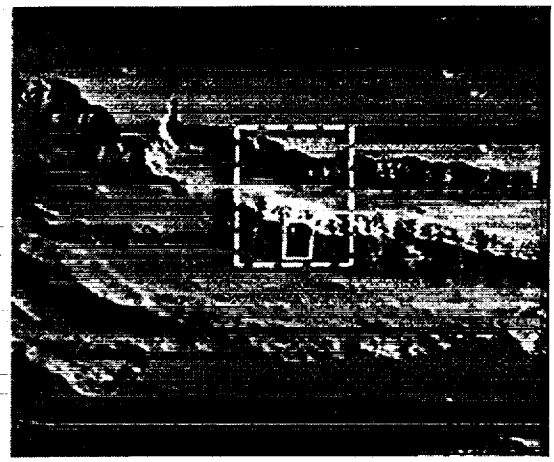

Figure 13. Sedimentary layers in Coprates Chasma

use on steep slopes (it is most effective on slopes ranging from 70-85 degrees) so a site with the sheerest cliffs would greatly facilitate the successful completion of the primary mission objective. The site also needed to be as close to the equator as possible to mitigate the effects of Martian seasons on the power provided by the solar panels.

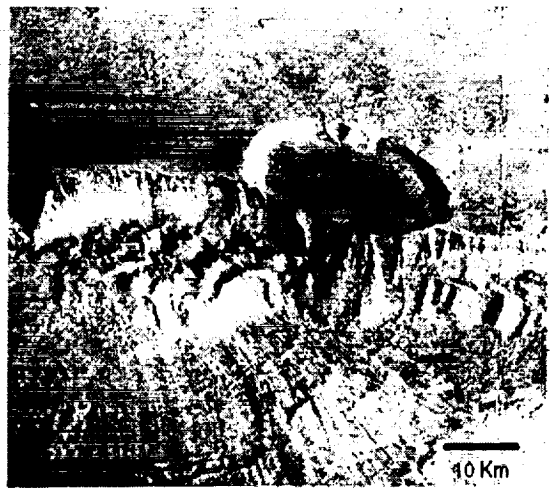

Figure 14. Gangis Chasma

Due to the many constraints and necessities presented by the proposed mission, the team's first selection of the possible landing sites is along the Coprates Chasma. This canyon system is

also located in the eastern region of Valles Marineris—along 7° and 17° south and between 69° and 52° west. The site located at Coprates Chasma has a much larger area for landing. The image shown in Figure 13 is a section of the canyon taken by the Mars Orbital Camera, the region width is approximately 100 km. As can be seen, the region surrounding the cliff edges is relatively smooth and the canyon walls are greatly sloped, allowing a good descent path for the Cliffhanger. The area around Coprates Chasma is void of excessive impact crater regions, allowing for smooth landing regions and traversing paths. The only requirement for landing in this region is to be within 1-2 kilometers of the canyon edge, allowing landing along any point of the canyon. Upon closer inspection of the region in the small white box in the above picture of Coprates Chasma, the layered regions are very distinct.

Table 3. Site Selection Examples

Canyon	Slop	Advantages	Disadvantages
Ophir	TBD	Smooth landing site	Not much data
Coprates	75 - 85	arge landing rea. Has a teep sloped anyon wall.	Not much data on smoothness of landing area,
Gangis	First 400 m up to 60, landslides near bottom of canyon where slope is minimal	rater bed is ood site for ander xperiments. rovides mooth, flat ath from ander to liffhanger ite.	Small area for landing (crater only 27 km wide) which may make precise landing very difficult
Candor	TBD	TBD	Not much data

These regions of layers are the primary mission of the Cliffhanger to inspect and remove samples, pictures, and other experiments from the canyon edges.

A second example of possible landing site is the large crater located on the boundary of Aurorae Planum and the southern rim of Gangis Chasma (approximately 48 degrees West and 8 degrees South) shown in Figure 13. This area is located near the eastern region of Valles Marineris.

6. CONCLUSIONS, RECOMMENDATIONS

FUTURE STUDIES AND LESSONS LEARNED

The ideas presented in this report are, of course, only preliminary investigations into the areas of rope-climbing robots and long-term observatories on Mars. Successful and cost effective completion of either mission objective will require much research into each of the design thoughts given by the team, no matter how basic or complex they may seem. It will also be necessary to make final decisions in the areas of experiment selection and redundancy versus cost.

Rope-Climbing Robotics

One of the most important areas for further study lies in the area of rope-climbing robotics. Many of the designs presented in this report have not been given more than the most rudimentary practical investigation. It will be vital to conduct extensive testing of these designs in a terrestrial setting to see, for example, how the cliffhanger will perform when exposed to various canyon wall angles and surface features. The robot has been designed to have the capability for locomotion at any angle (including somewhat uphill slopes) but maximum effective motion will be achieved at descent angles from 70-85 degrees. Further testing could suggest ways to make the robot more mobile on flat surfaces without sacrificing its descending capabilities. The usefulness of these robotics tests would extend far beyond the canyon walls of Mars. As stated earlier, many terrestrial applications exist for climbing robots—these uses will facilitate finding support and funding for such tests.

Site Selection

The results of these tests would also assist in another key area for successful primary mission completion. By characterizing the exact strengths and weaknesses of the final cliffhanger design, it will be possible to make a more effective site selection. Detailed, high-resolution images and reliefs of possible landing sites will be necessary in choosing the site that is most clear of debris with the most consistent angle of descent down the canyon wall. The suggestions put forward by this report are dependent on relatively low-resolution images without relevant MOLA data.

Power for the Mission

There is also a need for further investigation into the area of power production. While solar panels and batteries are capable of providing the power necessary for the mission, the team feels it is necessary to add a "safe mode" of operation to the lander and rover for the secondary mission. In this mode, the rover will return to the bay in which it was transported to the planet and the lander will retract all unnecessary instrumentation. It will also be necessary to retract the solar panels and survive solely on stored battery power. In long-term emergencies, such as lengthy dust storms, which can blanket an area for months, this situation would be far from ideal. So the team proposes adding an additional power source capable of at least keeping the base warm enough to prevent equipment damage. Several power options are available for this, including combusting reactive metals such as lithium for both heat and power and a nuclear power source such as the RTG's employed by NASA in the past. The nuclear engine would seem to be the best choice based strictly on performance criteria, but investigation into public policy and ecological concerns will be necessary before such a choice can be implemented.

Instrumentation for the Mission

Finally, it will be extremely important for scientists to carefully review all that is known or suspected of the evolutionary history of the planet. It will be possible to include instruments specifically designed to test theories and models of Martian history as well as instruments to make more general measurements. The cliffhanger was created as a modular design, allowing a variety of experiments to be performed while the robot descends the canyon walls. And, because samples will be returned to the landing site, far more in-depth studies will be possible through instruments contained in the lander.

These and other design and safety factors must be taken into account before the designs for the mission can be finalized. There were, of course, lessons to be learned from past successful and failed planetary missions but the adventurous nature of this particular mission will require research in entirely new directions. But the magnitude of the questions answered by this mold-breaking mission combined with its effect on the design of future manned missions and use in terrestrial applications will ensure that this research is not completed in vein.

7. OUTREACH

The following university and public activities were executed during the project to raise the academic and public awareness of the importance of space exploration and Mars missions:

December 3 , 1999, Penn State Mars Polar Lander Event and Mars Society MarsFest. Presentation and website development during worldwide celebration of space exploration on the occasion of America's return to Mars on the Mars Polar Lander mission. Events was held around the world by Mars Society chapters and other participating organizations for public outreach and to promote understanding Mars and Space Exploration.

April 7-8, 2000

HEDS-UP presentation at regional student conference for the American Institute of Aeronautics and Astronautics on April 7-8 at Penn State. http://navier.aero.psu.edu/~aiaa/conf/

April 8, 2000

HEDS-UP presentation booth. Space Day event at Penn State organized by the PA Space Grant Consortium (PSGC) for all Penn State groups who are involved in space-related research and education to exhibit information about their programs at this public event. Saturday, April 8, 2000, from ~11:00am to 2:00pm in the Alumni Hall of the HUB/Robeson Center.

April 26, 2000

HEDS-UP presentation at Penn State forum to discuss the formation of Space Colonization Institute at Penn State.

April 29, 2000:

HEDS-UP MARS ROBOTICS event at Penn State. Time and place: Saturday, April 29, 2000 from 10:30 a.m. to 1:00 p.m. in the 108 Wartik Lab. During the event, students outlined future robotic Mars missions to help the Human Exploration and Development of Mars.

August 10-13, 2000

Presentation is being planned at the International MARS SOCIETY Convention. The Third International Mars Society Convention, August 10-13, 2000 at Ryerson Polytechnic University, Toronto, Canada.

Mars Society and Mars Interest Groups: The basic concepts approached during the project were consulted and discussed with PSU Mars Society members and other departments like Astronomy, Aerospace, Mechanical, and Electrical. A lot of other ideas, not mentioned in this report, were discussed with these groups.

World Wide Web: The www web page; http://www.engr.psu.edu/ee/pub/ee497d/ was maintained on a daily basis throughout the project to raise the academic and public awareness of the importance of space exploration and Mars missions. All the major research topics of the project were highlighted and discussed. The web site is linked to all Mars and Space Exploration interest groups like for example NASA sites, Mars Society http://www.marssociety.com group, Mars Missions web page http://marsweb.jpl.nasa.gov, Mars Exploration; http://cmex-www.arc.nasa.gov, and others.

Publications:

All reports submitted by Penn State HEDS-UP team members are published on our Web Site as mentioned in the next paragraph. All report contain much more references covering the science of Mars and robotics.

8. REFERENCES

Student Papers published at Penn State HEDS-UP Website

http://www.engr.psu.edu/ee/pub/ee497d/

[1] Michael Schrader, "Mars in the Universe"
[2] Kevin F. Sloan, "Water On Mars"
[3] Carlos A. Mosquera, "The Atmosphere of Mars"
[4] Shubh Krishna and Jean Hsu, "Seasons on Mars"
[5] Joseph Yagloski Jr. and Christian Feisel, " Mars Geology and Volcanic Activity"
[6] Chris Carlins, "Mars Interior"
[7] Brian Sosnowchik and Nikki Thornton, "The Biology of Mars"
[8] Ben Weber, "Facts on the Polar Regions of Mars"
[9] Alysha Holmes and Mike Jordan, "Mars Future - Terraforming"
[10] Michael Graham, "Mars Interest Groups and Outreach"
[11] Joe Fledderman, "The Surface of Mars"
[12] Gregg O'Marr, "The Surface of Mars"
[13] Taite Merriman, "Mars Maps"
[14] Gregg O'Marr, "Locomotion: Legs and Artificial Muscle"
[15] Ben Weber, "Robotic Locomotion"
[16] Brian Sosnowchik and Jean Hsu, "Actuation Devices"
[17] Joe Fledderman and Chris Carlins, "Viable Uses for Sensors on a Future Mars Mission"
[18] Kevin Sloan, Michael Schrader, Shubh Krishna, "Navigation on Mars"
[19] David Borowski, Mike Jordan, Ben Webber, "Resource Production on Mars", to be published.
[20] Joseph Yagloski, Chad Laufer, Christian Feisel, Joe Fledderman, Ben Webber, "Robotic Experiments", to be published
[21] Mike Graham, Nikki Thorton, Taite Merriman, "Science Experiments on Mars"
[22] Christian Feisel, Chad Lauffer, Joseph Yagloski Jr., "Building Robot Model"
[23] Mike Jordan, Mike Graham, Mike Schrader, Taite Merriman, "Lander Mission and Long Term Observatory on Mars", TBP
[24] Shubh Krishna, Joe Yagloski, Nikki Thornton, Chris Feisel, Jean Hsu, Ben Webber, "Rover Design and Finctions in Penn State HEDS-UP Mars Mission", TBP
[25] Chris Carlins, Greg O'Murr, Brian Sosnowchik, Kevin Sloan, Joe Fledderman, Dave Borowski, "Cliffhanger Design"

Other Relevant Publications:

[26] NASA, "Exploring Mars Forum", second HEDS-UP Forun held at Lunar and Planetary Institute, Houston, TX, May 6-7, 1999, http://cass.jsc.nasa.gov/lpi/HEDS-UP/forum99.html
[27] Mars Pathfinder NASA Website, March 1997, http://mars.jpl.nasa.gov/MPF/mpf/ . Includes: MicroRover Characteristics, Mars Pathfinder Fact Sheet, Mars Pathfinder Instrument Descriptions, Microrover Flight Experiment Control and Navigation Subsystem, Mars Pathfinder Mission Science and Instruments, Mars Pathfinder Science Objectives, Mars Pathfinder Mission Rover Sojourner, Mars Pathfinder Mission Landing Site.
[28] Arden Albee, Steven Battel, Richard Brace, at al, "Report on the Loss of the Mars Polar Lander and Deep Space 2 Missions", 22 March 2000, Jet Propulsion Laboratory, California Institute of technology.
[29] NASA, "OuterPlanets Program" and "Europa Orbiter Mission Project Description", April 1999, http://outerplanets.LaRC.NASA.gov/

[30] M.B.Duke, editor, "Mars Surface Mission Workshop", Lunar and Planetary Institute, Houston, TX, October 4-5, 1997
[31] V.C. Gulick, "Mars 2005 Sample Return Workshop" at NASA Ames research Center, Lunar and Planetary Institute Technical Report Number 97-01, March 25-27, 1996
[32] NASA, "Mars Polar Lander / Deep Space 2", Press Kit, December 1999
[33] Lunar and Planetary Institute, workshop on new views of the Moon, "Integrated Remotely Sensed, Geophysical, and Sample Datasets", September 18-20, 1998
[34] Thomas J. Allred, "Medical Considerations in the Colonization of Mars", FACEP FCAP Unitah Basin Medical Center, Roosevelt, UT, January 2000.
[35] Arthur G. Stephenson, at al., "Mars Climate Orbiter Mishap Investigation Borad Phase I Report", November 10, 1999
[36] William J. O'Neil, Manager, "Mars Sample Return Mission 2003 Lander Additional Payload (AP)", Mars Surveyor program, Proposal Information Package, NASA, Jet Propulsion Laboratory, California Institute of technology, June 3, 1999.
[37] Paul O. Wieland, "Designing for Human Presence in Space: An Introduction to Environmental Control and Life Support Systems", George C. Marshall Space Flight Center, Alabama, NASA Reference Publication 1324, 1994.
[38] David C. Swanson, "Performance Model Incorporating Weather-Related Constrains for Fields of Unattended Ground sensors", The Applied research Laboratory, Penn State University, Technical Report.

Moon-based Advanced Reusable Transportation Architecture The *MARTA* Project

Georgia Institute of Technology
Graduate Program

Contributors:

Roger Alexander, Ryan Bechtel, Ted Chen, Tim Cormier, Sachin Kalaver, Mehmet Kirtas, Jung-Ho Lewe, Leland Marcus, Dave Marshall, Matt Medlin, James McIntire, Doug Nelson, Diego Remolina, Andy Scott, John Weglian

Faculty Advisor:
Dr. John R. Olds
Assistant Professor, School of Aerospace Engineering
Director, Space Systems Design Laboratory
Georgia Institute of Technology

ABSTRACT

The Moon-based Advanced Reusable Transportation Architecture (MARTA) Project conducted an in-depth investigation of possible Low Earth Orbit (LEO) to lunar surface transportation systems capable of sending both astronauts and large masses of cargo to the Moon and back. This investigation was conducted from the perspective of a private company operating the transportation system for a profit. The goal of this company was to provide an Internal Rate of Return (IRR) of 25% to its shareholders.

The technical aspect of the study began with a wide open design space that included nuclear rockets and tether systems as possible propulsion systems. Based on technical, political, and business considerations, the architecture was quickly narrowed down to a traditional chemical rocket using liquid oxygen and liquid hydrogen. However, three additional technologies were identified for further investigation: aerobraking, in-situ resource utilization (ISRU), and a mass driver on the lunar surface.

These three technologies were identified because they reduce the mass of propellant used. Operational costs are the largest expense with propellant cost the largest contributor. ISRU, the production of materials using resources on the Moon, was considered because an Earth to Orbit (ETO) launch cost of $1600 per kilogram made taking propellant from the Earth's surface an expensive proposition. The use of an aerobrake to circularize the orbit of a vehicle coming from the Moon towards Earth eliminated 3,100 meters per second of velocity change (Delta V), eliminating almost 30% of the 11,200 m/s required for one complete round trip. The use of a mass driver on the lunar surface, in conjunction with an ISRU production facility, would reduce the amount of propellant required by eliminating using propellant to take additional propellant from the lunar surface to Low Lunar Orbit (LLO). However, developing and operating such a system required further study to identify if it was cost effective.

The vehicle was modeled using the Simulated Probabilistic Parametric Lunar Architecture Tool (SPPLAT), which incorporated the disciplines of Weights and Sizing, Trajectories, and Cost. This tool used ISRU propellant cost, Technology Reduction Factor (a dry weight reduction due to improved technology), and vehicle engine specific impulse as inputs. Outputs were vehicle dry weight, total propellant used per trip, and cost to charge the customer in order to guarantee an IRR of 25%. SPPLAT also incorporated cost estimation error, weight estimation error, market growth, and ETO launch cost as uncertainty variables. Employing SPPLAT over a range of inputs produced the following results.

Based on the stipulation that the venture be profitable, the price to charge the customer was highly dependent on ISRU propellant cost and relatively insensitive to the other inputs. The best estimate of ISRU cost is $1000/kg, and results in a price to charge the customer of $2600/kg of payload. If ISRU cost can be reduced to $160/kg, the price to the customer is reduced to just $800/kg of payload. Additionally, the mass driver was only cost effective at an ISRU propellant cost greater than $250/kg, although it reduced total propellant used by 35%.

In conclusion, this mission is achievable with current technology, but is only profitable with greater research into the enabling technology of ISRU propellant production.

Acronyms

AHP	Analytic Hierarchy Process	MARTA	Moon-based Advanced Reusable Transportation Architecture
CER	Cost Estimating Relationship		
DDT&E	Design, Development, Testing, and Evaluation	NAFCOM96	1996 NASA Air Force Cost Model
EBIT	Earnings Before Interest and Taxes	NPV	Net Present Value
ELM	Earth Launch Mass	RFP	Request For Proposals
EOI	Earth Orbit Insertion	RSE	Response Surface Equation
ERO	Elliptical Refueling Orbit	RSM	Response Surface Methodology
ETO	Earth To Orbit		
GEO	Geostationary Orbit	SPPLAT	Simulated Probabilistic Parametric Lunar Architecture Tool
IRR	Internal Rate of Return		
ISRU	In-situ Resource Utilization		
LEO	Low Earth Orbit	TEI	Trans-Earth Injection
LLO	Low Lunar Orbit	TFU	Theoretical First Unit cost
LLTV	Lunar Lander and Transfer Vehicle	TLI	Translunar Injection
		TRF	Technology Reduction Factor
LTV	Lunar Transfer Vehicle	WBS	Weight Breakdown Statement
		WAF	Weight Adjustment Factor

1. Introduction

More than thirty years after Neil Armstrong first walked on the Moon, the scientific community is experiencing a renewed interest in Earth's only natural satellite. The recent Clementine and Lunar Prospector missions have revealed that there is still much more to discover about the Moon. These discoveries have led small companies like Orbital Technologies to complete studies in attempts to verify that ice exists at each of the Moon's two polar regions. At the same time, groups like Artemis Society International are advocating the establishment of privately financed permanent human colonies on the Moon for the sole purpose of making a profit.

While seemingly unrelated at first glance, each of these lunar missions has a single unifying feature. They all are dependent on the construction and operation of a commercially viable Earth-Moon transportation system. Considering the declining budgets approved each year for the National Aeronautics and Space Administration (NASA), the government will not be able to fund a transportation system of the type that is needed. Instead the financial backing for the program must come from private industry. Since the driving force behind any private industry venture is profit, there must be a level of return on the investment commensurate with the risk involved in developing such a transportation system.

The need for an Earth-Moon transportation system combined with the financial requirement that the system be profitable was the impetus for designing a Moon-based Advanced Reusable Transportation Architecture (The MARTA Project). The goals of the project were to design a transportation system capable of moving astronauts and large amounts of cargo between a space station in Low Earth Orbit (LEO) and the lunar surface.

The main mission requirements envisioned for this study are as follows:

1) 10 flights/year of 20 MT cargo
2) 5 flights/year of 40 MT cargo
3) 3 flights/year of 60 MT cargo
4) 4 manned flights/year of 5 astronauts
5) Half of all cargo and astronauts are delivered to a polar base and the other half to an equatorial base
6) Cargo must be delivered to the Moon within 4 weeks of launch from the Earth
7) Manned missions must not take longer than 5 days in transit

Additional requirements for the project include that all of the astronauts taken to the Moon must be returned to LEO, while the return cargo load is half the size of the outbound cargo load. Annual market growth is expected to be 5%, but could range from 0% to 15%. NASA would contribute 50% of the money required for Design, Development, Testing, and Evaluation (DDT&E) of the system and would be a guaranteed customer for seventeen years after 2018, the initial year of operation. A final requirement for the design to be successful was that a private company

that undertakes the development of the system would be able to make a 25% rate of return on their initial investment over the life of the project.

2. Problem Approach

The MARTA team took a novel approach to the design process. In an attempt to provide oversight and reduce mistakes, the whole team was divided into two smaller teams, the Design Team and the Review Team. The Design Team went through the steps outlined in the sections that follow and periodically provided the Review Team with data. The Review Team then performed their own completely independent analysis to verify or refute the results generated by the Design Team. If the two results differed, the Review Team would offer suggestions and generate "what if" scenarios to insure that the Design Team considered all of the possibilities.

2.1 Earth to Moon Transportation Architecture Selection Process

To minimize the possibility of overlooking a potential solution, the Design Team entered the process without preconceived notions regarding the final architecture. As such, it was difficult to narrow down an essentially infinite design space to a single architecture. The only insight the design team had into the problem before the brainstorming session was that the propellant usage of the system needed to be minimized if the operation was expected to be profitable. This fact came from a preliminary economic analysis that indicated the largest overall costs associated with the Earth-Moon transportation system were operations costs. For an in-space system like this one, operations cost translates almost directly into propellant cost (See Section 2.2 for more details). Thus, going into the brainstorming session, the team knew that reducing the propellant usage was a necessity. After brainstorming, the following four architectures were identified as most promising: a momentum-transfer tether system, a nuclear thermal rocket system, an electric propulsion system, and a chemical liquid rocket engine combined with an in-situ resource utilization (ISRU) program to provide propellant. Representative images of each of these systems appear below as Figure 1. The figure shows (from left to right) a satellite accelerating via a momentum-transfer tether, a nuclear thermal rocket engine, an electric rocket engine, and a chemical liquid rocket engine.

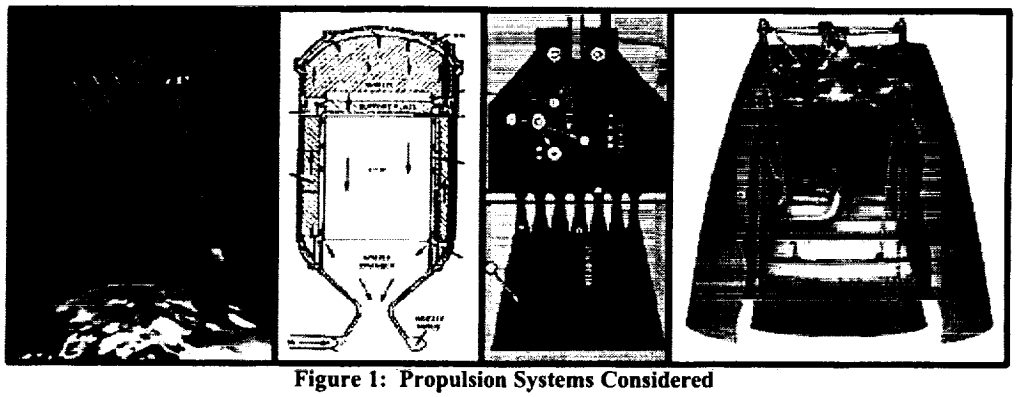

Figure 1: Propulsion Systems Considered

With these four systems identified, more detailed analyses provided a more complete idea of the main benefits each offered as well as the main drawbacks to the systems. The detailed analysis also allowed for a systematic down-selection process that resulted in a single architecture. To ensure an unbiased down-selection process, the design team employed a tool called the Analytic Hierarchy Process (AHP). AHP allowed direct comparison of each candidate architecture to each of the other architectures on a one-to-one basis. The process highlighted the strengths and weaknesses of each candidate and allowed the team to pick the overall strongest option. The results of the AHP showed that the tether system was not safe enough to be used with a human system. The main reason for this decision was that if the spacecraft missed the tether, it would not be able to enter the required orbit and could jeopardize the lives of the astronauts on board. Nuclear thermal rockets were eliminated from consideration because the design team felt that the environmental lobby would not allow a nuclear reactor to orbit Earth on a regular basis. The third candidate, an electric propulsion system, was eliminated because of time considerations. The current state of the art in electric propulsion required a three-month period to move a satellite from LEO to Geostationary Orbit (GEO). As such, it would take too long to move a vehicle from LEO all the way to the Moon. This left the

chemical liquid rocket system that used lunar resources to produce propellants on the Moon. This architecture was attractive based on the fact it uses proven technology and with ISRU it has the potential to use relatively low cost propellants since the cost of launching propellant from the Earth would be prohibitive.

One piece of technology that was included in each of the proposed system architectures was the use of an aerobrake maneuver through Earth's atmosphere when returning from the Moon. This procedure is used to further minimize the propellant usage and decrease the associated costs. The aerobrake minimized propellant usage because without it, the vehicle would have to burn its engine to slow down enough to be captured in Earth orbit and dock with the station. For safety reasons, the team decided against employing the aerobraking procedure on the astronaut transfer missions.

An additional method of reducing overall propellant use was the implementation of numerous fuel depots, including one in LLO, one in LEO, and several in intermediate elliptical refueling orbits (EROs). This option would allow for a smaller vehicle dry mass due to a smaller fuel capacity. However, as the vehicle dry mass was small compared to the payload mass, there was limited advantage to having more than one refueling stop. Thus, all the depots except for one in an ERO were eliminated. Additional analysis of the orbital mechanics of a depot in ERO showed that the depot's orbit would precess too much and would limit the launch opportunities to two per month.

In order to maintain the usefulness of in-space refueling, a just-in-time refueling plan was developed. Using additional vehicles to carry the additional propellant needed, the orbital precession of a fuel depot was avoided, as the refueling vehicle would be sent only as needed.

2.2 In-Situ Resource Utilization (ISRU) Research

Human settlement of space must eventually involve the utilization of space resources. A key question is whether the use of such resources can be leveraged to reduce the costs and increase the profitability of near-term space development plans. An early application will most likely be space-based propellant production. While Earth-To-Orbit (ETO) launch costs remain high, use of space-based propellants looks promising. This is because the high cost of earth-based propellants allows even a relatively massive, inefficient space-based propellant manufacturing facility to be cost competitive. If ETO launch costs drop, the design requirements of an economically viable propellant manufacturing facility become more stringent.

2.2.1 Economics of Lunar Propellants

The team decided to investigate the use of lunar propellants in its lunar transportation architecture for two reasons. First, initial economic assumptions made the use of Earth-based propellants financially impossible, so the only alternative, lunar propellants, had to be investigated. ETO launch costs were assumed to be $1600/kg of payload for a third generation reusable launch vehicle while payment for transporting payload from LEO to the lunar surface was initially targeted at $800/kg. Considering only propellant cost, it would have been necessary for each kilogram of propellants to transport two kilograms of payload from LEO to the lunar surface in order to break even. Such a high payload to propellant mass ratio (m_{PL}/m_p) is not feasible for near-term LTVs. In a Boeing study from 1993, a representative LTV traveling between LEO and LLO has a payload/propellant ratio of approximately one [1]. The baseline architecture in this study has a payload/propellant ratio of 0.26, largely because it acts as both a lunar surface lander and a transfer vehicle and must overcome the Moon's gravity. To break even just on the ETO cost of transporting propellant without considering investment and hardware procurement costs, the baseline architecture would need to charge $6000/kg to transport cargo from LEO to the lunar surface.

2.2.2 Lunar Polar Ice

The second reason for examining lunar propellant production was the new data available from the Clementine and Lunar Prospector missions that most likely indicate large quantities of water are frozen in cold traps at the lunar poles [2]. In 1996, the Clementine mission discovered permanently shadowed craters at both poles of the Moon -- the large Aitken basin in the south, and a series of smaller craters in the north. There may also exist permanent shadows in the bottoms of deep craters as much as 25 degrees from the poles. One preliminary radar experiment on Clementine postulated the existence of ice in these cold traps.

Two billion years ago, the Moon was close enough to the earth that its axis of revolution was unstable and there were no cold traps on the lunar surface. As the Moon's distance from Earth increased, its axis stabilized and ice from comet and meteor impacts began to accumulate in permanent shadow. Constant bombardment by meteors led to mixing of the ice deposits with surrounding regolith and prevented its dispersal by sublimation. About two meters of regolith has accumulated in this fashion since the formation of the cold traps, so ice is not expected below that depth [2].

Lunar Prospector's neutron spectrometer measured the flux of neutrons of various energies scattering off of the hydrogen trapped in the surface regolith. Figure 2 shows maps of hydrogen concentration at the lunar poles based on these measurements [3]. The darker color represents larger amounts of hydrogen, which indicates the presence of water. Preliminary data analysis indicates that there are 260 million metric tons (MT) of ice at the lunar poles, with 200 million MT in the south and 60 million MT in the north. The data are less sure in the north because the diameter of the cold trap craters there is near the resolution of the neutron spectrometer. Better results will become available in late 2000 after further data reduction [4].

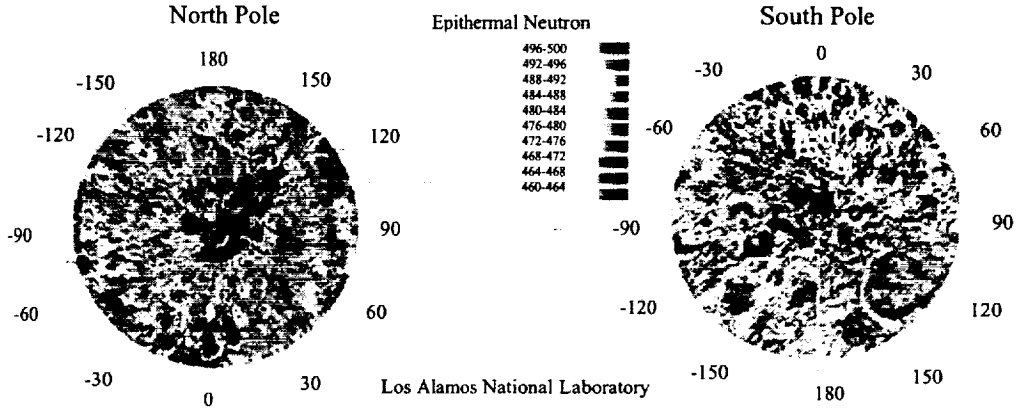

Figure 2: Polar H2 Concentrations from Lunar Prospector Neutron Spectrometer [3]

Producing liquid hydrogen and oxygen propellants from lunar polar ice involves several functional groups:

1) Autonomous rovers for regolith feed/slag transportation
2) Solar thermal furnace for water evaporation
3) Condenser for water vapor collection
4) Electrolysis unit for production of oxygen and hydrogen from water
5) Heat exchanger for liquefaction of propellants
6) Cryogenic storage system

The rovers must work in the extreme conditions of permanent shadow, and the scale of the operation could tax rover automation or strain its mass budget. The solar thermal furnace should be simple enough, given its location on a crater rim in permanent sunlight and the low temperatures required for evaporation compared to other ISRU techniques to be described. Water electrolysis is a space-proven system in the Russian Mir space station's Elektron oxygen generation unit, and in reverse in the space shuttle's fuel cells. Finally, cryogenic storage in the cold traps should be simple. Thus, it appears that the main technical challenges confronting the development of such a system are related to collection and dispersal of the regolith due to the cold operating temperatures and high material throughput.

Given these uncertainties, it is difficult to generate useful cost figures for this propellant production system. Orbital Technologies of Madison, WI recently performed a lunar transportation architecture study to evaluate the effects of different levels of ISRU [3]. Their overall evaluation criterion was Earth launch mass (ELM). The architecture includes two reusable vehicles, an orbital transfer vehicle and a lander, and maintenance/propellant resupply depots in LEO, LLO, and on the lunar surface. Nominal mission length for this study is twenty years. The launch mass savings and ETO launch cost results of the study are shown in Table 1 and Table 2 respectively. Utilizing both lunar hydrogen and lunar oxygen leads to ELM savings of 67% in this case. Before trying to quantify this result in a cost model, it will be helpful to look at other ISRU techniques that have been researched other groups.

Table 1: Launch Mass Savings

	No ISRU	Lunar LOX	Lunar LOX & LH2
ELM	8000 MT	3900 MT	2600 MT
% Savings	-	52.50%	67.50%

Table 2: ETO Launch Cost

	No ISRU	Lunar LOX	Lunar LOX & LH2
at $10,000/kg	$80 billion	$39 billion	$26 billion
at $1,600/kg	$12.8 billion	$6.24 billion	$4.16 billion

2.2.3 Other ISRU Methods

Prior to the discovery of ice at the lunar poles, ISRU research focused on the production of oxygen from regolith. Oxygen composes an average of 40% of lunar regolith. There are three main methods of extraction: chemical reaction, vacuum pyrolysis, and silica melt electrolysis [5]. According to Lunar Prospector's principal investigator, Dr. Alan Binder, no detailed research has yet been done on evaporation and electrolysis of polar ice. As a result, the closest reference process would be vacuum pyrolysis. Both processes involve simple heating of lunar material, but vacuum pyrolysis of dry regolith requires much higher temperatures, on the order of 2000 K, before useful products result. Vaporizing water from cold-trap regolith would require heating only to 400 K, just above the boiling point of water. Vacuum pyrolysis techniques need not deal with the cryogenic temperatures faced in cold traps, but since the process would probably occur away from the poles, the facility would either stand-down half the time or incur a mass penalty due to a power storage system for operation during the lunar night. Current state of the art vacuum pyrolysis, used widely in earth-based metal processing, uses batch sizes of 30 MT [5].

2.2.4 System Scale and Cost

The major difference between available studies of pyrolysis facilities and the MARTA lunar transportation architecture is the scale of operation. In 1993, Sherwood and Woodcock sized an oxygen production facility to produce 100 MT of propellant per year. Since one of Sherwood and Woodcock's landers required 25 MT of propellant to make one flight from the lunar surface to LLO and back, the production capability allowed them to make four such flights per year [1]. Production facility mass was 190 MT. In the baseline MARTA architecture, with market growth of 5% per year, annual ISRU propellant production requirements ramp up from 1800 MT in year one to 4000 MT in the final year of the program 17 years later. Assuming 100% efficient extraction of the 2% of ice crystals in the cold trap regolith, a 30 MT batch of regolith yields 0.6 MT of water. Producing 2000 MT of propellant annually requires 3300 batches or 100,000 MT of processed regolith in a continuous process. In 1999, a graduate team at Caltech's Laboratory for Space Mission Design examined a facility for producing oxygen and hydrogen from lunar polar ice and generated the curve in Figure 3 for facility mass as a function of required annual propellant [6]. For reference, the Sherwood and Woodcock data point is also included on the figure. Their model of the cold trap regolith assumed water to be 14% by mass of the cold trap regolith; more recent analysis indicates there is only 2% by mass. Their plant mass to produce 2000 MT of propellant annually is 25 MT, much less than the 190 MT required in the Boeing study to produce just 100 MT of oxygen annually. Due to the widely varying results of current studies, ISRU cost was treated parametrically for the MARTA project.

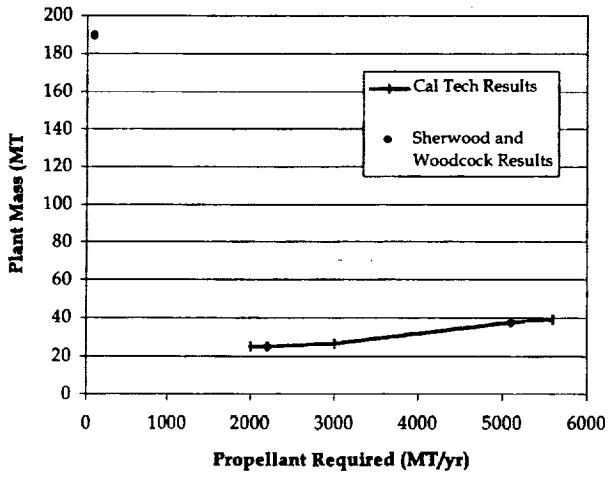

Figure 3: Production Facility Mass vs. Propellant Required [6]

2.3 Lunar Surface Architecture Selection Process

In order to make the chosen architecture work financially, the propellants needed to fuel the rocket vehicles must be produced on the lunar surface. Since substantial amounts of ice exist at the lunar poles, it makes sense to locate a propellant production facility at one of the poles (See Section 2.2 for more details on this.). Because some of the missions will be to the equator, there needs to be a way to refuel the vehicles landing at the equatorial site. This problem lead to an investigation intended to identify the optimal system architecture for transfer of propellant from the poles to the equator. Options considered included various combinations of lander vehicles, roving trucks, and a mass driver. The landing vehicles would be used to land at either the equator or poles and have the capability to jump from base to base if needed. The roving truck would be capable of navigating the 2730 kilometers from the polar base to the equator allowing transfer of cargo, people and propellant. The mass driver would be used to launch propellant into Low Lunar Orbit (LLO).

The mass and power requirement of the truck vehicle as well as the enormous travel distance required were deemed too difficult without excessive DDT&E costs. These technical and financial difficulties removed the truck from consideration. The remaining options were narrowed to the following choices: 1) a two-lander system with one vehicle sized for equatorial landings and the other for polar missions 2) a single lander that would land at both bases 3) a single lander in conjunction with a mass driver for launching propellants into LLO.

The required mass, propellant usage, and program cost for each option was calculated for the remaining candidates. Parametrically varying the ISRU propellant price per kilogram allowed the design team to generate the graph in Figure 4. Immediately evident is that the two-lander scheme has an overall higher program cost than a single vehicle option.

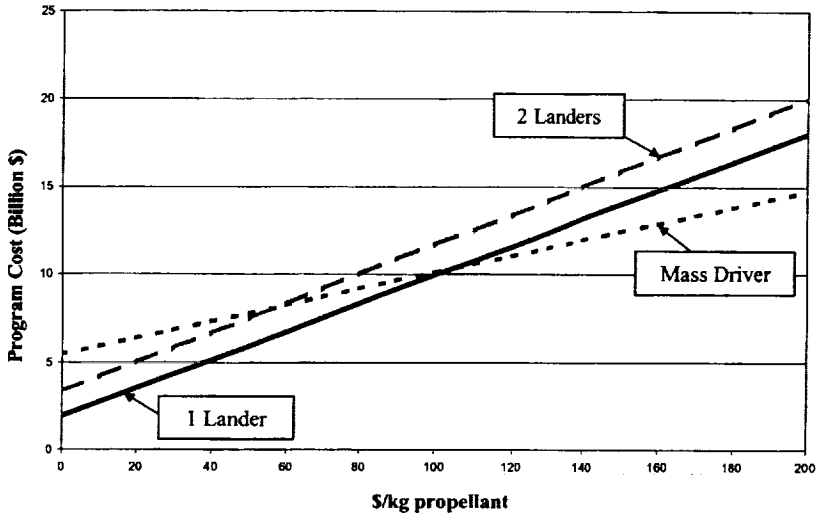

Figure 4: Lunar Surface and LLO Architecture Study

Perhaps the most valuable information obtained from Figure 4 is the fact that the single lander line intersects the mass driver line at $100 per kilogram. This implies a trade-off exists between the two configurations. If propellant can be made cheaply on the Moon, then it is best to use a more propellant hungry all-lander system. However, if propellant is very costly to produce on the lunar surface, the propellant savings of using the mass driver make this option more appealing. The $100 per kilogram intersection was identified during this simplified trade study and does not reflect the final results. After more detailed analysis, the actual intersection was found to be at $250 per kilogram. As such, Figure 4 is included to underline the importance of ISRU cost to the system architecture. It also points out that defining the final system configuration cannot be done unless ISRU cost is determined with confidence.

2.4 Simulated Probabilistic Parametric Lunar Architecture Tool Development

In order to calculate the mass, size, and cost of the transportation system being designed, it was necessary to create various models. These models needed to be flexible so that they could adapt to changes in the project as it

was refined throughout the design process. The following sections detail how the Simulated Probabilistic Lunar Architecture Tool (SPPLAT) was developed.

2.4.1 Weights and Sizing

A traditional Weight Breakdown Statement (WBS) was used in the formulation of the Weights and Sizing (W&S) model. The Weight Breakdown Statement is provided in detail in Section 3.1.1.

This model used Solver, the Excel optimization routine, to minimize the dry weight and propellant used for a given engine specific impulse (I_{sp}) and a combined Weight Adjustment Factor (WAF). This WAF was composed of two separate parts. The first was a Technology Reduction Factor (TRF) that modeled how much dry weight could be reduced due to advances in materials technology. The second was a Weight Estimating Error that modeled the inaccuracies in the W&S model itself. Both factors were expressed as percentages, and they were multiplied together to form the combined WAF.

Response Surface Analysis was used in modeling the W&S for use in a Monte Carlo Simulation. Response surface analysis generates an equation for the desired variable, (e.g. dry mass of the vehicle) using the control variables as inputs. A Response Surface Equation (RSE) was generated from 110 converged point designs that spanned the design space. The control variables for the RSE were I_{sp} and the WAF. I_{sp} was varied from 450 seconds to 500 seconds in 5-second increments, while the WAF was varied from 80% to 125% in 5% increments. This RSE was then used as the W&S model in the ultimate design tool, SPPLAT.

In order to have this tool generate values for each line item of the WBS, it was necessary to be able to calculate component masses from the vehicle dry mass. The extreme cases of the design space were analyzed and line items were identified as either fixed or variable masses (For example, avionics were a fixed mass for this mission architecture that stayed constant while tank mass changes based on engine I_{sp}). The variable mass line items were proportioned to the dry weight remaining after the fixed mass items were removed. These ratios were then applied to the RSE value of the vehicle dry weight to calculate the line item masses. The reason for developing the tool in this manner was to allow SPPLAT to generate the entire WBS from a single RSE.

2.4.2 Costing and Business Analysis

In order to determine the profitability of the business, an Excel spreadsheet model was created that included the following functions:

1) Costing of the Lunar Lander and Transfer Vehicles (LLTVs) using weight-based parametric Cost Estimating Relationships
2) Fleet size estimation and acquisition
3) Mass driver costing and payload capacity
4) Income and cash flows statements for calculation of project Net Present Value, (NPV)

The cost of the LLTVs was determined using weight-based Cost Estimating Relationships (CERs). The CERs used were from the 1996 NASA Air Force Cost Model (NAFCOM96). These CERs are based upon shuttle-era launch vehicle technology, and in many ways do not reflect the actual nature or technology of an in-space vehicle. However, since no reusable in-space transfer vehicle has ever been constructed, there are currently no CERs directly applicable to this project. In order to account for the differences between the hardware represented in the NAFCOM96 CERs and MARTA's LLTVs, complexity factors were used to modify the cost by linear multiplication. The costs obtained from the CERs were multiplied by these complexity factors to adjust the estimated cost up or down to obtain a more realistic cost model of the LLTV.

The LLTV costs were divided into two areas, DDT&E and a Theoretical First Unit cost (TFU). DDT&E represents all of the engineering and prototyping efforts required prior to the manufacture of the first vehicle. TFU represents the cost of building a single vehicle, with no learning curve or rate effects included. This analysis assumed that the main engine would be an off-the-shelf item, and that the RCS thrusters would be available off-the-shelf with only minor modifications. Most likely, this engine will be something similar to the SPW2000 engine under joint development by Snecma and Pratt and Whitney. The SPW2000 is being designed to produce 50,000 lbf of thrust with an I_{sp} of 460 sec. As a result, no DDT&E for main engines was included, and a substantially reduced DDT&E for RCS thrusters was used. The complexity factors used in the costing model are included in Table 3.

Table 3: LTV Complexity Factors

Vehicle Weight Group	DDT&E Complexity	TFU Complexity
Structure & Tank	0.8	1.0
RCS	0.1	1.0
Aerobrake	0.8	1.0
Primary Power	0.5	0.5
Electrical Conv/Dist	0.5	0.5
Environmental Contro	0.2	0.5
Avionics	0.2	0.7
Main Engine	0.0	1.0

As can be seen, substantial reductions were assumed for primary power, electrical conversion/distribution, environmental control and avionics DDT&E and TFU. Since substantial technological changes have occurred in these areas since the Shuttle development, this was deemed appropriate. The other TFU costs were left unchanged in order to be conservative. In addition to these hardware-related costs, costs were included for various systems and testing operations. These were calculated as a percent of total hardware costs. The percentages used are shown in Table 4. In addition to all of the above costs, a 20% margin was included to account for miscellaneous program costs that might be incurred.

Table 4: LTV Non-Hardware Cost Percentages

	Complexity Factor Adjustment on NAFCOM Results for	Complexity Factor Adjustment on NAFCOM
System Test Hardware	20%	-
Integration, Assembly, Check	12%	25%
System Test Ops	14%	-
Ground Support Equip.	6%	-
System Eng. & Integration	20%	4.50%
Program Management	5%	5%

The fleet size is based on the number of round trips as well as necessary support flights needed each year. For each of these flight types, a total flight time, including ground processing and maintenance, was determined. Using these times, the total required fleet size was calculated for each year. The trip time and flight assumptions used are shown in Table 5. The assumption was made that any operations on the lunar surface (loading/unloading) require two days. Any flight that arrives in LEO will spend seven days there for maintenance and inspection. The vehicles in the fleet will be rotated through the different flight types so that all vehicles receive periodic maintenance in LEO.

Table 5: Trip Time and Flight Assumptions

Flight Type	Total Round Trip Flight Time (days)	Flights per Round Trip Cargo Flight	Flights per Round Trip Passenger Flight
Cargo (60 MT)	19	1.0	-
Passenger (5 people)	15	-	1
LLO Refueling	4	2	-
ERO Refueling	12	1	-
Equatorial Base Refueling	4	0.5	0.5

In any year that a larger fleet size is required than the previous year, the program is charged for the acquisition of a new vehicle. A learning curve effect of 95% was used for this acquisition. In other words, every time the total number of vehicles built doubles, the cost to acquire the next vehicle decreases by 5%. As shown in Table 6, this process resulted in maximum fleet sizes of 3 vehicles in the 0% and 5% growth cases. For the 15% growth case, the fleet size reaches 10 in the final program year.

Table 6: Vehicles Required for Different Annual Growth Rates

Annual Flight Growth Rate	Max Number of Vehicles Required
0%	3
5%	3
15%	10

Income and cash flow statements were prepared in order to calculate the project Net Present Value (NPV). A number of assumptions were made in the preparation of these statements. These assumptions are shown in Table 7 below.

Table 7: Accounting Assumptions Used for Income Statements

Fleet DDT&E Period	3 years
DDT&E Start Period	2014
Maintenance Costs per Cargo or Passenger Flight	$1 M
Lunar Surface Operations Cost	$10 M/yr
LTV Depreciation Method	Straight-line, 10 year lifetime
Mass Driver Depreciation Method	Straight-line, 15 year lifetime
Main Engine Life	100 flights

The cost of lunar propellants was treated as an independent variable, and the cargo revenue per kilogram necessary to produce zero NPV for a given cost of propellants was calculated. This step was necessary in order design a system that would meet the goal of returning a 25% rate of return for the private company that operates it. The goal was to calculate the price per kilogram that the company would need to charge NASA (the customer) in order to make the required return. This was easily accomplished by assuming that the market demand (the government-sponsored payload) would not change with changing cargo revenues. The added NPV generated by an additional $1 per kilogram of payload was determined. Since NPV is a linear operator, all that was required to determine the zero NPV cargo price was to divide the NPV for the nominal case by this $1/kg NPV. The result was then added or subtracted from the nominal cargo price to determine the zero NPV cargo price. This became the major financial metric used to evaluate the various mission configurations.

2.5 Setting up the Design of Experiments (DOE)

In order to gauge the effects of changing ISRU cost on the economics of the project, a design of experiment (DOE) matrix was set up to perform a response surface analysis using SPPLAT. Response surface analysis generates an equation for the desired variable, (e.g. price to charge customer) using the control variables as inputs. Because the use of a lunar mass driver was handled as a discrete variable, two separate response surfaces were created. Both response surfaces used ISRU cost, rocket engine I_{sp}, and weight adjustment factor (WAF) as control variables. The inputs for the design of experiments analysis are shown in Table 8.

Table 8: Design of Experiments Matrix

Run	x_1 Isp (sec.)	x_2 ISRU ($/kg)	x_3 Weight Red. (%)	Mass Driver
1	460	50	0	Yes
2	460	50	20	
3	460	5000	0	
4	460	5000	20	Yes
5	500	50	0	
6	500	50	20	
7	500	5000	0	Yes
8	500	5000	20	
9	480	2525	10	
10	460	2525	10	Yes
11	500	2525	10	
12	480	50	10	
13	480	5000	10	Yes
14	480	2525	0	
15	480	2525	20	
16	460	50	0	No
17	460	50	20	
18	460	5000	0	
19	460	5000	20	No
20	500	50	0	
21	500	50	20	
22	500	5000	0	No
23	500	5000	20	
24	480	2525	10	
25	460	2525	10	No
26	500	2525	10	
27	480	50	10	
28	480	5000	10	No
29	480	2525	0	
30	480	2525	20	

In order to make the design more robust, an uncertainty analysis using Monte Carlo simulation was also performed. The mass estimate, cost estimate, market expansion rate, and ETO cost per kg were allowed to vary between the limits shown in Table 9. The flow of this process is illustrated in Figure 5. For a given run of the DOE, 5000 Monte Carlo iterations were performed. For each iteration, a random value was picked within the range of each of the noise variables. The Monte Carlo analysis provided mean and standard deviation response surfaces. The end result was a group of response surface equations (RSE) capable of modeling the output parameters over the entire range of the inputs for both architecture selections. The RSEs of interest in this project are: 1) Price to charge the customer that results in a 25% rate of return for the business, 2) The vehicle dry mass, and 3) Propellant required to complete on cargo transfer. A sample response surface is shown in Figure 6. For simplicity, this surface demonstrates the effect on vehicle dry weight of varying I_{sp} and ISRU cost. The color contours are used to help show the curvature of the surface. The optimal design was selected by using SPPLAT to find the combination of control variables that resulted in the minimum price to charge the customer. The uncertainty analysis using the noise variables allowed the design to team to associate a confidence level with this price to charge. In other words, the uncertainty analysis allows the design team to asses how likely it is that a combination of control variables will minimize the price to charge.

Table 9: Noise Variable Ranges for the Monte Carlo Simulation

Noise Variable	Minimum	Most Likely	Maximum
Mass Estimate	-20%	0%	25%
Cost Estimate	-5%	5%	15%
Market Expansion	0%	5%	15%
ETO Cost per kg	$800	$1,600	$5,000

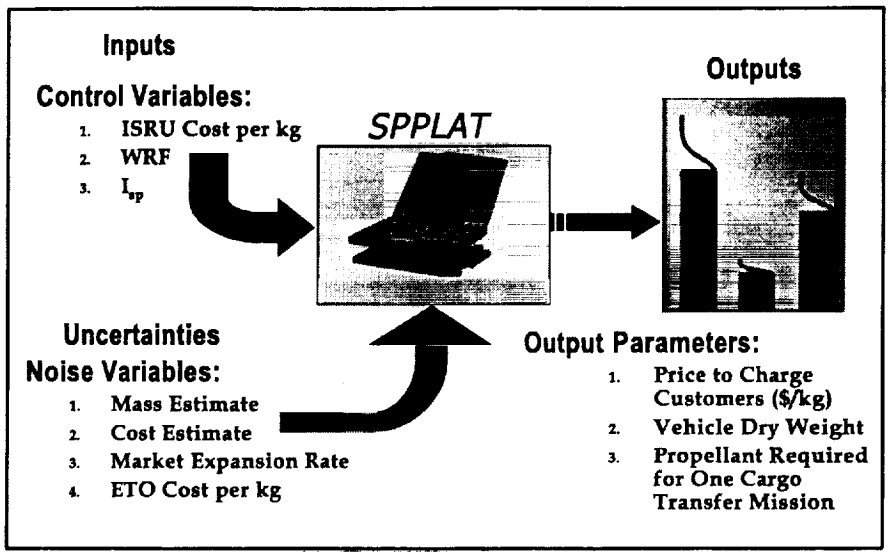

Figure 5: Uncertainty Analysis Flowchart

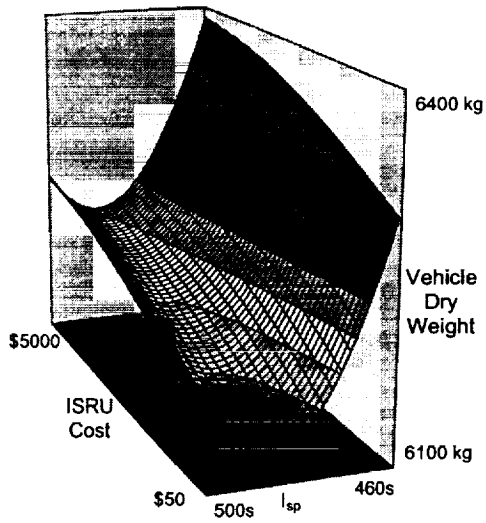

Figure 6: Representative Response Surface

3. Results

3.1 Baseline Operations/Architecture

The final mission architecture consists of a MARTA operated facility at the Moon's South Pole which is both the center of overall operations as well as the location of the propellant production facility which makes liquid oxygen and liquid hydrogen from lunar water ice. The South Pole was chosen because the majority of the lunar ice is located there. If necessary, a similar facility can be constructed at the North Pole. The system uses a combined lunar lander and transfer vehicle (LLTV) design that allows a single vehicle to take returning cargo or astronauts to LEO and then inbound cargo or astronauts to the Moon's surface. This same vehicle design also functions as an in-space refueling vehicle during a transfer mission. MARTA maintains no infrastructure at the Moon's equator, but supplies transportation services to the NASA base.

3.1.1 Vehicle Description

The MARTA vehicle serves as both lunar lander and in-space transfer vehicle. It remains as one unit throughout the entire mission. The aerobrake is used to capture into Earth orbit in the cargo and refueling missions,

whereas a propulsive burn is used to capture a vehicle carrying astronauts. The low thrust requirement for lift off from the Moon enables the same engine to be used for launch, landing, and all in-space propulsive burns. A three-view of the baseline MARTA vehicle is shown in Figure 7.

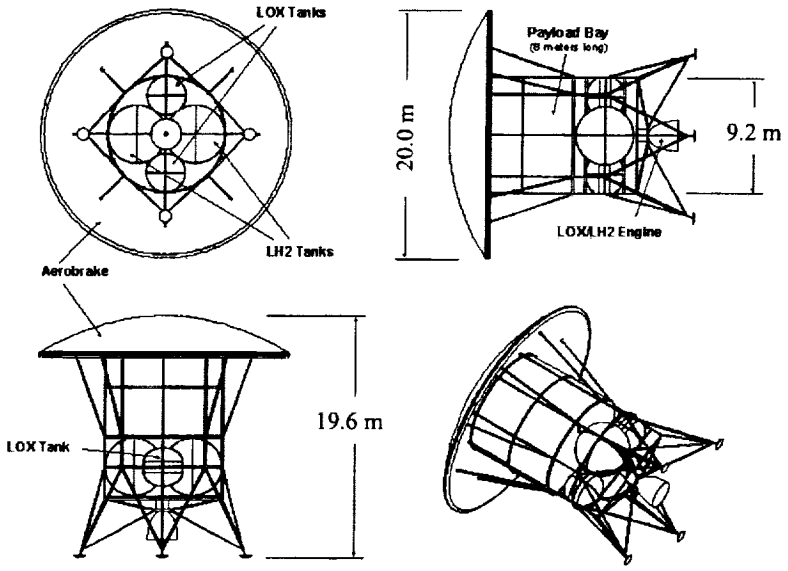

Figure 7: Three View of the MARTA Transfer Vehicle

The vehicle is designed to accommodate four different configurations, as shown in Figure 8. Each of these different payloads is fitted in the payload compartment either while the MARTA vehicle is docked in LEO or is on the surface of the Moon.

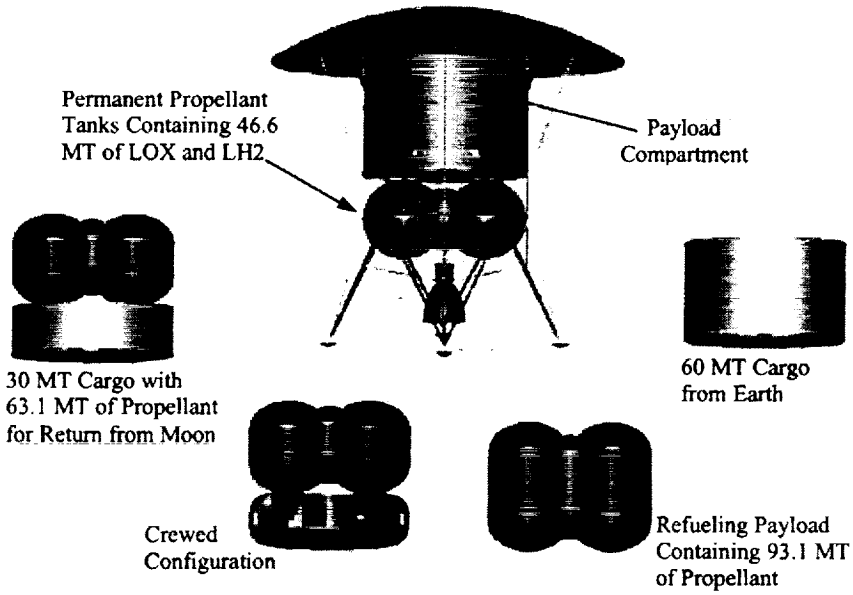

Figure 8: MARTA Transfer Vehicle with Various Configurations

Due to the low forces required for an in-space system, the vehicle itself is relatively light, as can be seen in the component weight breakdown given Table 10. The numbers in Table 10 apply to the vehicle regardless of the mission. Only the contents of the payload compartment change when the vehicle is outfitted for one of its various missions. Estimates show that the vehicle can expect to experience a maximum of 0.1 Earth g's during the aerobraking procedure and a maximum of 0.33 Earth g's during landing on the lunar surface. A finite element analysis shows that the truss structure designed for the vehicle is strong enough to withstand 1.5 Earth g's.

Table 10: Baseline Vehicle Weight Breakdown Statement

1.0	Body Group			1400 kg
	1.1	Primary Structure	825 kg	
	1.2	Thrust Structure	175 kg	
	1.3	LOX Tank	150 kg	
	1.4	LH2 Tank	250 kg	
2.0	Landing Gear			325 kg
3.0	LOX/LH2 Engine			325 kg
4.0	RCS Propulsion			125 kg
5.0	Aerobrake			1025 kg
6.0	Primary Power			1075 kg
7.0	Electrical Conversion and Distribution			400 kg
8.0	Environmental Control			375 kg
9.0	Avionics			375 kg
10.0	Margin			825 kg
	Dry Mass			**6250 kg**

3.1.2 Trajectory Description

An example cargo transfer scenario starts on the Moon's surface at the South Pole as shown in Figure 9. Two vehicles are required for the entire mission, the first carrying the cargo and the second carrying additional propellant for refueling. The cargo vehicle leaves the Moon's surface carrying 30 MT of returning cargo and 109.7 MT of additional propellant. The refueling vehicle carries 139.7 MT of additional propellant. Both vehicles burn all 46.6 MT of propellant in the permanently attached tanks in order to produce the 1700 m/s ΔV necessary to reach LLO.

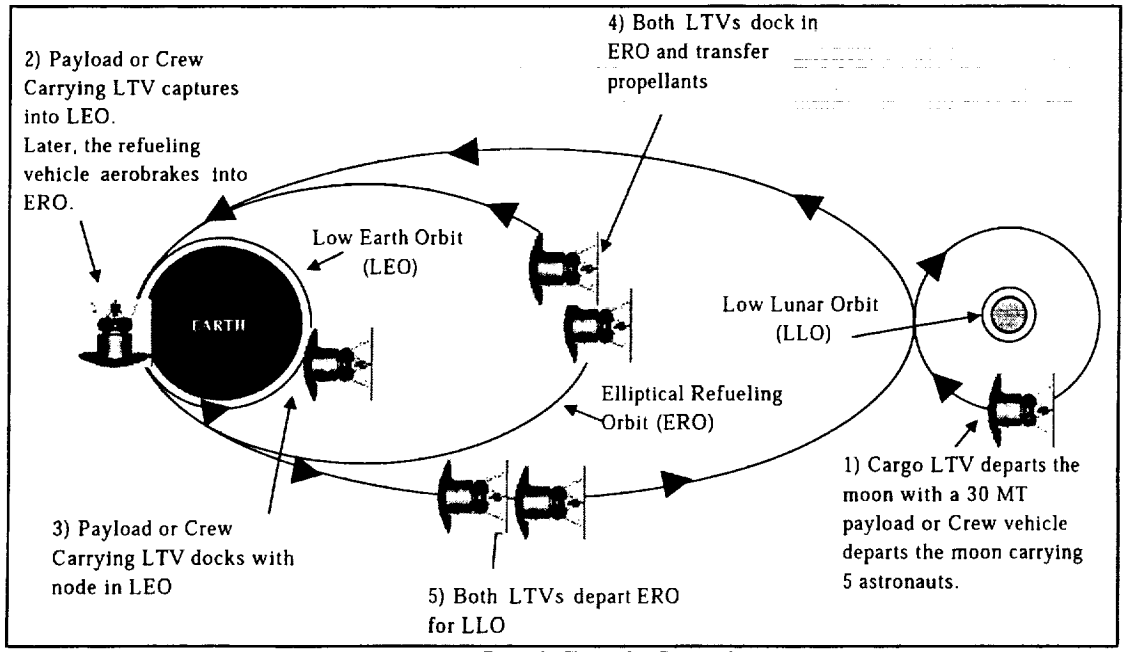

Figure 9: Sample Transfer Scenario

Once in LLO, each vehicle takes 16.4 MT from its additional propellant in order to make the 800 m/s ΔV for the TEI burn. Both vehicles then spend 5 days in transit to Earth. The cargo vehicle conducts 12 aerobrake passes (adding another 5 days to the transfer) through the atmosphere to produce the ΔV of 3100 m/s needed to capture into LEO. It then performs a rendezvous with the transportation node and swaps out the 30 MT returning cargo for 60 MT of outbound cargo.

Once the cargo vehicle has completed the cargo transfer and any necessary maintenance, it uses all its remaining fuel to make the 2400 m/s ΔV needed to enter an elliptical refueling orbit (ERO) where it will meet the refueling vehicle to take on the propellants needed to get back to the Moon. Not needing to be in LEO, the refueling vehicle aerobrakes directly into the ERO to rendezvous with the cargo vehicle. At this point, the cargo vehicle takes on sufficient propellant to complete the trip to the Moon. The cargo and refueling vehicles both burn to produce the 700 m/s needed to enter the transfer back to lunar orbit. At the Moon, each vehicle burns its engine to generate the 800 m/s of ΔV required to enter a polar LLO and then burns again for 1700 m/s to return to the surface. The cargo vehicle lands at either the South Pole or the equator (as required by cargo manifesting) while the refueling vehicle lands at the South Pole to begin the cycle again.

Because the cargo mission outlined above takes too much time to comfortably transfer astronauts using the same methods, a separate mission scenario was developed for astronaut missions. The main difference between the two scenarios is found in the leg of the trip from the Moon to LEO. Instead of the aerobraking procedure used with the cargo, the astronaut missions use the MARTA vehicle rocket engine to provide the ΔV necessary to capture into LEO. This maneuver is possible because the crew module is small enough that the vehicle can carry enough propellant to successfully complete the maneuver. Once the vehicle carrying the astronauts leaves LEO, it follows the same procedure as the cargo mission.

3.1.3 Mass Driver Description

Various mass driver designs were considered in an attempt to find the best one for the mission. Figure 10 below shows two such alternative designs that were investigated. Pictured on the left is a single one-way mass driver track powered by a large solar power array. On the right is a mass driver design which includes a deceleration section of track utilizing re-usable "buckets" that hold the payload during launch.

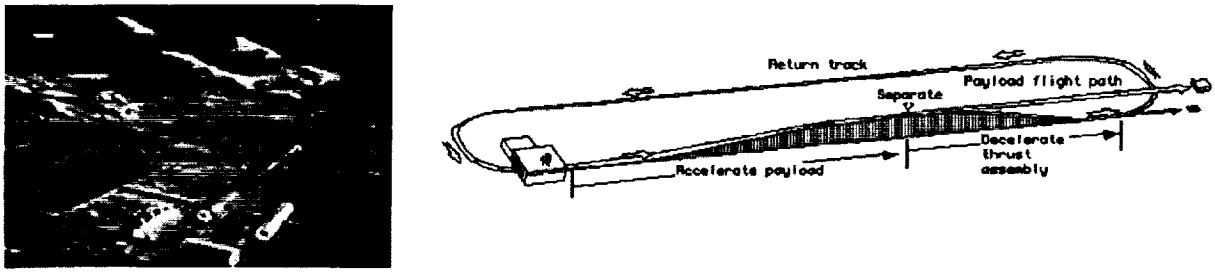

Figure 10: Sample Mass Driver Architectures

The mass driver operates by accelerating the payload using magnetic attraction. The magnetic field is generated by a linear synchronous motor timed by feedback of the payload's position along the track. The final section of the track is devoted to dampening any disturbances and correctly aligning the payload to minimize trajectory error. The payload will have some reaction control correction ability to correct for any small launch spread. The main components of the system are super conducting wire and silicon-controlled rectifiers. The chosen system is powered by nuclear generators although solar power could be used if political considerations make use of nuclear power an issue. An efficiency of 92% is assumed for the conversion of electrical energy to kinetic energy.

The mass driver system breakdown is provided in Table 11 below. All mass, power and cost estimates are based on the work of the late G. K. O'Neill of Princeton University [7]. The first rows of the table are design dependent variables. The baseline design is sized to generate the ΔV of 1700 m/s that is required for LLO insertion. The 20 Earth-g load requirement was found to be a good compromise between excessive track length and the maximum loading the structural system could reasonably handle. The mass of propellants launched per year is calculated from the number of cargo flights multiplied by their propellant usage requirement. The "chunk" size represents the mass of the payload launched by each shot of the mass driver. It was determined that 30 MT would be most convenient if the mass driver is to be used later for launching cargo.

The remaining rows in Table 11 are outputs based on the design variables. Total system mass includes both the mass driver system as well as the power generating and storage facilities. The annual recurring cost accounts for costs associated with each launch as well as track maintenance. Non-recurring cost accounts for DDT&E, TFU, transport of system to lunar surface, track construction, power generation and power storage facilities.

Table 11: Baseline Mass Driver System Requirements

Mass Driver	
ΔV to Reach LLO	1,700 m/s
Mass Launched per Year	2,000,000 kg/yr
Number of g's at Launch	20
"Chunk" Size	30,000 kg
Length of Track	7,400 m
Total Launcher Mass	36,800 kg
Total System Mass	57,600 kg
Total Power	295,000 W
Estimated Annual Recurring Cost	$919,300
Estimated Non-Recurring Cost	$1,922,900,000

3.1.4 Baseline Cost Breakdown

A profitable 25% rate of return was set in the business case, and cost per kilogram of lunar propellants was varied, along with engine I_{sp} and weight technology reduction factor. ISRU cost was the driving parameter, followed by use of a mass driver. Customer price is fairly insensitive to engine Isp and WAF. Varying lunar propellant cost leads to variation in the price charged to the customer for transporting cargo from LEO to the lunar surface. The results of the team's trade study are shown in Figure 11.

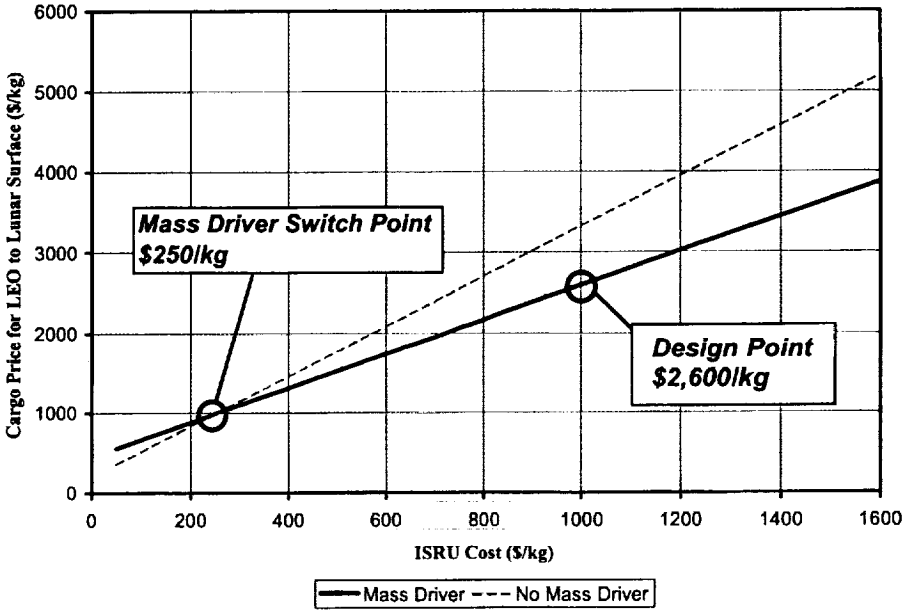

Figure 11: Customer Price as a Function of ISRU Cost

If propellant price can be brought down to $160/kg, the original RFP price goal of $800/kg can be achieved. The team feels that a propellant price of $1000/kg, which yields a cargo price of $2600/kg, is a reasonable goal that can motivate ISRU technology development over the next 18 years before IOC.

Using SPPLAT's cost model as described in Section 2.4.2, a cost breakdown was found for the baseline vehicle as shown in Table 12. The price to charge customers per kg for transfer from LEO to the Moon was the main output of the model based on obtaining an NPV of zero with a discount rate of 25%. The largest expense was approximately $48 billion for ISRU propellants over the life of the program.

Table 12: Baseline Cost Breakdown

Price to Charge Customers for LEO to Moon Transfer	2600/kg
IRR	25%
NPV	$0
Vehicle DDT&E	$1,000 M
LTV ETO Launch Costs	$570 M
ISRU Propellant Costs	$47,650 M
Mass Driver DDT&E	$2,300 M
Operations Costs	$1,500 M
Fleet Acquisition Costs	$1,000 M
Life Cycle Costs	$54,000 M
Total Revenue	$74,000 M

3.2 Results of the Design of Experiments

The results of the DOE provide a robust assessment of the effects of the control variables, also showing the effects of uncertainty in the design relationships via the noise variables. The RSEs themselves are very accurate. Goodness of fit analysis shows that the equations possess very high R-squared (R^2) values. High R^2 values indicate a good match between the RSE and the original data points. With the exception of the vehicle dry mass standard deviation equation, all of the R^2 values are above 0.996.

The RSE's show that the price to charge the customer per kg of payload should be set to $2600/kg of cargo and $2 million/person to provide a 25% rate of return for the baseline design. These price figures require the use of a lunar mass driver because the baseline ISRU cost is high enough to warrant its use. If the design is implemented without the use of the mass driver, the prices to charge the customer increase by approximately 22%. Using the available standard deviation RSE's, the optimum price combination shows that the price will fall within 7% of the quoted mean prices with 95% confidence levels.

Because the number of astronaut flights is smaller than the number of cargo flights, the price to charge per astronaut does not change noticeably. For cargo missions, within the range of input variables specified, the minimum possible price to charge is $307/kg. This price results when a lunar mass driver is not used, the engine I_{sp} is increased to 500s, the cost per kilogram for ISRU production is brought to $50, and a 20% technology reduction factor (TRF) used.

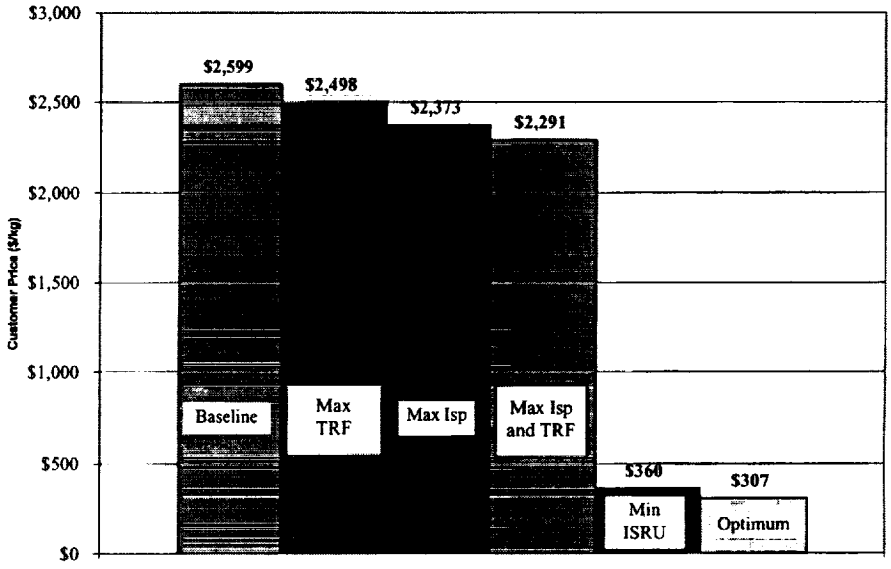

Figure 12: Price to charge customer per kg of payload for the optimal and baseline design cases

A comparison of different designs to the baseline vehicle is shown in Figure 12. Increasing the I_{sp} of the rocket engine to 500 sec only reduces the price to charge the customer for a kilogram of cargo to $2373/kg, and increasing the TRF to 20% only reduces the price to $2498/kg. The combined benefit of implementing both advances in technology provides a savings of 12% to the customer. However, investing in ISRU technology and reducing the cost per kilogram of ISRU production to $50 results in a savings of 86%. It should be noted that the use of a lunar mass driver is no longer beneficial once the cost of ISRU propellants is brought below $250/kg. Therefore, the cost of ISRU propellants has a significant impact on the economics of this design. Not only does a low ISRU cost allow the price per kilogram of payload to reach very low levels, but it also removes the need to invest in additional technology, namely the lunar mass driver. Figure 13 shows how sensitive the price to charge the customer is to the cost of ISRU propellant production.

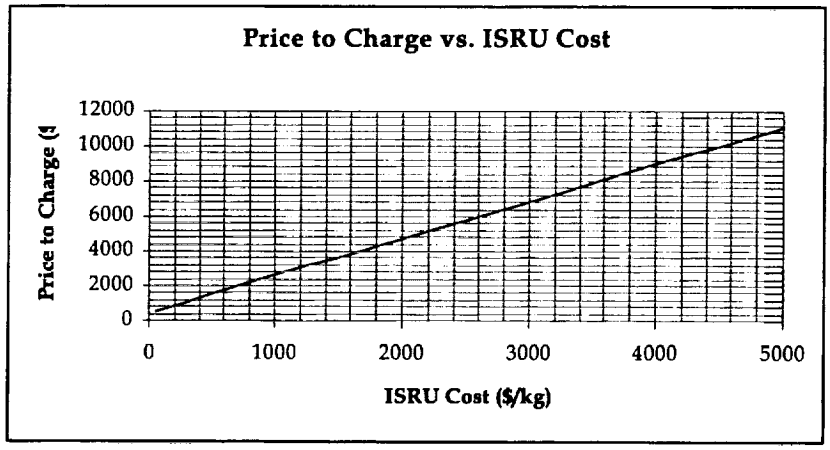

Figure 13: Effects of ISRU Cost on the Price to Charge the Customer

3.3 Independent Verification of Results

As discussed in Section 2, a Review Team paralleled the work of the Design Team throughout the design process. The Review Team used the same architecture but completed an independent analysis of the vehicle. The Review Team used more conservative values such as a different schedule requiring more vehicles, a heavier aerobrake based on current technology, and certain assumptions for the cost estimation such as a higher complexity factor for the RCS system. DDT&E for the main engine was also included in this verification analysis. The results of this analysis were within 13% of the price determined for the baseline case by the Design Team.

4. Conclusions and Recommendations

The main conclusion reached from this project is that it is currently possible to build a commercially viable and technologically feasible Earth-Moon transportation system even though it would be costly. The MARTA vehicle presented does not rely on any advanced technologies or require any technical advances to become a reality. However, the most important feature of the architecture is not the vehicle. In order to make this a profitable venture, the cost of producing propellants on the Moon must be controlled. In fact, this one technology is the single largest factor in determining how much a company must charge in order to make a 25% return. As such, NASA or other similar groups should focus resources on developing a low cost lunar ISRU facility.

Another important result of the study is that the use of a mass driver is not a necessary requirement for the system as outlined. In fact, it only improves the business case for the system when the cost of ISRU production is in excess of $250/kg. This fact reiterates the importance of lowering the cost of an ISRU facility. By reducing the cost below $250/kg, it is possible to significantly reduce the complexity of the system and time needed to develop and deploy it because the mass driver is no longer necessary.

The final conclusion is that moderately improving the I_{sp} of liquid oxygen/liquid hydrogen fueled rocket and reducing the mass of the vehicle through advanced materials technologies does help reduce the cost of the system. But, the effects are only marginal. As a result, the MARTA team does not feel it is justified to spend research dollars trying to improve these two technologies when today's technologies work almost equally as well. Instead, all resources should be concentrated on lowering the cost of an ISRU facility.

5. Outreach

The most important outreach operation of the MARTA Project is to the scientific community. By identifying a key driver in reducing the cost of an Earth-Moon transportation system, the MARTA team feels it has made an invaluable contribution to the exploration and commercial development of the Moon.

Additionally, the team has extended its outreach to the political arena. A MARTA team member lobbied members of Congress in March 2000 to help publicize the importance of utilizing space resources to provide access to space for everyone interested. MARTA has also been in contact with Lunar Prospector principal investigator Dr. Alan Binder about the MARTA design, learning from him some of the nuances of the results from Lunar Prospector and discussing his plans for commercial lunar exploration beginning with missions based on data purchase.

6. Acknowledgements

The members of the design team would like to express their utmost gratitude to Dr. Olds, for his guidance during every stage of the design. The project could not have taken place without the invaluable experience he helped pass on to us. We would also like to thank to those who have preceded us at Georgia Tech: Ashraf Charania, Dave McCormick, Irene Budianto, Laura Ledsinger, Dave Way, John Bradford, Kris Cowart, and Brad St. Germain for their support and advice throughout the project. Lastly, we would like to thank Dr. Alan Binder for providing us with previously unpublished data about the Lunar Prospector Mission and discussing his plans for commercial follow-on missions.

7. Works Cited

1. Sherwood, B., and Woodcock, G.R. "Cost and Benefits of Lunar Oxygen: Economics, Engineering, and Operations" in *Resources of Near-Earth Space*. Lewis, J., et al, eds. University of Arizona Press, Tucson, AZ. 1993.
2. Binder, A. "Lunar Prospector: Overview" *Science* v.281, 4 Sept 1998. p.1475.
3. Rice, E.E. *Development of Lunar Ice / Hydrogen Recovery System Architecture*. NASA/NIAC Research Grant 07600-021 OTC-G083-FR-2000-1. Orbital Technologies Corp., Madison, WI. 1 Jan 2000. niac.usra.edu/files/studies/final_report/html/341Rice/341Rice.html4.
4. Gruener, J.E., "Lunar Prospector's Mother Lode" *Lunar News* , No. 64, Dec 1999. Planetary Missions and Materials Branch, Earth Science & Solar System Exploration Division, Johnson Space Center, NASA. www-curator.jsc.nasa.gov/lunar/lnews/Lndec99/Prospector.html
5. Senior, C. L. "Lunar Oxygen Production by Pyrolysis," in *Resources of Near-Earth Space*. Lewis, J., et al, eds. University of Arizona Press, Tucson, AZ. 1993.
6. Baker, R. S. *Tlaloc Project Final Report*. California Institute of Technology, Laboratory for Spacecraft and Mission Design. June 1999. http://www.lsmd.caltech.edu/ae125/tlalocReport.pdf
7. Chilton, F.; Hibbs, B.; Kolm, H.; O'Neill, G.K.; and Phillips, J.; Electromagnetic Mass Drivers, in Space-Based Manufacturing from Nonterrestrial Materials, Progress in Astronautics and Aeronautics, vol. 57, AIAA, New York, 1977, pp. 37-61.
8. Arnold, W.; Bowen, S.; Cohen, S.; Kaplan, D.; Fine, K.; Kolm, M.; Newman, J.; O'Neill, Snow, W.; Mass Drivers III: Engineering. Space Resources and Space Settlements. NASA SP-428, 1979, pp. 119-157.
9. Cordell, B., O. Steinbronn. "An Analysis of Possible Advanced Space Strategies Featuring the Role of Space Resource Utilization" IAA-88-587. 39th Congress of the International Astronautical Federation, Bangalore, India. 8-15 Oct 1988.
10. Duke, M.B., R.J. Gustafson, and E.E. Rice. "Mining of Lunar Polar Ice" AIAA-98-1069. 36th Aerospace Sciences Meeting & Exhibit, Reno, NV. 12-15 Jan 1998.
11. Fegley, B., and Swindle, T.D. "Lunar Volatiles: Implications for Lunar Resource Utilization" in *Resources of Near-Earth Space*. Lewis, J., et al, eds. University of Arizona Press, Tucson, AZ. 1993.
12. Lewis, J., M.S. Matthews, and M.L. Guerrieri, eds. *Resources of Near-Earth Space*. University of Arizona Press, Tucson, AZ. 1993.
13. McKay, M.F., D.S. McKay, and M.B. Duke, eds. *Space Resources* NASA SP-509 vols.1-5. Johnson Space Center, Houston, TX. 1992.
14. Repic, E., Waldron, R., McMclure, W., and Woo, H. "Mission and Transportation System Applications of In-Situ-Derived Propellants" in *Resources of Near-Earth Space*. Lewis, J., et al, eds. University of Arizona Press, Tucson, AZ. 1993.
15. Staehle, R.L., et al., "Lunar Base Siting" in *Resources of Near-Earth Space*. Lewis, J., et al, eds. University of Arizona Press, Tucson, AZ. 1993.

Red Mars – Green Mars?
Mars Regolith as a Growing Medium

Embry-Riddle Aeronautical University
Daytona Beach, Florida

Advisor
Dr. Robert N. McGrath
Assistant Professor – Aviation Business Administration Department

Students

Rebecca Burgher
Tony DeTora
Holly Fisher
Michael Stein

1.0 Abstract

This project has been designed to determine if it is possible to grow plants that will provide a significant portion of the NASA-defined human nutritional requirements utilizing Martian regolith as the growing medium. Some alteration of the Martian regolith in addition to the introduction of a fertilizer is desirable in order to achieve this goal, but this alteration can be accomplished with little disruption to activities that are expected at a human-inhabited Mars base.

In 1987 Amos Banin "cautiously suggested that from the physical and chemical view points, the Martian soil may constitute an appropriate medium for plant growth." [1] With the Pathfinder science data confirming or supporting most of the necessary assumptions and estimates, it can now be suggested with much less caution that Martian soil is an appropriate medium. Despite this optimistic view, there will be no way to make this more than merely a suggestion until Martian regolith is either returned to earth or humans are finally brought to Mars.

2.0 NASA-defined Human Nutritional Requirements

Spaceflight introduces the human body to extremes not normally experienced in daily life. To supplement the body's natural protections for some of the negative effects that can occur, important nutrients must be included in an astronaut's diet.

To combat dehydration as well as reduce the risk of kidney stones, a recommended water intake of one milliliter per kcal of energy consumed. An average size astronaut of 70 kg requires about 3,000 kcal per day to remain at a constant weight and temperature. Because of the problem of calcium loss in weightlessness, fat should be a large component, (as high as 30 to 35 percent) of the astronaut's daily calorie intake. For the same reason, although a high protein diet would combat muscle loss, it would also impede calcium absorption, and therefore is recommended at 12 to 15 percent of the average diet, with further insight needed. [2]

A number of vitamins are also vital to an astronaut's health. Specifically, fat-soluble vitamins A, D, E, and K are necessary for both men and women. Water-soluble vitamins such as B_{12}, B_6, Thiamin, Riboflavin, Floate, Niacin, Biotin, and Pantothenic Acid are also important for human health. In addition to calcium, minerals such as phosphorous, magnesium, sodium, and potassium must be included in the diet of a long-term space traveler. Finally, trace elements such as iron, copper, manganese, fluoride, zinc, selenium, iodine, and chromium should be considered and included. [2]

After completing this study of essential nutrients, the following list of plants that could supply many of these necessary elements was developed. A mix of these 14 plants can provide nearly all of the required nutrients, with the lacking components being made up with vitamin/mineral supplements.

1. Wheat
2. Soybeans
3. Lettuce
4. Potato
5. Tomato
6. Spinach
7. Sweet Potato
8. Peanuts
9. Cow Peas
10. Dried Beans
11. Strawberry
12. Cabbage
13. Charod
14. Carrot

In addition to these 14 plants, a diet for a Mars base could be supplemented with celery, peppers, rice, snap beans, broccoli and various other plants to increase the variety of food consumed as well as maximizing nutrient inclusion without relying upon supplements. These inclusions will neither significantly effect the desired growing environment, nor increase the necessary growing area.

Vitamin and mineral supplements can be brought from earth to help provide the essentials to base inhabitants, and some foodstuffs could also be brought to further diversify the available foods.

3.0 Growth Requirements/ Preferences

All fourteen required varieties of plant identified have different temperature, light, soil type, moisture, and pH requirements for optimum growth. While potato and cabbage prefer a temperature range of 60°F – 70°F, and sweet potato prefers an even warmer 70°F – 80°F, wheat is optimized at a cooler temperature. Lettuce requires 1" of rain per week while wheat prefers fairly dry and soybeans prefer more moisture. Soybeans obtain their nitrogen from the air, not through the soil. Sweet potato prefers acidic soil while spinach doesn't grow well in acidic soil which may well prevent the use of Martian regolith for it's growth. Strawberry can grow in a variety of soil types while spinach prefers a sandy loam and carrot requires a deep, rich soil for optimization.

Optimum growth of all plants is not required, and some tradeoffs are required in order to develop a simple facility that can provide these needs. There will be several separate growing areas at differing levels of each of these requirements. Wheat will be grown by itself in a cool greenhouse with a constant day cycle to increase the yield. Other areas will have earth-normal day/night cycles and temperature range of either 60°F – 70°F or 70°F – 80°F.

Nutrients that are required for plant growth are broken down into macro-nutrients, those required on a large scale, and micro-nutrients, those that are required in much smaller scales. Macro-nutrients can not all be supplied by the Martian regolith, just as they can not be supplied by earth soil.

Table 1 – Macro-nutrient Levels in Terrestrial and Martian Soils [3]

Element	Terrestrial Soil (Avg wt %)	Mars Soil (Avg wt %)
N	0.14	Not determined
P	0.06	0.30
K	0.83	0.08
Ca	1.37	4.1
Mg	0.5	3.6
S	0.07	2.9

Micro-nutrients are also available in the Martian regolith. Fe is found in non-crystalline form, Zn, Cu and Mo are available at similar levels to that of earth soils.

4.0 Martian Regolith

The composition of Martian regolith appears to be uniform or nearly uniform throughout the planetary surface. This is most likely due to years, perhaps hundreds of millions of years, of storms carrying and intermixing the surface fines. [1] This theory is supported by the extreme similarities in the composition of the samples, as can be seen in Table 2, taken from each of the Viking sites as well as the Pathfinder soil data. The Viking sites are approximately 6500 km apart while the Pathfinder site is in a different hemisphere. [4]

The data provided from the regolith tested during the Pathfinder mission displayed slightly different qualities than the Viking tests as shown in Table 2, but Pathfinder was designed to provide a more detailed picture than the Viking missions. Both of these have differed to some degree from the SNC meteorites' composition, specifically in the increased presence of Si in the soil samples.

The oxides found during Mars Pathfinder mission using an Alpha Proton X-Ray Spectrometer agree with the inferred mineralogy from the Viking sites as can be seen in Table 3. The Viking landing craft were not equipped to directly measure the mineralogy of the soil, but the figures have been determined based upon the chemical composition and modeling.

The Martian regolith itself forms a loosely packed, porous medium in which plants will be able to grow and support the necessary root structures. Since the regolith contains a high proportion of smectite clays, the minerals stabilize the pH at the slightly acidic range (pH 5-6). These minerals also have a high exchange capacity, providing a large pool of exchangeable ions.

Table 2 – Elemental Composition of Martian Soils

Element	Pathfinder A-2, Soil [5]	Pathfinder A-4, Soil [5]	Pathfinder A-5, Soil [5]	Viking 1 Lander Site [6]
	Weight %	Weight %	Weight %	Weight %
Carbon [C]	-	-	-	-
Oxygen [O]	42.5	43.9	43.2	-
Sodium [Na]	3.2	3.8	2.6	-
Magnesium[Mg]	5.3	5.5	5.2	5.0 +/- 2.5
Aluminum [Al]	4.2	5.5	5.4	3.0 +/- 0.9
Silicon [Si]	21.6	20.2	20.5	20.9 +/- 2.5
Phosphorus [P]	-	1.5	1.0	-
Sulfur [S]	1.7	2.5	2.2	3.1 +/- 0.5
Chlorine [Cl]	-	0.6	0.6	0.7 +/- 0.3
Potassium [K]	0.5	0.6	0.6	< 0.25
Calcium [Ca]	4.5	3.4	3.8	4.0 +/- 0.8
Titanium [Ti]	0.6	0.7	0.4	0.5 +/- 0.2
Chromium [Cr]	0.2	0.3	0.3	-
Manganese [Mn]	0.4	0.4	0.5	-
Iron [Fe]	15.2	11.2	13.6	12.7 +/- 2.0
Nickel [Ni]	-	-	0.1	-
Not Directly Detected*	-	-	-	50.1 +/- 4.3
Sum	100	100	100	49.9

* Includes H_2O, NaO, CO_2, NO_x, and trace amounts of Rb, Sr, Y and Zr

Table 3 – Oxides in Martian Soils

Oxide	Pathfinder A-2, Soil [5]	Pathfinder A-4, Soil [5]	Pathfinder A-5, Soil [5]	Viking Chryse Planitia [7, 8]	Viking Utopia Planitia [7, 8]
	Weight %	Weight %	Weight %	Weight %	Weight %
Na_20	4.3	5.1	3.6	-	-
MgO	8.7	9.0	8.6	6	6
Al_2O_3	8.0	10.4	10.1	7.3	7*
SiO_2	46.1	43.3	43.8	44	43
SO_3	4.3	6.2	5.4	6.7	7.9
K_2O	0.6	0.7	0.7	<0.5	<0.5
CaO	6.3	4.8	5.3	5.7	5.7
TiO_2	1.1	1.1	0.7	0.62	0.54
MnO	0.5	0.5	0.6	-	-
Fe_2O_3	19.5	14.5	17.5	17.5	17.3
Cl	-	-	-	0.8	0.4
Other	-	-	-	2	2
Totals (approx)	99	96	96	91	90

* Inferred from available data

5.0 Comparison of Regolith to Requirements

Plants require N, P, K, Ca, Mg and S in considerable quantities and Fe, Mn, Zn, Cu, B and Mo in trace quantities. The Martian regolith contains P, Ca, Mg, S, Fe, Zn, Cu and Mo in sufficient quantities. N is available in the atmosphere, but it is not expected to provide the full needs of plant growth. K is available in small amounts in the regolith – this will also need to be supplemented. There is no evidence of B on the planet Mars. Mn is present in the Shergotty meteorite in amounts of less than 0.5% by weight. [3]

Most of the elements that are required are available, but the specific detailed mineralogy and the ease with which the plants could use them in their present form is unknown. Fertilization will be needed to provide some essential elements.

Other elements provide special concern due to the specific nature of the Martian regolith. Aluminum is present in a smaller concentration than is common in earth soils, but due to the acidic conditions on Mars, it may be a toxic level for plants. Chloride is found in amounts that may prevent plant life from taking in water, which would have an immediately detrimental effect upon the plants in question. [3]

6.0 Genetic Alteration of Plants

Some of the plants might be altered through the use of genetic engineering to more suitably inhabit the Martian landscape, or a controlled environment utilizing Martian regolith. Most genetic alteration of plants involves splicing genes specifically to confer resistance to some form of virus or insect. There have been advances, however, in providing plants with drought resistance, increased iron content and tolerance to normally toxic levels of aluminum. [9] These alterations are truly beyond the scope of this paper, the students involved and most of the individuals worldwide working on genetic engineering of plants.

7.0 Alteration of Regolith to Meet Growth Requirements

Clearly, the addition of a fertilizer will be required to produce the desired plants on Mars in a healthy environment. This fertilizer will need to provide significant nitrogen and potassium levels plus small amounts of manganese and boron. In the extremely unlikely situation that one of the elements contained in the Martian regolith is in a form that can not be easily utilized by the plants, there will need to be additional steps taken to ensure acceptable nutrient solubility and usability.

The aluminum and chloride presence in the regolith will need to be counteracted or the elements will need to be removed from the soil. Silicon has been shown to prevent toxicity of metals, but it is unclear how well this will work in the Martian environment. [10] This problem may be overcome by leaching the excess soluble salts from the regolith.

8.0 Preliminary Greenhouse Configuration

The greenhouse configuration can be seen in Figure 1 and is designed to separate the plant growth into six different areas. Each of these greenhouses is identical, provides a "shirtsleeve" environment, and will provide the desired temperature, humidity and pressure. The airlocks attach each greenhouse to a tunnel system as shown in Figure 2. This tunnel system provides for easy movement between the different greenhouse areas and allows for future expansion.

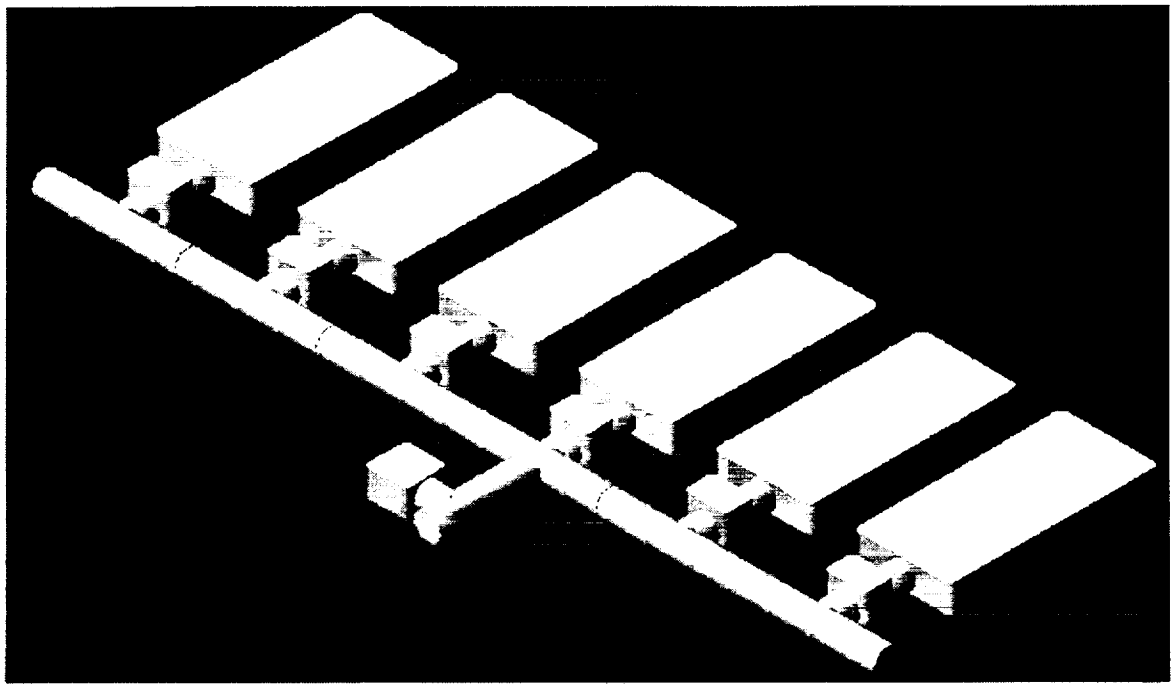

Figure 1 – Greenhouse Array

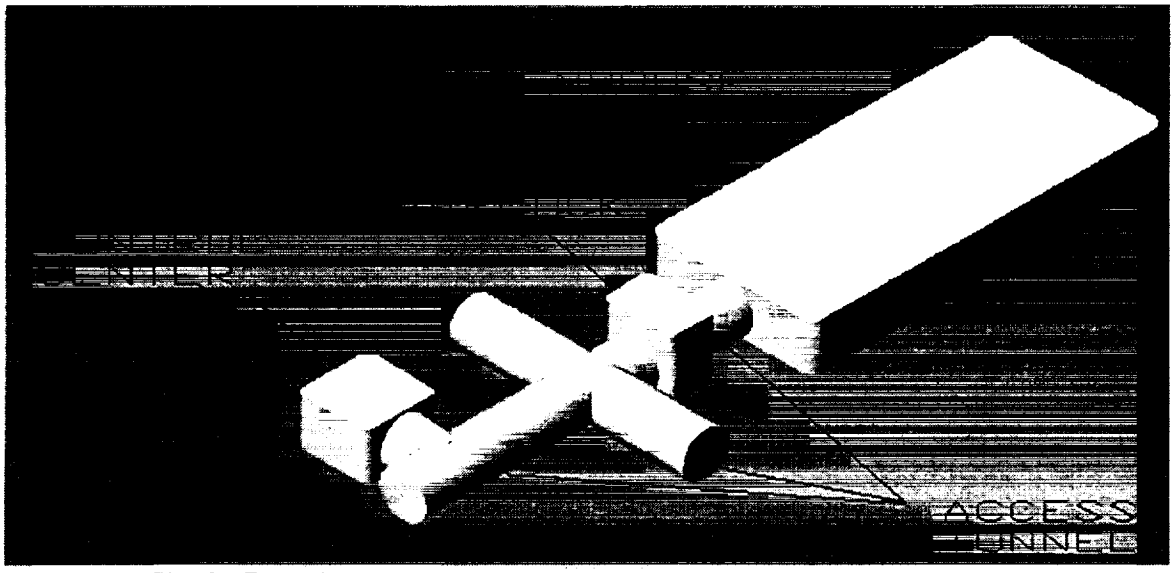

Figure 2 – Single Greenhouse

Each greenhouse has the same layout, enabling each to be used for any of the growing environments. This layout configuration can be viewed in Figure 3. Figure 4 provides a top view of a single greenhouse while Figure 5 provides a side view of the configuration.

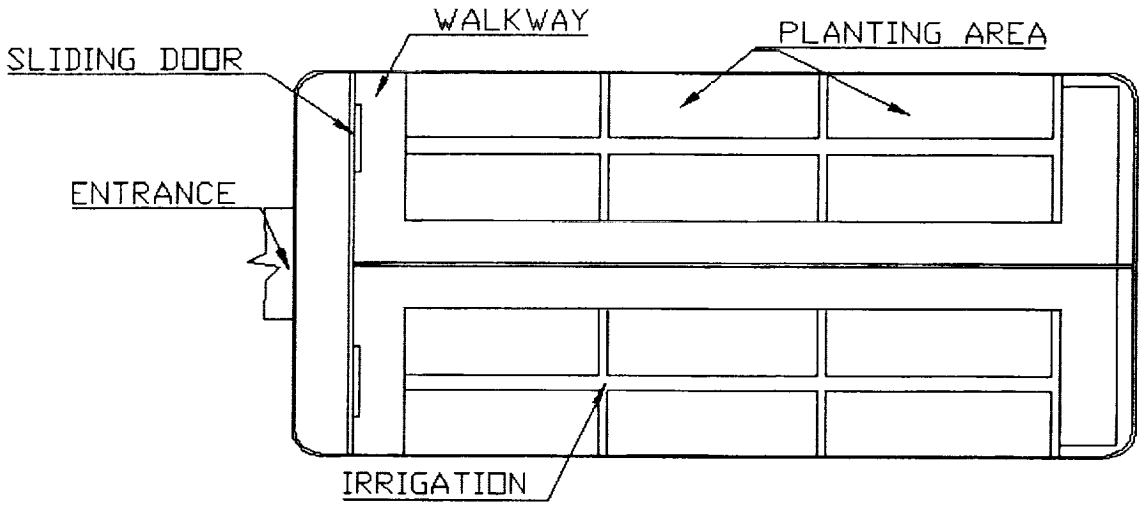

Figure 3 – Layout: Single Greenhouse

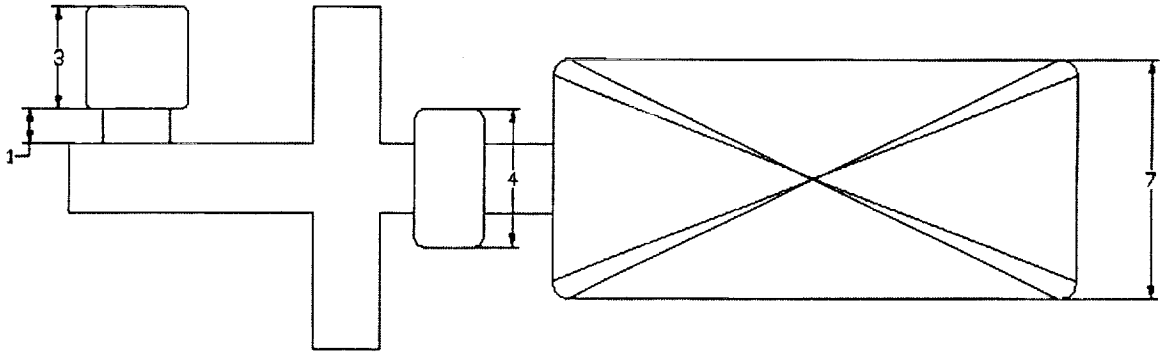

Figure 4 – Top View: Single Greenhouse [All Dimensions in meters]

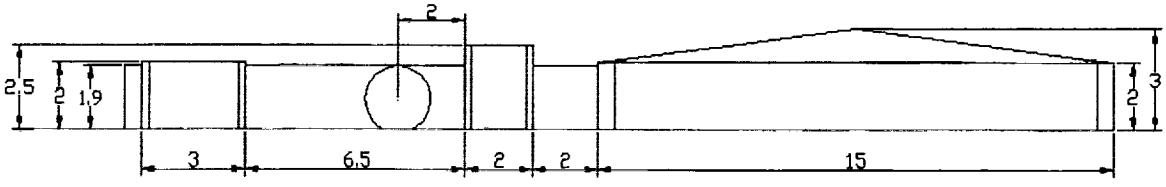

Figure 5 – Side View: Single Greenhouse [All Dimensions in meters]

9.0 Conclusion

Although certain assumptions can be made at this time based upon the information that is currently available, no real answers to the main question can be resolved without increased knowledge about the Martian regolith. There appear to be no major obstacles to the utilization of regolith as a growing medium, but the unknowns continue to be considerable.

The data received from the Pathfinder mission were astounding in their variety, complexity and relative consistency with the Viking data from 20 years earlier. This variety, complexity and relative consistency has not led to any major new insights on this specific topic. No new evidence was uncovered to bolster or refute a claim of regolith as a growing medium.

Ideas regarding the use of Martian regolith as a growing medium have been published as early as 1987 [1] when much less was specifically known about the composition of the Martian regolith. With the Pathfinder science data confirming most of the existing estimates and assumptions, the work that Banin, Stoker, Ming and others have done are now more confidently the proper path to follow. The path, however, is blocked by a lack of knowledge.

What is truly needed to glean greater insight into the issue is Martian regolith. This can be achieved by bringing regolith back to humans to test it or by bringing humans to Mars.

References

1. Banin, Amos, 1987. Mars Soil – A Sterile Regolith or a Medium for Plant Growth? In: The Case for Mars III: Strategies for exploration – general interest and overview. American Astronautical Society, San Diego, pp 559-571.
2. Lane, Helen W., Rice, Barbara, L., Wogan, Christine F., 1991. Nutritional Requirements for Space Station *Freedom* Crews. NASA Conference Publication 3146.
3. Stoker, C.R., Gooding, J.L., Roush, T., Banin, A., Burt, D., Clark, B.C., Flynn, G., and Gwynne, O., 1993. The physical and chemical properties and resource potential of martian surface soils. In: Resources of Near-Earth Space. The University of Arizona Press, Tucson pp 659-707.
4. Rieder, R., Economou, T., Wanke, H., Turkevich, A., Crisp, J., Bruckner, J., Dreibus, G., and McSween, Jr., H.Y. 1997. The chemical composition of martian soils and rocks returned from the mobile alpha proton X-ray spectrometer: Preliminary results from the X-ray mode. In: Science, Volume 278, December 5, 1997.
5. Mars Pathfinder Science Results Website. http://mars.jpl.nasa.gov/MPF/science/science-index.html
6. Meyer, Thomas R., and McKay, Christopher P., 1995. Using the Resources of Mars for Human Settlements, American Astronautical Society Paper AAS 95-489. In: Strategies for Mars: A guide to human exploration. American Astronautical Society, San Diego pp 393-442.
7. Ming, Douglas W., Golden, D.C., and Henninger, Donald L., 1993. Utilization of On-Site Resources for Regenerative Life Support Systems at Lunar and Martian Outposts. SAE Technical Paper 932091.
8. Clark, B.C., Baird, A.K., Weldon, R.J., Tsusaki, D.M., Schnable, L., and Candelaria, M.P., 1982. Chemical composition of martian fines. Journal of Geophys. Research, 87, 10059-10067.
9. Tangley, Laura, 2000. Engineering the harvest. In: U.S. News & World Report, March 13, 2000, pp 46-47.
10. Bugbee, Bruce. Why add silicon to nutrient solutions? In: Hydroponics website http://www.hbci.com/~wenonah/hydro/makhydro.htm

LIST OF FORUM PARTICIPANTS

John Abbott
Embry-Riddle Aeronautical University

Jhason Abuan
University of Maryland

David L. Akin
University of Maryland

Roger Alexander
Georgia Institute of Technology

Ben Armentrout
University of Washington

Abigail Bazin
Colorado School of Mines

Ryan S. Bechtel
Georgia Institute of Technology

Avi Belinsky
Seattle, Washington

David Black
Lunar and Planetary Institute

Angela Braun
University of Texas, Austin

Nathan S. Brown
California Institute of Technology

Rebecca Burgher
Embry-Riddle Aeronautical University

James D. Burke
Jet Propulsion Laboratory (Retired)

Dan Butler
University of Texas, Austin

Chris Carlins
Pennsylvania State University

Robert Cataldo
NASA Glenn Research Center

Diana Chai
University of California, Berkeley

Vincent Chang
University of California, Berkeley

David Chu
University of California, Berkeley

Stephen M. Clifford
Lunar and Planetary Institute

Jordan Conley
Rowan University

John Connolly
NASA Johnson Space Center

Timothy A. Cormier
Georgia Institute of Technology

Keith T. Crowe
Colorado School of Mines

Tony De Tora
Embry-Riddle Aeronautical University

Chuong Dinh
Wichita State University

Truong V. Dinh
Wichita State University

David S. Draper
NASA Johnson Space Center

Michael B. Duke
Lunar and Planetary Institute

Dean Edmonston
Wichita State University

Alvin B. Eisenberg
Boeing

Holly Fisher
Embry-Riddle Aeronautical University

Joe Fledderman
Pennsylvania State University

Wallace Fowler
University of Texas, Austin

David C. Gan
University of California, Berkeley

Colin Graham
University of Colorado

Michael Graham
Pennsylvania State University

James P. Gross
Colorado School of Mines

Elyus Gwin
University of California, Berkeley

Anne C. Hadreas
University of California, Berkeley

Samantha Harper
University of California, Berkeley

Don Henninger
NASA Johnson Space Center

Jason Hinkle
University of Colorado

Christopher Hirata
California Institute of Technology

Alysha Holmes
Pennsylvania State University

Jean Hsu
Pennsylvania State University

Oscar Hsu
University of Maryland

Michael Jordan
Pennsylvania State University

Satchidanand A. Kalaver
Georgia Institute of Technology

David Kaplan
NASA Johnson Space Center

Heidi Kappes
University of Washington

Ben Kirk
University of Texas, Austin

Wojciech Klimkiewicz
Pennsylvania State University

Roy Klusendorf
Oceaneering Space Systems

Robert D. Knecht
Colorado School of Mines

Ted Kutrumbos
University of Colorado

Lawrence Kuznetz
University of California, Berkeley

Pascal Lee
NASA Ames Research Center

Devon Lefler
Rowan University

Jung-Ho Lewe
Georgia Institute of Technology

Loy-Yik Liew
Wichita State University

Ravi Malla
Wichita State University

Humboldt C. Mandell
NASA Johnson Space Center

Anthony Marchese
Rowan University

Weston R. Marlatt
Colorado School of Mines

Edward D. McCullough
Boeing RSS

Michael McGee
Lockheed Martin Astronautics

David S. McKay
NASA Johnson Space Center

Barbara J. McKinney
Colorado School of Mines

Jeffrey J. Mendel
University of California, Berkeley

Ben Mottinger
University of Colorado

Jason Muckenthaler
University of Colorado

Gawad Nagati
Wichita State University

Douglas K. Nelson
Georgia Institute of Technology

Deborah J. Neubek
NASA Johnson Space Center

Seet Wai Ng
Wichita State University

John R. Olds
Georgia Institute of Technology

Gregg O'Marr
Pennsylvania State University

Michael A. O'Neal
NASA Kennedy Space Center

Peter C. Pawlowski
University of Maryland

Lewis L. Peach Jr.
USRA Headquarters

Shane Pixton
Embry-Riddle Aeronautical University

David S. Portree
Freelance Writer

Andrew Potter
Lunar and Planetary Institute

Brent J. Pounds
Colorado School of Mines

Robert Reed
University of Maryland

Mahmut Reyhanoglu
Embry-Riddle Aeronautical University

Christopher Roberts
Embry-Riddle Aeronautical University

Lanny Rudner
University of California, Berkeley

Eric Schell
University of Colorado

Derek M. Shannon
California Institute of Technology

Kevin Sloan
Pennsylvania State University

Brian Sosnowchik
Pennsylvania State University

Paul Spudis
Lunar and Planetary Institute

Michael Stein
Embry-Riddle Aeronautical University

Frieda B. Taub
University of Washington

Nikki Thornton
Pennsylvania State University

Kevin Turner
University of Maryland

Phillip N. Tyler
Colorado School of Mines

Ben Weber
Pennsylvania State University

John E. Weglian
Georgia Institute of Technology

Scott White
University of Texas, Austin

Dan Wicklund
University of Colorado

Dalziel Wilson
University of California, Berkeley

Miki Yamada
University of California, Berkeley

Corissa Young
University of Colorado

Rommel Zara
University of Maryland